DISSERTATION

DEVELOPMENT OF LC-MS AND DEGRADATION TECHNIQUES FOR THE ANALYSIS OF FUNGAL-DERIVED CHITIN

Submitted by

Christopher L. Allison

Department of Chemistry

In partial fulfillment of the requirements

For the Degree of Doctor of Philosophy

Colorado State University

Fort Collins, Colorado

Summer 2020

Doctoral Committee:

Advisor: Melissa M. Reynolds

Delphine Farmer
Travis Bailey
Ketul Popat

ABSTRACT

DEVELOPMENT OF LC-MS AND DEGRADATION TECHNIQUES FOR THE ANALYSIS OF FUNGAL-DERIVED CHITIN

The research contained within this dissertation began with the following question: Can liquid chromatography-mass spectrometry (LC-MS) be used as a screening method for fungal infections? The ensuing projects investigated various aspects of that question, taking a ground-up approach that started with the analysis of the simplest constituents of the biomarkers used, chitin and chitosan. The complexity of the systems investigated was gradually increased, culminating in the extraction and detection of these biomarkers from pertinent fungal cells. Chitin constitutes 10-30% of the mass of filamentous fungi. While not found endogenously, it is the second most abundant naturally-occurring polysaccharide, next to cellulose. Chitin is composed of >50% *N*-acetylglucosamine (GlcNAc) and D-glucosamine (GlcN). In nature and in numerous applications, chitin can be deacetylated to produce chitosan. Chitosan is the deacetylated (>50% GlcN) counterpart to chitin and is also found in some species of fungi. This dissertation began with the development of electrospray ionization mass spectrometry (ESI-MS) methods to analyze GlcN and GlcNAc, as well as oligomers composed of both residues. The optimization of methods to analyze the components of chitin served as the foundation on which to advance the applicability of these methods. Following method optimization, the ability of mass spectrometry to analyze polymeric chitosan was explored. Detecting polymeric chitosan was determined to be infeasible using ESI-MS; hence, the focus of subsequent studies was turned to the use of degradation studies to generate low molecular weight chemical fingerprints that could be correlated to the presence of

chitin and chitosan. The first experiments performed to study the degradation of chitosan evaluated the impact nitrosating conditions have on the structure of chitosan. Both mass spectrometry and spectroscopic methods were used to track the formation of a degradation product, 2,5-anhydro-D-mannose (2,5-AM), to demonstrate that nitrous acid-based conditions induce degradation in polymeric chitosan. Following these experiments, degradation studies were expanded to include a wider range of starting materials. Chitosan polymer was used again, in addition to two chitin polymers with varied degrees of deacetylation. In addition to examining the effect of nitrosating conditions on these polymers, degradation methods were expanded to include hydrochloric acid (HCl), hydrogen peroxide (H_2O_2), and enzymatic degradation agents (lysozyme, lipase, and hemicellulase). The susceptibility of each polymer to degradation protocols was assessed by ESI-MS or LC-MS analysis of degradation products generated. Results from these studies indicated that HCl, H_2O_2, HNO_2, and lysozyme generate distinct products from chitin and chitosan polymers. Identification of unique chemical fingerprints produced from chitin and its derivatives provided the necessary information to apply these studies to pertinent fungal cells. The final experiments in this dissertation apply cleanup, cell lysis, degradation methods, and LC-MS to identify GlcN produced from *Aspergillus niger* fungi. Cumulatively, the following research contains a thorough overview of degradation methods for chitin and its derivates, along with the characterization of low molecular weight fingerprints that each protocol generates. ESI-MS or LC-MS methods were used to identify low molecular weight products formed during degradation. Finally, both degradation and LC-MS methods were applied to *Aspergillus niger* to validate that representative fungal species can be detected using the proposed techniques.

TABLE OF CONTENTS

CHAPTER 1

BACKGROUND AND INTRODUCTION

1.1 Overview

During the course of the research contained in this dissertation, the prevailing motivation was to determine the efficacy of liquid chromatography-mass spectrometry (LC-MS) as a diagnostic tool for fungal infections. Diagnostics for fungal infections often take weeks to provide results, and sometimes render false negatives. Inconsistency or delays in currently used diagnostics present the need for sensitive screening methods such as those proposed in this dissertation. Subsequent research projects span a variety of approaches; however, their common purpose was to increase the knowledge of two distinct components pertinent to this objective. The first aspect of this system investigated was chitin, the biomarker proposed to allow detection of fungal infections. Chitin and its derivatives vary greatly in size, solubility, and susceptibility to chemical modifications. Given this, a thorough understanding of its chemical nature is critical to the ultimate goal of creating a diagnostic method for fungal infections. The second system explored was the instrumentation proposed to allow the detection of fungi. LC-MS is an analytical technique that links chemical separations with a sensitive detector. Both components are complex, customizable systems that have increased in complexity, applicability, and frequency since their discovery. A thorough discussion of each of these topics is imperative to understanding the research covered in following chapters. In this chapter, chitin and its derivatives (primarily chitosan) are discussed in detail, along with their incidence, chemical properties, and applications. Mass spectrometry is introduced, alongside an overview of how mass spectrometers ionize and detect various

compounds. High-performance liquid chromatography is covered in the context of its pairing with mass spectrometry. The prior use of LC-MS to analyze chitin derivatives is considered, along with the applications of these studies. Finally, the importance of improving diagnostic methods for fungal infections is highlighted. By discussing the systems of interest and the need for improved diagnostic methods, this chapter highlights the importance of the research contained later in this dissertation. Furthermore, it provides rationale for the selection of both the biomarker and the detection method used to address whether LC-MS may serve as a diagnostic tool for fungal infections. **Figure 1.1** highlights how the proposed methods may be used to screen for fungi.

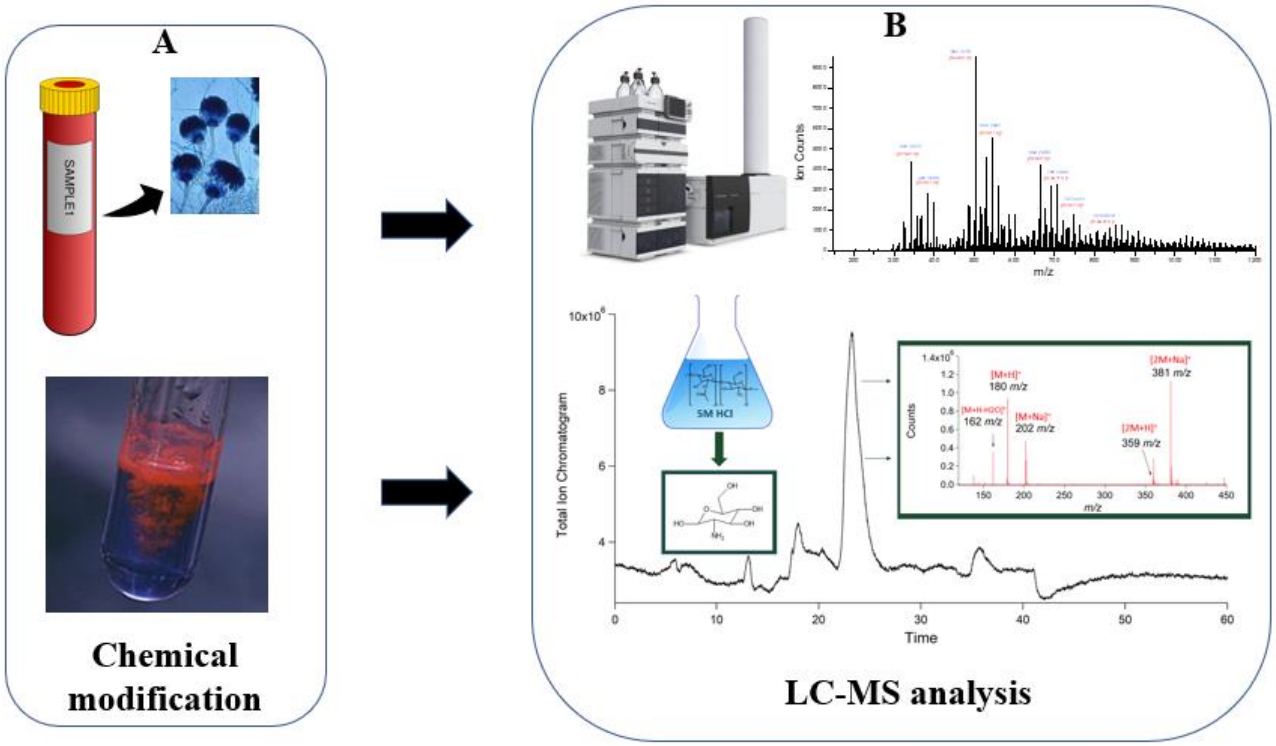

Figure 1.1: Overview of the proposed use of LC-MS to detect fungal infections. Different aspects of research are represented by each inset. Inset **A** represents the necessary chemical modifications to produce a molecular indicator of fungi. Inset **B** represents the analytical method development required to detect the signal produced by the molecular indicator.

1.2 Introduction

Chitin and its derivatives, especially chitosan, have been heavily studied in biomedical research[1,2]. Numerous studies have closely examined chitosan's biocompatible, antimicrobial, and wound-healing properties, among others[3–5]. Chitosan and its derivatives are analyzed by a variety of methods, including size exclusion chromatography, infrared spectroscopy, nuclear magnetic resonance spectroscopy, viscometry, and others[6–8]. Mass spectrometry can be used to characterize chitosan; however, its use is largely restricted to analyzing low molecular weight species[9,10]. While some large molecules such as proteins are routinely analyzed using mass spectrometry and multiple charging[11,12], multiply-charging polymers for analysis is less common[13,14]. The routine use of mass spectrometry to analyze polymeric chitosan is discouraged due to several complications encountered in the analysis of oligomers. These include the formation of various adducts, as well as the formation of multiple charge states for each polymeric species[13,15]. Rather than attempting to deconvolute significantly complicated polymeric spectra, inferences are often made by the analysis of the degradation products of chitosan[9,10,16,17]. Given that the degradation of chitosan has been well-studied and is controllable[18,19], mass spectrometric analysis of its degradation products can elucidate information about both the products and the parent polymer. Mass spectrometric analysis of the degradation products of chitin and chitosan provides specific molecular information that offers insight into degradation processes. Additionally, for researchers interested in making chitosan oligosaccharides (COS) in-house, characterization of the specific products generated by degradation protocols is highly useful. Using high-performance liquid chromatography (HPLC) to separate the low molecular weight components of chitosan, including COS, glucosamine (GlcN), and *N*-acetylglucosamine (GlcNAc) with hydrophilic interaction liquid chromatography (HILIC) columns has been explored[20–22]. The development of well-defined

degradation methods to produce a low molecular weight fingerprint would allow LC-MS to act as a detection method for chitin and chitosan polymers. Given that these polysaccharides are constituents of fungal cell walls[23], the detection of chitin could serve as a diagnostic tool for fungal infections in appropriately equipped clinical laboratories.

1.3 Polymers and polysaccharides

1.3.1 Incidence and classifications

Polymers are used worldwide for a huge range of applications. They occur in everyday applications like shopping bags, and can also be found in high-tech materials like Kevlar vests and biomedical implants[24,25]. Plastics, fibers, and a host of other synthetic and naturally-occurring materials are comprised of polymers[26]. Polymers are macromolecules composed of a large number of smaller molecules linked together. The smallest molecular components are known as monomers, and polymers can be composed from just a few to thousands of these subunits[27]. This gives polymers a vast size range, ranging in size from a few thousand to several million Daltons. If only a few monomers are joined together, the molecule is referred to as an oligomer. Generally, the masses of these is <10 kDa[28]. Oligomers can be further subcategorized into dimers (two linked monomers), trimers (three monomers), tetramers, and so forth. Oligomers are structurally identical to their parent polymers but with differing properties as a consequence of their lower molecular weight[29]. Polymers composed of one type of monomer are called homopolymers. Not all polymers contain just one type of monomer subunit, however[30]. Copolymers consist of two distinct monomer units, and these subunits may occur randomly, in blocks, or in alternating fashion[31]. In addition, polymers may also be classified as linear or branched. Linear polymers are characterized by a continuous chain of carbon-carbon bonds, in which the remaining two valence bonds are attached to hydrogens or hydrocarbon moieties[32]. Conversely, branched polymers contain secondary

polymer chains linked to their primary backbone, resulting in a variety of three-dimensional structures and multiple chain ends per molecule[33].

Many polymers are durable materials that age slowly and retain their properties over time. While these are desirable properties in many instances, this has resulted in a worldwide increase of waste buildup[34]. The desire to minimize persistent waste products has sparked interest in the use of biodegradable polymers with the potential for reuse, recycling, and non-toxic degradation[35,36]. Polysaccharides are a prominent class of naturally occurring polymers with wide applicability. Polysaccharides are cyclolinear polyethers formed by condensation reactions of sugars[37] and linked by glycosidic bonds. These are bonds in which the anomeric hydroxyl group of a monosaccharide joins with a hydroxyl group on another subunit, creating water as a byproduct[38,39]. The breakdown of polysaccharides is facilitated by the presence of glycosidic bonds, which are highly susceptible to hydrolysis[40]. This produces simple sugars as degradation products, providing a non-toxic degradation pathway. Cellulose, chitin, starch, and glycogen are all examples of polysaccharides. Together, these compose a majority of biomass in the world as constituents of vegetation, fungi, and arthropods[41–43].

1.3.2 Chitin and its derivatives

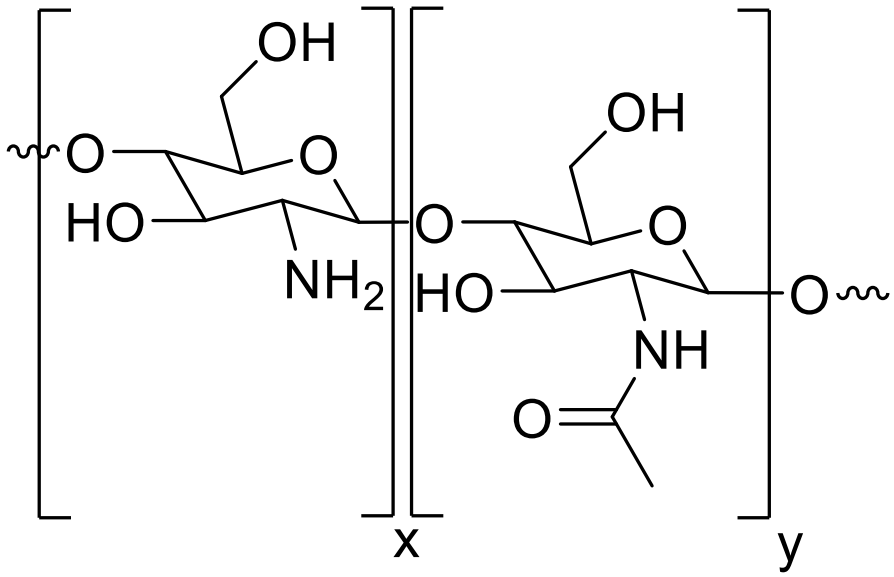

Figure 1.2: Generic structure of chitin/chitosan. Subunit "x" shows a GlcN residue. Subunit "y" shows a GlcNAc residue. In larger species, subunits are randomly distributed and occur in varying proportions in a given sample.

Chitin is the second-most abundant polysaccharide found in nature, next to cellulose. It is found in marine crustaceans, arthropods, and fungi, and confers rigidity to the exoskeleton of its parent organism[26,42,44]. Chitin is a branched polymer composed of repeating *N*-acetylglucosamine (GlcNAc) monomers. It is insoluble in the majority of solutions, dissolving only in specific organic solvents like hexafluoroacetone, hexafluoro-2-propanol, or *N,N*-dimethylacetamide in the presence of lithium[45]. An estimated 10^{10}-10^{12} tons of chitin are produced in nature annually, making it a readily available byproduct of the seafood harvesting industry[46]. Fungal sources, especially *Aspergillus niger,* also represent a sizable source of chitin[47]. Physically, chitin is a white, inelastic compound that forms crystalline microfibrils[48,49]. Given the quantity of chitin produced annually, in some coastal areas chitin is considered to be a source of beach pollution[50]; however, chitin-degrading enzymes found in many organisms render it biodegradable[51].

As chitin's inability to dissolve in commonly used solvents renders it largely intractable, it is often chemically modified to produce chitosan. Chitosan is generally obtained via the alkaline deacetylation of chitin. Industrially derivatizing chitin from marine crustacean waste to chitosan is a four-step process. This includes 1) deproteinization, in which bonds are disrupted between chitin and proteins. 2) Demineralization occurs next, which is implemented to remove minerals such as calcium carbonate. 3) Decoloration removes excess pigmentation, and 4) deacetylation chemically modifies chitin to chitosan by hydrolyzing the *N*-acetyl group to a primary amine[50]. Deacetylation is rarely complete, and yields a copolymer consisting of randomly distributed D-glucosamine (GlcN, >50%) and GlcNAc, as shown in **Figure 1.2**. Chitosan has greatly increased applicability in comparison to chitin. This is partially due to its ability to dissolve in acidic aqueous solutions, and partly due to the reactivity of the primary amine in GlcN subunit[52,53]. Both properties are conferred by the deacetylation of GlcNAc monomers to GlcN. Chitosan is soluble in pH < 6.0 solutions with compositions of >50% GlcN[54]. While chitin and chitosan are usually differentiated based on their proportion of GlcN to GlcNAc, the European Chitin Society asserts that chitin and chitosan should be classified based on solubility in a 0.1 M acetic acid solution with soluble materials being referred to as chitosan and insoluble as chitin[55]. For the purposes of this dissertation "chitin" will refer to polymers with proportions of GlcNAc greater than 50%, and "chitosan" will refer to polymers with proportions of GlcN greater than 50%. Chitosan has many desirable properties including biocompatibility, non-toxicity, and biodegradability[56,57]. Modification of chitin's *N*-acetyl group to a primary amine confers an increased ability for chitosan to be derivatized and otherwise modified[58,59]. Chitosan varies in size, depending on the source and methods used to convert it from chitin[60]. Chitosan is a beige to white-colored powder[61,62]. It is

commercially available from many vendors, and commonly ranges between 3800 and 500,000 g/mol with degrees of *N*-acetylation from 2% - 40%[63,64].

The biodegradable, biocompatible, and non-toxic properties of chitosan have given it great applicability in medical research. Chitin and chitosan-based materials have been applied extensively in tissue-engineering. Chitin-based materials have been fabricated into several forms of scaffolds, including hydrogels, films, tubes, and three-dimensional porous structures[65,66]. These have demonstrated the ability to facilitate regenerative cell growth while providing beneficial effects such as enhanced cellular function and biomolecule regulation[67,68]. Chitin/nanosilver composite scaffolds have been made for wound-healing applications, exhibiting both antimicrobial and blood-clotting properties[69]. Chitosan has been fabricated into microspheres, which have been investigated for their potential as drug carriers[70]. In addition, chitosan microspheres are hemostatic, and have been implemented in bandages, sponges, and other wound dressings[71]. In addition to its applications in cell regeneration and wound healing, chitosan has demonstrated the ability to inhibit microbial growth. Chitosan has been utilized for its antimicrobial properties in healthcare, including applications in wound-healing, dentistry, and ophthalmology[72–75]. Its antimicrobial uses extend beyond healthcare into food preservation textile fabrication, where it inhibits long-term bacterial proliferation[75–77]. Chitosan's antibacterial properties have been demonstrated against *E. coli*, as well as *Actinobacillus* and *Streptococcus* species, among others[78–80]. Chitosan is polycationic in solution; it is thought that its cationic primary amines are significant contributing factors to its antibacterial behavior[75,81]. These interact with negatively charged groups contained on prokaryotic cell walls, ultimately, resulting in cell surface alterations, lysis, and death[82].

The functionality of chitosan can be further enhanced via production of low molecular weight COS. These compounds have molecular weights of <3000 g/mol, and are commonly

produced in-house. Decreasing the molecular weight of chitosan confers increased solubility, as COS easily dissolve in neutral water[83]. COS are non-cytotoxic and are easily processed by the human body. They are absorbed through the intestine and are eventually excreted in urine[84]. Their increased solubility, straightforward breakdown and *in-vivo* disposal make COS a frequent target for derivatizations for drug delivery[85–87]. In addition to being easily biodegradable, COS display many of the same biological properties that give chitosan its appeal. These include wound-healing, anti-inflammatory, and antimicrobial properties, although its antimicrobial effects are less pronounced[88–91]. Consistent with their parent polymers, COS are comprised of GlcN and GlcNAc monomers joined by β-1,4 glycosidic bonds. Research involving COS commonly uses shorthand nomenclature to describe the components of oligomers. Rather than list oligomers of a specific composition by using the full subunit name, GlcNAc is referred to by the letter "A", while GlcN is referred to by the letter "D." These letters stand for "acetylated" versus "deacetylated" monomer units, respectively[92]. As an example, a chitosan oligomer containing three GlcN and one GlcNAc residue would be referred to as "D3A1." This nomenclature will be used in following chapters. In this dissertation, COS are characterized in a variety of studies. Their high solubility makes them detectable using LC-MS. Additionally, the predictable nature by which COS form allows inferences to be made about their parent polymers following their detection.

1.3.3 Chitin in fungi

Chitin (and chitosan, to a lesser extent) is found in the cell walls of filamentous fungi. Fungi are widespread in areas inhabited by humans. Exposure to airborne fungal spores is unavoidable for most; however, infection is quite rare in all but immunocompromised individuals[93]. Only around 1% of fungal species have the ability to cause fungal infection, which can occur superficially as skin infections (e.g. athlete's foot) or invasively[94,95]. Invasive fungal

infections are extremely deadly, being associated with mortality rates of over 50%[96,97]. Invasive fungal infections include a variety of systemic infections, extending to the blood, heart lungs, and other internal locations[98–100]. Given the ubiquity of airborne spores, pulmonary fungal infections are of significant concern to immunocompromised patients[101,102]. Over 10,000,000 cases occur annually, making these a significant global concern[103]. Screening methods used to diagnose fungal infections often result in delayed treatment or misdiagnoses. Cultures can take weeks to provide results, while microscopy and other relatively fast methods are prone to false negatives due to their reliance on visible indicators[104,105]. Inconsistency and delays in current testing methods presents the need for sensitive screening methods such as those proposed in this dissertation. The fungi implicated in pulmonary infections are usually filamentous, and include species from *Aspergillus, Cryptococcus,* and *Pneumocystis* genera[96,101]. Chitin confers rigidity to the cell walls of filamentous fungi, composing a total of 10-30% of their dry mass[106,107]. While humans contain chitinases and other enzymes capable of degrading chitin, neither chitin nor chitosan are not found endogenously in humans[108,109]. Given this, methods to detect chitin by LC-MS offer the potential to serve as an effective diagnostic tool for fungal infections. Decreasing both the time to diagnosis and the incidence of false negatives is crucial to immunocompromised patient health.

1.4 Liquid chromatography - mass spectrometry

1.4.1 Development of modern mass spectrometers

In its earliest forms, mass spectrometry was first used in the 1910s to demonstrate the existence of isotopes, for which F.W. Aston won the 1922 Nobel Prize in Chemistry[110]. In the 1940s, the petroleum industry adopted techniques to perform quantitative analysis of hydrocarbons in process streams[111]. The presence of mass spectrometry grew over the next 40 years; however, ionization methods all shared a reliance on gas-phase collisions between a charged particle and the

analyte, limiting its use to compounds already volatilized. Researchers struggled with the problem of how to bring large molecules into the gas phase until the 1980s, when the field exploded with so-called "soft" ionization techniques capable of producing ions from thermally labile or nonvolatile compounds[112]. Fast-atom bombardment (FAB) was the first technique capable of ionizing non-volatile compounds; however, its incidence waned following the introduction of more sensitive ionization methods[113,114]. These include matrix-assisted laser desorption ionization (MALDI) and electrospray ionization (ESI), both of which were invented later in the 1980s[115,116]. MALDI and ESI remain two of the most popular ionization methods, with improved versions regularly being developed since their advent. These are paired with a variety of mass analyzers, allowing instruments to be built and customized for the analysis of a plethora of compounds. Modern mass spectrometric methods are often used in tandem with separations methods like high-performance liquid chromatography. These techniques facilitate analysis of complex mixtures of compounds, providing a sensitive detector for separations and expanding the applications for mass spectrometry[111,117].

1.4.2 Ionization sources

The first step to successfully perform mass spectrometry is to generate charged ions in the gaseous phase. This is done via the use of ionization sources[111,117]. Modern mass spectrometers include a wide range of sources, which can be categorized into three general groups: gas phase ion sources, desorption ion sources, and ambient desorption sources[117]. The two most common gas phase sources are electron impact (EI) and chemical ionization (CI) sources[118]. These are used in conjunction with gas chromatography systems, and function by ionizing compounds already in the gaseous phase. Desorption sources include FAB, ESI, MALDI, and a range of others[117]. Desorption sources broadly function by converting solid or liquid phase samples into gas-phase

ions. Ambient ionization sources such as desorption electrospray ionization (DESI) and direct analysis in real time (DART) sources facilitate ionization through desorption[119]. One of the key advantages to ambient ionization sources is their ability to ionize samples with little or no pretreatment. Sources can be further subcategorized into hard or soft ionization sources. Hard ionization sources fragment compounds, resulting in multiple *m/z* peaks per analyte[111]. On the other hand, soft ionization methods result in little to no fragmentation. MALDI and ESI are the two most common desorption methods, both of which are soft ionization sources. Both are conducive for ionization of polar analytes like metabolites, peptides, or biopolymers and feature the highest mass limits of all ion sources[117]. MALDI sources are frequently used for applications such as protein analysis or imaging; however, due to difficulties pairing MALDI with liquid chromatography, LC-MS systems typically utilize ESI[120,121]. Due to its easy pairing with separations, methods contained in the dissertation make use of an ESI source, which is covered in greater detail below.

Table 1.1: Commonly used ionization sources and their compatibility with various separations techniques.

Ionization method	**Separation pairing**
Electron Impact (EI)	GC
Chemical Ionization (CI)	GC
Atmospheric Pressure Chemical Ionization (APCI)	LC
Electrospray Ionization (ESI)	LC
Matrix-Assisted Laser Desorption Ionization (MALDI)	Usually none; sometime modified to be compatible with LC

Since its inception, ESI has steadily remained one of the most common ionization sources in mass spectrometry[122–124]. Its flexibility is one of the primary reasons for its prevalence in modern analytical chemistry, as it is capable of ionizing small compounds (<100 Da) up to proteins with masses of hundreds of thousands of Daltons[125,126]. For applications where a separation step is desired, ESI holds an advantage over MALDI due to its easy pairing with LC methods. ESI is used to analyze compounds dissolved in volatile solvents. Electrospray droplets are generated following injection of the analyte into a volatile mobile phase. Their formation is induced as the mobile phase is sprayed through a nebulizing needle at atmospheric pressure to which a high voltage is applied. Solvent evaporation is encouraged by concurrent inert gas flow, often nitrogen. Highly charged droplets of these solutions are produced, followed by solvent evaporation. As evaporation continues, charged droplets continue to shrink, ultimately resulting in the ejection of charged ions. This leaves behind gaseous ions, facilitating the ionization of labile compounds with little to no fragmentation[115,127]. These ions are electrostatically directed into a capillary leading into the instrument where ions are subjected to focusing, filtering and sometimes fragmentation steps before entering the detector[12,127–129]. **Figure 1.3** shows an overview of ion formation in ESI.

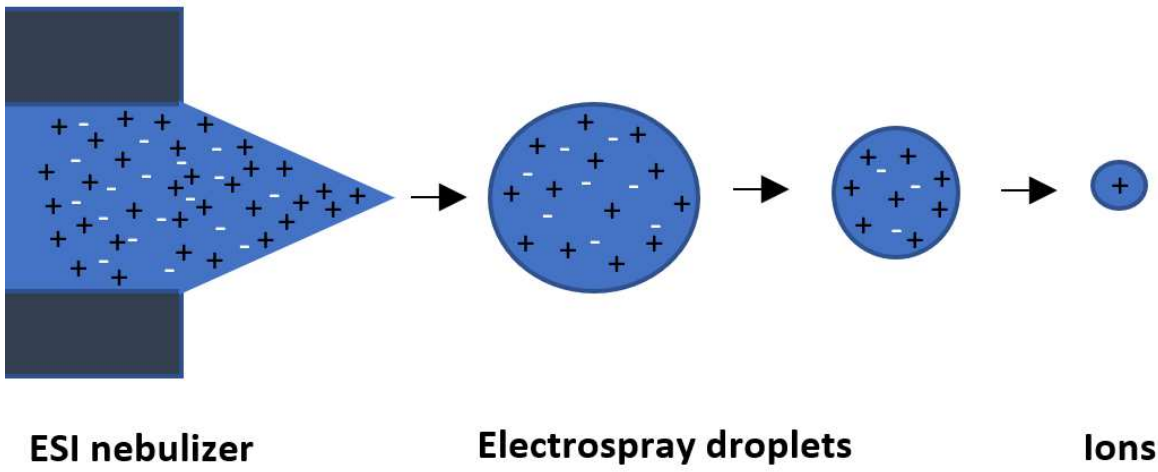

Figure 1.3: ESI ionization process showing the formation of positive ions within the source.

1.4.3 Mass analyzers

Table 1.2: Mass analyzers with approximated mass limits.

Mass analyzer	Mass range *m/z*	Resolution
Quadrupole	4000	≤2000
Time-of-flight (TOF)	No theoretical limit	≤3000
Orbitrap	6000	≤150,000
Fourier transform ion cyclotron resonance (FT-ICR)	6000	≤1,000,000

Following ionization, mass analyzers are used separate ions with different mass-to-charge, or *m/z* ratios. These include ion traps, quadrupoles, time-of-flights (TOF), Orbitraps, and Fourier transform ion cyclotron resonance (FT-ICR) mass analyzers. Different mass analyzers are utilized in different circumstances for their varying properties, including their resolution and upper mass limits, as shown in **Table 1.2**[111,117]. A mass analyzer's resolution is one of its most significant features. Resolution is described by the equation $R = m/\Delta m$ where m is the nominal mass of a mass spectral peak and Δm is the difference between two adjacent peaks with equal intensity[130–132]. Increased resolution facilitates differentiation between ions with lower mass differences. Upper mass limits vary from ~4000 Daltons in quadrupoles to Megadaltons in TOFs[133–135]. A TOF mass analyzer was used for studies covered within this dissertation. While not as sensitive as some detectors, TOFs facilitate the detection of a wide range of analytes, due to their flexible mass ranges.

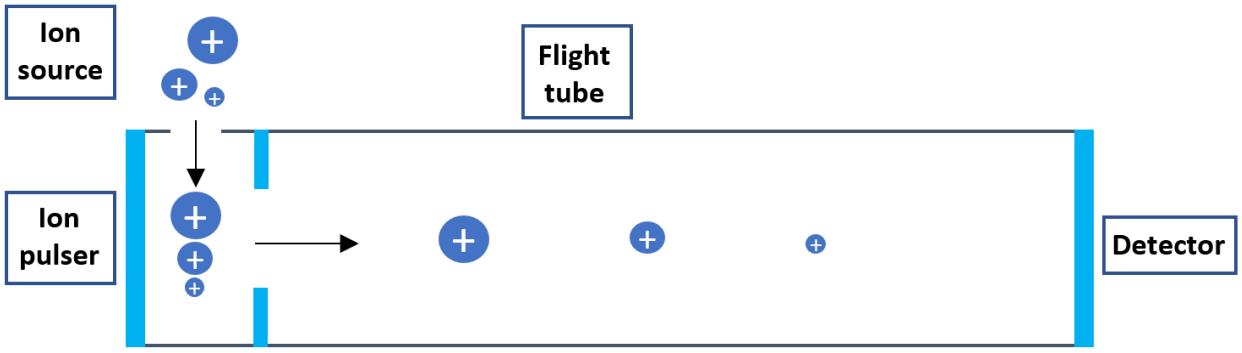

Figure 1.4: Schematic of a time-of-flight mass analyzer.

TOF flight tubes are generally one meter in length. In mass spectrometers containing TOFs, a nearly parallel stream of ions travels from the source through focusing steps (e.g. a quadrupole) and into an ion pulser[136]. The ion pulser emits a high-voltage pulse in the same polarity to the ion stream, accelerating the ions through a flight tube under high vacuum. In the flight tube, the ions separate based on their *m/z* ratio, ultimately reaching the detector and producing a signal that can be observed in mass spectra[137–140]. **Figure 1.4** shows an overview of the separation of charged ions in a flight tube. For the sake of simplicity, the flight tube shown above contains a linear flight path, at the end of which is a detector. However, many modern TOFs contain reflectrons, which are ion mirrors, at the opposite end of the flight tube. Reflectrons cause a parabolic reversal of the ion stream, effectively doubling the TOF's flight path[141–143]. The relationship between resolution and flight time is described by $R = m/\Delta m = t/2\Delta t = L/2\Delta x$, where m = mass, t = flight time, L is the distance and x is the width of a cluster of ions in the flight tube[144]. Through use of a reflectron, L is maximized, thereby increasing analyzer resolution[145,146]. TOF mass analyzers theoretically have no upper mass limit, which encourages their use in applications involving large biological samples[147,148]. Hence, they are frequently used in tandem with desorption sources like MALDI or ESI in research involving large singly- or multiply charged molecules, like proteins.

1.4.4 Liquid chromatography - mass spectrometry

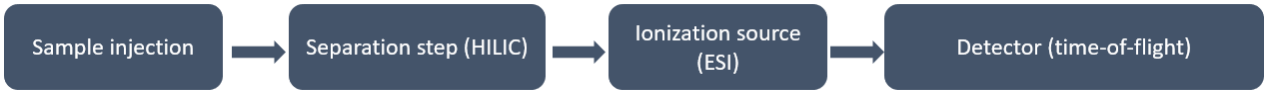

Figure 1.5: Simplified scheme of sample flow through an LC-MS system.

Analysis of complex mixtures greatly benefits from the introduction of a separation technique like liquid chromatography. The absence of an LC step can lead to ion suppression in complex samples[149,150]. Ion suppression is broadly defined as a decreased quantity of charged ions that reach the detector. Ion suppression often occurs with the presence of compounds with low volatility, such as in biological matrices[149]. ESI is frequently used as a detector in tandem with separations techniques like HPLC or in recent years, ultra-high-performance liquid chromatography (UHLPC). This step is implemented prior to ionization, as shown in **Figure 1.5**. Mass spectrometry is the most sensitive detector available for HPLC. Interfacing these two techniques allows compounds to be separated prior to ionization by their polarity, chemical structure, or molecular weight[151]. This addresses ion suppression by minimizing the number of signals produced in the ionization source at a given time. LC-MS allows eluates to be characterized by both their retention time and *m/z* ratio, providing secondary validation of an analyte's presence. This gives mass spectrometers a significant advantage over ultraviolet (UV) or diode array detectors (DAD), which rely on retention time as their only identifier. Two subcategories of HPLC include normal-phase and reversed-phase, based on the stationary phase the column contains. Normal-phase chromatography stationary phases are hydrophilic and are therefore conducive to retaining polar compounds[152–154]. Reversed-phase columns contain nonpolar stationary phases, making them more effective at retaining hydrophobic compounds[155–157]. The ability to tailor column selectivity to separate certain analytes in tandem with sensitive ionization methods like

ESI makes LC-MS an excellent technique for qualitatively or quantitatively identifying trace analytes in complex matrices[158–160]. Modern LC-MS systems are used in a vast range of applications that extend from industrial analysis of petroleum to pharmaceutical quantitation, and from environmental analyses to metabolic screenings[161–164].

1.5 LC-MS in polymer characterization

1.5.1 Analysis of chitin and other polymers by mass spectrometry

Mass spectrometry has been used to characterize some polymers. MALDI is often the preferred mass spectrometric ionization method for polymer analysis, due to its ability to ionize molecules with high molecular weights without multiply charging them[165]. However, MALDI suffers from several drawbacks, including lack of reproducibility and a high likelihood of fragmentation within the source[166–169]. Additionally, MALDI is not compatible with traditional LC systems, requiring specialized systems to interface the two techniques[170–172]. Large compounds ionized using ESI are often multiply charged. Multiply charging ions reduces the *m/z* of large compounds to ranges measurable by the detector. Multiple charging usually occurs via acquisition of positively charged ions, but can sometimes occur via proton abstraction[173,174]. While multiply-charging large molecules for ESI analysis has been very successful with nucleic acids and proteins, multiply charging polymers has been met with limited success[175].

The analysis of polymeric chitin by mass spectrometry is not feasible due to chitin's insolubility in compatible solvents. However, polymeric chitosan is soluble in acidic aqueous solutions[176,177]. In literature, the use of mass spectrometry to analyze chitosan has been limited to its oligomeric components. Both MALDI and ESI have been used to analyze chitosan oligomers[178–181]. Mass spectrometry has been used to analyze COS produced by enzymatic

degradation, and is sometimes used to characterize derivatized COS[182–184]. Since chitosan is composed of GlcN and GlcNAc, COS molecules can include any number of these subunits. In addition, a range of adducts can form with each of these compounds. This yields fairly complex spectra that include $[M + H]^+$, $[M + Na]^+$, $[M + K]^+$, and $[M - H_2O + H]^+$ adducts[184,185].

1.5.2 HPLC of chitin and its derivatives

HPLC has been used to analyze COS as well as its constituent monomers. While reverse-phase columns (e.g. C18 columns) are commonly used for separating many organic compounds, they are not conducive for separating polar molecules like COS. Hence, separating underivatized COS, GlcN and GlcNAc requires the use of HILIC columns[186–188]. Combining LC methods with ESI enhances its analytical capabilities as LC-MS has the potential to be quantitative. Additionally, the use of chromatography allows COS to be detected in complex matrices, where ion suppression may be problematic. While mass spectrometry has been used in the analysis of COS, a survey of recent literature indicates that more superficial methods are more common[189,190]. The use of mass spectrometry as a standalone technique offers great potential for better understanding the degradation processes used to create COS, as it provides specific identification of the compounds produced[191]. Chapters 3 and 4 in this dissertation discuss the depolymerization of chitin and chitosan, and the production of compounds that may result during certain derivatizations. While many of these studies were performed using mass spectrometry without a prior separation step, samples in which a complex matrix was presented required the use of chromatography. Chapter 5 discusses the use of LC-MS to detect the degradation products of polymeric chitin in fungi. The analysis of biological systems such as these necessitates separation to combat ion suppression, and if desired, to allow quantitative studies. The mass percent of pathogenic fungi ranges from 10-30% polymeric chitin. Given this, methods to detect chitin hold the potential to serve as novel, sensitive

diagnostic methods for fungi. Due to the absence of well-defined methods of analysis, both mass spectrometry and LC-MS are frequently overlooked as techniques to analyze chitin derivatives. The projects found in ensuing chapters investigate the ability, advantages, and novel ways that LC-MS can be used to analyze chitin derivatives.

1.6 Dissertation overview

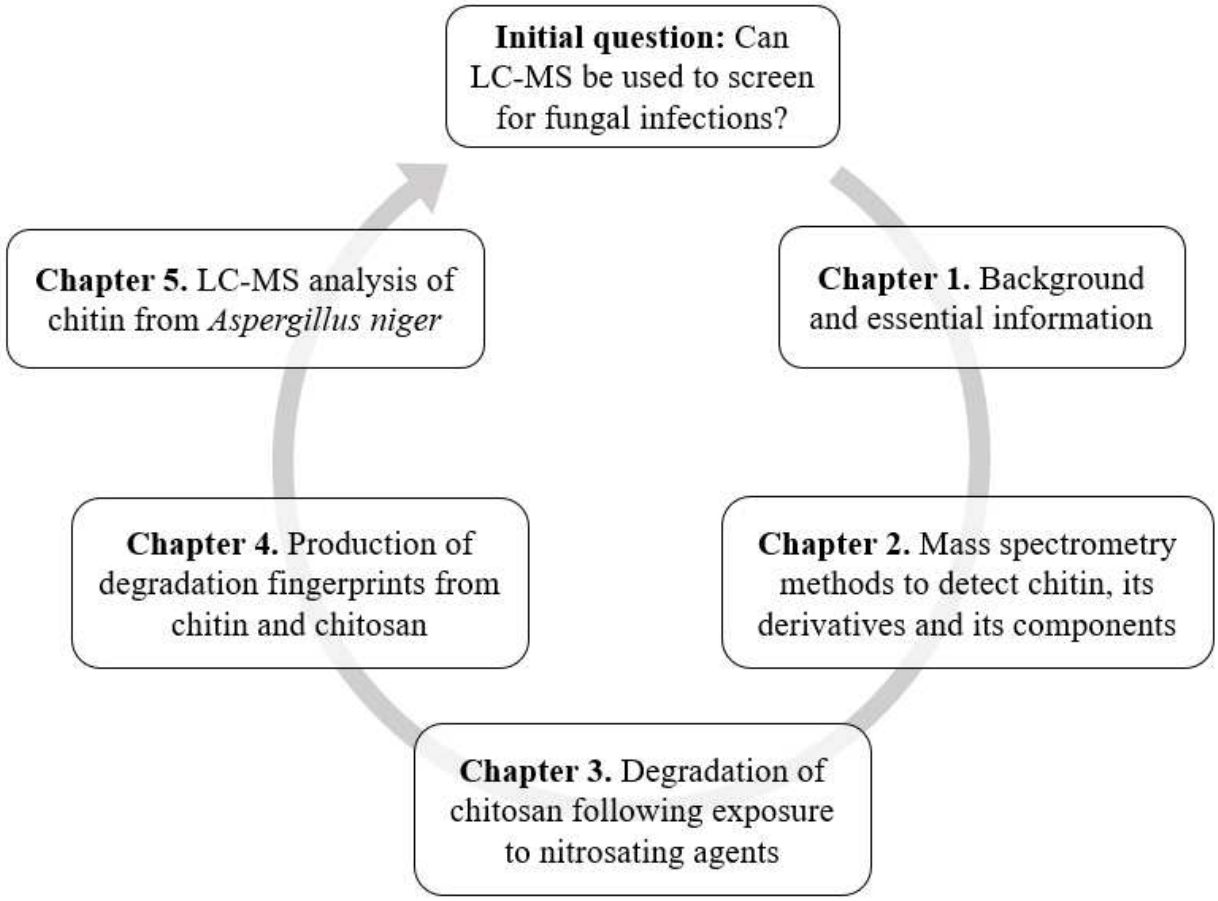

Figure 1.6: Dissertation overview showing the initial research question and pertinent goals achieved. Each box is representative of a phase of research that corresponds to a chapter in this dissertation.

The research contained in this dissertation outlines progress toward answering the question that brought about this body of work: Can LC-MS be used as a screening method for fungal infections? Chronologically, the research contained in this dissertation followed a course as shown in **Figure 1.6**. During preliminary phases of research, the absence of literature precedence to provide guidance regarding preliminary steps in research was evident. Hence, this body of work takes a ground-up approach, beginning with method development to analyze chitin and chitosan's building blocks in chapter 2. These are presented along with experiments addressing whether

polymeric chitosan can be analyzed using mass spectrometry. ESI methods were optimized to increase the ionization efficiency of low molecular weight standards including GlcN, GlcNAc, and COS. Additionally, we found that our methods were not effective for the analysis of polymeric chitosan. Chapter 3 investigates the ability of nitrosating agents to degrade chitosan, with degradation being tracked using mass spectrometry and FTIR. We found that chitosan polymers undergo degradation to produce GlcN, GlcNAc, 2,5-anhydro-d-mannose (2,5-AM) and COS upon exposure to some nitrosating agents, especially those that involve the use of acids. Significantly, this research highlights the first use of our methods to track the degradation of chitin derivatives. In chapter 4, the susceptibility of a variety of chitin and chitosan polymers was explored by exposing these to acids, oxidizing agents, and nitrosating agents. Using direct injection mass spectrometry, we found that strong acids degrade all species of chitin and chitosan, while oxidizing agents and nitrosating agents only effectively degrade deacetylated polymers. Finally, in Chapter 5, we address the feasibility of detecting fungal-derived chitin using mass spectrometry. To accomplish this, we paired sample cleanup methods, cell lysis procedures and solid-phase extraction with HILIC-ESI-TOF-MS to identify GlcN produced from *Aspergillus niger.* Ultmately, the research contained in this dissertation confirms that LC-MS has the capability as a diagnostic method for fungal infections, as proposed at the beginning of this work.

CHAPTER 1 – REFERENCES

(1) SINGH, D. K.; RAY, A. R. *Biomedical Applications of Chitin, Chitosan, and Their Derivatives*; Marcel Dekker Inc., 2007; Vol. 40. https://doi.org/10.1081/MC-100100579.

(2) Park, B. K.; Kim, M.-M. Applications of Chitin and Its Derivatives in Biological Medicine. *Int. J. Mol. Sci* **2010**, *11*, 5152–5164. https://doi.org/10.3390/ijms11125152.

(3) Chi, R.; Cheung, F.; Ng, T. B.; Wong, J. H.; Chan, W. Y. Marine Drugs Chitosan: An Update on Potential Biomedical and Pharmaceutical Applications. *Mar. Drugs* **2015**, *13*, 5156–5186. https://doi.org/10.3390/md13085156.

(4) Devlieghere, F.; Vermeulen, A.; Debevere, J. Chitosan: Antimicrobial Activity, Interactions with Food Components and Applicability as a Coating on Fruit and Vegetables. *Food Microbiol.* **2004**, *21* (6), 703–714. https://doi.org/10.1016/j.fm.2004.02.008.

(5) Ueno, H.; Mori, T.; Fujinaga, T. *Topical Formulations and Wound Healing Applications of Chitosan*; 2001; Vol. 52.

(6) Beri, R. G.; Walker, J.; Reese, E. T.; Rollings, J. E. Characterization of Chitosans via Coupled Size-Exclusion Chromatography and Multiple-Angle Laser Light-Scattering Technique. *Carbohydr. Res.* **1993**, *238* (C), 11–26. https://doi.org/10.1016/0008-6215(93)87002-A.

(7) Kasaai, M. R.; Arul, J.; Charlet, G. Intrinsic Viscosity–Molecular Weight Relationship for Chitosan. *J. Polym. Sci. Part B Polym. Phys.* **2000**, *38* (19), 2591–2598. https://doi.org/10.1002/1099-0488(20001001)38:19<2591::AID-POLB110>3.0.CO;2-6.

(8) Lavertu, M.; Xia, Z.; Serreqi, A. N.; Berrada, M.; Rodrigues, A.; Wang, D.; Buschmann, M. D.; Gupta, A. A Validated 1H NMR Method for the Determination of the Degree of Deacetylation of Chitosan. *J. Pharm. Biomed. Anal.* **2003**, *32* (6), 1149–1158. https://doi.org/10.1016/S0731-7085(03)00155-9.

(9) Li, J.; Chen, L.; Meng, Z.; Dou, G. Development of a Mass Spectrometry Method for the Characterization of a Series of Chitosan. *Int. J. Biol. Macromol.* **2019**, *121*, 89–96. https://doi.org/10.1016/j.ijbiomac.2018.09.194.

(10) Cord-Landwehr, S.; Ihmor, P.; Niehues, A.; Luftmann, H.; Moerschbacher, B. M.; Mormann, M. Quantitative Mass-Spectrometric Sequencing of Chitosan Oligomers Revealing Cleavage Sites of Chitosan Hydrolases. *Anal. Chem.* **2017**, *89* (5), 2893–2900. https://doi.org/10.1021/acs.analchem.6b04183.

(11) Lomeli, S. H.; Peng, I. X.; Yin, S.; Ogorzalek Loo, R. R.; Loo, J. A. New Reagents for Increasing ESI Multiple Charging of Proteins and Protein Complexes. *J. Am. Soc. Mass Spectrom.* **2010**, *21* (1), 127–131. https://doi.org/10.1016/j.jasms.2009.09.014.

(12) Banerjee, S.; Mazumdar, S. Electrospray Ionization Mass Spectrometry: A Technique to Access the Information beyond the Molecular Weight of the Analyte. *Int. J. Anal. Chem.* **2012**, *2012*, 40. https://doi.org/10.1155/2012/282574.

(13) Characterization and Analysis of Polymers - Wiley - Google Books https://books.google.com/books?id=IWqmp9oMToIC&pg=PA191&lpg=PA191&dq=polymer+multiple+charging+esi&source=bl&ots=fZP6zDIhGK&sig=ACfU3U2AqfQ423andgXUp8NFEPqDShisZw&hl=en&ppis=_c&sa=X&ved=2ahUKEwijtonFxLvoAhVInJ4KHft4DEsQ6AEwD3oECAwQAQ#v=onepage&q=polymer multiple charging esi&f=false

(accessed Mar 27, 2020).

(14) O'Connor, P. B.; McLafferty, F. W. Oligomer Characterization of 4—23 KDa Polymers by Electrospray Fourier Transform Mass Spectrometry. *J. Am. Chem. Soc.* **1995**, *117* (51), 12826–12831. https://doi.org/10.1021/ja00156a021.

(15) Steinkoenig, J.; Cecchini, M. M.; Reale, S.; Goldmann, A. S.; Barner-Kowollik, C. Supercharging Synthetic Polymers: Mass Spectrometric Access to Nonpolar Synthetic Polymers. *Macromolecules* **2017**, *50* (20), 8033–8041. https://doi.org/10.1021/acs.macromol.7b02018.

(16) Maldini, M.; Montoro, P.; Piacente, S.; Pizza, C. ESI-MS, ESI-MS/MS Fingerprint and LC-ESI-MS Analysis of Proathocyanidins from Bursera Simaruba Sarg Bark. *Nat. Prod. Commun.* **2009**, *4* (12), 1671–1674.

(17) Wattjes, J.; Niehues, A.; Cord-Landwehr, S.; Hoßbach, J.; David, L.; Delair, T.; Moerschbacher, B. M. Enzymatic Production and Enzymatic-Mass Spectrometric Fingerprinting Analysis of Chitosan Polymers with Different Nonrandom Patterns of Acetylation. *J. Am. Chem. Soc.* **2019**, *141* (7), 3137–3145. https://doi.org/10.1021/jacs.8b12561.

(18) Agnihotri, S. A.; Kulkarni, V. D.; Kulkarni, A. R.; Aminabhavi, T. M. Degradation of Chitosan and Chemically Modified Chitosan by Viscosity Measurements. *J. Appl. Polym. Sci.* **2006**, *102* (4), 3255–3258. https://doi.org/10.1002/app.24663.

(19) Jennings, J. A. Controlling Chitosan Degradation Properties in Vitro and in Vivo. In *Chitosan Based Biomaterials*; Elsevier Inc., 2017; Vol. 1, pp 159–182. https://doi.org/10.1016/B978-0-08-100230-8.00007-8.

(20) Choi, Y. J.; Kim, E. J.; Piao, Z.; Yun, Y. C.; Shin, Y. C. Purification and Characterization of Chitosanase from Bacillus Sp. Strain KCTC 0377BP and Its Application for the Production of Chitosan Oligosaccharides. *Appl. Environ. Microbiol.* **2004**, *70* (8), 4522–4531. https://doi.org/10.1128/AEM.70.8.4522-4531.2004.

(21) Asthana, C.; 1, I. D.; Peterson, G. M.; 2, S.; Patel, R. P. Development and Validation of a Novel High Performance Liquid Chromatography-Coupled with Corona Charged Aerosol Detector Method for Quantification of Glucosamine in Dietary Supplements. **2019**. https://doi.org/10.1371/journal.pone.0216039.

(22) Pedrali, A.; Bleve, M.; Capra, P.; Jonsson, T.; Massolini, G.; Perugini, P.; Marrubini, G. Determination of N-Acetylglucosamine in Cosmetic Formulations and Skin Test Samples by Hydrophilic Interaction Liquid Chromatography and UV Detection. *J. Pharm. Biomed. Anal.* **2015**, *107*, 125–130. https://doi.org/10.1016/j.jpba.2014.12.014.

(23) Deguchi, S.; Tsujii, K.; Horikoshi, K. In Situ Microscopic Observation of Chitin and Fungal Cells with Chitinous Cell Walls in Hydrothermal Conditions. *Sci. Rep.* **2015**, *5*. https://doi.org/10.1038/srep11907.

(24) Dickson, A. N.; Barry, J. N.; McDonnell, K. A.; Dowling, D. P. Fabrication of Continuous Carbon, Glass and Kevlar Fibre Reinforced Polymer Composites Using Additive Manufacturing. *Addit. Manuf.* **2017**, *16*, 146–152. https://doi.org/10.1016/j.addma.2017.06.004.

(25) Manivasagam, G.; Dhinasekaran, D.; Rajamanickam, A. Biomedical Implants: Corrosion and Its Prevention-A Review Coating on Implants for Biomedical Applications View Project Create New Project “Corrosion Analysis of SPD Magnesium Material” View

Project Biomedical Implants: Corrosion and Its Prevention-A Review. *Recent Patents Corros. Sci.* **2010**, *2*, 40–54. https://doi.org/10.2174/1877610801002010040.

(26) Rinaudo, M. Chitin and Chitosan: Properties and Applications. *Prog. Polym. Sci.* **2006**, *31* (7), 603–632. https://doi.org/10.1016/j.progpolymsci.2006.06.001.

(27) Odian, G. *Principles of Polymerization*; John Wiley & Sons, Inc., 2004. https://doi.org/10.1002/047147875x.

(28) Litvinova, L. S. SYNTHETIC POLYMERS | Thin-Layer (Planar) Chromatography. In *Reference Module in Chemistry, Molecular Sciences and Chemical Engineering*; Elsevier, 2013. https://doi.org/10.1016/b978-0-12-409547-2.04944-1.

(29) Roncali, J.; Garnier, F.; Lemaire, M.; Garreau, R. Poly Mono-, Bi- and Trithiophene: Effect of Oligomer Chain Length on the Polymer Properties. *Synth. Met.* **1986**, *15* (4), 323–331. https://doi.org/10.1016/0379-6779(86)90081-0.

(30) Hamley, I. W. *The Physics of Block Copolymers*; 1998.

(31) Alternating Copolymers - Google Books https://books.google.com/books?hl=en&lr=&id=P4TrBwAAQBAJ&oi=fnd&pg=PA1&dq=copolymers&ots=W8drM0Uj0R&sig=l80vdghN8pLAwD-YIQ8o6WcDWcE#v=onepage&q=copolymers&f=false (accessed Mar 27, 2020).

(32) Dodiuk, H.; Goodman, S. H. Handbook of Thermoset Plastics (Third Edition). In *Handbook of Thermoset Plastics*; Elsevier Inc., 2014; pp 1–12. https://doi.org/10.1016/B978-1-4557-3107-7.00001-4.

(33) Mai, D. J.; Schroeder, C. M. Single Polymer Dynamics of Topologically Complex DNA.

Current Opinion in Colloid and Interface Science. Elsevier Ltd December 1, 2016, pp 28–40. https://doi.org/10.1016/j.cocis.2016.08.003.

(34) White, J. R. Polymer Ageing: Physics, Chemistry or Engineering? Time to Reflect. *Comptes Rendus Chim.* **2006**, *9* (11–12), 1396–1408. https://doi.org/10.1016/j.crci.2006.07.008.

(35) Zhang, Z.; Ortiz, O.; Goyal, R.; Kohn, J. Biodegradable Polymers. In *Principles of Tissue Engineering: Fourth Edition*; Elsevier Inc., 2013; pp 441–473. https://doi.org/10.1016/B978-0-12-398358-9.00023-9.

(36) Murphy, M. B.; Mikos, A. G. Chapter Twenty-Two - Polymer Scaffold Fabrication. In *Principles of Tissue Engineering (Third Edition)*; Robert, L., Robert, L., Joseph VacantiA2 - Robert Lanza, R. L., Joseph, V., Eds.; Academic Press, 2007; pp 309–321. https://doi.org/http://dx.doi.org/10.1016/B978-012370615-7/50026-3.

(37) BeMiller, J. N. Polysaccharides. In *Carbohydrate Chemistry for Food Scientists*; Elsevier, 2019; pp 103–157. https://doi.org/10.1016/b978-0-12-812069-9.00005-4.

(38) Sapuan, S. M.; Tamrin, K. F.; Nukman, Y.; El-Shekeil, Y. A.; Hussin, M. S. A.; Aziz, S. N. A. Natural Fiber-Reinforced Composites: Types, Development, Manufacturing Process, and Measurement. In *Comprehensive Materials Finishing*; Elsevier Inc., 2017; Vol. 1–3, pp 203–230. https://doi.org/10.1016/B978-0-12-803581-8.09183-9.

(39) Bhat, G.; Kandagor, V. Synthetic Polymer Fibers and Their Processing Requirements. In *Advances in Filament Yarn Spinning of Textiles and Polymers*; Elsevier Ltd., 2014; pp 3–30. https://doi.org/10.1533/9780857099174.1.3.

(40) Biermann, C. J. Hydrolysis and Other Cleavages of Glycosidic Linkages in Polysaccharides. *Adv. Carbohydr. Chem. Biochem.* **1988**, *46* (C), 251–271. https://doi.org/10.1016/S0065-2318(08)60168-7.

(41) Bajpai, P. Wood and Fiber Fundamentals. In *Biermann's Handbook of Pulp and Paper*; Elsevier, 2018; pp 19–74. https://doi.org/10.1016/b978-0-12-814240-0.00002-1.

(42) Daraghmeh, N. H.; Chowdhry, B. Z.; Leharne, S. A.; Al Omari, M. M.; Badwan, A. A. Chitin. In *Profiles of Drug Substances, Excipients and Related Methodology*; Academic Press Inc., 2011; Vol. 36, pp 35–102. https://doi.org/10.1016/B978-0-12-387667-6.00002-6.

(43) Fabritius, H.; Sachs, C.; Raabe, D.; Nikolov, S.; Friák, M.; Neugebauer, J. Chitin in the Exoskeletons of Arthropoda: From Ancient Design to Novel Materials Science; Springer, Dordrecht, 2011; pp 35–60. https://doi.org/10.1007/978-90-481-9684-5_2.

(44) Winkler, S. . K. D. L. Biosynthesized Materials: Properties and Processing. **2001**, 609–615. https://doi.org/10.1016/B0-08-043152-6/00117-0.

(45) Kurita, K. Controlled Functionalization of the Polysaccharide Chitin. *Progress in Polymer Science (Oxford)*. Elsevier Ltd 2001, pp 1921–1971. https://doi.org/10.1016/S0079-6700(01)00007-7.

(46) Yan, N.; Chen, X. Sustainability: Don't Waste Seafood Waste. *Nature*. Nature Publishing Group August 10, 2015, pp 155–157. https://doi.org/10.1038/524155a.

(47) BeMiller, J. N. Starch-Based Gums. In *Industrial Gums: Polysaccharides and Their Derivatives: Third Edition*; Elsevier Inc., 2012; pp 579–600.

https://doi.org/10.1016/B978-0-08-092654-4.50025-5.

(48) Hoell, I. A.; Vaaje-Kolstad, G.; Eijsink, V. G. H. Structure and Function of Enzymes Acting on Chitin and Chitosan. *Biotechnol. Genet. Eng. Rev.* **2010**, *27* (1), 331–366. https://doi.org/10.1080/02648725.2010.10648156.

(49) Merzendorfer, H.; Zimoch, L. Chitin Metabolism in Insects: Structure, Function and Regulation of Chitin Synthases and Chitinases. *Journal of Experimental Biology*. December 2003, pp 4393–4412. https://doi.org/10.1242/jeb.00709.

(50) Dutta, P. K.; Duta, J.; Tripathi, V. S. Chitin and Chitosan: Chemistry, Properties and Applications. *J. Sci. Ind. Res. (India).* **2004**, *63* (1), 20–31. https://doi.org/10.1002/chin.200727270.

(51) Singh Rathore, A.; Gupta, R. D. Chitinases from Bacteria to Human: Properties, Applications, and Future Perspectives. **2015**. https://doi.org/10.1155/2015/791907.

(52) Qin, C.; Li, H.; Xiao, Q.; Liu, Y.; Zhu, J.; Du, Y. Water-Solubility of Chitosan and Its Antimicrobial Activity. *Carbohydr. Polym.* **2006**, *63* (3), 367–374. https://doi.org/10.1016/j.carbpol.2005.09.023.

(53) Roy, J. C.; Salaün, F.; Giraud, S.; Ferri, A.; Chen, G.; Guan, J. Solubility of Chitin: Solvents, Solution Behaviors and Their Related Mechanisms. In *Solubility of Polysaccharides*; InTech, 2017. https://doi.org/10.5772/intechopen.71385.

(54) Kumirska, J.; Czerwicka, M.; Kaczy??ski, Z.; Bychowska, A.; Brzozowski, K.; Th??ming, J.; Stepnowski, P. Application of Spectroscopic Methods for Structural Analysis of Chitin and Chitosan. *Mar. Drugs* **2010**, *8* (5), 1567–1636. https://doi.org/10.3390/md8051567.

(55) European Chitin Society; Domard, A.; EUCHIS '95 (1 1995.09.11-13 Brest); International Conference of the European Chitin Society (EUCHIS) (1 1995.09.11-13 Brest). *Proceedings of the 1st International Conference of the European Chitin Society : Held in Brest, France, September 11-13, 1995*; André, 1996.

(56) Koide, S. S. Chitin-Chitosan: Properties, Benefits and Risks. *Nutrition Research*. Elsevier June 1, 1998, pp 1091–1101. https://doi.org/10.1016/S0271-5317(98)00091-8.

(57) Dai, T.; Tanaka, M.; Huang, Y. Y.; Hamblin, M. R. Chitosan Preparations for Wounds and Burns: Antimicrobial and Wound-Healing Effects. *Expert Review of Anti-Infective Therapy*. NIH Public Access July 2011, pp 857–879. https://doi.org/10.1586/eri.11.59.

(58) Harish Prashanth, K. V.; Tharanathan, R. N. Chitin/Chitosan: Modifications and Their Unlimited Application Potential-an Overview. *Trends in Food Science and Technology*. Elsevier March 1, 2007, pp 117–131. https://doi.org/10.1016/j.tifs.2006.10.022.

(59) Zhang, J.; Xia, W.; Liu, P.; Cheng, Q.; Tahirou, T.; Gu, W.; Li, B. Chitosan Modification and Pharmaceutical/Biomedical Applications. *Marine Drugs*. Multidisciplinary Digital Publishing Institute (MDPI) July 2010, pp 1962–1987. https://doi.org/10.3390/md8071962.

(60) Khanmohammadi, M.; Elmizadeh, H.; Ghasemi, K. Investigation of Size and Morphology of Chitosan Nanoparticles Used in Drug Delivery System Employing Chemometric Technique. *Iran. J. Pharm. Res.* **2015**, *14* (3), 665–675. https://doi.org/10.22037/ijpr.2015.1761.

(61) Yen, M. T.; Mau, J. L. Selected Physical Properties of Chitin Prepared from Shiitake Stipes. *LWT - Food Sci. Technol.* **2007**, *40* (3), 558–563.

https://doi.org/10.1016/j.lwt.2005.10.008.

(62) Fai, A. E. C.; Stamford, T. C. M.; Stamford-Arnaud, T. M.; Santa-Cruz, P. D.; Da Silva, M. C. F.; Campos-Takaki, G. M.; Stamford, T. L. M. Physico-Chemical Characteristics and Functional Properties of Chitin and Chitosan Produced by Mucor Circinelloides Using Yam Bean as Substrate. *Molecules* **2011**, *16* (8), 7143–7154. https://doi.org/10.3390/molecules16087143.

(63) Antonino, R. S. C. M. D. Q.; Fook, B. R. P. L.; Lima, V. A. D. O.; Rached, R. Í. D. F.; Lima, E. P. N.; Lima, R. J. D. S.; Covas, C. A. P.; Fook, M. V. L. Preparation and Characterization of Chitosan Obtained from Shells of Shrimp (Litopenaeus Vannamei Boone). *Mar. Drugs* **2017**, *15* (5). https://doi.org/10.3390/md15050141.

(64) Chang, A. K. T.; Frias, R. R.; Alvarez, L. V.; Bigol, U. G.; Guzman, J. P. M. D. Comparative Antibacterial Activity of Commercial Chitosan and Chitosan Extracted from Auricularia Sp. *Biocatal. Agric. Biotechnol.* **2019**, *17*, 189–195. https://doi.org/10.1016/j.bcab.2018.11.016.

(65) Berger, J.; Reist, M.; Mayer, J. M.; Felt, O.; Gurny, R. Structure and Interactions in Chitosan Hydrogels Formed by Complexation or Aggregation for Biomedical Applications. *European Journal of Pharmaceutics and Biopharmaceutics*. Elsevier 2004, pp 35–52. https://doi.org/10.1016/S0939-6411(03)00160-7.

(66) Jiang, T.; Kumbar, S. G.; Nair, L. S.; Laurencin, C. T. Biologically Active Chitosan Systems for Tissue Engineering and Regenerative Medicine. *Curr. Top. Med. Chem.* **2008**, *8* (4), 354–364.

(67) Drewa, T.; Adamowicz, J.; Lysik, J.; Polaczek, J.; Pielichowski, J. Chitosan Scaffold

Enhances Nerve Regeneration within the in Vitro Reconstructed Bladder Wall: An Animal Study. *Urol. Int.* **2008**, *81* (3), 330–334. https://doi.org/10.1159/000151414.

(68) VandeVord, P. J.; Matthew, H. W. T.; DeSilva, S. P.; Mayton, L.; Wu, B.; Wooley, P. H. Evaluation of the Biocompatibility of a Chitosan Scaffold in Mice. *J. Biomed. Mater. Res.* **2002**, *59* (3), 585–590. https://doi.org/10.1002/jbm.1270.

(69) Madhumathi, K.; Sudheesh Kumar, P. T.; Abhilash, S.; Sreeja, V.; Tamura, H.; Manzoor, K.; Nair, S. V.; Jayakumar, R. Development of Novel Chitin/Nanosilver Composite Scaffolds for Wound Dressing Applications. *J. Mater. Sci. Mater. Med.* **2010**, *21* (2), 807–813. https://doi.org/10.1007/s10856-009-3877-z.

(70) Sinha, V. R.; Singla, A. K.; Wadhawan, S.; Kaushik, R.; Kumria, R.; Bansal, K.; Dhawan, S. Chitosan Microspheres as a Potential Carrier for Drugs. *International Journal of Pharmaceutics*. Elsevier April 15, 2004, pp 1–33. https://doi.org/10.1016/j.ijpharm.2003.12.026.

(71) Hu, Z.; Zhang, D. Y.; Lu, S. T.; Li, P. W.; Li, S. D. Chitosan-Based Composite Materials for Prospective Hemostatic Applications. *Marine Drugs*. MDPI AG August 4, 2018. https://doi.org/10.3390/md16080273.

(72) Felt, O.; Carrel, A.; Baehni, P.; Buri, P.; Gurny, R. Chitosan as Tear Substitute: A Wetting Agent Endowed with Antimicrobial Efficacy. *J. Ocul. Pharmacol. Ther.* **2000**, *16* (3), 261–270. https://doi.org/10.1089/jop.2000.16.261.

(73) Decker, E. M.; Von Ohle, C.; Weiger, R.; Wiech, I.; Brecx, M. A Synergistic Chlorhexidine/Chitosan Combination for Improved Antiplaque Strategies. *J. Periodontal Res.* **2005**, *40* (5), 373–377. https://doi.org/10.1111/j.1600-0765.2005.00817.x.

(74) Logesh, A. R.; Thillaimaharani, K. A.; Sharmila, K.; Kalaiselvam, M.; Raffi, S. M. Production of Chitosan from Endolichenic Fungi Isolated from Mangrove Environment and Its Antagonistic Activity. *Asian Pac. J. Trop. Biomed.* **2012**, *2* (2), 140–143. https://doi.org/10.1016/S2221-1691(11)60208-6.

(75) Raafat, D.; Sahl, H. G. Chitosan and Its Antimicrobial Potential - A Critical Literature Survey. *Microbial Biotechnology*. Wiley-Blackwell March 2009, pp 186–201. https://doi.org/10.1111/j.1751-7915.2008.00080.x.

(76) Rhoades, J.; Roller, S. Antimicrobial Actions of Degraded and Native Chitosan against Spoilage Organisms in Laboratory Media and Foods. *Appl. Environ. Microbiol.* **2000**, *66* (1), 80–86. https://doi.org/10.1128/AEM.66.1.80-86.2000.

(77) El-Tahlawy, K. F.; El-Bendary, M. A.; Elhendawy, A. G.; Hudson, S. M. The Antimicrobial Activity of Cotton Fabrics Treated with Different Crosslinking Agents and Chitosan. *Carbohydr. Polym.* **2005**, *60* (4), 421–430. https://doi.org/10.1016/j.carbpol.2005.02.019.

(78) Tsai, G. J.; Su, W. H. Antibacterial Activity of Shrimp Chitosan against Escherichia Coli. *J. Food Prot.* **1999**, *62* (3), 239–243. https://doi.org/10.4315/0362-028x-62.3.239.

(79) Ikinci, G.; Şenel, S.; Akincibay, H.; Kaş, S.; Erciş, S.; Wilson, C. G.; Hincal, A. A. Effect of Chitosan on a Periodontal Pathogen Porphyromonas Gingivalis. *Int. J. Pharm.* **2002**, *235* (1–2), 121–127. https://doi.org/10.1016/S0378-5173(01)00974-7.

(80) Choi, B. K.; Kim, K. Y.; Yoo, Y. J.; Oh, S. J.; Choi, J. H.; Kim, C. Y. In Vitro Antimicrobial Activity of a Chitooligosaccharide Mixture against Actinobacillus Actinomycetemcomitans and Streptococcus Mutans. *Int. J. Antimicrob. Agents* **2001**, *18*

(6), 553–557. https://doi.org/10.1016/S0924-8579(01)00434-4.

(81) Muzzarelli, R.; Tarsi, R.; Filippini, O.; Giovanetti, E.; Biagini, G.; Varaldo, P. E. Antimicrobial Properties of N-Carboxybutyl Chitosan. *Antimicrob. Agents Chemother.* **1990**, *34* (10), 2019–2023. https://doi.org/10.1128/AAC.34.10.2019.

(82) Je, J. Y.; Kim, S. K. Chitosan Derivatives Killed Bacteria by Disrupting the Outer and Inner Membrane. *J. Agric. Food Chem.* **2006**, *54* (18), 6629–6633. https://doi.org/10.1021/jf061310p.

(83) Yin, H.; Du, Y.; Dong, Z. Chitin Oligosaccharide and Chitosan Oligosaccharide : Two Similar but Different Plant Elicitors. **2016**, *7* (April), 2014–2017. https://doi.org/10.3389/fpls.2016.00522.

(84) Muanprasat, C.; Chatsudthipong, V. Chitosan Oligosaccharide: Biological Activities and Potential Therapeutic Applications. *Pharmacology and Therapeutics*. Elsevier Inc. February 1, 2017, pp 80–97. https://doi.org/10.1016/j.pharmthera.2016.10.013.

(85) Lee, J. Y.; Termsarasab, U.; Lee, M. Y.; Kim, D. H.; Lee, S. Y.; Kim, J. S.; Cho, H. J.; Kim, D. D. Chemosensitizing Indomethacin-Conjugated Chitosan Oligosaccharide Nanoparticles for Tumor-Targeted Drug Delivery. *Acta Biomater.* **2017**, *57*, 262–273. https://doi.org/10.1016/j.actbio.2017.05.012.

(86) Akhlaghi, S. P.; Berry, R. C.; Tam, K. C. Surface Modification of Cellulose Nanocrystal with Chitosan Oligosaccharide for Drug Delivery Applications. *Cellulose* **2013**, *20* (4), 1747–1764. https://doi.org/10.1007/s10570-013-9954-y.

(87) Chitosan and Its Derivatives as Self-Assembled Systems for Drug Delivery. In *Controlled*

Drug Delivery; Elsevier, 2015; pp 85–125. https://doi.org/10.1016/b978-1-907568-45-9.00003-2.

(88) Azuma, K.; Osaki, T.; Minami, S.; Okamoto, Y. Anticancer and Anti-Inflammatory Properties of Chitin and Chitosan Oligosaccharides. *J. Funct. Biomater.* **2015**, *6* (1), 33–49. https://doi.org/10.3390/jfb6010033.

(89) Lv, X.; Liu, Y.; Song, S.; Tong, C.; Shi, X.; Zhao, Y.; Zhang, J.; Hou, M. Influence of Chitosan Oligosaccharide on the Gelling and Wound Healing Properties of Injectable Hydrogels Based on Carboxymethyl Chitosan/Alginate Polyelectrolyte Complexes. *Carbohydr. Polym.* **2019**, *205*, 312–321. https://doi.org/10.1016/j.carbpol.2018.10.067.

(90) Hosseinnejad, M.; Jafari, M. Evaluation of Different Factors Affecting Antimicrobial Properties of Chitosan. *Int. J. Biol. Macromol.* **2016**, *85*, 467–475. https://doi.org/10.1016/j.ijbiomac.2016.01.022.

(91) Zivanovic, S.; Basurto, C. C.; Chi, S.; Davidson, P. M.; Weiss, J. Molecular Weight of Chitosan Inn Uences Antimicrobial Activity in Oil-in-Water Emulsions. *J. Food Prot.* **2004**, *67* (5), 952–959. https://doi.org/10.4315/0362-028X-67.5.952.

(92) Chitin, Chitosan, Oligosaccharides and Their Derivatives: Biological ... - Google Books https://books.google.com/books?hl=en&lr=&id=ChXOBQAAQBAJ&oi=fnd&pg=PP1&ots=KCQQZ31ddE&sig=P0rLvUmo3UZSCYbGkpBr81qWsHk#v=onepage&q=d2a2&f=false (accessed Mar 30, 2020).

(93) Fungal Infections - Protect Your Health | Fungal Diseases | CDC https://www.cdc.gov/fungal/features/fungal-infections.html (accessed May 12, 2020).

(94) Veríssimo, C. Fungal Infections. In *Environmental Mycology in Public Health: Fungi and Mycotoxins Risk Assessment and Management*; Elsevier Inc., 2015; pp 27–34. https://doi.org/10.1016/B978-0-12-411471-5.00003-X.

(95) Badiee, P.; Hashemizadeh, Z. Opportunistic Invasive Fungal Infections: Diagnosis & Clinical Management. *Indian Journal of Medical Research*. Indian Council of Medical Research 2014, pp 195–204.

(96) Chowdhary, A.; Agarwal, K.; Meis, J. F. Filamentous Fungi in Respiratory Infections. What Lies Beyond Aspergillosis and Mucormycosis? *PLoS Pathogens*. Public Library of Science April 1, 2016. https://doi.org/10.1371/journal.ppat.1005491.

(97) Brown, G. D.; Denning, D. W.; Gow, N. A. R.; Levitz, S. M.; Netea, M. G.; White, T. C. Hidden Killers: Human Fungal Infections. *Science Translational Medicine*. December 19, 2012. https://doi.org/10.1126/scitranslmed.3004404.

(98) Invasive Candidiasis | Candidiasis | Types of Fungal Diseases | Fungal Diseases | CDC https://www.cdc.gov/fungal/diseases/candidiasis/invasive/index.html (accessed May 12, 2020).

(99) Enoch, D. A.; Ludlam, H. A.; Brown Correspondence, N. M. Invasive Fungal Infections: A Review of Epidemiology and Management Options. https://doi.org/10.1099/jmm.0.46548-0.

(100) Groll, A. H.; Shah, P. M.; Mentzel, C.; Schneider, M.; Just-Nuebling, G.; Huebner, K. Trends in the Postmortem Epidemiology of Invasive Fungal Infections at a University Hospital. *J. Infect.* **1996**, *33* (1), 23–32. https://doi.org/10.1016/S0163-4453(96)92700-0.

(101) Li, Z.; Lu, G.; Meng, G. Pathogenic Fungal Infection in the Lung. *Front. Immunol.* **2019**, *10* (JUL). https://doi.org/10.3389/fimmu.2019.01524.

(102) Limper, A. H. The Changing Spectrum of Fungal Infections in Pulmonary and Critical Care Practice: Clinical Approach to Diagnosis. *Proceedings of the American Thoracic Society*. May 15, 2010, pp 163–168. https://doi.org/10.1513/pats.200906-049AL.

(103) GAFFI. Fungal Disease Frequency | Gaffi - Global Action Fund for Fungal Infections https://www.gaffi.org/why/fungal-disease-frequency/ (accessed Apr 12, 2020).

(104) Laboratory tests for fungal infection | DermNet NZ https://dermnetnz.org/topics/laboratory-tests-for-fungal-infection/ (accessed May 12, 2020).

(105) Bosshard, P. P. Incubation of Fungal Cultures: How Long Is Long Enough? *Mycoses* **2011**, *54* (5), e539-45. https://doi.org/10.1111/j.1439-0507.2010.01977.x.

(106) Ohno, N. *2.17 Yeast and Fungal Polysaccharides*.

(107) Lenardon, M. D.; Munro, C. A.; Gow, N. A. R. Chitin Synthesis and Fungal Pathogenesis. *Current Opinion in Microbiology*. Elsevier August 2010, pp 416–423. https://doi.org/10.1016/j.mib.2010.05.002.

(108) Kzhyshkowska, J.; Gratchev, A.; Goerdt, S. Human Chitinases and Chitinase-Like Proteins as Indicators for Inflammation and Cancer. *Biomark. Insights* **2007**, *2*, 117727190700200. https://doi.org/10.1177/117727190700200023.

(109) Kumar, A.; Zhang, K. Y. J. Human Chitinases: Structure, Function, and Inhibitor Discovery. In *Advances in Experimental Medicine and Biology*; Springer New York LLC,

2019; Vol. 1142, pp 221–251. https://doi.org/10.1007/978-981-13-7318-3_11.

(110) The Nobel Prize in Chemistry 1922 https://www.nobelprize.org/prizes/chemistry/1922/summary/ (accessed Jun 2, 2020).

(111) Skoog, D.; West, D.; Holler, J.; Crouch, S. *Fundamentals of Analytic Chemistry*; Brooks/Cole Cengage Learning, 2014.

(112) SIUZDAK, G. An Introduction to Mass Spectrometry Ionization: An Excerpt from The Expanding Role of Mass Spectrometry in Biotechnology, 2nd Ed.; MCC Press: San Diego, 2005. *J. Assoc. Lab. Autom.* **2004**, *9* (2), 50–63. https://doi.org/10.1016/j.jala.2004.01.004.

(113) Claeys, M.; Claereboudt, J. *Fast Atom Bombardment Ionization in Mass Spectrometry*, 3rd ed.; Elsevier Ltd., 2016. https://doi.org/10.1016/B978-0-12-803224-4.00320-4.

(114) Lafont, R.; Dauphin-Villemant, C.; Warren, J. T.; Rees, H. H. *Ecdysteroid Chemistry and Biochemistry ☆*; 2017. https://doi.org/10.1016/b978-0-12-809633-8.04026-7.

(115) Ho, C. S.; Lam, C. W. K.; Chan, M. H. M.; Cheung, R. C. K.; Law, L. K.; Lit, L. C. W.; Ng, K. F.; Suen, M. W. M.; Tai, H. L. Electrospray Ionisation Mass Spectrometry: Principles and Clinical Applications. *Clin. Biochem. Rev.* **2003**, *24* (1), 3–12.

(116) Jackson, S. N.; Woods, A. S. The Development of Matrix-Assisted Laser Desorption Ionization (MALDI) Mass Spectrometry. In *The Encyclopedia of Mass Spectrometry*; Elsevier, 2016; pp 124–131. https://doi.org/10.1016/b978-0-08-043848-1.00015-8.

(117) Harris, D. C. *Quantitative Chemical Analysis, 9th Ed.*; Springer Science and Business Media LLC, 2015; Vol. 407. https://doi.org/10.1007/s00216-015-9059-6.

(118) Badman, E. R.; Chrisman, P. A.; McLuckey, S. A. A Quadrupole Ion Trap Mass Spectrometer with Three Independent Ion Sources for the Study of Gas-Phase Ion/Ion Reactions. *Anal. Chem.* **2002**, *74* (24), 6237–6243. https://doi.org/10.1021/ac026020w.

(119) Takáts, Z.; Wiseman, J. M.; Cooks, R. G. Ambient Mass Spectrometry Using Desorption Electrospray Ionization (DESI): Instrumentation, Mechanisms and Applications in Forensics, Chemistry, and Biology. *Journal of Mass Spectrometry*. October 2005, pp 1261–1275. https://doi.org/10.1002/jms.922.

(120) Nadler, W. M.; Waidelich, D.; Kerner, A.; Hanke, S.; Berg, R.; Trumpp, A.; Rösli, C. MALDI versus ESI: The Impact of the Ion Source on Peptide Identification. *J. Proteome Res.* **2017**, *16* (3), 1207–1215. https://doi.org/10.1021/acs.jproteome.6b00805.

(121) Cole, R. B. Electrospray and MALDI Mass Spectrometry https://books.google.com/books?hl=en&lr=&id=A0ccqBiov78C&oi=fnd&pg=PT13&dq=maldi+ionization+sources&ots=5fWlu7OY6h&sig=wtdFzokZKZTvF9H1SqwonJKu6VA#v=onepage&q=maldi ionization sources&f=false (accessed May 8, 2020). https://doi.org/10.1002/9780470588901.

(122) Trauger, S. A.; Webb, W.; Siuzdak, G. Press Peptide and Protein Analysis with Mass Spectrometry.

(123) Bruins, A. P. Mass Spectrometry with Ion Sources Operating at Atmospheric Pressure. *Mass Spectrom. Rev.* **1991**, *10* (1), 53–77. https://doi.org/10.1002/mas.1280100104.

(124) Covey, T. R.; Thomson, B. A.; Schneider, B. B. Atmospheric Pressure Ion Sources. *Mass Spectrom. Rev.* **2009**, *28* (6), 870–897. https://doi.org/10.1002/mas.20246.

(125) Fenn, J. B.; Mann, M.; Meng, C. K.; Wong, S. F.; Whitehouse, C. M. Electrospray Ionization for Mass Spectrometry of Large Biomolecules. *Science*. 1989, pp 64–71. https://doi.org/10.1126/science.2675315.

(126) Wilm, M. Principles of Electrospray Ionization. *Molecular and Cellular Proteomics*. American Society for Biochemistry and Molecular Biology July 2011. https://doi.org/10.1074/mcp.M111.009407.

(127) Konermann, L.; Ahadi, E.; Rodriguez, A. D.; Vahidi, S. Unraveling the Mechanism of Electrospray Ionization. *Anal. Chem.* **2013**, *85* (1), 2–9. https://doi.org/10.1021/ac302789c.

(128) Kebarle, P. A Brief Overview of the Present Status of the Mechanisms Involved in Electrospray Mass Spectrometry. *J. Mass Spectrom.* **2000**, *35* (7), 804–817. https://doi.org/10.1002/1096-9888(200007)35:7<804::AID-JMS22>3.0.CO;2-Q.

(129) Gygi, S. P.; Aebersold, R. Mass Spectrometry and Proteomics. *Current Opinion in Chemical Biology*. Current Biology Ltd October 1, 2000, pp 489–494. https://doi.org/10.1016/S1367-5931(00)00121-6.

(130) *Resolving Power and Mass Resolution Technical Overview Instrument Resolving Power and Mass Resolution*.

(131) USA Inc, J. *How Resolution Is Defined*.

(132) Fiehn Lab - Mass Resolution and Resolving Power https://fiehnlab.ucdavis.edu/projects/seven-golden-rules/mass-resolution (accessed May 8, 2020).

(133) SCHERMANN, J.-P. Spectroscopy and Modeling of Biomolecular Building Blocks. In *Spectroscopy and Modeling of Biomolecular Building Blocks*; Elsevier, 2008; pp 129–207. https://doi.org/10.1016/B978-044452708-0.50004-6.

(134) Wenzel, R. J.; Matter, U.; Schultheis, L.; Zenobi, R. Analysis of Megadalton Ions Using Cryodetection MALDI Time-of-Flight Mass Spectrometry. *Anal. Chem.* **2005**, *77* (14), 4329–4337. https://doi.org/10.1021/ac0482054.

(135) Lee, J.; Reilly, P. T. A. Limitation of Time-of-Flight Resolution in the Ultra High Mass Range. *Anal. Chem.* **2011**, *83* (15), 5831–5833. https://doi.org/10.1021/ac201537b.

(136) Agilent - intro to TOF.pdf - OneDrive https://colostate-my.sharepoint.com/personal/kdenef_colostate_edu/_layouts/15/onedrive.aspx?id=%2Fpersonal%2Fkdenef_colostate_edu%2FDocuments%2FMS general papers%2FAgilent - intro to TOF.pdf&parent=%2Fpersonal%2Fkdenef_colostate_edu%2FDocuments%2FMS general papers (accessed May 8, 2020).

(137) Principles of MALDI-TOF Mass Spectrometry : SHIMADZU (Shimadzu Corporation) https://www.shimadzu.com/an/lifescience/maldi/princpl1.html (accessed May 8, 2020).

(138) Region, A. *Time-of-Flight Analyzer and Method*; 1992; Vol. 160.

(139) Cotter, R. J. Time-of-Flight Mass Spectrometry: An Increasing Role in the Life Sciences. *Biol. Mass Spectrom.* **1989**, *18* (8), 513–532. https://doi.org/10.1002/bms.1200180803.

(140) Grix, R.; Kutscher, R.; Li, G.; Grüner, U.; Wollnik, H.; Matsuda, H. A Time-of-Flight Mass Analyzer with High Resolving Power. *Rapid Commun. Mass Spectrom.* **1988**, *2* (5), 83–85. https://doi.org/10.1002/rcm.1290020503.

(141) Boesl, U.; Weinkauf, R.; Schlag, E. W. Reflectron Time-of-Flight Mass Spectrometry and Laser Excitation for the Analysis of Neutrals, Ionized Molecules and Secondary Fragments. *International Journal of Mass Spectrometry and Ion Processes*. Elsevier January 15, 1992, pp 121–166. https://doi.org/10.1016/0168-1176(92)80001-H.

(142) Mamyrin, B. A. Laser Assisted Reflectron Time-of-Flight Mass Spectrometry. *Int. J. Mass Spectrom. Ion Process.* **1994**, *131* (C), 1–19. https://doi.org/10.1016/0168-1176(93)03891-O.

(143) Doroshenko, V. M.; Cotter, R. J. Ideal Velocity Focusing in a Reflectron Time-of-Flight Mass Spectrometer. *J. Am. Soc. Mass Spectrom.* **1999**, *10* (10), 992–999. https://doi.org/10.1016/S1044-0305(99)00067-7.

(144) Hoffmann Edmond de, S. V. Mass Spectrometry: Principles and Applications, 3rd Edition - Edmond de Hoffmann, Vincent Stroobant. 2007, pp 1–4.

(145) Biomedical Mass Spectrometry Resource | WUSTL.edu » TOF MS Resolution and Mass Measurement Accuracy https://msr.dom.wustl.edu/tof-ms-resolution-mass-measurement-accuracy/ (accessed May 8, 2020).

(146) *Time-of-Flight Mass Spectrometry Technical Overview*.

(147) Yi-Wei Tang, C. W. S. Advanced Techniques in Diagnostic Microbiology https://books.google.com/books?id=pDb3tqQkvRsC&pg=PA499&lpg=PA499&dq=tof+has+no+theoretical+upper+mass+limit&source=bl&ots=xJfOUC0Qj8&sig=ACfU3U2GDfqsflpXqPeBgnOqGes9P-hXUA&hl=en&sa=X&ved=2ahUKEwir0N32paXpAhXbGM0KHcChDOEQ6AEwA3oECAcQAQ#v=onepage&q=tof has (accessed May 8, 2020).

(148) Jerzy Silberring, Ralph Ekman, D. M. D. Mass Spectrometry and Hyphenated Techniques in Neuropeptide Research https://books.google.com/books?id=ITjQb77X2OIC&pg=PA61&lpg=PA61&dq=tof+has+no+theoretical+upper+mass+limit&source=bl&ots=wmAPBvKmMi&sig=ACfU3U1V7oRZfI6qKAlUmDd0erxdlI63FA&hl=en&sa=X&ved=2ahUKEwir0N32paXpAhXbGM0KHcChDOEQ6AEwAHoECAgQAQ#v=onepage&q=tof has n (accessed May 8, 2020).

(149) Annesley, T. M. Ion Suppression in Mass Spectrometry. *Clinical Chemistry*. July 1, 2003, pp 1041–1044. https://doi.org/10.1373/49.7.1041.

(150) Furey, A.; Moriarty, M.; Bane, V.; Kinsella, B.; Lehane, M. Ion Suppression; A Critical Review on Causes, Evaluation, Prevention and Applications. *Talanta*. Elsevier B.V. October 15, 2013, pp 104–122. https://doi.org/10.1016/j.talanta.2013.03.048.

(151) Lozano-Sánchez, J.; Borrás-Linares, I.; Sass-Kiss, A.; Segura-Carretero, A. Chromatographic Technique: High-Performance Liquid Chromatography (HPLC). In *Modern Techniques for Food Authentication*; Elsevier, 2018; pp 459–526. https://doi.org/10.1016/b978-0-12-814264-6.00013-x.

(152) Dudley, E.; Bond, A. E. Phosphoproteomic Techniques and Applications. In *Advances in Protein Chemistry and Structural Biology*; Academic Press Inc., 2014; Vol. 95, pp 25–69. https://doi.org/10.1016/B978-0-12-800453-1.00002-6.

(153) Mizzen, C. A. Purification and Analyses of Histone H1 Variants and H1 Posttranslational Modifications. *Methods Enzymol.* **2004**, *375*, 278–297. https://doi.org/10.1016/S0076-6879(03)75019-8.

(154) Neue, U. D.; Alden, B. A.; Iraneta, P. C.; Mëndez, A.; Grumbach, E. S.; Tran, K.; Diehl,

D. M. *HPLC Columns for Pharmaceutical Analysis*; Elsevier Inc., 2005; Vol. 6. https://doi.org/10.1016/S0149-6395(05)80048-0.

(155) Royle, L. Separation of Glycans and Monosaccharides. In *Liquid Chromatography: Applications: Second Edition*; Elsevier Inc., 2017; Vol. 2, pp 183–200. https://doi.org/10.1016/B978-0-12-805392-8.00007-4.

(156) Poole, C. F.; Lenca, N. Reversed-Phase Liquid Chromatography. In *Liquid Chromatography: Fundamentals and Instrumentation: Second Edition*; Elsevier, 2017; Vol. 1, pp 91–123. https://doi.org/10.1016/B978-0-12-805393-5.00004-X.

(157) Robards, K.; Haddad, P. R.; Jackson, P. E. High-Performance Liquid Chromatography—Separations. In *Principles and Practice of Modern Chromatographic Methods*; Elsevier, 2004; pp 305–380. https://doi.org/10.1016/b978-0-08-057178-2.50009-1.

(158) Tautenhahn, R.; Bottcher, C.; Neumann, S. Highly Sensitive Feature Detection for High Resolution LC/MS. *BMC Bioinformatics* **2008**, *9* (1), 504. https://doi.org/10.1186/1471-2105-9-504.

(159) Mirnaghi, F. S.; Chen, Y.; Sidisky, L. M.; Pawliszyn, J. Optimization of the Coating Procedure for a High-Throughput 96-Blade Solid Phase Microextraction System Coupled with LC-MS/MS for Analysis of Complex Samples. *Anal. Chem.* **2011**, *83* (15), 6018–6025. https://doi.org/10.1021/ac2010185.

(160) Levin, Y.; Schwarz, E.; Wang, L.; Leweke, F. M.; Bahn, S. Label-Free LC-MS/MS Quantitative Proteomics for Large-Scale Biomarker Discovery in Complex Samples. *J. Sep. Sci.* **2007**, *30* (14), 2198–2203. https://doi.org/10.1002/jssc.200700189.

(161) Henion, J.; Brewer, E.; Rule, G. Peer Reviewed: Sample Preparation for LC/MS/MS: Analyzing Biological and Environmental Samples. *Anal. Chem.* **1998**, *70* (19), 650A-656A. https://doi.org/10.1021/ac981991q.

(162) Lu, W.; Bennett, B. D.; Rabinowitz, J. D. Analytical Strategies for LC-MS-Based Targeted Metabolomics. *J. Chromatogr. B Anal. Technol. Biomed. Life Sci.* **2008**, *871* (2), 236–242. https://doi.org/10.1016/j.jchromb.2008.04.031.

(163) Dark, W. A.; Associates, W.; McFadden, W. H. *The Role of HPLC and LC-MS in the Separation and Characterization of Coal Liquefaction Products*.

(164) Lee, M. S.; Kerns, E. H. LC/MS Applications in Drug Development. *Mass Spectrom. Rev.* **1999**, *18* (3-4), 187–279. https://doi.org/10.1002/(SICI)1098-2787(1999)18:3/4<187::AID-MAS2>3.0.CO;2-K.

(165) Payne, M. E.; Grayson, S. M. Characterization of Synthetic Polymers via Matrix Assisted Laser Desorption Ionization Time of Flight (MALDI-TOF) Mass Spectrometry. *J. Vis. Exp.* **2018**, *2018* (136). https://doi.org/10.3791/57174.

(166) Gusev, A. I.; Wilkinson, W. R.; Proctor, A.; Hercules, D. M. Improvement of Signal Reproducibility and Matrix/Comatrix Effects in MALDI Analysis. *Anal. Chem.* **1995**, *67* (6), 1034–1041. https://doi.org/10.1021/ac00102a003.

(167) Albrethsen, J. Reproducibility in Protein Profiling by MALDI-TOF Mass Spectrometry. *Clin. Chem.* **2007**, *53* (5), 852–858. https://doi.org/10.1373/clinchem.2006.082644.

(168) Köcher, T.; Engström, Å.; Zubarev, R. A. Fragmentation of Peptides in MALDI In-Source Decay Mediated by Hydrogen Radicals. *Anal. Chem.* **2005**, *77* (1), 172–177.

https://doi.org/10.1021/ac0489115.

(169) Demeure, K.; Gabelica, V.; De Pauw, E. A. New Advances in the Understanding of the In-Source Decay Fragmentation of Peptides in MALDI-TOF-MS. *J Am Soc Mass Spectrom* **2010**, *21*, 1906–1917. https://doi.org/10.1016/j.jasms.2010.07.009.

(170) El-Aneed, A.; Cohen, A.; Banoub, J. Mass Spectrometry, Review of the Basics: Electrospray, MALDI, and Commonly Used Mass Analyzers. *Applied Spectroscopy Reviews*. Taylor & Francis Group 2009, pp 210–230. https://doi.org/10.1080/05704920902717872.

(171) *Interfacing Liquid Chromatography and Tandem MALDI Mass Spectrometry*.

(172) Bodnar, W. M.; Blackburn, R. K.; Krise, J. M.; Moseley, M. A. Exploiting the Complementary Nature of LC/MALDI/MS/MS and LC/ESI/MS/MS for Increased Proteome Coverage. *J. Am. Soc. Mass Spectrom.* **2003**, *14* (9), 971–979. https://doi.org/10.1016/S1044-0305(03)00209-5.

(173) Liu, X.; Cole, R. B. A New Model for Multiply Charged Adduct Formation Between Peptides and Anions in Electrospray Mass Spectrometry. *J. Am. Soc. Mass Spectrom* **2011**, *22*, 2125–2136. https://doi.org/10.1007/s13361-011-0255-0.

(174) Harvey, D. J. Fragmentation of Negative Ions from Carbohydrates: Part 1. Use of Nitrate and Other Anionic Adducts for the Production of Negative Ion Electrospray Spectra from N-Linked Carbohydrates. *J. Am. Soc. Mass Spectrom.* **2005**, *16* (5), 622–630. https://doi.org/10.1016/j.jasms.2005.01.004.

(175) Tapia, J. B.; Hibbard, H. A. J.; Reynolds, M. M. Derivatization of Dextran for Multiply

Charged Ion Formation and Electrospray Ionization Time-of-Flight Mass Spectrometric Analysis. *J. Am. Soc. Mass Spectrom.* **2017**, *28* (10), 2201–2208. https://doi.org/10.1007/s13361-017-1717-9.

(176) Pillai, C. K. S.; Paul, W.; Sharma, C. P. Chitin and Chitosan Polymers: Chemistry, Solubility and Fiber Formation. *Prog. Polym. Sci.* **2009**, *34*, 641–678. https://doi.org/10.1016/j.progpolymsci.2009.04.001.

(177) Ravindra, R.; Krovvidi, K. R.; Khan, A. A. Solubility Parameter of Chitin and Chitosan. *Carbohydr. Polym.* **1998**, *36* (2–3), 121–127. https://doi.org/10.1016/S0144-8617(98)00020-4.

(178) Li, K.; Liu, S.; Xing, R.; Yu, H.; Qin, Y.; Li, R.; Li, P. High-Resolution Separation of Homogeneous Chitooligomers Series from 2-Mers to 7-Mers by Ion-Exchange Chromatography. *J. Sep. Sci.* **2013**, *36* (7), 1275–1282. https://doi.org/10.1002/jssc.201200935.

(179) Cabrera, J. C.; Van Cutsem, P. Preparation of Chitooligosaccharides with Degree of Polymerization Higher than 6 by Acid or Enzymatic Degradation of Chitosan. *Biochem. Eng. J.* **2005**, *25*, 165–172. https://doi.org/10.1016/j.bej.2005.04.025.

(180) Li, J.; Du, Y.; Yang, J.; Feng, T.; Li, A.; Chen, P. Preparation and Characterisation of Low Molecular Weight Chitosan and Chito-Oligomers by a Commercial Enzyme. *Polym. Degrad. Stab.* **2005**, *87* (3), 441–448. https://doi.org/10.1016/j.polymdegradstab.2004.09.008.

(181) Chen, M.; Zhu, X.; Li, Z.; Guo, X.; Ling, P. Application of Matrix-Assisted Laser Desorption/Ionization Time-of-Flight Mass Spectrometry (MALDI-TOF-MS) in

Preparation of Chitosan Oligosaccharides (COS) with Degree of Polymerization (DP) 5-12 Containing Well-Distributed Acetyl Groups. *Int. J. Mass Spectrom.* **2010**, *290* (2–3), 94–99. https://doi.org/10.1016/j.ijms.2009.12.008.

(182) Bahrke, S.; Einarsson, J. M.; Gislason, J.; Haebel, S.; Letzel, M. C.; Peter-Katalinić, J.; Peter, M. G. Sequence Analysis of Chitooligosaccharides by Matrix-Assisted Laser Desorption Ionization Postsource Decay Mass Spectrometry. *Biomacromolecules* **2002**, *3* (4), 696–704. https://doi.org/10.1021/bm020010n.

(183) Akiyama, K.; Kawazu, K.; Kobayashi, A. A Novel Method for Chemo-Enzymatic Synthesis of Elicitor-Active Chitosan Oligomers and Partially N-Deacetylated Chitin Oligomers Using N-Acylated Chitotrioses as Substrates in a Lysozyme-Catalyzed Transglycosylation Reaction System. *Carbohydr. Res.* **1995**, *279* (C), 151–160. https://doi.org/10.1016/0008-6215(95)00288-X.

(184) Cabrera, J. C.; Van Cutsem, P. Preparation of Chitooligosaccharides with Degree of Polymerization Higher than 6 by Acid or Enzymatic Degradation of Chitosan. *Biochem. Eng. J.* **2005**, *25* (2), 165–172. https://doi.org/10.1016/j.bej.2005.04.025.

(185) Chen, M.; Zhu, X.; Li, Z.; Guo, X.; Ling, P. Application of Matrix-Assisted Laser Desorption/Ionization Time-of-Flight Mass Spectrometry (MALDI-TOF-MS) in Preparation of Chitosan Oligosaccharides (COS) with Degree of Polymerization (DP) 5â€“12 Containing Well-Distributed Acetyl Groups. *Int. J. Mass Spectrom.* **2010**, *290*, 94–99. https://doi.org/10.1016/j.ijms.2009.12.008.

(186) Calvano, C. D.; Zambonin, C. G.; Jensen, O. N. Assessment of Lectin and HILIC Based Enrichment Protocols for Characterization of Serum Glycoproteins by Mass Spectrometry.

J. Proteomics **2008**, *71* (3), 304–317. https://doi.org/10.1016/j.jprot.2008.06.013.

(187) Staples, G. O.; Bowman, M. J.; Costello, C. E.; Hitchcock, A. M.; Lau, J. M.; Leymarie, N.; Miller, C.; Naimy, H.; Shi, X.; Zaia, J. A Chip-Based Amide-HILIC LC/MS Platform for Glycosaminoglycan Glycomics Profiling. *Proteomics* **2009**, *9* (3), 686–695. https://doi.org/10.1002/pmic.200701008.

(188) Dong, X.; Shen, A.; Gou, Z.; Chen, D.; Liang, X. Hydrophilic Interaction/Weak Cation-Exchange Mixed-Mode Chromatography for Chitooligosaccharides Separation. *Carbohydr. Res.* **2012**, *361*, 195–199. https://doi.org/10.1016/j.carres.2012.08.022.

(189) Lu, Y.; Shah, A.; Hunter, R. A.; Soto, R. J.; Schoenfisch, M. H. S-Nitrosothiol-Modified Nitric Oxide-Releasing Chitosan Oligosaccharides as Antibacterial Agents. *Acta Biomater.* **2015**, *12* (1), 62–69. https://doi.org/10.1016/j.actbio.2014.10.028.

(190) Allison, C. L.; Lutzke, A.; Reynolds, M. M. Examining the Effect of Common Nitrosating Agents on Chitosan Using a Glucosamine Oligosaccharide Model System. *Carbohydr. Polym.* **2019**, *203*. https://doi.org/10.1016/j.carbpol.2018.09.052.

(191) Allison, C. L.; Lutzke, A.; Reynolds, M. M. Identification of Low Molecular Weight Degradation Products from Chitin and Chitosan by Electrospray Ionization Time-of-Flight Mass Spectrometry. *Carbohydr. Res.* **2020**, *493*, 108046. https://doi.org/10.1016/j.carres.2020.108046.

CHAPTER 2

ESI METHODS FOR THE DETECTION OF CHITIN AND CHITOSAN'S DEGRADATION PRODUCTS

2.1 Overview

To address whether LC-MS can be used to screen for fungal infections, experiments began with a ground-up analysis of the low molecular weight components of chitosan. Electrospray ionization (ESI) methods were optimized for the detection of the simplest units that comprise chitosan polymers. Glucosamine (GlcN), *N*-acetylglucosamine (GlcNAc), and chitosan oligosaccharides (COS) composed of assorted combinations of these monomers were used to build these methods. Eventually, these methods were applied to polymeric chitosan. These studies implemented direct injection ESI methods, bypassing prior separation steps to target the ionization efficiency for this class of analytes. The experiments contained in this chapter focus on increasing the ionization efficiency of mass spectrometric methods, and explore the capabilities and the limitations of ESI-MS to analyze chitin derivatives.

The use of LC-MS to analyze chitin derivatives presents several challenges. Perhaps the most prevalent of these is that in its native polymeric state, chitin is insoluble in aqueous mobile phases that would enable its analysis by LC-MS. This necessitates one of two approaches: 1) modifying chitin to a soluble derivative such as chitosan, or 2) degrading chitin to produce a low molecular weight fingerprint, such as soluble GlcNAc oligomers. Both of these approaches involve chemical modification to produce compounds for which detection suggests the presence of chitin.

Chitosan is a common derivative of chitin that is soluble in acidic aqueous solutions. Depolymerization protocols used to produce GlcNAc oligomers often deacetylate chitin as well, especially those involving acidic treatments. Numerous studies indicate that chitin can be depolymerized and deacetylated in one-step treatments at both industrial and research scales. Given this, it seemed intuitive to begin mass spectrometric method development using low molecular weight COS. Several questions were addressed during the studies covered in this chapter. Firstly, what are the optimal mass spectrometric conditions to enable the detection of COS? In these experiments, a COS model system was used to produce methods with increased ionization efficiency compared to methods used for routine analyses. Parameters deemed to impact ionization efficiency were systematically varied and then optimized. We found that the mobile phase composition, fragmentor voltage, and ionization polarity all have a strong impact on the ability of COS to produce signals in ESI-MS. Following the optimization of mass spectrometric methods for COS, these were applied to address the second question: Can polymeric chitosan be detected using mass spectrometry? Our results and those in literature show that mass spectrometry can be used to characterize COS and the monomers that compose chitosan; however, these studies have been limited to species that only contain a few residues. In this chapter, studies were performed in which polymeric chitosan was suspended in acidic aqueous solutions, then analyzed using ESI time-of-flight (TOF) mass spectrometry. These experiments sought to multiply charge chitosan to produce *m/z* signals within the range of the TOF that was used. However, no multiply charged signals were observed in mass spectra obtained during these experiments, indicating that these methods were ineffective for the analysis of polymeric chitosan. Given the difficulty experienced in multiply charging polymeric chitosan, the focus of the research following this was

shifted to producing low molecular weight fingerprints that could be related back to the presence of chitin or chitosan polymers.

2.2 Introduction

2.2.1 Analysis of chitin, chitosan, and their components by mass spectrometry

The analysis of chitosan by mass spectrometry has been confined to low molecular weight species. The molecular weight of chitosan is usually reduced via chemical or enzymatic modifications prior to characterization, but sometimes occurs by physical modifications during instrumental analysis. Some of the first studies using mass spectrometry to analyze chitosan occurred prior to the widespread use of soft ionization sources. Electron impact (EI) sources have been used to study the thermal behavior of chitin and chitosan by producing fragment ions from polymers with varying degrees of deacetylation[1,2]. EI sources have also been used to study the thermal stability of chitosan when forming complexes with ions such as silver[3]. The introduction of matrix-assisted laser desorption ionization (MALDI) and electrospray ionization (ESI) ion sources later facilitated the analysis of chitosan oligomers without prior fragmentation. Both ESI and MALDI have been used to characterize chitosan oligomers produced by chemical and enzymatic degradation methods[4–6]. MALDI has been used to characterize oligomers with degrees of polymerization of up to 24 and with molecular weights of ~4200 g/mol[7]; however, the analysis of species larger than this has not been explored.

For applications in which quantitation is desired, ESI is preferred over MALDI due to the ability of ESI to be easily paired with HPLC. Large molecules like proteins are often multiply charged during ESI[8,9]. The formation of adducts with multiple positive charges decreases the *m/z* ratio of large molecules to a range detectable by most common mass analyzers. Even in mass

analyzers with theoretically high mass limits, multiply charging large compounds is beneficial for analysis, as this decreases a compound's *m/z* ratio to ranges where resolving power and mass accuracy are maximized[10]. Given the prevalence and advantages of multiply charging proteins using ESI[11–13], experiments were performed to answer whether polymeric chitosan may behave in a similar fashion. Chitosan is polycationic in solution[14,15], which suggested that carefully optimizing ionization conditions then applying these settings to larger polymeric species might facilitate polymeric chitosan analysis by mass spectrometry.

Analysis of the low molecular weight constituents of chitosan by mass spectrometry has been well established. COS are made frequently in medical research, and have been separated and detected using LC-MS[16,17]. The monomers that compose chitin and chitosan have applications in the fields of human health and supplements, and have both been well-studied using mass spectrometry and LC-MS. Glucosamine (GlcN) is found endogenously in cartilage and is taken as a dietary supplement for joint support[18,19]. It is routinely analyzed using mass spectrometry, HPLC, and LC-MS systems that implement a variety of detectors. *N*-acetylglucosamine (GlcNAc) is also used as a dietary supplement, and has also been studied using mass spectrometry, HPLC, and LC-MS. Both GlcN and GlcNAc are usually separated using hydrophilic interaction liquid chromatography (HILIC) columns[20,21]. HILIC columns contain polar stationary phases, which are used in conjunction with a mobile phase containing an aqueous component. The hydrophilic nature of HILIC stationary phases results in the formation of a layer of water at a molecular level, facilitating analyte partitioning[22]. This allows compounds to be separated that may not be retained on more common reverse-phase (e.g. C18) columns. Mass spectrometric analysis of both GlcN and GlcNAc is usually performed in positive ion mode, as these compounds are usually easily protonated in ESI[23,24].

2.2.2 Approach

The experiments contained in this chapter utilize electrospray ionization time-of-flight mass spectrometry (ESI-TOF-MS). ESI is frequently used in both research laboratories and clinical facilities. This source was selected to ensure methods would be directly transferrable from research laboratories to hospitals, given the end goal of developing a medical diagnostic technique. TOF mass analyzers are commonly used in tandem with ESI, and are popular for several reasons. Firstly, they facilitate accurate mass measurements, which allow compound assignments for ions based on their mass defects, rather than by just their nominal masses. Mass defects are defined as the difference between a compound's monoisotopic mass and its nominal mass, and these values vary depending on the nuclear binding energy of a compound[25,26]. The use of accurate mass measurements allows the differentiation of compounds with equivalent nominal masses. In addition to having the capacity to make accurate mass measurements, TOFs can analyze a large range of analytes, ranging from under 100 Daltons up to Megadaltons[27]. TOFs are commonly used to analyze large, multiply charged ions like proteins. The motivation to perform equivalent analyses on multiply charged polymeric chitosan guided the selection of mass analyzer for these experiments.

Optimization studies targeted two mass spectrometric components to maximize the ionization efficiency of chitosan. Generally, these can be classified into modifications to the mobile phase, and optimization of ion source parameters. In ESI-MS, samples are introduced into a flow of polar solvent which is subsequently infused into the source. Common solvents include methanol, acetonitrile, and water. The effectiveness of these solvents increases with their relative volatility. For instance, water is a highly polar molecule. However, acetonitrile is a more effective solvent in many situations due to its higher volatility. Despite its lower volatility, water is still

commonly used in ESI methods, as some polar analytes are insoluble in organic solvents. This often necessitates the use of a partially aqueous mobile phase to prevent analyte precipitation. Additives are often used to increase the effectiveness of ESI methods. Low concentrations of formic or acetic acid (~0.1% volume/volume) are often used in positive ion mode ESI. These acidify the mobile phase and can act as proton donors to encourage the formation of protonated adducts[28]. Ammonia can be used in negative ion mode to increase solution pH to induce the opposite effect as acids[29]. In these studies, the use of mobile phases with varied proportions of organic and aqueous solvents was investigated, as was the impact additives had on ionization.

Following the introduction of samples into the mobile phase flow, the mixture is sprayed through an ESI needle at atmospheric pressure alongside the application of a strong electric potential. Solvent droplets undergo evaporation, ultimately resulting in the formation of volatilized ions. These are electrostatically drawn into a capillary, undergo focusing steps (often via a quadrupole), then are analyzed by a mass analyzer. Several parameters are important to consider when optimizing ESI methods. One of these is the capillary voltage, which is applied at the entrance of the capillary. The purpose of the capillary voltage is to guide ions from the spray chamber toward the instrument's accelerating and focusing regions[30]. The fragmentor voltage is applied to the opposite interior side of the capillary. Its purpose is to increase the velocity at which ions travel from the spray chamber, which is at atmospheric pressure, to the interior high-pressure region (~10^{-7} torr) of the instrument[31]. Low fragmentor voltages may be insufficient to draw ions into the instrument, whereas excessive fragmentor voltages may fragment ions, making analyte identification difficult. In the following studies, the capillary and fragmentor voltages were optimized to maximize the number of signals in mass spectra, indicating that greater ionization efficiency had been achieved.

2.3 Materials and Methods

2.3.1 Materials

D-Glucosamine hydrochloride (99.9%) was obtained from Calbiochem (Darmstadt, DE). *N*-Acetyl-D-glucosamine (>98.0%) was obtained from TCI (Portland, OR). Chitosan oligosaccharides (<3000 MW, 93% deacetylated) were obtained from Carbosynth (Compton, Berkshire, UK). Low molecular weight chitosan (96% deacetylated) and ammonium acetate (≥98%), were obtained from Sigma Aldrich. LC-MS grade MeOH and LC-MS grade H_2O were obtained from EMD Millipore (Burlington, MA). LC-MS vials were purchased from Agilent (Santa Clara, CA). Glacial acetic acid and glass media storage bottles were purchased from Fisher Scientific (Waltham, MA). A NE-1000 programmable single syringe pump was acquired from New Era Pump Systems (New York, New York). LC syringes were obtained from Hamilton (Reno, NV).

2.3.2 Sample preparation

Samples were prepared by adding ~10 mg of sample to a scintillation vial then adding an appropriate amount of solvent to create a solution with a concentration of 1 mg/mL. LC-MS grade water was used as a solvent for glucosamine, *N*-acetylglucosamine, and chitosan oligosaccharides. A 1% acetic acid solution was used to dissolve chitosan polymer. Vials were vortexed for 10 seconds and the resulting solutions filtered through 0.2-μm filters into LC-MS vials. Vials were stored at -20 °C until analysis.

2.3.3 Mass Spectrometry

Mass spectra were acquired using an Agilent 6224 high resolution time-of-flight mass spectrometer (Agilent, Palo Alto, CA, USA). For studies involving the characterization of chitosan

oligosaccharides in positive ionization mode, a multimode ion source was equipped and set to electrospray ionization mode. For studies involving the characterization of glucosamine, *N*-acetylglucosamine, and chitosan polymer, a dual electrospray ionization source was equipped. For studies involving the characterization of chitosan oligosaccharides in negative ionization mode, a dual electrospray ionization source was equipped. Samples were prepared and injected into the solvent flow, bypassing any prior separation step. For syringe injection experiments performed with chitosan polymer, 500 μL of 1 mg/mL chitosan polymer solution was drawn into a Hamilton glass LC syringe. The syringe was attached to a NE-1000 syringe pump with a flow rate of 100 μL/minute directly into the ionization source. Data was acquired over 5 minutes.

The mobile phase used was composed of methanol and water. The proportions tested can be found in **Table 2.1.** Following optimization of mobile phase proportions, 0.1% v/v acetic acid was added to both components to compare the ionization efficiency of samples with and without acidic additives. In all experiments, the flow rate was set to 0.200 mL/min. Other mass spectrometric parameters were as follows: 60 V skimmer voltage, 650 V octupole voltage, 45 psig nebulizer pressure, and 10 L min^{-1} gas flow at 250 °C (N_2). The capillary voltage and fragmentor voltage were tested in the ranges shown in **Table 2.1.**

Table 2.1: Mass spectrometric parameters modified during method development.

Method development parameter	**Range tested**
Mobile phase composition: MeOH:H_2O	5:95 – 95:5
Capillary voltage	2000 V – 4000 V
Fragmentor voltage	20 V – 50 V

Initial optimization studies were performed in positive ionization mode. Glucosamine, *N*-acetylglucosamine, and chitosan oligosaccharides were characterized in both positive ionization mode and negative ionization mode. Experiments analyzing chitosan polymer were performed in positive ionization mode. The detection range for all scans was set to 120-3200 *m/z*.

2.4 Data analysis

Raw data was viewed and processed using Agilent MassHunter Workstation® software's Qualitative Analysis program, with subsequent analyses being carried out using Microsoft Excel®.

2.4. Results and Discussion

2.4.1 Ion prediction and screening

Prior to sample analysis, the monoisotopic masses for GlcN, GlcNAc and oligomers composed of these were calculated. Structures were built in ChemDraw and *m/z* predictions were made in both ChemDraw and MassHunter software suites. These values were compiled into **Table 2.2.** For all oligomers, GlcN residues are referred to as "D," or deacetylated subunits, while GlcNAc residues are referred to as "N" subunits.

Table 2.2: Compilation of low molecular weight chitosan monomers and oligomers with the potential to appear in mass spectra.

Compounds		**Calculated monoisotopic masses of ESI adducts**				
Species	**Formula**	**$[M-H_2O+H]^+$**	**$[M+H]^+$**	**$[M+Na]^+$**	**$[M-H]^-$**	**$[M+Cl]^-$**
2,5-AM	$C_6H_{10}O_5$	145.0495	163.0601	185.0420	161.0455	197.0222
2,5-AM	$C_6H_{12}O_6$	163.0601	181.0707	203.0526	179.0561	215.0328
D1A0	$C_6H_{13}NO_5$	162.0761	180.0866	202.0686	178.0721	214.0488
D0A1	$C_8H_{15}NO_6$	204.0866	222.0973	244.0792	220.0827	256.0593
D2A0	$C_{12}H_{24}N_2O_9$	323.1449	341.1555	363.1374	339.1409	375.1176

D1A1	$C_{14}H_{26}N_2O_{10}$	365.1555	383.1660	405.1480	381.1515	417.1281
D0A2	$C_{16}H_{28}N_2O_{11}$	407.1660	425.1766	447.1585	423.1620	459.1387
D3A0	$C_{18}H_{35}N_3O_{13}$	484.2137	502.2243	524.2062	500.2097	536.1864
D2A1	$C_{20}H_{37}N_3O_{14}$	526.2243	544.2348	566.2168	542.2203	578.1970
D1A2	$C_{22}H_{39}N_3O_{15}$	568.2348	586.2454	608.2273	584.2308	620.2075
D0A3	$C_{24}H_{41}N_3O_{16}$	610.2454	628.2560	650.2379	262.2414	662.2181
D4A0	$C_{24}H_{46}N_4O_{17}$	645.2825	663.2931	685.2750	661.2785	697.2552
D3A1	$C_{26}H_{48}N_4O_{18}$	687.2931	705.3036	727.2856	719.2840	755.2607
D2A2	$C_{28}H_{50}N_4O_{19}$	729.3036	747.3142	769.2961	745.2996	781.2763
D1A3	$C_{30}H_{52}N_4O_{20}$	771.3142	789.3248	811.3087	787.3102	823.2869
D5A0	$C_{30}H_{57}N_5O_{21}$	806.3513	824.3619	846.3438	822.3473	858.3240
D0A4	$C_{32}H_{54}N_4O_{21}$	813.3248	831.3353	853.3173	829.3208	865.2975
D3A2	$C_{34}H_{61}N_5O_{23}$	890.3724	908.3830	930.3650	906.3685	942.3451
D6A0	$C_{36}H_{68}N_6O_{25}$	967.4201	985.4307	1007.4126	983.4161	1019.3928

2.4.2 Optimization of mass spectrometric parameters

Prior to optimization studies, COS were analyzed with a mass spectrometric method used for routine analyses. This was provided by the Central Instrument Facility at Colorado State University. The mass spectrometric parameters that remained constant through optimization experiments are as follows: 0.200 mL/min flow rate, 60 V skimmer voltage, 650 V octupole voltage, 45 psig nebulizer pressure, and 10 L min^{-1} gas flow at 250 °C (N_2). Parameters that were optimized can be found in **Table 2.3**. A sample mass spectra can be seen in **Figure 2.1**.

Table 2.3: Initial mass spectrometric parameters.

Parameter	*Mobile phase*	*Fragmentor voltage*	*Capillary voltage*	*Additives*
Value	100% MeOH	120 V	2500 V	None

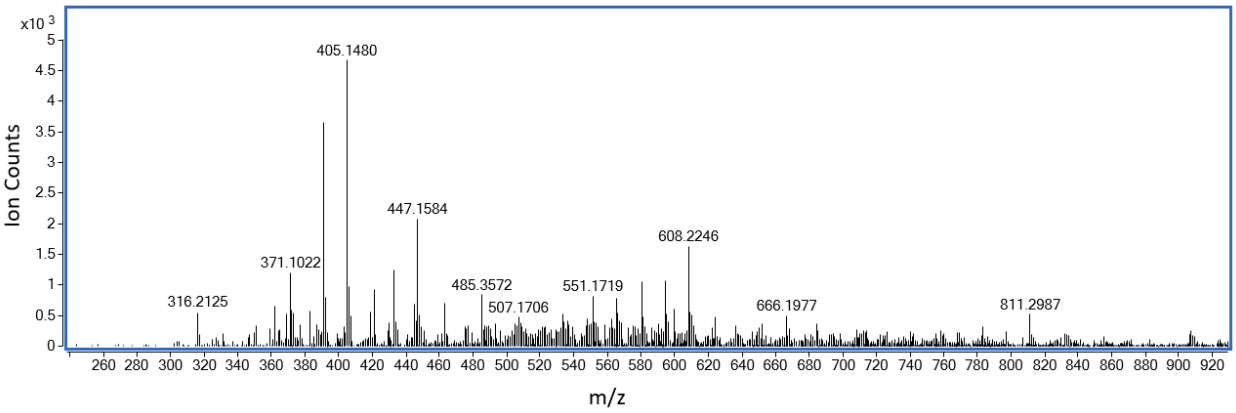

Figure 2.1: Mass spectrum of COS using a non-optimized method.

Using the provided method with no modifications, several signals were observed that indicated the presence of COS. The signal at 363 *m/z* corresponds to an ion with a molecular formula matching that of a sodiated GlcN dimer, $[C_{12}H_{24}N_2O_9 + Na]^+$. The signal at 405 *m/z* corresponds to an ion with a molecular formula matching that of a sodiated GlcN-GlcNAc dimer, $[C_{14}H_{26}N_2O_{10} + Na]^+$. The signal at 447 *m/z* corresponds to an ion with a molecular formula matching that of a sodiated GlcNAc dimer, $[C_{16}H_{28}N_2O_{11} + Na]^+$. The signal at 566 *m/z* corresponds to an ion with a molecular formula matching that of a sodiated D2A1 trimer, $[C_{20}H_{37}N_3O_{14} + Na]^+$. The signal at 608 *m/z* corresponds to an ion with a molecular formula matching that of a sodiated D2A2 tetramer, $[C_{28}H_{50}N_4O_{19} + Na]^+$. The signal at 811 *m/z* corresponds to an ion with a molecular formula matching that of a sodiated D1A3 tetramer, $[C_{30}H_{52}N_{24}O_{20} + Na]^+$.

The goal of initial experiments was to maximize analyte solubility while retaining a volatile mobile phase. GlcN residues are not soluble in methanol; however, the addition of water to the mobile phase allows GlcN to dissolve. To prevent analytes from potentially crashing out of solution following their injection into the solvent stream, an aqueous component was introduced into the mobile phase composition. The aqueous mobile phase component was varied in 10% increments from 10% to 90% of the total, with the remainder consisting of methanol. Additional experiments were run at 95% and at 5% aqueous compositions. To track the impact the aqueous component may have on the ionization efficiency, the peak ion abundances were tracked in all spectra obtained. All experiments were performed in triplicate. The results from these experiments is shown in **Figure 2.2**.

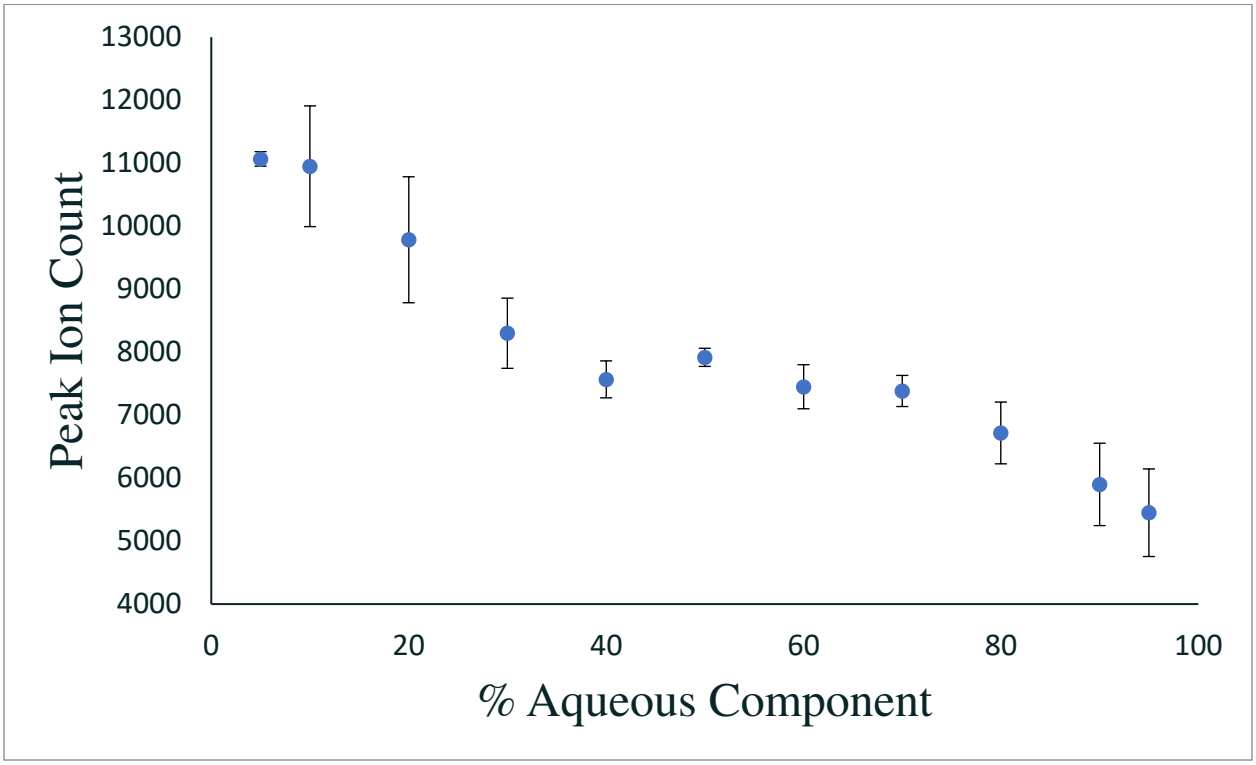

Figure 2.2: The peak observed ion count with an increasing aqueous mobile phase component. This figure shows the impact of the aqueous mobile phase component on the ionization efficiency for COS.

Overall, a downward trend was observed in the peak ion count as the aqueous component increased. This was expected, as the vapor pressure of water is considerably higher than that of methanol. However, introducing an aqueous component greatly increased the number of signals observed in subsequent mass spectra. Representative mass spectra using 100% methanol versus 50:50 MeOH:H_2O mobile phase are shown in **Figure 2.3**.

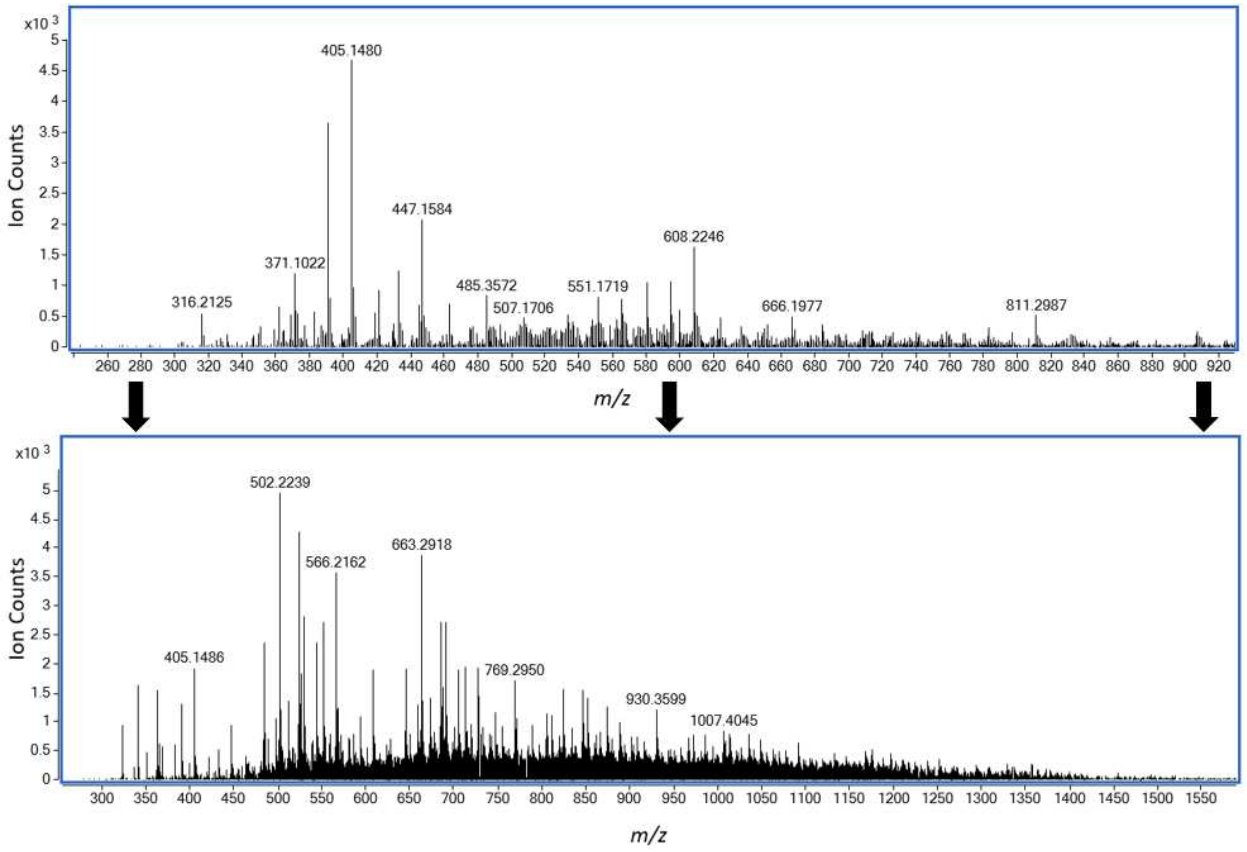

Figure 2.3: Mass spectrum of COS before and after the introduction of a mobile phase aqueous component. The mobile phase used in the top spectrum was 100% methanol. The mobile phase used in the bottom spectrum was 50:50 MeOH:H_2O.

Prior to the introduction of water into the mobile phase, signals observed in mass spectra included 363, 405, 447, 566, 608, and 811 *m/z*. The presence of water in the mobile phase significantly increased the number of signals observed, with the addition of peaks at 341, 383, 502, 544, 586, 628, 663, 705, 747, 789, and 824 *m/z*. The addition of these peaks that were previously

predicted indicates that using an exclusively organic mobile phase inhibits COS ion production in ESI. To balance decreased ionization efficiency with analyte compatibility, a mobile phase composed of 50% MeOH and 50% H_2O was used for subsequent studies.

Following the addition of an aqueous mobile phase component, the impact of acidic additives on ionization was assessed. This was done by adding 0.1% acetic acid by volume to both mobile phase components used. Two prominent signals (D1A1 and D3A0) were selected as representative analytes and the ion counts as well as the proportion of sodiated to protonated adducts were tracked. **Figure 2.4** provides a visual indication of this data. The addition of 0.01% acetic acid only resulted in slight trends toward higher observed ion counts. Ion counts increased slightly for both protonated and sodiated adducts. Interestingly, an appreciable difference between the proportion of protonated and sodiated adducts was not observed. These results were consistent for the representative analytes, as well as those not shown.

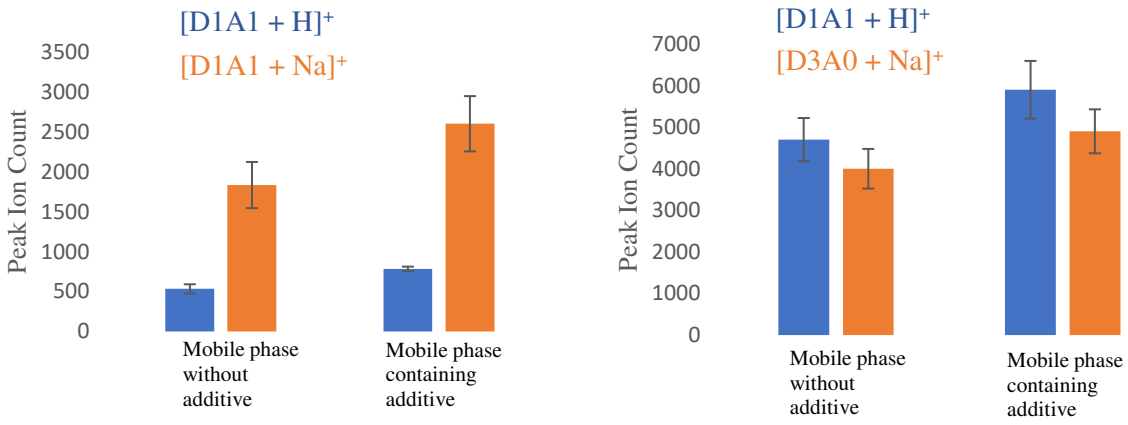

Figure 2.4: Ion abundance for representative oligomers before and after the addition of 0.1% acetic acid to the mobile phase.

The next parameters optimized were the fragmentor voltage and the capillary voltage. For capillary voltage optimization, the mobile phase held at 50:50 water:methanol and the fragmentor

voltage was held at 20 V. The capillary voltage was varied between 2000 and 4000 V by 500 V increments and the peak ion counts were tracked. Samples were analyzed in triplicate. We did not notice an appreciable trend in ionization efficiency while varying the capillary voltage, as shown in **Figure 2.5**. This indicated that even at the lowest value tested (2000 V), the capillary voltage was sufficient to draw a maximum number of ions from the spray chamber into the capillary.

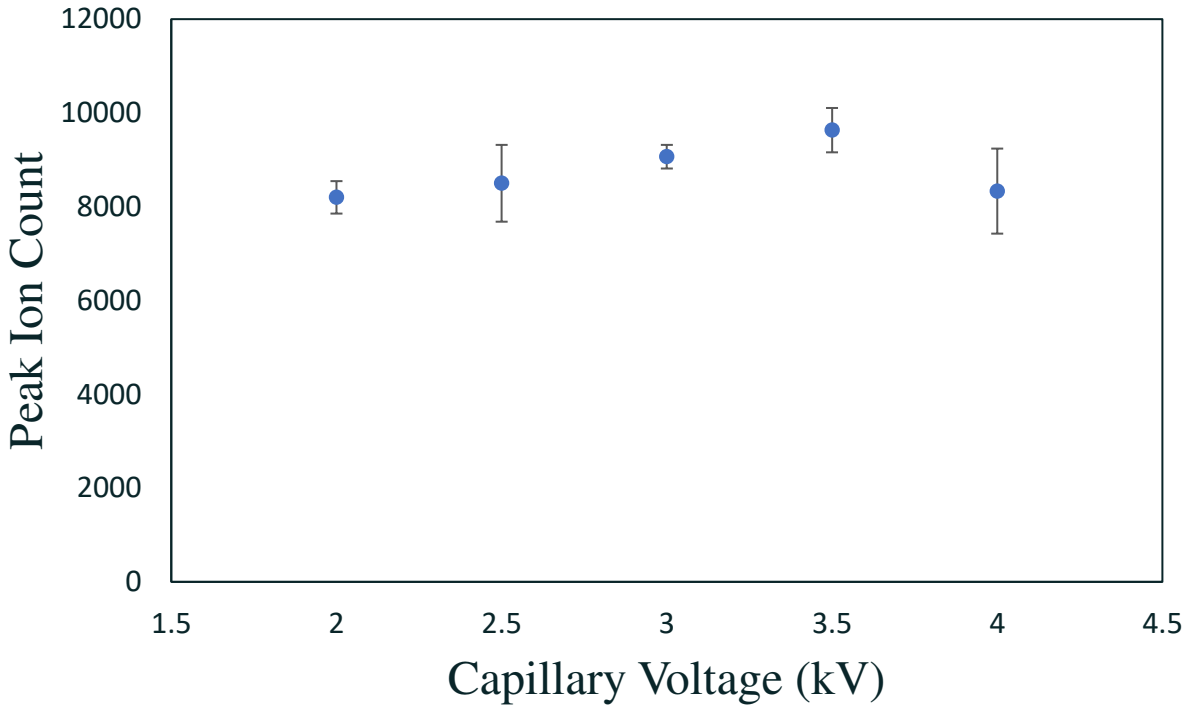

Figure 2.5: The change in peak observed ion count in mass spectrometry methods with varied capillary voltages.

For fragmentor voltage optimization, the mobile phase was set to 50:50 methanol and water, while the capillary voltage was held at **3500 V.** The fragmentor voltage was varied between 5 and 50 V by 10 V increments. We analyzed a 1 mg/mL COS standard in triplicate and tracked the peak observed ion counts. This plot can be seen in **Figure 2.6**. Results indicated that increasing the fragmentor voltage significantly increased the ionization efficiency during these experiments.

This suggested that at the lower levels tested, the fragmentor voltage was insufficient to accelerate ions from the atmospheric pressure spray chamber to the high-pressure regions of the instrument.

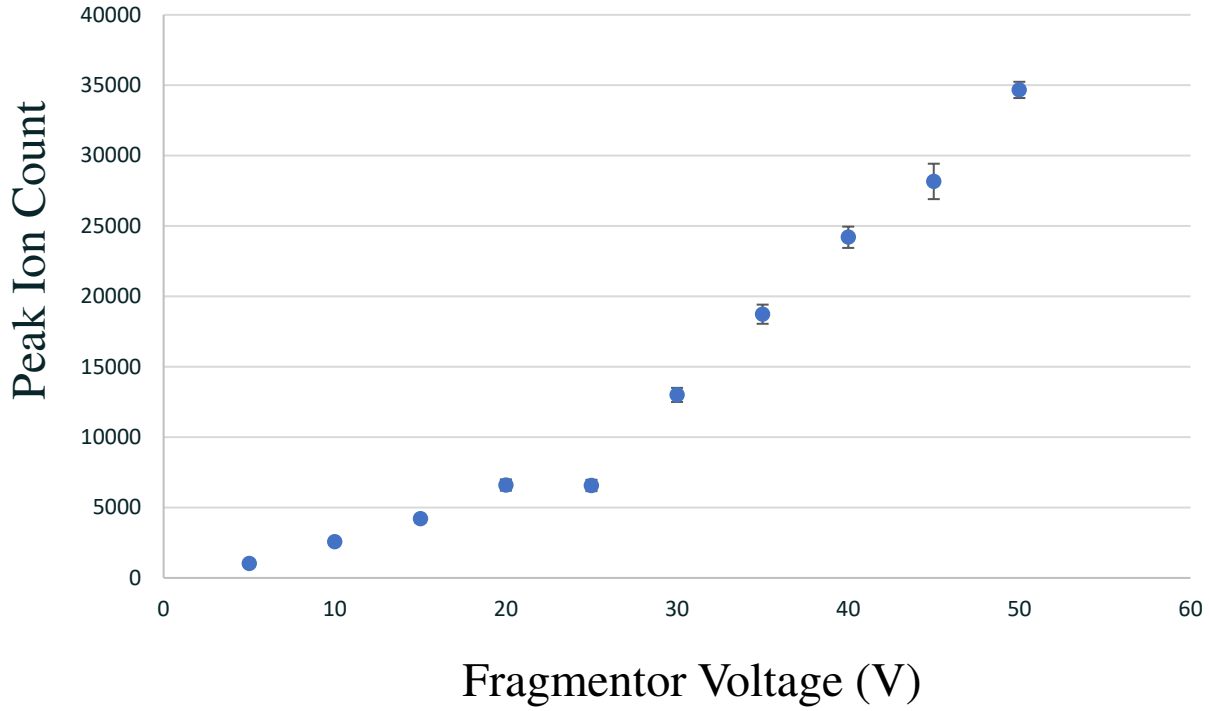

Figure 2.6: Changes in peak ion count observed in mass spectrometry methods with varied fragmentor voltages.

2.4.3 Final characterization – positive ionization mode

Initially, COS were characterized using positive ionization mode due to indications within literature that GlcN, GlcNAc, and COS readily form protonated adducts in ESI[23,24,32]. Using positive ionization mode, signals were detected representing a total of twelve compounds, as shown in the bottom spectrum in **Figure 2.3** and summarized in **Table 2.3**. In addition to protonated adducts, high abundances of sodiated adducts were also observed. Sodiated adducts are a common occurrence in mass spectra obtained in positive ionization mode. These are an artefact of glass manufacturing, and hence, their origin can often be traced to glassware that solvents come in contact with or are stored in[33]. In the case of these experiments, this was likely from the media

bottles in which mobile phase solvents were stored. It is usually considered preferable to produce protonated adducts rather than sodiated, since the presence of both effectively doubles the number of signals for a given number of compounds in mass spectra. However, alternative storage containers (e.g. Teflon) are prohibitively expensive, which leads to many mass spectrometrists screening for both adduct possibilities in most situations.

Table 2.3: Signals observed in mass spectra of COS following the addition of an aqueous mobile phase component.

Signal (*m/z*)	**Ion**	**Formula**
341	$[D2A0 + H]^+$	$C_{12}H_{24}N_2O_9$
383	$[D1A1 + H]^+$	$C_{14}H_{26}N_2O_9$
425	$[D0A2 + H]^+$	$C_{16}H_{28}N_2O_{11}$
502	$[D3A0 + H]^+$	$C_{18}H_{35}N_3O_{13}$
544	$[D2A1 + H]^+$	$C_{20}H_{37}N_3O_{14}$
586	$[D1A2 + H]^+$	$C_{22}H_{39}N_3O_{15}$
628	$[D0A3 + H]^+$	$C_{24}H_{41}N_3O_{16}$
663	$[D4A0 + H]^+$	$C_{24}H_{46}N_4O_{17}$
705	$[D3A1 + H]^+$	$C_{26}H_{48}N_4O_{18}$
747	$[D2A2 + H]^+$	$C_{28}H_{50}N_4O_{19}$
789	$[D1A3 + H]^+$	$C_{30}H_{52}N_4O_{20}$
824	$[D5A0 + H]^+$	$C_{30}H_{57}N_5O_{21}$

2.4.4 Final characterization – negative ionization mode

Following characterization studies in positive ion mode, COS were analyzed in negative ionization mode to assess if this may facilitate the detection of compounds not previously observed. All source parameters remained constant in these experiments. 50:50 methanol and water were used without any additives. The 0.01% acetic acid additive was not used in negative ion mode experiments; decreasing the pH would likely be counterproductive to the formation of $[M - H]^-$ adducts. Using negative ionization mode, signals were detected representing GlcN, GlcNAc, and eight relevant oligomers. A representative mass spectrum can be seen in **Figure 2.7**.

All signals identifiable as COS can be found in **Table 2.4**. Interestingly, no $[M - H]^-$ adducts were observed in the mass spectra obtained. Rather, chlorinated $[M + Cl]^-$ adducts were produced. While chlorinated adducts are not common, they have been reported to form in negative ion mode when analyzing compounds lacking acidic sites[34,35]. GlcN, GlcNAc, and COS have not previously been reported to form chlorinated adducts. However, the presence of basic amines and lack of carboxyl groups suggests that these compounds would be good candidates for the formation of chlorinated adducts. Given the uncommon nature of these adducts, isotopic patterns were used to identify all signals proposed to be chlorinated adducts. The two stable chlorine isotopes are 35 g/mol (75.77%) and 37 g/mol (24.23%), giving chlorinated ions a unique, recognizable isotopic pattern in which their mass spectral abundance directly mirrors the proportion of isotopes.

Table 2.4: Signals observed in mass spectra of COS in negative ionization mode.

Signal (*m/z*)	**Compound**	**Formula**
214	D1A0	$C_6H_{13}NO_5$
256	D0A1	$C_8H_{15}NO_6$
375	D2A0	$C_{12}H_{24}N_2O_9$
417	D1A1	$C_{14}H_{26}N_2O_9$
459	D0A2	$C_{16}H_{28}N_2O_{11}$
536	D3A0	$C_{18}H_{35}N_3O_{13}$
578	D2A1	$C_{20}H_{37}N_3O_{14}$
620	D1A2	$C_{22}H_{39}N_3O_{15}$
697	D4A0	$C_{24}H_{46}N_4O_{17}$

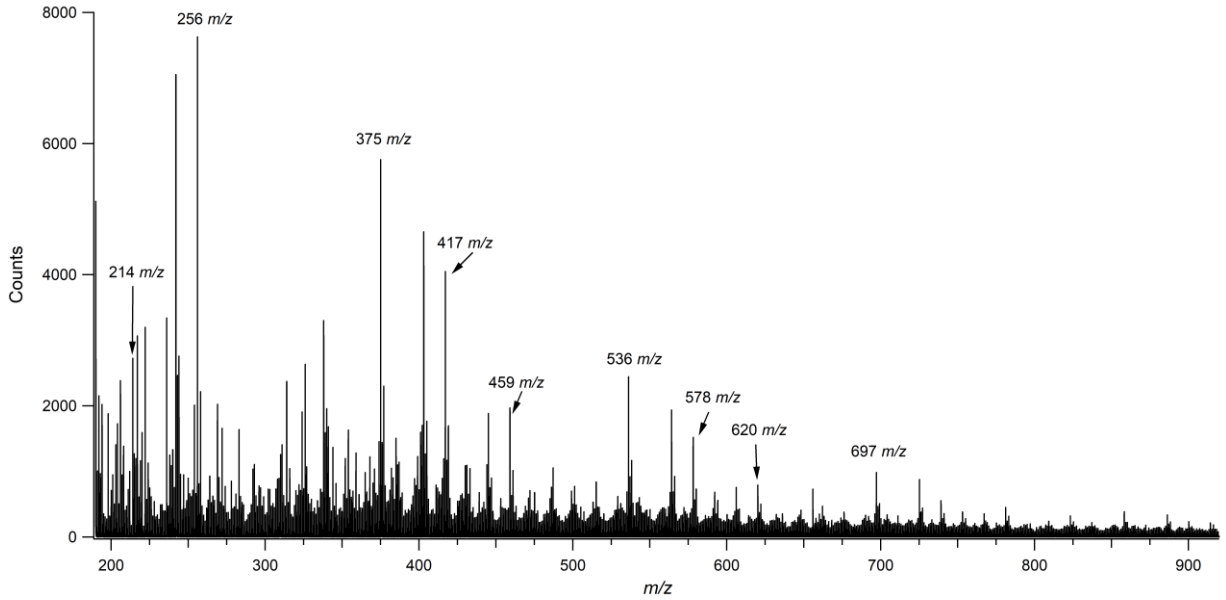

Figure 2.7: Representative mass spectrum of COS analyzed in negative ionization mode. All marked signals are indicative of chlorinated adducts.

2.4.5 Mass spectrometry of chitosan polymer

Our experiments attempting to multiply charge polymeric chitosan were not successful. Despite using an acidic aqueous solutions to ensure solvation and the use of mass spectrometric conditions conducive to ionization of oligomeric chitosan, multiply charged envelopes were not observed that would indicate the presence of multiply-charged chitosan polymers. The analyte used was low molecular weight chitosan from Sigma-Aldrich®, which was reported to have a molecular weight of 50-130 kDa. Polymers in this range would contain over 300 residues at the minimum end of the range to more than 800 residues at the higher mass range. The TOF used has an accurate mass range of 100-3200 *m/z.* Charges required to decrease the *m/z* ratios of these compounds to an appropriate range would be 16 charges at the low range (50,000 Da/16^+ = 3125 *m/z*), up to 41 at the upper range (130,000 Da/41^+ = 3171 *m/z*). Ions with charge states of greater than this are commonly seen in the literature[12,36]. While the default setting of the TOF used is its accurate mass range (100-3200 *m/z*), it can be set to operate in nominal mass mode, which extends its range to 20,000 *m/z* while allowing nominal mass measurements. Charges

required to decrease the *m/z* ratios of polymers to an appropriate range would be 3 charges at the low range (50,000 Da/3^+ = 16,667 *m/z*), up to 7 charges at the upper range (130,000 Da/7^+ = 18,571 *m/z*). Despite these charge states being easily achievable with proteins, multiply charged envelopes indicating the presence of polymeric chitosan were not observed, even after modifying the TOF parameters to nominal mass settings. In addition, experiments were performed in which aqueous chitosan was infused directly into the source, bypassing the introduction of the sample into the mobile phase, thereby eliminating the possibility for analytes to crash out of solution. During these experiments, signals indicating the presence of multiply charged chitosan polymer were not observed. Literature investigations imply that this may likely due to the tendency of chitosan to remain coiled in solution, even when fully dissolved[37–39]. Studies indicate that proteins that undergo successful multiple charging in ESI usually uncoil at least partially in solution[40]. In fact, a protein's ESI charge state can be used as a direct indicator of the extent of its coiling in solution[41]. Similar studies investigating the ability of dextran to multiply charge were met with limited success, with only oligomers of up to 1821 g/mol successfully acquiring multiple charges[42]. Given this information, it seems highly unlikely that chitosan polymer will undergo multiple charging in ESI. Hence, these studies were abandoned in favor of studying degradation methods to produce low molecular weight fingerprints from polymeric chitosan.

2.5 Conclusions

In the preceding experiments, parameters were optimized to develop methods conducive to the ionization of COS. To accomplish this, we analyzed a 1 mg/mL solution of COS and assessed whether signals were produced, as well as the peak intensity under certain conditions. In the development of these final methods, we used conditions that encouraged the formation of ions at their highest abundances. The mobile phase considerations we took into account were the

proportions of organic to aqueous solvents and the presence of mobile phase additives. The introduction of an aqueous component of the mobile phase increased the number of COS signals from six to eleven, indicating that this is a critical component to include in mass spectrometric methods for COS analysis. The introduction of an acidic component into the mobile phase increased the abundance of both protonated and sodiated adducts. The source parameters taken into consideration were the capillary voltage and the fragmentor voltage. The capillary voltage was not found to have a significant effect on the ion abundances of COS in the range tested. Increasing the fragmentor voltage was found to increase the ionization efficiency in the range tested. COS were characterized in both positive ionization mode and negative ionization modes. Eleven signals in positive ionization mode and nine signals in negative ionization mode could be corroborated with the constituents of chitosan. Analyzing polymeric chitosan using mass spectrometry was not successful using the methods developed for COS, or after modifications to injection methods and the mass analyzer.

Cumulatively, the studies performed in this chapter indicate that ESI-TOF-MS is well-suited for the analysis of chitosan's components, including GlcN, GlcNAc, and COS composed of these monomers. These compounds ionize in both positive and negative ionization modes. However, methods using positive ionization mode produced more signals that could be corroborated to COS than those using negative ionization mode. Using both solvent flow injection methods and syringe injections into the ionization source, we did not observe signals indicating that polymeric chitosan had multiply charged using ESI-TOF-MS. Fungi contain polymeric chitin and/or chitosan that can exceed 1 megadalton in size. Therefore, our original proposal of using chitin or chitosan as a marker for fungal infections necessitates non-direct detection methods. To facilitate this, the next phases of research covered in subsequent chapters focus on developing and

defining methods to degrade chitin and chitosan, then identifying the low molecular weight compounds produced from these. In conjunction with this, we continued using mass spectrometry to establish the efficacy of degradation methods, and to identify chemical fingerprints that these produce. The mass spectrometric information and methods used in this chapter provide a crucial starting point for methods used in subsequent chapters.

CHAPTER 2 – REFERENCES

(1) Mattai, J.; Hayes, E. R. Characterization of Chitosan by Pyrolysis-Mass Spectrometry. *J. Anal. Appl. Pyrolysis* **1982**, *3* (4), 327–334. https://doi.org/10.1016/0165-2370(82)80019-3.

(2) Nieto, J. M.; Peniche-Covas, C.; Padro´n, G. Characterization of Chitosan by Pyrolysis-Mass Spectrometry, Thermal Analysis and Differential Scanning Calorimetry. *Thermochim. Acta* **1991**, *176* (C), 63–68. https://doi.org/10.1016/0040-6031(91)80260-P.

(3) Peniche-Covas, C.; Jiménez, M. S.; Núñez, A. Characterization of Silver-Binding Chitosan by Thermal Analysis and Electron Impact Mass Spectrometry. *Carbohydr. Polym.* **1988**, *9* (4), 249–256. https://doi.org/10.1016/0144-8617(88)90043-4.

(4) Wattjes, J.; Niehues, A.; Cord-Landwehr, S.; Hoßbach, J.; David, L.; Delair, T.; Moerschbacher, B. M. Enzymatic Production and Enzymatic-Mass Spectrometric Fingerprinting Analysis of Chitosan Polymers with Different Nonrandom Patterns of Acetylation. *J. Am. Chem. Soc.* **2019**, *141* (7), 3137–3145. https://doi.org/10.1021/jacs.8b12561.

(5) Cord-Landwehr, S.; Ihmor, P.; Niehues, A.; Luftmann, H.; Moerschbacher, B. M.; Mormann, M. Quantitative Mass-Spectrometric Sequencing of Chitosan Oligomers Revealing Cleavage Sites of Chitosan Hydrolases. *Anal. Chem.* **2017**, *89* (5), 2893–2900. https://doi.org/10.1021/acs.analchem.6b04183.

(6) Cabrera, J. C.; Van Cutsem, P. Preparation of Chitooligosaccharides with Degree of Polymerization Higher than 6 by Acid or Enzymatic Degradation of Chitosan. *Biochem. Eng. J.* **2005**, *25*, 165–172. https://doi.org/10.1016/j.bej.2005.04.025.

(7) Chen, M.; Zhu, X.; Li, Z.; Guo, X.; Ling, P. Application of Matrix-Assisted Laser Desorption/Ionization Time-of-Flight Mass Spectrometry (MALDI-TOF-MS) in Preparation of Chitosan Oligosaccharides (COS) with Degree of Polymerization (DP) 5â€“12 Containing Well-Distributed Acetyl Groups. *Int. J. Mass Spectrom.* **2010**, *290*, 94–99. https://doi.org/10.1016/j.ijms.2009.12.008.

(8) Wong, S. F.; Meng, C. K.; Fenn, J. B. Multiple Charging in Electrospray Ionization of Poly(Ethylene Glycols). *J. Phys. Chem.* **1988**, *92* (2), 546–550. https://doi.org/10.1021/j100313a058.

(9) Loo, J. A.; Udseth, H. R.; Smith, R. D.; Futrell, J. H. Collisional Effects on the Charge Distribution of Ions from Large Molecules, Formed by Electrospray-Ionization Mass Spectrometry. *Rapid Commun. Mass Spectrom.* **1988**, *2* (10), 207–210. https://doi.org/10.1002/rcm.1290021006.

(10) Polfer, N. C. Supercharging Proteins: How Many Charges Can a Protein Carry? *Angew. Chemie Int. Ed.* **2017**, *56* (29), 8335–8337. https://doi.org/10.1002/anie.201704527.

(11) Kumar Kailasa, S.; Hasan, N.; Wu, H. F. Identification of Multiply Charged Proteins and Amino Acid Clusters by Liquid Nitrogen Assisted Spray Ionization Mass Spectrometry. *Talanta* **2012**, *97*, 539–549. https://doi.org/10.1016/j.talanta.2012.05.011.

(12) Lomeli, S. H.; Peng, I. X.; Yin, S.; Ogorzalek Loo, R. R.; Loo, J. A. New Reagents for Increasing ESI Multiple Charging of Proteins and Protein Complexes. *J. Am. Soc. Mass Spectrom.* **2010**, *21* (1), 127–131. https://doi.org/10.1016/j.jasms.2009.09.014.

(13) Sampson, J. S.; Hawkridge, A. M.; Muddiman, D. C. Generation and Detection of Multiply-Charged Peptides and Proteins by Matrix-Assisted Laser Desorption

Electrospray Ionization (MALDESI) Fourier Transform Ion Cyclotron Resonance Mass Spectrometry. *J. Am. Soc. Mass Spectrom.* **2006**, *17* (12), 1712–1716. https://doi.org/10.1016/j.jasms.2006.08.003.

(14) Cheung, R. C. F.; Ng, T. B.; Wong, J. H.; Chan, W. Y. Chitosan: An Update on Potential Biomedical and Pharmaceutical Applications. *Marine Drugs*. MDPI AG August 1, 2015, pp 5156–5186. https://doi.org/10.3390/md13085156.

(15) Bose, A.; Wong, T. W. Oral Colon Cancer Targeting by Chitosan Nanocomposites. **2018**. https://doi.org/10.1016/B978-0-12-813741-3.00018-2.

(16) Kim, J.; Kim, J.; Hong, J.; Lee, S.; Park, S.; Lee, J.; Kim, J. LC – MS / MS Analysis of Chitooligosaccharides. *Carbohydr. Res.* **2013**, *372*, 23–29. https://doi.org/10.1016/j.carres.2013.02.007.

(17) Su, Y.; Hu, Y.; Du, Y.; Huang, X.; He, J.; You, J.; Yuan, H.; Hu, F. Redox-Responsive Polymer-Drug Conjugates Based on Doxorubicin and Chitosan Oligosaccharide- g -Stearic Acid for Cancer Therapy. *Mol. Pharm.* **2015**, *12* (4), 1193–1202. https://doi.org/10.1021/mp500710x.

(18) Dasgupta, A.; Klein, K. Herbal and Other Dietary Supplements That Are Antioxidants. In *Antioxidants in Food, Vitamins and Supplements*; Elsevier, 2014; pp 295–315. https://doi.org/10.1016/b978-0-12-405872-9.00016-1.

(19) Jerosch, J.; Jimenez, S. Effects of Glucosamine and Chondroitin Sulfate on Cartilage Metabolism in OA: Outlook on Other Nutrient Partners Especially Omega-3 Fatty Acids. *Int. J. Rheumatol.* **2011**, *2011*, 17. https://doi.org/10.1155/2011/969012.

(20) Shao, Y.; Alluri, R.; Mummert, M.; Koetter, U.; Lech, S. A Stability-Indicating HPLC Method for the Determination of Glucosamine in Pharmaceutical Formulations. *J. Pharm. Biomed. Anal.* **2004**, *35* (3), 625–631. https://doi.org/10.1016/j.jpba.2004.01.021.

(21) Pedrali, A.; Bleve, M.; Capra, P.; Jonsson, T.; Massolini, G.; Perugini, P.; Marrubini, G. Determination of N-Acetylglucosamine in Cosmetic Formulations and Skin Test Samples by Hydrophilic Interaction Liquid Chromatography and UV Detection. *J. Pharm. Biomed. Anal.* **2015**, *107*, 125–130. https://doi.org/10.1016/j.jpba.2014.12.014.

(22) Retention and Selectivity of Polar Neutral Molecules in HILIC | Sigma-Aldrich https://www.sigmaaldrich.com/technical-documents/articles/analytical/pharmaceutical/hilic-polar-neutral-molecules.html (accessed May 18, 2020).

(23) Banoub, J.; Boullanger, P.; Lafont, D.; Cohen, A.; El Aneed, A.; Rowlands, E. In Situ Formation of C-Glycosides during Electrospray Ionization Tandem Mass Spectrometry of a Series of Synthetic Amphiphilic Cholesteryl Polyethoxy Neoglycolipids Containing N-Acetyl-D-Glucosamine. *J. Am. Soc. Mass Spectrom.* **2005**, *16* (4), 565–570. https://doi.org/10.1016/j.jasms.2005.01.003.

(24) Roda, A.; Sabatini, L.; Barbieri, A.; Guardigli, M.; Locatelli, M.; Violante, F. S.; Rovati, L. C.; Persiani, S. Development and Validation of a Sensitive HPLC-ESI-MS/MS Method for the Direct Determination of Glucosamine in Human Plasma. *J. Chromatogr. B Anal. Technol. Biomed. Life Sci.* **2006**, *844* (1), 119–126. https://doi.org/10.1016/j.jchromb.2006.07.013.

(25) Sleno, L. The Use of Mass Defect in Modern Mass Spectrometry. *J. Mass Spectrom.*

2012, *47* (2), 226–236. https://doi.org/10.1002/jms.2953.

(26) Pourshahian, S. Mass Defect from Nuclear Physics to Mass Spectral Analysis. *J. Am. Soc. Mass Spectrom.* **2017**, *28* (9), 1836–1843. https://doi.org/10.1007/s13361-017-1741-9.

(27) Fuerstenau, S. D.; Benner, W. H. Molecular Weight Determination of Megadalton DNA Electrospray Ions Using Charge Detection Time-of-flight Mass Spectrometry. *Rapid Commun. Mass Spectrom.* **1995**, *9* (15), 1528–1538. https://doi.org/10.1002/rcm.1290091513.

(28) Impact of Mobile Phase Additives on LC-MS Sensitivity, Demonstrated using Spice Cannabinoids | Sigma-Aldrich https://www.sigmaaldrich.com/technical-documents/articles/analytical/bioanalytical/lcms-spice-cannabinoids.html (accessed May 19, 2020).

(29) Liang, Y.; Guan, T.; Zhou, Y.; Liu, Y.; Xing, L.; Zheng, X.; Dai, C.; Du, P.; Rao, T.; Zhou, L.; et al. Effect of Mobile Phase Additives on Qualitative and Quantitative Analysis of Ginsenosides by Liquid Chromatography Hybrid Quadrupole-Time of Flight Mass Spectrometry. *J. Chromatogr. A* **2013**, *1297*, 29–36. https://doi.org/10.1016/j.chroma.2013.04.001.

(30) Hughes, J.; Fandino, A.; Mcintyre, D.; Presser, D.; Stone, P.; Szczesnieski, A.; Tichy, S.; Weil, D.; Phillips, L. *Agilent 6400 Series Triple Quadrupole LC/MS/MS Users Workshop North America QQQ Method Development and Optimization MassHunter Quant: Method Setup Peak Detection Optimization Quant Troubleshooting*.

(31) Cronan, P. *Introduction to Mass Spectrometry Ionization Sources, Ion Trajectory, and Method Development*; 2012.

(32) Kumirska, J.; Czerwicka, M.; Kaczyński, Z.; Bychowska, A.; Brzozowski, K.; Thöming, J.; Stepnowski, P. Application of Spectroscopic Methods for Structural Analysis of Chitin and Chitosan. *Mar. Drugs* **2010**, *8* (5), 1567–1636. https://doi.org/10.3390/md8051567.

(33) Mortier, K. A.; Zhang, G. F.; Van Peteghem, C. H.; Lambert, W. E. Adduct Formation in Quantitative Bioanalysis: Effect of Ionization Conditions on Paclitaxel. *J. Am. Soc. Mass Spectrom.* **2004**, *15* (4), 585–592. https://doi.org/10.1016/j.jasms.2003.12.013.

(34) Cole, R. B.; Zhu, J. Chloride Anion Attachment in Negative Ion Electrospray Ionization Mass Spectrometry†. *Rapid Commun. Mass Spectrom.* **1999**, *13* (7), 607–611. https://doi.org/10.1002/(SICI)1097-0231(19990415)13:7<607::AID-RCM530>3.0.CO;2-2.

(35) Zhu, J.; Cole, R. B. Formation and Decompositions of Chloride Adduct Ions, [M + Cl]-, in Negative Ion Electrospray Ionization Mass Spectrometry. *J. Am. Soc. Mass Spectrom.* **2000**, *11* (11), 932–941. https://doi.org/10.1016/S1044-0305(00)00164-1.

(36) Yin, S.; Loo, J. A. Top-down Mass Spectrometry of Supercharged Native Protein-Ligand Complexes. *Int. J. Mass Spectrom.* **2011**, *300* (2–3), 118–122. https://doi.org/10.1016/j.ijms.2010.06.032.

(37) Chattopadhyay, D. P.; Inamdar, M. S. Aqueous Behaviour of Chitosan. *Int. J. Polym. Sci.* **2010**, *2010*. https://doi.org/10.1155/2010/939536.

(38) Gowariker, V.; … N. V.-P.; 1986, undefined. Polymer Solutions. *New Age Int. New Delhi …*.

(39) Polymers, A. T.-P. C. of; 1972, undefined. Rheological Properties of Polymers in

Viscofluid State. *MIR Publ. Moscow, Russ.*

(40) NIR, I.; FELDMAN, Y.; ASERIN, A.; GARTI, N. Surface Properties and Emulsification Behavior of Denatured Soy Proteins. *J. Food Sci.* **1994**, *59* (3), 606–610. https://doi.org/10.1111/j.1365-2621.1994.tb05573.x.

(41) Konermann, L.; Douglas, D. J. Equilibrium Unfolding of Proteins Monitored by Electrospray Ionization Mass Spectrometry: Distinguishing Two-state from Multi-state Transitions. *Rapid Commun. Mass Spectrom.* **1998**, *12* (8), 435–442. https://doi.org/10.1002/(SICI)1097-0231(19980430)12:8<435::AID-RCM181>3.0.CO;2-F.

(42) Tapia, J. B.; Hibbard, H. A. J.; Reynolds, M. M. Derivatization of Dextran for Multiply Charged Ion Formation and Electrospray Ionization Time-of-Flight Mass Spectrometric Analysis. *J. Am. Soc. Mass Spectrom.* **2017**, *28* (10), 2201–2208. https://doi.org/10.1007/s13361-017-1717-9.

CHAPTER 3

EFFECTS OF NITROSATING AGENTS ON CHITOSAN'S STRUCTURE

3.1 Overview

The first application of the methods developed in Chapter 2 was to track the degradation of chitosan polymer under the influence of nitrosating agents. As chitin's most common derivative, chitosan is frequently modified to enhance its functionality in medical research. Modifications to and derivatizations often involve exposing chitosan polymers to compounds that may not be chemically innocuous. A survey of literature in which chitosan derivatives are modified to produce nitrosating agents led to a question: Is chitosan's structural integrity retained during these derivatizations, or do these result in appreciable degradation? The applications of nitrosated chitosan derivatives are usually medical in nature, so a thorough understanding of potential byproducts is crucial to these materials eventually gaining FDA approval. We hypothesized that the exposure of chitosan to harsh chemical agents render it susceptible to degradation, and that this can be monitored by screening the potential low molecular weight degradation products via mass spectrometry. To test this, we exposed chitosan polymer to a variety of nitrosating conditions, then used mass spectrometry to assess whether degradation had occurred.

Chitosan has received substantial attention as a biomaterial due to its unique properties. It has become increasingly common to derivatize chitosan to produce nitric oxide (NO)-releasing materials that exert various therapeutic effects through the action of NO. It is generally the case that these NO-releasing polymers are prepared by exposure to high-pressure NO or nitrosating agents like nitrous acid (HNO_2) or alkyl nitrites (RONO). In our study, mass spectrometry and

spectroscopic methods demonstrate that both monomeric and oligomeric glucosamine experience chemical alteration after exposure to HNO_2-based nitrosating conditions from the literature. In polymeric chitosan, HNO_2-based nitrosating conditions were found to induce degradation through the formation of 2,5-anhydro-D-mannose and oligosaccharides. In contrast, the RONO *tert*-butyl nitrite and high-pressure NO were not found to significantly degrade or otherwise alter the structure of glucosamine or its oligomers, supporting the suitability of these approaches.

3.2 Introduction

Nitric oxide (NO) is ubiquitous in mammalian biochemistry, where it is produced by the vascular endothelium to regulate vasodilation, immune cells (*e.g.*, macrophages) as an antimicrobial agent, and nerve cells as a critical neurotransmitter[1]. These physiological roles have led to the conscription of exogenous NO as a therapeutic agent. Because NO is highly reactive and exhibits a short half-life under physiological conditions, the use of more stable NO prodrugs has greatly facilitated the continuing development of NO-based therapies. These prodrugs typically take the form of molecules or specific functional groups that spontaneously decompose to form NO[2]. In recent years, the fabrication of biomaterials ranging from bulk polymers to nanomaterials that exhibit NO-forming properties has received considerable attention[3,4]. Due to their natural origin and medically-useful properties, polysaccharides have been frequently modified to include NO donor moieties. As early as 1996, Smith *et al.* demonstrated that NO-forming *N*-diazeniumdiolate groups could be grafted to the branched polysaccharide dextran (consisting of α-1,6 and α-1,3-linked glucose units)[5]. This principle was later applied to the glycosaminoglycan heparin, which is commonly used in medicine as an anticoagulant[6]. More recently, chitosan (a naturally-derived copolymer consisting of β-1,4-linked D-glucosamine [GlcN] and *N*-acetyl-D-glucosamine [GlcNAc]) has been investigated as a platform for NO delivery applications. Lu *et*

al. produced water-soluble NO-releasing chitosan oligosaccharides (COS) bearing *N*-diazeniumdiolate groups that were found to exhibit pronounced antibacterial effects against *Pseudomonas aeruginosa*[7]. It was subsequently demonstrated that the antibacterial properties of NO-releasing COS could be preserved when using the *S*-nitrosothiol functional group as an alternative NO donor[8]. The versatility of chitosan as a biomaterial and the broad therapeutic potential of NO has led to the use of chitosan-derived NO-releasing materials for proposed applications that include disruption of bacterial biofilms[9], transdermal delivery of NO[10], treatment of Crohn's disease[11], wound-healing[12,13], and prevention of platelet adhesion[14]. In general, this category of material is intended to exert therapeutic effects through the spontaneous production of NO in a biological environment.

Chitosan is typically obtained from alkaline deacetylation of chitin, a biopolymer of GlcNAc that occurs as a structural component of the shells of marine crustaceans and fungal cell walls[15]. This deacetylation is rarely complete and yields a copolymer consisting predominantly of GlcN (>50%) and GlcNAc that can be dissolved in aqueous acid and exhibits hemostatic, antimicrobial, and wound-healing properties[16]. These properties have been paired with the known physiological effects of NO to produce NO-releasing chitosan derivatives for therapeutic applications. The primary approach to the development of such materials involves the chemical derivatization of chitosan to include thiol or secondary amine groups, which be subsequently converted to *S*-nitrosothiols or *N*-diazeniumdiolates that generate gaseous NO in response to an appropriate trigger (*e.g.*, light or pH). In the specific case of thiol-bearing chitosan derivatives, treatment with HNO_2 may form *S*-nitrosothiols according to the equation $RSH + HNO_2 \rightarrow RSNO + H_2O$[17]. Because chitosan is composed of structurally complex repeating units derived from both GlcN and GlcNAc, there is significant potential for undesirable reactions with other functional groups. For

example, it is known that the reaction of HNO_2 with alcohols results in the formation of alkyl nitrites[18]. More importantly, the reaction of HNO_2 with aliphatic primary amines results in the initial formation of a primary nitrosamine, followed by further reaction to yield an unstable aliphatic diazonium intermediate[19]. In the case of GlcN, nitrogen gas is displaced from this intermediate by an internal rearrangement, resulting in ring-contraction and the formation of 2,5-anhydro-D-mannose (2,5-AM)[19]. As an example, Claustre *et al.* (among others) previously prepared 2,5-AM by the deamination of GlcN hydrochloride using $NaNO_2$ and a strong cation-exchange resin[20,21]. It has been established by substantial prior work that this reactivity extends to polymers that include GlcN structural units, often inducing depolymerization[22,23].

In an idealized scenario, the preparation of an NO-releasing chitosan derivative is achieved through a sequence of reactions in which a precursor to an NO donor (a thiol in the case of *S*-nitrosothiols and secondary amine in the case of *N*-diazeniumdiolates) is grafted to the polysaccharide, followed by exposure of this conjugate to chemical agents that are intended to form an NO donor from the grafted functional group. However, the ability of the primary amine group of GlcN to react under such conditions renders the polymer susceptible to chemical alteration or degradation that may impact its proposed structure or function. Both nitrous acid (HNO_2) and alkyl nitrites (RONO) function as *nitrosating agents* (formal donors of NO^+) in solution that may effect the conversion of nucleophilic functional groups to nitrosated derivatives[2,18]. This reactivity is often exploited in the synthesis of NO-releasing compounds such as *S*-nitrosothiols through treatment of thiol precursors with HNO_2. For instance, Lu *et al*. treated a solution of thiol-bearing chitosan oligosaccharides with sodium nitrite under acidic conditions to produce an *S*-nitrosated derivative[8]. Simon-Walker *et al.* immersed titania nanotube arrays

coated with a chitosan-thioglycolic acid conjugate in *tert*-butyl nitrite (*t*-BuONO) to impart NO release properties through the putative formation of *S*-nitrosothiol functional groups[14].

However, GlcN units in chitosan may undergo undesirable reactions in the presence of HNO_2/RONO that result in significant structural alteration. The *N*-nitrosation of aliphatic primary amines by HNO_2 is known to result in deamination through diazotization and subsequent displacement of N_2[19]. This reactivity occurs in the Demjanov and Tiffeneau-Demjanov rearrangements and has been clearly established to occur in the case of glucosamine, where it results in the formation of 2,5-AM[20,24], as shown in **Figure 3.1A**. The deamination of chitosan itself using HNO_2 is accompanied by depolymerization and the production of 2,5-AM in a manner analogous to the reaction of monomeric GlcN[21]. The ability of HNO_2 to initiate the deamination and depolymerization of polysaccharides is not confined to chitosan, and also occurs in the case of heparin and other polymers that contain GlcN units[22,25,26]. Other functional groups present in chitosan may also react in the presence of nitrosating agents, including alcohols[27] and amides[28].

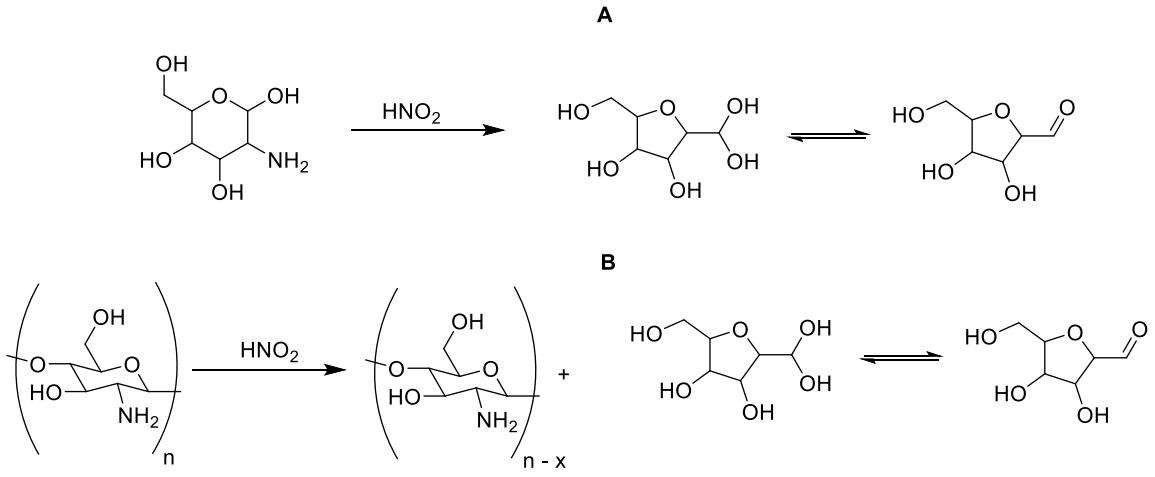

Figure 3.1: Scheme **A** shows 2,5-AM formation from glucosamine as a result of exposure to HNO_2. Scheme **B** shows 2,5-AM formation as a result of a GlcN polymer or oligomer exposure to HNO_2, where n represents the degree of polymerization and x represents the number of repeating units in the cleaved segment.

It is evident that exposure of chitosan to nitrosating agents is not chemically innocuous, and may result in depolymerization or other structural alterations. Curiously, this phenomenon has been largely ignored during the development of NO-releasing materials derived from chitosan. NO-releasing chitosan derivatives are rarely subjected to rigorous analytical scrutiny following their synthesis, and it remains unclear if the original structure and behavior of the polysaccharide is retained, yielding the possibility of chemical modifications to its structure such as those shown in **Figure 3.1B**. This work seeks to elucidate the structural changes that may be induced in chitosan following exposure to common conditions used to produce NO-releasing derivatives. The chief structural constituents of chitosan (GlcN and GlcNAc), a COS model system, and chitosan itself were variously exposed to HNO_2, *t*-BuONO, and gaseous NO to replicate typical literature protocols for the synthesis of *S*-nitrosothiols and *N*-diazeniumdiolates, the most frequent NO donors grafted to chitosan. The products were characterized through a combination of ^{1}H and ^{13}C nuclear magnetic resonance (NMR), attenuated total reflectance Fourier transform infrared spectroscopy (ATR-FTIR), and time-of-flight mass spectrometry (MS).

3.3 Materials and methods

3.3.1 Materials

Chitosan oligosaccharides (COS, <3000 MW, 93% deacetylated) were obtained from Carbosynth (Compton, Berkshire, UK). Chitosan (PROTASAN UP B 90/20, 80 kDa MW, 96% deacetylated) was obtained from NovaMatrix (Sandvika, Norway). D-Glucosamine hydrochloride (99.9%) was obtained from Calbiochem (Darmstadt, DE). *N*-Acetyl-D-glucosamine (<98.0%) was obtained from TCI (Portland, OR). Sodium methoxide (98%) and *tert*-butyl nitrite (*t*-BuONO, 90%) were obtained from Alfa Aesar (Haverhill, MA). Anhydrous ACS grade diethyl ether, ACS grade sodium nitrite (97.0%), concentrated hydrochloric acid, HPLC grade methanol, and LC-MS

grade water were obtained from EMD Millipore (Burlington, MA). Anhydrous ethanol was obtained from Pharmco (Brookfield, CT).

3.3.2 Spectroscopic characterization

Infrared (IR) spectra were collected using attenuated total reflectance (ATR) on a Nicolet 6700 FT-IR spectrometer (Thermo Electron Corp., Madison, WI, USA) fitted with a Smart iTR ATR sampling accessory and a ZnSe crystal plate. Nuclear magnetic resonance (NMR) spectra (^{1}H) were acquired using a Bruker Avance Neo 400 spectrometer. Deuterium oxide (D_2O) was used to dissolve GlcN, GlcNAc, and COS samples, while a 1 M solution of deuterium chloride in D_2O (DCl/D_2O) was generally used to dissolve chitosan. Samples were dissolved at a concentration of either 50 mg mL^{-1} (COS and chitosan) or 100 mg mL^{-1} (GlcN and GlcNAc) and compounds that experience pronounced mutarotation were allowed to equilibrate for 1 day prior to analysis.

3.3.3 Mass spectrometry

Mass spectra were acquired using an Agilent 6224 time-of-flight mass spectrometer (Agilent, Palo Alto, CA, USA) equipped with a dual electrospray ion source. Samples were prepared at a concentration of ~1 mg ml^{-1} in LC/MS grade water. The solutions were injected directly into the source without a pre-separation step at a flow rate of 0.220 mL/min using an Agilent 1260 high-performance quaternary liquid chromatograph (Agilent, Palo Alto, CA, USA) with an isocratic mobile phase composed of 50:50 methanol:water. Spectra were acquired in negative ion mode. The ion source conditions were as follows: 2500V capillary voltage, 120V fragmentor voltage, 60V skimmer voltage, 250V octupole voltage, 10 L min^{-1} gas flow (N_2), and 45 psig nebulizer pressure. The detection range was set to 120-3200 *m/z*.

3.3.4 Experimental conditions

Nitrous acid protocol. GlcN hydrochloride (0.323 g, 1.5 mmol), GlcNAc (0.332 g, 1.5 mmol), COS (0.242 g, approximately 1.5 mmol based on the mass of the GlcN repeating unit), or chitosan (0.242 g) was measured into a 20-mL scintillation vial, dissolved in LC-MS grade water, and cooled to 0 °C using an ice bath. Equimolar quantities (1.5, 0.75, or 0.15 mmol) of hydrochloric acid (5 M) and an aqueous solution of sodium nitrite (0.515 g mL^{-1}) were added. The total volume of each solution was 5 mL, and the sealed vials were agitated at 0 °C for 2 h. Following this reaction period, the solvent and other volatiles were removed under vacuum (<100 mTorr) to obtain a constant weight.

Alkyl nitrite protocol. GlcN hydrochloride (0.323 g, 1.5 mmol), GlcNAc (0.332 g, 1.5 mmol), or COS (0.242 g, approximately 1.5 mmol) was measured into a 20-mL scintillation vial. Each sample was immersed in excess *t*-BuONO (2 mL) without additional solvent for 2 h at 0 °C, then the liquid was removed from the insoluble oligosaccharide by pipette. Samples were then washed with diethyl ether and placed under vacuum (<100 mTorr) until a constant weight was obtained. A modified form of this protocol was also evaluated in which the respective substrate was agitated in a mixture of 2 mL of *t*-BuONO and 2 mL of LC-MS grade water.

High-pressure NO protocol. COS (30 mg, approximately 0.19 mmol) were suspended in a 5.4 mM sodium methoxide solution in either methanol (2 mL) or methanol/water (2 mL, 6:4 v/v). The suspensions were placed in polymer-coated Parr hydrogenation vessels and pressurized to 100 psi with NO gas for 36 h using a high-pressure line. Suspensions were agitated using magnetic stir plates for the duration of the experiments. O_2 was rigorously excluded from the experiments by thorough purging with argon gas.

Low-pressure NO protocol. GlcN hydrochloride (0.323 g, 1.5 mmol) or COS (0.242 g, approximately 1.5 mmol) were added to 20-mL scintillation vials and dissolved in 5 mL of LC-MS grade water. A constant flow of NO gas was bubbled through each solution for 10 min, then the sealed vials were allowed to stand for 16 h at ambient temperature (22 °C). The solvent and other volatiles were removed under vacuum (<100 mTorr) until the samples reached a constant weight. A modified form of this protocol was also evaluated in which both NO and air were bubbled through the solution simultaneously.

3.4 Results and discussion

3.4.1 Nitrous acid protocol

To evaluate the effect of HNO_2 on chitosan, we selected a COS model system that facilitates characterization of low molecular weight oligosaccharide units by MS. COS (approximately 1.5 mmol, as estimated by the repeating unit mass of GlcN) was dissolved in LC-MS grade water at 0 °C and treated with 1, 0.5, and 0.1 molar equivalents (relative to GlcN) of HNO_2 that was formed *in situ* from the reaction of $NaNO_2$ and hydrochloric acid. The concentrations of HNO_2 were 300, 150, and 30 mM, respectively. Vigorous bubbling was immediately observed at the two higher concentrations and was attributable to the production of nitrogen gas as a consequence of the deamination of GlcN units. Bubbling remained visually detectable even at 30 mM HNO_2, and was largely complete within several minutes. After agitating for 2 h at 0 °C, the solvent was removed under vacuum to isolate the solid products for further characterization. COS species with 2-5 residues were observed *via* MS in negative ion mode as $[M + Cl]^-$ chlorinated adducts. After exposure to HNO_2 at concentrations greater than 0.1 mole equivalents, new ion formation was observed at 197 *m/z* $[C_6H_{10}O_5 + Cl^-]$ and at 215 *m/z* $[C_6H_{12}O_6 + Cl^-]$, corresponding to 2,5-AM and its putative hydrated form. Higher molecular weight species were not observed to undergo similar

rearrangements; however, this does not necessarily preclude their existence. Decreased ionization efficiency due to molecule size combined with a relatively low conversion rate leaves the possibility that high molecular weight rearrangements are below the limit of detection given the methods used. Non-monomeric species decreased in relative proportion to GlcN and GlcNAc for all hydrochloric acid concentrations, indicating that exposure to even relatively dilute concentrations of hydrochloric acid exerts a degradative effect on the oligomer. 2,5-AM was detectable by MS after exposure to HNO_2 concentrations greater than 0.1 mole equivalent, indicating that the anticipated HNO_2-mediated deamination proceeds even at concentrations substantially lower than are used in literature.

Due to substantial peak overlap and the absence of definitive assignments, identification of the 2,5-AM product is less certain using ^{1}H NMR. The initial ^{1}H NMR spectrum of COS is characterized by a broad region between 4.0 and 3.3 ppm that is attributable to C3-C6 protons of the hexose structure, while upfield features at 3.1 and 2.0 ppm are assigned to C2 and *N*-acetyl protons from GlcNAc units, respectively[29]. C1 protons overlap with the HDO peak at 4.8 ppm and are not independently resolved. Several minor peaks occur in the range of 8.4-8.0 ppm that likely arise from oxidation of GlcN or GlcNAc units during commercial preparation of the oligosaccharide using H_2O_2 [30]. Upon treatment with 1 eq. of HNO_2, a fine structure emerges from the broad oligomeric peaks that is characteristic of small molecule formation, accompanied by the development of new peaks at 5.1, 4.1, and 4.0 ppm as shown in **Figure 3.2** that are presumably attributable to downfield protons of 2,5-AM. These features remain detectable after treatment with 0.5 eq. of HNO_2, but are no longer clearly resolved at 0.1 eq. of HNO_2. ATR-FTIR remained generally consistent with the starting material. This collected data indicates that the deamination of GlcN units by HNO_2 is not quantitative, but occurs to a detectable extent by MS and ^{1}H NMR.

We note that the reactions in this study were performed at comparatively low hydrochloric acid concentrations of 300-30 mM. In comparison, literature conditions used to prepare NO-releasing chitosan derivatives have used significantly higher concentrations (as much as 1.25 M)[8]. It is therefore sensible to consider the likelihood that hydrochloric acid itself may independently degrade chitosan. Treatment of chitosan with hydrochloric acid is commonly used to reduce chain length through hydrolysis. Li *et al.* evaluated the ability of hydrochloric acid to degrade chitosan to GlcN *via* β-1,4-glycosidic bond cleavage at varying concentrations[31]. In this study, GlcN formation as a result of acid hydrolysis was observed at hydrochloric acid concentrations in the range of 4-10 M[31]. Given this possibility, considerable hydrolytic degradation of COS could reasonably be expected under highly acidic conditions that may limit the preservation of higher molecular weight species in reaction products. In general, it seems inadvisable to attempt the nitrosation of chitosan (or other GlcN -containing polymers) using HNO_2, particularly in the presence of concentrated hydrochloric acid.

To determine whether the formation of 2,5-AM could be identified following treatment of chitosan (80 kDa MW) with HNO_2, the polymer was suspended in water (in which the non-cationic form exhibited poor solubility in the absence of acid) and exposed to 1 equivalent of HNO_2. As in the case of COS, evolution of gas was apparent following the addition of sodium nitrite. The product was subsequently isolated and characterized by MS and ^{1}H NMR. Mass spectra showed oligomeric species formation along with GlcNAc at 256 *m/z* and 2,5-AM at 215 *m/z*, as shown in **Figure 3.3**. IR indicated generally conserved absorbances. In the ^{1}H NMR spectrum of chitosan in 1 M DCl/D_2O, C1 protons of deacetylated and acetylated units are present at 4.8 and 4.5 ppm, respectively. The broad resonances ranging from 4.0 to 3.3 ppm are largely attributable to C3-C6 protons, with the C2 protons of deacetylated units appearing upfield at 3.0 ppm. The methyl

protons of *N*-acetyl groups produce a minor signal at 1.9 ppm. Following exposure to 1 eq. of HNO_2, the spectrum is substantially altered and is no longer recognizable. While changes occur throughout the spectrum, the appearance of a prominent multiplet at 4.9 ppm that is accompanied by triplets at 4.0 and 3.9 ppm is consistent with the product identified as 2,5-AM in experiments carried out with COS.

To elucidate differences in reactivity between GlcN and GlcNAc units of chitosan, both compounds were treated with HNO_2 under conditions identical to those used for the COS study. GlcN itself was observed by MS in negative ion mode as the chlorinated adduct at 214 *m/z* [$C_6H_{13}NO_5 + Cl^-$], and remained detectable in the samples after treatment with HNO_2. As expected from literature precedence[20,24], 2,5-AM was also observed at 197 [$C_6H_{10}O_5 + Cl^-$] and 215 *m/z* [$C_6H_{12}O_6 + Cl^-$]. The ^{1}H NMR spectrum of GlcN displays diagnostic peaks appearing downfield of HDO at 5.43 (d, J = 3.6 Hz) and 4.94 ppm (d, J = 8.5 Hz) and can be assigned to the resonances of α- GlcN and β- GlcN, respectively. Following exposure to HNO_2, an apparent doublet develops at 5.08 ppm (J = 5.2 Hz), with less clearly resolved features appearing at 4.17 and 4.04 ppm. Collectively, these are the sole distinguishable ^{1}H NMR features that result from exposure of GlcN to HNO_2, although subtle changes are present elsewhere in the spectra. These modifications can be seen in **Figure 3.4**. ATR-FTIR spectra indicated generally conserved absorbances. In the case of the *N*-acetylated monomer MS of the starting material exhibited a peak at 256 m/z [$C_8H_{15}NO_6 + Cl]^-$ that corresponded to GlcNAc. MS of products treated with HNO_2 displayed the same peak, without the formation of 2,5-AM or other products. The combined MS and spectroscopic data acquired for GlcN after exposure to HNO_2 supports deamination and concomitant rearrangement of the substrate to 2,5-AM, as predicted by prior reports[19,24]. Notably, ^{1}H NMR indicates that the reaction does not proceed to completion with a stoichiometric quantity of HNO_2, and the majority

of GlcN is recovered at the end of the reaction. In contrast with the results for GlcN, there is no evidence that GlcNAc is sensitive to structural changes in the presence of HNO_2. Since the COS utilized in this study primarily consist of GlcN structural units, it is unsurprising that the formation of 2,5-AM is detectable in their mass spectra following reaction with HNO_2. Mass spectra of chitosan following exposure to HNO_2 indicated that polysaccharide degradation and hydrated 2,5-AM formation at 215 *m/z* occurred upon exposure to all reactant concentrations used as indicated by previously unobserved oligomer and monomer species.

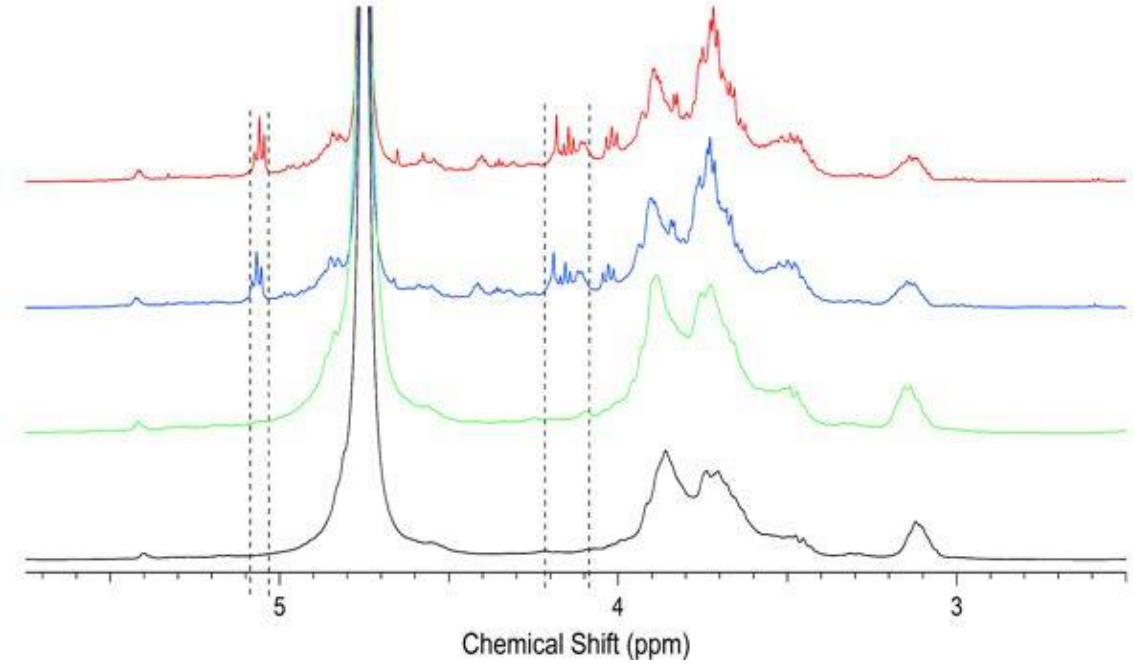

Figure 3.2: Overlay of COS species subjected to nitrous acid protocol where black = starting material, green = 0.1 mole equivalents HCl, blue = 0.5 mole equivalents HCl and red = 1 mole equivalent of HCl.

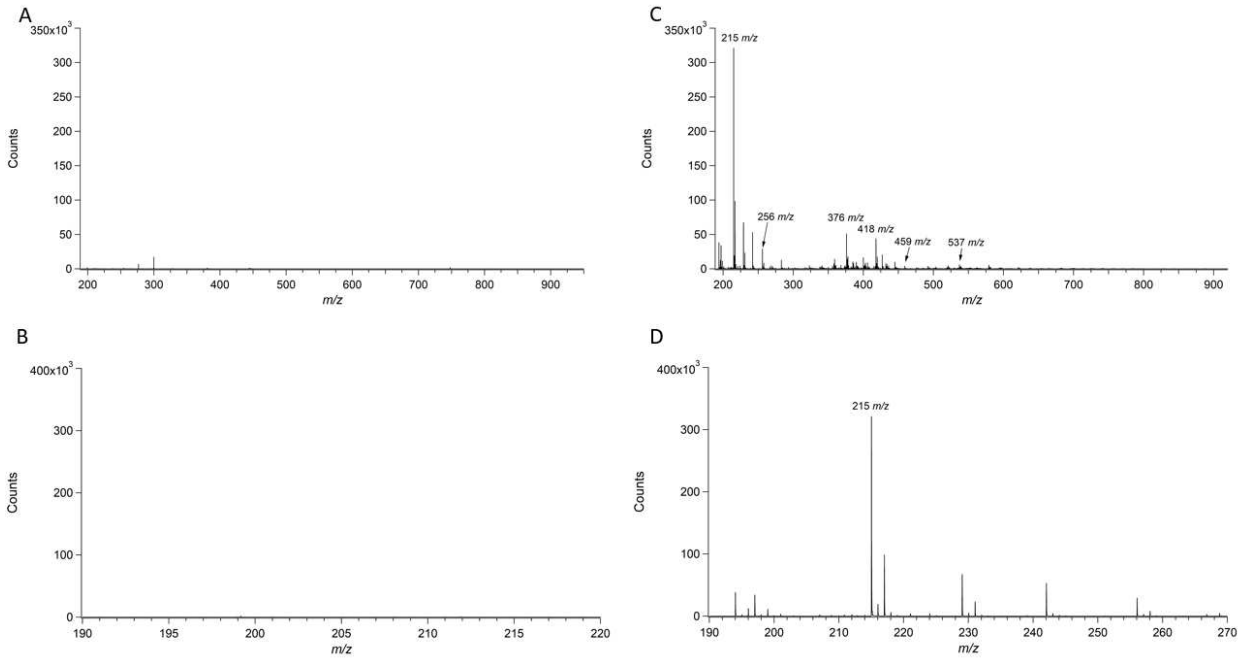

Figure 3.3: Mass spectra of 80 kDa chitosan before and after exposure to HNO_2. Insets A and B show the full spectrum and the magnification of the area of interest, respectively of unadulterated chitosan. Insets C and D show the full spectrum and magnification of the area of interest where the peak at 215 *m/z* is indicative of a compound with a formula consistent with a chlorinated hydrated 2,5-anhydro-D-mannose adduct, $[C_6H_{10}O_5 + Cl]^-$. The peak at 256 *m/z* is indicative of a compound with a molecular formala consistent with a chlorinated GlcNAc adduct, $[C_8H_{15}NO_6 + Cl]^-$. Remaining labeled peaks are indicative of compounds with molecular formulas consistent with the chlorinated COS adducts listed in **Table B.1** in the Appendix B.

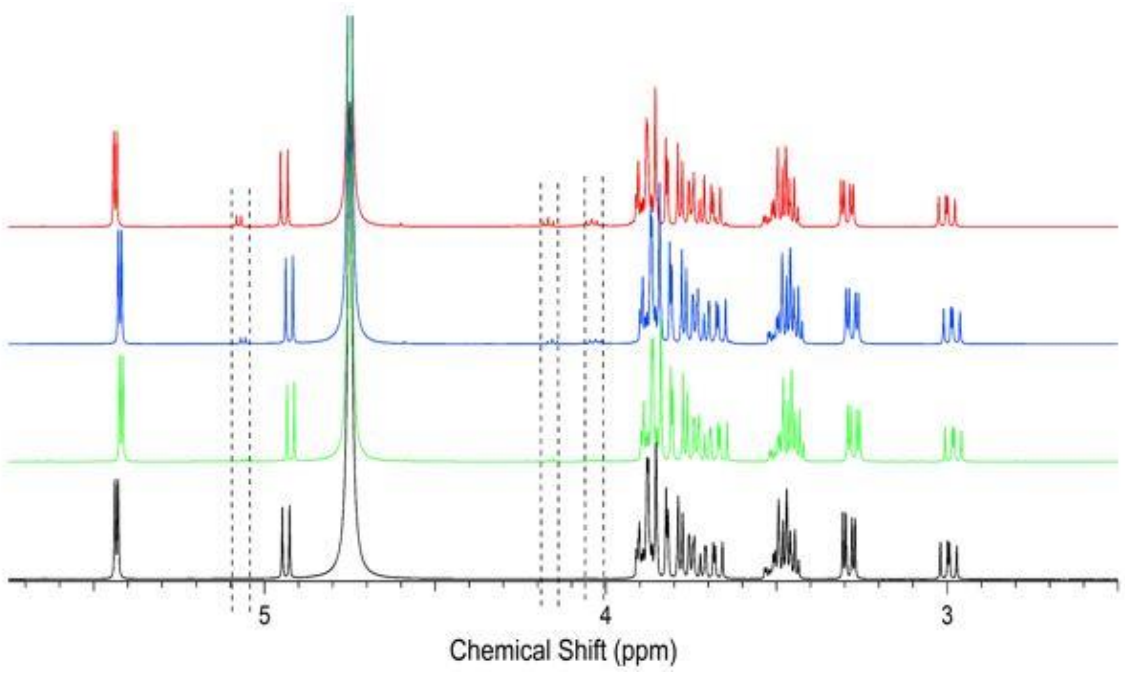

Figure 3.4: Overlay of GlcN subjected to nitrous acid protocol where black = starting material, green = 0.1 mole equivalents HCl, blue = 0.5 mole equivalents HCl and red = 1 mole equivalent of HCl.

3.4.2 Alkyl nitrite protocol

Alkyl nitrites are the chief alternative to HNO_2 in the preparation of RSNOs, and have been previously used to achieve the *S*-nitrosation of thiol-bearing chitosan derivatives[14]. While alkyl nitrites may be directly synthesized from alcohols and HNO_2, several examples are commercially available. Both mono and polysaccharides are predictably insoluble in alkyl nitrites, and previous approaches to synthesis of NO-forming chitosan derivatives involved the exposure of the polymer to *t*-BuONO under heterogeneous conditions[13]. We found that the suspension of COS, GlcN, and GlcNAc in 2 mL of neat *t*-BuONO for 2 h at 0 °C did not produce any detectable 2,5-AM by MS, and *m/z* ratios corresponding to the starting material were preserved. This indicates that nitrosation protocols based on alkyl nitrites *in the absence of water* may have limited effect on the structure of GlcN and GlcNAc. Alkyl nitrites are known to participate in nitrosyl exchange reactions with alcohols ($R_1OH + R_2ONO \rightarrow R_1ONO + R_2OH$), yet this process is either unfavorable with the hydroxyl groups of GlcN/GlcNAc units or the product is unstable in water and is undetected by MS[27]. Following separation from *t*-BuONO under vacuum, ATR-FTIR spectra of COS, GlcN, and GlcNAc did not reveal the development of any new peaks or a decrease in the O-H stretching region, which corroborates a general lack of reactivity and the absence of *O*-nitrosation. This lack of reactivity was further supported by ^{1}H NMR, where no alteration of the normal spectra of COS, GlcN, and GlcNAc was resolved. Since alkyl nitrites are susceptible to HNO_2-forming hydrolysis ($RONO + H_2O \rightarrow ROH + HNO_2$)[32,33]. it was reasoned that the presence of both *t*-BuONO and water could result in the formation of an equilibrium concentration of HNO_2 that would serve as a more potent nitrosating agent. To evaluate this hypothesis, COS were exposed to a 1:1 mixture of *t*-BuONO and water over 2 h at 0 °C. Mass spectra displayed previously unobserved peaks at 215

m/z, indicative of 2,5-AM formation along with decreased proportions of oligomeric to monomeric species. This suggests *t*-BuONO and water in tandem exert a degradative effect on chitosan, similarly to HNO_2 prepared from hydrochloric acid and sodium nitrite. ^1H NMR appeared to support the formation of a distinct product, with new peaks at 5.0, 4.1, and 4.0 ppm that correspond to those observed in the HNO_2 protocol and tentatively assigned to 2,5-AM. Similarly, 80 kDa chitosan was degraded by *t*-BuONO/water to an extent sufficient to render it soluble in D_2O, without the presence of acid. This apparent degradation was accompanied by the development of prominent peaks at 4.9, 4.0, and 3.9 ppm, as well as numerous additional features that remain unassigned. MS of these products suggested polysaccharide degradation occurred, indicated by the formation of relevant oligomers and monomers. Hydrated 2,5-AM was observed at 215 *m/z* along with GlcNAc at 256 *m/z.* As anticipated from the results obtained using the HNO_2 protocol, exposure of GlcN to *t*-BuONO/water produces new peaks at 5.04 (doublet), 4.13 and 4.00 ppm (triplets), while the spectrum of GlcNAc is unchanged. These results indicate that *t*-BuONO does not independently induce the rearrangement of GlcN or its polymeric derivatives, but presumably hydrolyzes in the presence of water to produce HNO_2.

3.4.3 High-pressure nitric oxide protocol

Multiple publications have reported the synthesis of NO-releasing chitosan derivatives containing *N*-diazeniumdiolate functional groups as NO donors[7]. *N*-Diazeniumdiolates are not formed by treatment of amines with nitrosyl transfer agents (*e.g.*, HNO_2 or alkyl nitrites) and are instead prepared *via* direct reaction with NO at high pressure, typically under basic conditions[9,34]. *N*-Diazeniumdiolates synthesized from primary amines exhibit poor stability, therefore the derivatization of chitosan to include secondary amine groups is required to produce useful NO donors with this approach[34]. The decomposition of an unstable primary *N*-diazeniumdiolate may

yield a variety of potential products, including simple regeneration of the parent amine and release of NO according to the equation $RNH(NO)_2 + H^+ \rightarrow RNH_2 + 2\ NO$[35]. In cases where the decomposition pathway is more complex, deamination, alkylation, and nitrosamine formation may be possible[34]. In rare cases, it has been reported that amides may also form *N*-diazeniumdiolates[36]. To assess the susceptibility of chitosan's GlcN and GlcNAc units to reaction under typical *N*-diazeniumdiolate formation conditions, suspensions of COS in both methanol and a methanol/water mixture were pressurized with 100 psi of NO for 3 days in the presence of sodium methoxide. MS of the isolated products was consistent with that of the starting material and lacked ions at 197 and 215 *m/z* associated with 2,5-AM. In addition, we did not observe the appearance of any ions that could be attributed to *N*-diazeniumdiolated GlcN or GlcNAc units or other hypothetical products. ^{1}H NMR and ATR-FTIR similarly failed to elucidate any clear chemical distinction between the COS samples before and after exposure to high-pressure NO. Consequently, no evidence exists to suggest that the saccharide structure of chitosan is irreversibly altered under a high-pressure NO atmosphere.

3.4.4 Low-pressure nitric oxide protocol

The potential sensitivity of chitosan (or any GlcN -containing polymer) to the *indirect* effects of NO is particularly important in the context of NO-releasing derivatives. Upon exposure to water and oxygen, NO may react to form HNO_2 according to the equation $4\ NO + O_2 + 2\ H_2O \rightarrow 4\ HNO_2$. Furthermore, the reaction of NO with oxygen alone produces NO_2 ($2\ NO + O_2 \rightarrow 2\ NO_2$), which may result in the reversible formation of dinitrogen trioxide (N_2O_3) through the reaction $NO + NO_2 \rightarrow N_2O_3$. Since both HNO_2 and N_2O_3 act as nitrosating agents, NO-releasing derivatives of chitosan may be susceptible to self-induced degradation that results from the production of NO under aerobic conditions. NO-releasing chitosan derivatives are rarely recharacterized at the end

of the NO release period, and it remains unclear if NO oxidation products are able to detectably alter the properties of the polysaccharide. When used *in vivo*, it may be anticipated that NO release from chitosan derivatives will result in a negligible local concentration of NO oxidation products due to rapid diffusion of NO and consumption by reaction with the biological environment (*e.g.*, hemoglobin). However, NO assay protocols used for characterization and *in vitro* experimental conditions (*e.g.*, bacteria studies) often confine materials to small volumes that could permit build-up of nitrosating agents. The feasibility of this scenario is supported by the antimicrobial effect of NO-releasing chitosan derivatives, a phenomenon that is mediated by the formation of reactive nitrogen species (RNS) that exert nitrosative stress on microorganisms. To investigate the ability of NO to affect the structure of monomeric GlcN and the COS model system, each substrate was dissolved in water and a constant flow of NO was bubbled through the solution for 10 min. To permit the reaction of NO with the initial equilibrium concentration of dissolved O_2, the solutions were not deoxygenated by inert gas. After recovery of GlcN and COS from solution by vacuum, MS of both substrates did not reveal any apparent change in ion distribution. In particular, MS of COS did not show a proportional decrease in higher molecular weight species or the presence of degradation products formed by direct exposure to HNO_2. This outcome was largely unremarkable, since the steady bubbling of NO is likely to displace O_2 and other dissolved gases and potentially remove volatile nitrosating species. From a practical standpoint, it is largely infeasible for any NO-releasing chitosan derivative to achieve a rate of NO production sufficient to achieve this effect. To evaluate the impact of NO in aqueous solution with *consistent* aeration, both NO and air were bubbled through solutions of COS. Following isolation, no 2,5-AM formation was detectable in COS, although lower proportions of oligosaccharides to monomers were observed. Furthermore, the formation of distinct products after this exposure was similarly

undetected by ^{1}H NMR. Interestingly, in the case of chitosan itself, GlcNAc and 2,5-AM residues were observed in the 80 kDa polysaccharide exposed to this protocol, although ^{1}H NMR failed to detect the expected product. In comparison, both MS and ^{1}H NMR readily detected the formation of the expected product in the case of GlcN. Since GlcNAc was not anticipated to exhibit any reactivity, it was not examined using this approach.

3.5 Conclusions

Because it has become increasingly common to utilize chitosan (in both oligomeric and polymeric forms) as a platform for NO delivery, this study evaluated the susceptibility of the polysaccharide to structural alteration in the presence of NO and common nitrosating agents such as HNO_2 and *t*-BuONO. The use of an oligomeric form of chitosan (COS) permitted facile characterization by MS and various spectroscopic techniques, and monomeric D-glucosamine (GlcN) and *N*-acetyl-D-glucosamine (GlcNAc) were examined as needed to model the unique chemical behavior of these structural units. We confirmed that chitosan is vulnerable to degradation by solution-phase exposure to HNO_2, which results in deamination of GlcN structural units, the formation of the ring-contracted product 2,5-anhydro-D-mannose (2,5-AM), and probable cleavage of anomeric bonds and depolymerization. This degradation is detectable even at an HNO_2 concentration of only 30 mM at 0 °C. In contrast, the use of an alkyl nitrite (*t*-BuONO) under heterogeneous conditions does not result in any identifiable changes to the structure of chitosan. Similarly, direct exposure to NO at both elevated pressure (100 psi) and when bubbled through a solution at ambient pressure had no effect on chitosan, indicating that the synthesis of grafted *N*-diazeniumdiolates is likely to proceed without impact on the structure of the polymer.

As outlined in this work, the susceptibility of GlcN units to deamination and rearrangement supports that HNO_2 is capable of altering the structure of the polysaccharide itself. This alteration

and loss of chemical functionality may be undesirable if biomaterials intend to harness the characteristic therapeutic properties of chitosan, which are directly derived from the structure of GlcN. Moreover, it is clear that comprehensive characterization is necessary for both chitosan and other GlcN -containing polymers that have been subjected to nitrosating conditions. In general, we advise the common-sense use of alkyl nitrites in the absence of water as a milder substitute for HNO_2 in nitrosation reactions involving chitosan or other polysaccharides that contain GlcN repeating units. We also observe that the formation of 2,5-AM serves as a useful fingerprint for the HNO_2-induced deamination of GlcN and can be reliably detected by both MS and ^1H NMR. By exploring the impact of various nitrosating conditions on the structure of GlcN polysaccharides, this work highlights the importance of rigorous characterization of materials to potentially degradative nitrosating processes.

CHAPTER 3 – REFERENCES

(1) Moncada, S.; Palmer, R. M. J.; Higgs, E. A. Nitric Oxide: Physiology, Pathophysiology, and Pharmacology. *Pharmacological Reviews*. 1991, pp 109–142.

(2) Miller, M. R.; Megson, I. L. Recent Developments in Nitric Oxide Donor Drugs. *British Journal of Pharmacology*. June 2007, pp 305–321. https://doi.org/10.1038/sj.bjp.0707224.

(3) Wo, Y.; Brisbois, E. J.; Bartlett, R. H.; Meyerhoff, M. E. Recent Advances in Thromboresistant and Antimicrobial Polymers for Biomedical Applications: Just Say Yes to Nitric Oxide (NO). *Biomaterials Science*. Royal Society of Chemistry August 1, 2016, pp 1161–1183. https://doi.org/10.1039/c6bm00271d.

(4) Yu, S.; Li, G.; Liu, R.; Ma, D.; Xue, W. Dendritic Fe_3O_4 @Poly(Dopamine)@PAMAM Nanocomposite as Controllable NO-Releasing Material: A Synergistic Photothermal and NO Antibacterial Study. *Adv. Funct. Mater.* **2018**, *28* (20), 1707440. https://doi.org/10.1002/adfm.201707440.

(5) Smith, D. J.; Chakravarthy, D.; Pulfer, S.; Simmons, M. L.; Hrabie, J. A.; Citro, M. L.; Saavedra, J. E.; Davies, K. M.; Hutsell, T. C.; Mooradian, D. L.; et al. Nitric Oxide-Releasing Polymers Containing the [N(O)NO]- Group. *J. Med. Chem.* **1996**, *39* (5), 1148–1156. https://doi.org/10.1021/jm950652b.

(6) Saavedra, J. E.; Mooradian, D. L.; Mowery, K. A.; Schoenfisch, M. H.; Citro, M. L.; Davies, K. M.; Meyerhoff, M. E.; Keefer, L. K. Conversion of a Polysaccharide to Nitric Oxide-Releasing Form. Dual-Mechanism Anticoagulant Activity of Diazeniumdiolated Heparin. *Bioorg. Med. Chem. Lett.* **2000**, *10* (8), 751–753. https://doi.org/10.1016/s0960-894x(00)00086-x.

(7) Lu, Y.; Slomberg, D. L.; Schoenfisch, M. H. Nitric Oxide-Releasing Chitosan

Oligosaccharides as Antibacterial Agents. *Biomaterials* **2014**, *35* (5), 1716–1724. https://doi.org/10.1016/j.biomaterials.2013.11.015.

(8) Lu, Y.; Shah, A.; Hunter, R. A.; Soto, R. J.; Schoenfisch, M. H. S-Nitrosothiol-Modified Nitric Oxide-Releasing Chitosan Oligosaccharides as Antibacterial Agents. *Acta Biomater.* **2015**, *12* (1), 62–69. https://doi.org/10.1016/j.actbio.2014.10.028.

(9) Reighard, K. P.; Schoenfisch, M. H. Antibacterial Action of Nitric Oxide-Releasing Chitosan Oligosaccharides against Pseudomonas Aeruginosa under Aerobic and Anaerobic Conditions. *Antimicrob. Agents Chemother.* **2015**, *59* (10), 6506–6513. https://doi.org/10.1128/AAC.01208-15.

(10) Pelegrino, M. T.; Weller, R. B.; Chen, X.; Bernardes, J. S.; Seabra, A. B. Chitosan Nanoparticles for Nitric Oxide Delivery in Human Skin. *Medchemcomm* **2017**, *8* (4), 713–719. https://doi.org/10.1039/c6md00502k.

(11) Shah, S. U.; Martinho, N.; Socha, M.; Pinto Reis, C.; Gibaud, S. Synthesis and Characterization of S-Nitrosoglutathione-Oligosaccharide-Chitosan as a Nitric Oxide Donor. *Expert Opin. Drug Deliv.* **2015**, *12* (8), 1209–1223. https://doi.org/10.1517/17425247.2015.1028916.

(12) Kim, J. O.; Noh, J. K.; Thapa, R. K.; Hasan, N.; Choi, M.; Kim, J. H.; Lee, J. H.; Ku, S. K.; Yoo, J. W. Nitric Oxide-Releasing Chitosan Film for Enhanced Antibacterial and in Vivo Wound-Healing Efficacy. *Int. J. Biol. Macromol.* **2015**, *79*, 217–225. https://doi.org/10.1016/j.ijbiomac.2015.04.073.

(13) Lutzke, A.; Pegalajar-Jurado, A.; Neufeld, B. H.; Reynolds, M. M. Nitric Oxide-Releasing S-Nitrosated Derivatives of Chitin and Chitosan for Biomedical Applications. *J. Mater. Chem. B* **2014**, *2* (42), 7449–7458. https://doi.org/10.1039/c4tb01340a.

(14) Simon-Walker, R.; Romero, R.; Staver, J. M.; Zang, Y.; Reynolds, M. M.; Popat, K. C.; Kipper, M. J. Glycocalyx-Inspired Nitric Oxide-Releasing Surfaces Reduce Platelet Adhesion and Activation on Titanium. *ACS Biomater. Sci. Eng.* **2017**, *3* (1), 68–77. https://doi.org/10.1021/acsbiomaterials.6b00572.

(15) Rinaudo, M. Chitin and Chitosan: Properties and Applications. *Progress in Polymer Science (Oxford)*. Pergamon July 1, 2006, pp 603–632. https://doi.org/10.1016/j.progpolymsci.2006.06.001.

(16) Croisier, F.; Jérôme, C. Chitosan-Based Biomaterials for Tissue Engineering. *European Polymer Journal*. Elsevier Ltd April 1, 2013, pp 780–792. https://doi.org/10.1016/j.eurpolymj.2012.12.009.

(17) Dicks, A. P.; Beloso, P. H.; Williams, D. L. H. Decomposition of S-Nitrosothiols: The Effects of Added Thiols. *J. Chem. Soc. Perkin Trans. 2* **1997**, *0* (8), 1429–1434. https://doi.org/10.1039/a701594a.

(18) Wang, P. G.; Xian, M.; Tang, X.; Wu, X.; Wen, Z.; Cai, T.; Janczuk, A. J. Nitric Oxide Donors: Chemical Activities and Biological Applications. *Chem. Rev.* **2002**, *102* (4), 1091–1134. https://doi.org/10.1021/cr000040l.

(19) Collins, C. J.; Collins, C. J. Reactions of Primary Aliphatic Amines with Nitrous Acid1. *Acc. Chem. Res.* **1971**, *4* (9), 315–322. https://doi.org/10.1021/ar50045a004.

(20) Claustre, S.; Bringaud, F.; Azéma, L.; Baron, R.; Périé, J.; Willson, M. An Easy Stereospecific Synthesis of 1-Amino-2,5-Anhydro-1-Deoxy-D-Mannitol and Arylamino Derivatives. *Carbohydr. Res.* **1999**, *315* (3–4), 339–344. https://doi.org/10.1016/s0008-6215(99)00040-3.

(21) Horton, D.; Philips, K. D. The Nitrous Acid Deamination of Glycosides and Acetates of 2-

Amino-2-Deoxy-D-Glucose. *Carbohydr. Res.* **1973**, *30* (2), 367–374. https://doi.org/10.1016/S0008-6215(00)81823-6.

(22) Conrad, H. E. Nitrous Acid Degradation of Glycosaminoglycans. *Curr. Protoc. Mol. Biol.* **1995**, *32* (1), 17.22.1-17.22.5. https://doi.org/10.1002/0471142727.mb1722as32.

(23) Shively, J. E.; Conrad, H. E. Formation of Anhydrosugars in the Chemical Depolymerization Of. **1976**, *15* (18), 3932–3942. https://doi.org/10.1021/bi00663a005.

(24) Plutschack, M. B.; McQuade, D. T.; Valenti, G.; Seeberger, P. H. Flow Synthesis of a Versatile Fructosamine Mimic and Quenching Studies of a Fructose Transport Probe. *Beilstein J. Org. Chem.* **2013**, *9*, 2022–2027. https://doi.org/10.3762/bjoc.9.238.

(25) Shively, J. E.; Conrad, H. E. Formation of Anhydrosugars in the Chemical Depolymerization of Heparin. *Biochemistry* **1976**, *15* (18), 3932–3942. https://doi.org/10.1021/bi00663a005.

(26) Vilar, R. E.; Ghael, D.; Li, M.; Bhagat, D. D.; Arrigo, L. M.; Cowman, M. K.; Dweck, H. S.; Rosenfeld, L. Nitric Oxide Degradation of Heparin and Heparan Sulphate. *Biochem. J.* **1997**, *324* (2), 473–479. https://doi.org/10.1042/bj3240473.

(27) Doyle, M. P.; Terpstra, J. W.; Pickering, R. A.; LePoire, D. M. Hydrolysis, Nitrosyl Exchange, and Synthesis of Alkyl Nitrttes. *J. Org. Chem.* **1983**, *48* (20), 3379–3382. https://doi.org/10.1021/jo00168a002.

(28) Lobl, T. J. *(No Title)*.

(29) Lavertu, M.; Xia, Z.; Serreqi, A. N.; Berrada, M.; Rodrigues, A.; Wang, D.; Buschmann, M. D.; Gupta, A. A Validated 1H NMR Method for the Determination of the Degree of Deacetylation of Chitosan. *J. Pharm. Biomed. Anal.* **2003**, *32* (6), 1149–1158. https://doi.org/10.1016/S0731-7085(03)00155-9.

(30) Tian, F.; Liu, Y.; Hu, K.; Zhao, B. The Depolymerization Mechanism of Chitosan by Hydrogen Peroxide. *J. Mater. Sci.* **2003**, *38* (23), 4709–4712. https://doi.org/10.1023/A:1027466716950.

(31) Li, B.; Zhang, J.; Bu, F.; Xia, W. Determination of Chitosan with a Modified Acid Hydrolysis and HPLC Method. *Carbohydr. Res.* **2013**, *366*, 50–54. https://doi.org/10.1016/j.carres.2012.11.005.

(32) Iglesias, E.; García-Río, L.; Leis, J. R.; Peña, M. E.; Williams, D. L. H. Evidence for Concerted Acid Hydrolysis of Alkyl Nitrites. *J. Chem. Soc. Perkin Trans. 2* **1992**, No. 10, 1673–1679. https://doi.org/10.1039/p29920001673.

(33) Crookes, M. J.; Williams, D. L. H. Nitrosation by Alkyl Nitrites. Part 5. Kinetics and Mechanism of Reactions in Acetonitrile. *J. Chem. Soc. Perkin Trans. 2* **1989**, No. 9, 1319. https://doi.org/10.1039/p29890001319.

(34) Salmon, D. J.; De Holding, C. L. T.; Thomas, L.; Peterson, K. V.; Goodman, G. P.; Saavedra, J. E.; Srinivasan, A.; Davies, K. M.; Keefer, L. K.; Miranda, K. M. HNO and NO Release from a Primary Amine-Based Diazeniumdiolate as a Function of PH. *Inorg. Chem.* **2011**, *50* (8), 3262–3270. https://doi.org/10.1021/ic101736e.

(35) Dutton, A. S.; Fukuto, J. M.; Houk, K. N. The Mechanism of NO Formation from the Decomposition of Dialkylamino Diazeniumdiolates: Density Functional Theory and CBS-QB3 Predictions. *Inorg. Chem.* **2004**, *43* (3), 1039–1045. https://doi.org/10.1021/ic0349609.

(36) Holland, R. J.; Klose, J. R.; Deschamps, J. R.; Cao, Z.; Keefer, L. K.; Saavedra, J. E. Direct Reaction of Amides with Nitric Oxide to Form Diazeniumdiolates. *J. Org. Chem.* **2014**, *79* (19), 9389–9393. https://doi.org/10.1021/jo501670e.

CHAPTER 4

COMPARISON OF DEGRADATION METHODS FOR CHITIN AND CHITOSAN USING MASS SPECTROMETRY AND LC-MS

4.1 Overview

In chapter 3, we used mass spectrometry to track the susceptibility of chitosan polymer to depolymerization by nitrous acid generated *in situ*. These results led to additional questions regarding the susceptibility of chitin derivatives to degradation agents. Firstly, how do different degradation agents impact the structural integrity of chitin and chitosan polymers with differing degrees of acetylation? A wide variety of conditions have been demonstrated to depolymerize chitosan and/or chitin; however, their comparative effectiveness has not been established. Secondly, which degradation products are formed following the exposure of chitin and chitosan to these degradation agents? A clear characterization of the low molecular weight products generated by degradation protocols is crucial to addressing the goal of detecting fungal-derived chitin. To answer these questions, we exposed a copolymer system composed of highly deacetylated chitosan (96% D-glucosamine), slightly deacetylated chitin (20-30% D-glucosamine), and completely acetylated chitin (100% *N*-acetylglucosamine) to three chemical degradation agents and three enzymatic degradation agents. We characterized and compared the low molecular weight degradation chemical fingerprints produced by these using direct injection mass spectrometry or LC-MS.

In addition to identifying the chemical fingerprints to facilitate the detection of polymeric chitin and chitosan, this chapter provide an overview of degradation protocols that can be followed to design chitosan oligosaccharides (COS) with desired compositions. The beneficial effects provided by COS make them of interest in medical research. The monomers that constitute COS confer distinct properties, so controlling COS composition during their production is significant. In this work, we degraded chitin and chitosan polymers and identified low molecular weight products such as COS that formed, using electrospray ionization time-of-flight mass spectrometry. Our results show that hydrochloric acid, hydrogen peroxide, and nitrous acid generate distinct products from chitin and chitosan. Hydrochloric acid degrades both chitin and chitosan polymers to produce glucosamine (GlcN) monomers and oligomers. Hydrogen peroxide degrades chitosan to produce GlcN and *N*-acetyl-D-glucosamine (GlcNAc) monomers and oligomers, and nitrous acid degrades chitosan to produce 2,5-anhydro-D-mannose. In addition to these methods of chemical degradation, several enzymes that have been reported to degrade chitosan were used, including lysozyme, lipase, and hemicellulase. Upon exposure to lysozyme, chitosan polymer and chitin polymer 1 produced GlcN, GlcNAc, and oligomers composed of these. Chitin polymer 2 was not degraded by lysozyme. We did not observe degradation in any instances when polymers were exposed to lipase and hemicellulase. Our studies show that COS composition is dictated by both the degradation protocol and the starting polymer. Additionally, our results enable selection of degradation protocols based on their ability to degrade chitin and chitosan and facilitate the production of COS with desired compositions.

4.2 Introduction

Chitin and chitosan are biopolymers that have been explored extensively for medical applications[1–3]. They are copolymers composed of randomly distributed GlcN and GlcNAc[4–6].

Chitin (>50% GlcNAc) was historically regarded as being intractable due to its limited solubility[7]. In recent years, however, the usefulness of chitin derivatives has led to an interest in deacetylating chitin to chitosan to improve its solubility. This deacetylation is rarely complete and yields a copolymer consisting predominantly of GlcN (>50% GlcN) and GlcNAc that is soluble in aqueous acid. Chitosan exhibits hemostatic, antimicrobial, and wound-healing properties[8,9] and is easily derivatized[10,11].

Degrading chitin and chitosan to produce low molecular weight COS is particularly useful, as COS are highly soluble in aqueous solvents and confer a variety of beneficial effects. GlcNAc oligomers with degrees of polymerization of up to 6 and GlcN oligomers with degrees of polymerization of up to 10 solubilize freely in neutral H_2O[12]. A plethora of unique health benefits are associated with COS, including antimicrobial, anti-inflammatory and anti-tumor properties, among others[13–16]. To further enhance these properties, COS are commonly derivatized and used as scaffolds with a range of chemical modifications. Applications for these derivatives include drug delivery, enhanced stability, and biocompatibility[11,17]. Derivatizations frequently make use of the primary amine of GlcN, rendering the proportion of GlcN to GlcNAc in COS an important factor[18–21]. The primary amine of GlcN has been implicated in the antibacterial properties of COS[22], and GlcNAc oligomers have shown the ability to reduce oxidative stress by scavenging free radicals[23].

While these studies indicate that COS composition is significant, there is a lack of research indicating appropriate methods to produce COS with desired compositions. Producing COS often involves exposing chitin or chitosan polymers to an oxidizing agent or acid. Acids such as hydrochloric acid (HCl) and Nitrous acid (HNO_2) have been used to depolymerize chitosan by distinct mechanisms[13,24,25]. Hydrogen peroxide is the most commonly used oxidizing agent used

to depolymerize chitosan for COS production[26–28]. In addition to chemical agents, chitin and chitosan are susceptible to degradation by some enzymes. Certain enzymes, such as chitinases and chitosanases, exhibit specific activity against these polysaccharides[29,30]. Enzymes produced endogenously by mammals, including humans, have been shown to successfully degrade chitin and its derivates[31]. Enzymes that have been reported to degrade chitin and chitosan include lysozyme, lipase, and hemicellulase[32–35]. Despite a heightened interest in producing COS, to the best of our knowledge, there is not a comparison of degradation protocols by the identification of the low molecular weight products. Degradation is commonly appraised using high-performance liquid chromatography, size-exclusion chromatography, and rheometry[36–38]. While these characterization techniques are capable of assessing degradation to an extent, they do not identify specific degradation products. We propose that degradation protocols used to produce COS yield distinct low molecular weight products that are dependent on both the degrading agent and the composition of the polymers used. The use of electrospray ionization time-of-flight mass spectrometry (ESI-TOF-MS) enables identification of the specific low molecular weight COS produced by degradation methods described in literature. Additionally, it allows us to evaluate the susceptibility of polymeric starting materials to degradation protocols by comparing COS and other low molecular weight products that form, such as GlcN and GlcNAc.

As many researchers produce COS in-house, this work allows selection of degradation methods to produce COS with desired monomer compositions. In this work, we characterized the low molecular weight products that were generated from chitin and chitosan polymers exposed to degradation conditions seen in literature. These low molecular weight products included COS, GlcN, GlcNAc and 2,5-anhydro-d-mannose. The polymers we used were comprised of varying size and degree acetylated chitin and chitosan. These included chitosan polymer (96%

deacetylated), chitin polymer 1 (20-30% deacetylated), and chitin polymer 2 (100% acetylated). Chitosan oligosaccharides (93% deacetylated), GlcN and GlcNAc were used in mass spectrometric method development to create a reference library of potential degradation products. Samples acquired from chitin and chitosan degradation were screened against this library to identify the resulting products. Polymer degradation products were identified after 1 h and 2 h of exposure to the selected reagents and again after 24 h by direct injection electrospray ionization mass spectrometry (ESI-MS).

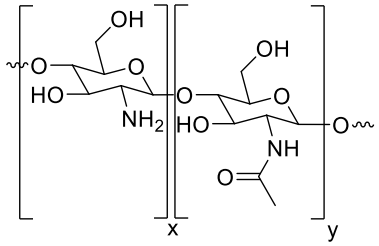

Figure 4.1. Generic structure of chitin (>50% GlcNAc) and chitosan (>50% GlcN) showing its GlcN (x) and GlcNAc (y) subunits.

Table 4.1: Polymers used for degradation studies.

Polymer	**Supplier**	**% Glucosamine units**	**% *N*-Acetylglucosamine units**
Chitin 1	Alfa Aesar	20-30[a]	70-80
Chitin 2	TCI	-	100[b]
Chitosan	Sigma Aldrich	96[c]	4

[a]Alfa Aesar certificate of analysis; [b]TCI certificate of analysis; [c]Sigma Aldrich certificate of analysis

4.3 Materials and Methods

4.3.1 Materials

D-Glucosamine hydrochloride (99.9%) was obtained from Calbiochem (Darmstadt, DE). Chitin polymer 2 (100% acetylated) and *N*-Acetyl-D-glucosamine (>98.0%) were obtained from TCI (Portland, OR). Chitosan oligosaccharides (<3000 MW, 93% deacetylated) were obtained from Carbosynth (Compton, Berkshire, UK). Low molecular weight chitosan (96% deacetylated), ammonium acetate (≥98%), hydrogen peroxide (30% w/w in H_2O), lipase (~200 units/g) from *Aspergillus niger,* and hemicellulase (~0.3-3.0 units/mg) from *Aspergillus niger* were obtained from Sigma Aldrich. Chicken egg white lysozyme (≥20,000 units/mg) and chitin polymer 1 (20-30% deacetylated) was obtained from Alfa Aesar. Concentrated HCl, ACS grade sodium nitrite (≥97.0%), LC-MS grade MeOH and LC-MS grade H_2O were obtained from EMD Millipore (Burlington, MA). Sodium hydroxide (pellets/certified ACS) were obtained from Thermo Fisher (Waltham, MA).

4.3.2 Spectroscopic characterization

Infrared (IR) spectra were collected using attenuated total reflectance (ATR) on a Nicolet 6700 FT-IR spectrometer (Thermo Electron Corp., Madison, WI, USA) fitted with a Smart iTR-ATR sampling accessory and a ZnSe crystal plate.

4.3.3 Mass spectrometry and LC-MS

4.3.3.1 Direct injection mass spectrometry

Mass spectra were acquired using an Agilent 6224 time-of-flight mass spectrometer (Agilent, Palo Alto, CA, USA) equipped with a dual electrospray ionization source. Products

acquired from degradations were characterized via direct injection mass spectrometry. At time intervals at 1 h, 2 h and 24 h, samples were removed via syringe and immediately injected into the instrument source, bypassing any prior separation step. An isocratic mobile phase composed of 50:50 MeOH:H_2O was used with a flow rate of 0.300 mL/min. Mass spectrometric parameters were as follows: 3500 V capillary voltage, 50 V fragmentor voltage, 60 V skimmer voltage, 650 V octupole voltage, 45 psig nebulizer pressure, and 10 L min^{-1} gas flow at 250 °C (N_2). Products from H_2O_2 and HCl degradations were analyzed in positive ion mode. Products from HNO_2 degradations were analyzed in negative ion mode. The detection range for all scans was set to 120-3200 *m/z*.

4.3.3.2 Liquid chromatography mass spectrometry

Products acquired from enzymatic degradation protocols were characterized using LC-MS. Samples were prepared by syringe extraction from vials containing the analyte, buffer and degrading agent. Aliquots were removed at 1 h, 4 h, 24 h, 3 d, and 7 d. These were filtered using Agilent PTFE Econofltr 0.2-µm filters. The filtered solutions were placed in a 110 °C oven for 10 minutes to deactivate enzymatic activity prior to sample analysis, then stored at -20 °C until analysis. Analytes were separated using an Agilent Zorbax SB-C18 rapid resolution column with dimensions of 4.6x150 mm and a 3.5-µm particle size. The mobile phase consisted of LC-MS grade acetonitrile and water, each containing a 0.1% formic acid additive. A 95:5 H_2O:ACN isocratic gradient was used with a variable flow rate. The flow rate was initially set at 0.300 mL/min and decreased to 0.050 mL/min between 3.30 and 4.00 minutes. The flow rate remained at 0.050 mL/min until 15 minutes then transitioned back to the starting conditions of 0.300 mL/min at 20 minutes. The source used was an Agilent dual electrospray ionization source operating in positive ion mode. The ion source conditions were as follows: 2500 V capillary voltage, 120 V

fragmentor voltage, 60 V skimmer voltage, 250 V octupole voltage, 10 L min^{-1} gas flow (N_2), and 45 psig nebulizer pressure. The detection range was set to 120-3200 *m/z*.

4.3.4 Degradation protocols

4.3.4.1 Chemical degradation protocols

For degradations performed with H_2O_2, 20 mg of each polymer was measured into separate 50 mL round-bottom flasks. 20 mL of 30% H_2O_2 was added directly to each flask and the resulting suspensions were stirred at 90 °C. Aliquots of approximately 1 mL were removed at 1 h and 2 h at a constant temperature. After these aliquots were removed, the reaction vessels were allowed to cool to room temperature (19 °C) under constant stirring and an additional aliquot was removed after 24 h. The collected aliquots were filtered through 0.2-μm filters and immediately analyzed using direct injection mass spectrometry in positive ionization mode. Mass spectrometry was performed on all replicates and spectra compared to assess the COS and monomers formed.

For degradations performed with HCl, 10 mg of each polymer was measured into separate 50 mL round-bottom flasks. 10 mL of 5 M HCl was added directly to each flask and the resulting suspensions were stirred at 90 °C. Aliquots of approximately 1 mL were removed after 1 h and 2 h at 90 °C and a third aliquot was removed after 24 h after the reaction vessel was allowed to return to room temperature (19 °C). Aliquots were filtered using 0.2-μm filters and immediately analyzed using direct injection mass spectrometry in positive ionization mode. Mass spectrometry was performed on all replicates and spectra compared to assess the COS and monomers formed.

For degradations performed with HNO_2, 100 mg of each polymer was measured into separate 50 mL round-bottom flasks, to which 9 mL of LC-MS grade H_2O was added. 340 mg sodium nitrite was added, followed immediately by 1 mL 5 M HCl dropwise to produce HNO_2 *in*

situ at an overall concentration of 0.5 M. The resulting suspensions were stirred at 90 °C. Aliquots of approximately 1 mL were removed after 1 h and 2 h at 90 °C and a third aliquot was removed after 24 h after the reaction vessel was allowed to return to room temperature (19 °C). Aliquots were filtered using 0.2-μm filters and immediately analyzed using direct injection mass spectrometry in negative ionization mode. Mass spectrometry was performed on all replicates and spectra compared to assess the COS and monomers formed.

4.3.4.2 Enzymatic degradation protocols

For degradations performed with lysozyme, 1 mM acetate buffer solution was made by adding an appropriate quantity of ammonium acetate to LC-MS grade water and adjusting the pH to 4.5 using dropwise addition of HCl and NaOH. 10 mL buffer solution was added to round-bottom flasks containing 20 mg analyte. The flasks were heated in a water bath to 40 °C and 10 mg lysozyme from chicken egg white was added to make an enzyme:chitosan mass ratio of 1:2. These suspensions were stirred for 7 days with aliquots removed at 1 hour, 4 hours, 24 hours, 3 days, and 7 days. Aliquots were immediately filtered using 0.2-μm filters into LC-MS vials and placed in a 110 °C oven for 10 minutes to cease further enzymatic activity, then stored at -20 °C until analysis.

For degradations performed with lipase, a 1 mM acetate buffer solution was made by adding an appropriate quantity of ammonium acetate to LC-MS grade water and adjusting the pH to 8.0 using dropwise addition of HCl and NaOH. 10 mL buffer solution was added to a round-bottom flask containing 20 mg analyte. The flasks were heated in a water bath to 40 °C and 10 mg lipase from *Aspergillus niger* was added to make an enzyme:chitosan mass ratio of 1:2. These suspensions were stirred for 7 days with aliquots removed at 1 hour, 4 hours, 24 hours, 3 days, and

7 days. Aliquots were immediately filtered using 0.2-μm filters into LC-MS vials and placed in a 110 °C oven for 10 minutes to cease further enzymatic activity, then stored at -20 °C until analysis.

For degradations performed with hemicellulase, a 1 mM acetate buffer solution was made by adding an appropriate quantity of ammonium acetate to LC-MS grade water and adjusting the pH to 4.5 using dropwise addition of HCl and NaOH. 10 mL buffer solution was added to a round-bottom flask containing 20 mg analyte. The flasks were heated in a water bath to 40 °C and 10 mg hemicellulase from *Aspergillus niger* was added to make an enzyme:chitosan mass ratio of 1:2. These suspensions were stirred for 7 days with aliquots removed at 1 hour, 4 hours, 24 hours, 3 days, and 7 days. Aliquots were immediately filtered using 0.2-μm filters into LC-MS vials and placed in a 110 °C oven for 10 minutes to cease further enzymatic activity, then stored at -20 °C until analysis.

4.3.5 Degradation product screening

Standards for GlcN, GlcNAc, COS, chitosan polymer, chitin polymer 1 and chitin polymer 2 were characterized by ATR-IR as well as ESI-TOF-MS in positive ionization mode. ATR-IR and mass spectra of starting materials can be found in Appendix D. A reference library was built for COS, GlcN, and GlcNAc standards characterized using MS; these mass spectra can be found in Appendix D. **Table B.1** in Appendix B contains calculated *m/z* values for monomers and oligomers of GlcN and GlcNAc corresponding to common adducts found in ESI-MS. Mass spectra from degradation experiments were compared to the reference ions obtained from these standards as well as in Appendix B, **Table B.1**. All degradation experiments were run in triplicate and analyzed via mass spectrometry.

4.4 Results and Discussion

4.4.1 Starting material characterization

Chitosan polymer, chitin polymer 1, and chitin polymer 2 were individually suspended in LC-MS grade H_2O, vortexed, and aliquots were drawn and analyzed via direct injection ESI-TOF-MS. Mass spectra from all compounds indicated that no low molecular weight compounds related to chitin or chitosan such as COS, GlcN, or GlcNAc were present from 120-3200 *m/z* that were later observed after these polymers were exposed to degradation protocols. These mass spectra can be found in Appendix B.

4.4.2 H_2O_2 degradation

The ability of H_2O_2 to degrade chitosan has been well established[26,27,38]. Low molecular weight COS are commonly produced by exposing the polymer directly to H_2O_2[39]. Alternatively, chitosan can first be dissolved in acidic aqueous solutions and then exposed to H_2O_2[40]. In these experiments, chitosan polymer, chitin polymer 1, and chitin polymer 2 were exposed directly to 30% H_2O_2, removed aliquots after 1 h, 2 h, and 24 h of exposure, and characterized the resulting COS and monomers using direct injection ESI-TOF-MS. COS and monomers produced from the H_2O_2 degradation of all polymers are summarized in **Table 4.2.**

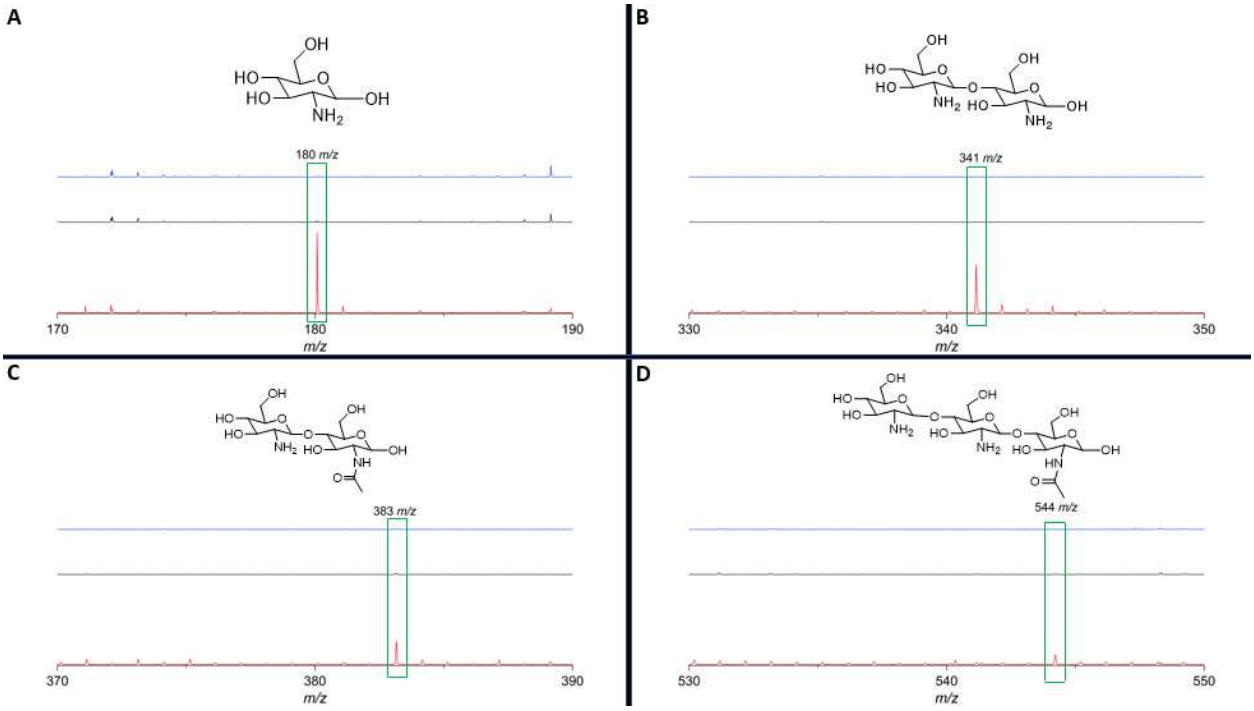

Figure 4.2: Mass spectra of chitin and chitosan polymers exposed to 30% H_2O_2 for 1 h. Chitosan polymer (96% GlcN) is shown in red. Chitin polymer 1 (20-30% GlcN) is shown in black. Chitin polymer 2 (~0% GlcN) is shown in blue. Following one hour of exposure to 30% H_2O_2, degradation products were only observed to form from chitosan polymer. Inset **A** shows a peak overlay for GlcN monomers. Inset **B** shows an overlay for GlcN dimers. Inset **C** shows an overlay for GlcN/GlcNAc dimers. Inset **D** shows a peak overlay for GlcN/GlcN/GlcNAc trimers.

Table 4.2: Summary of low molecular weight degradation products following exposure to 30% H_2O_2 and characterized by ESI-TOF-MS.

Analyte	Observed species	1 h	2 h	24 h
GlcN	$[C_6H_{13}NO_5 + H]^+$	X	X	
GlcNAc	$[C_8H_{15}NO_6 + H]^+$	X	X	
GlcN dimer	$[C_{12}H_{24}N_2O_9 + H]^+$	X		
GlcN/GlcNAc dimer	$[C_{14}H_{26}N_2O_9 + H]^+$	X	X	
2 GlcN, 1 GlcNAc trimer	$[C_{20}H_{37}N_3O_{14} + H]^+$	X		
1 GlcN, 2 GlcNAc trimer	$[C_{22}H_{39}N_3O_5 + H]^+$		X	

Mass spectra of chitosan polymer exposed to H_2O_2 for 1 h contained signals at 180, 341, 383, and 544 *m/z*. The signal at 180 *m/z* corresponds to an ion with a formula matching that of a protonated GlcN ion, $[C_6H_{13}NO_5 + H]^+$. The signal at 341 *m/z* corresponds to an ion with a molecular formula matching that of a protonated GlcN dimer, $[C_{12}H_{24}N_2O_9 + H]^+$. The signal at 383 *m/z* corresponds to an ion with a formula matching that of a protonated GlcN/GlcNAc dimer, $[C_{14}H_{26}N_2O_9 + H]^+$. The signal at 544 *m/z* corresponds to an ion with a formula matching that of a protonated GlcN/GlcNAc/GlcNAc trimer, $[C_{20}H_{37}N_3O_{14} + H]^+$.The signals at 180, 341, and 383 *m/z* were all observed in mass spectra taken after 2 h of H_2O_2 exposure, with the addition of a signal at 222 *m/z*, indicative of a compound with a formula matching that of a protonated GlcNAc ion, $[C_8H_{15}NO_6 + H]^+$. Following 24 h of exposure, all compounds observed at 2 h remained visible. **Table 4.3** summarizes chitosan polymer's degradation products following 24 h of exposure to 30% H_2O_2. Replicates of all corresponding mass spectra can be found in Appendix D.

Table 4.3: Degradation products generated from chitosan polymer exposed to 30% H_2O_2 over 24 hours.

Analyte	*m/z* observed	1 h	2 h	24 h
GlcN, $[C_6H_{13}NO_5 + H]^+$	180 *m/z*	X	X	X
GlcNAc, $[C_8H_{15}NO_6 + H]^+$	222 *m/z*		X	X
GlcN dimer, $[C_{12}H_{24}N_2O_9 + H]^+$	341 *m/z*	X	X	X
GlcN/GlcNAc dimer $[C_{14}H_{26}N_2O_9 + H]^+$	383 *m/z*	X	X	X
2 GlcN, 1 GlcNAc trimer, $[C_{20}H_{37}N_3O_{14} + H]^+$	544 *m/z*	X		

Low concentrations of H_2O_2 have been reported to induce degradation of partially deacetylated chitosan via random 1,4-β-D glycosidic bond cleavage, after which chain-end scissions occur, producing a series of oligosaccharides[40,41]. This was reflected in results by the

range of COS and monomers observed when chitosan polymer was exposed to H_2O_2. The relative ratio of GlcN monomers to GlcN dimers increased from 1.9 ± 0.3 to 8.8 ± 7.2 from 1 h to 24 h, suggesting that GlcN dimers were hydrolyzed to monomers. Similarly, the signal observed at 544 *m/z* decreased in abundance during the times measured and disappeared completely by 2 h, suggesting a similar fate. In contrast, GlcNAc monomers were not visible in mass spectra until 2 h of exposure and increased in relative abundance compared to GlcN between 2 h and 24 h. These trends suggest that GlcN-GlcN bonds have a higher susceptibility to hydrolysis than GlcNAc-GlcN or GlcNAc-GlcNAc glycosidic bonds, as an equal susceptibility to hydrolysis would yield equivalent abundances of these ions over time.

GlcN, GlcNAc, and COS were not observed in mass spectra of chitin polymer 1 exposed to 30% H_2O_2 for 1 h. Following 2 h of exposure, signals were visible at 180, 383 and 447 *m/z*. The signals at 180 and 383 *m/z* correspond to ions with molecular formulas matching those of protonated GlcN monomers and GlcN/GlcNAc dimers. The signal at 447 corresponds to an ion with a formula matching that of a sodiated GlcNAc dimer, $[C_{16}H_{28}N_2O_{11} + Na]^+$. Following 24 h of exposure, the signals previously observed at 2 h remained visible, with new signal formation at 222 and 586 *m/z*. The signal at 222 *m/z* is indicative of an ion with a formula matching that of a protonated GlcNAc monomer. The signal at 586 is indicative of a compound with a formula matching that of a trimer composed of one GlcN and two GlcNAc subunits, $[C_{22}H_{39}N_3O_5 + H]^+$. Replicates of all corresponding mass spectra can be found in Appendix D. Chitin polymer 1 had a reported a deacetylation of 20-30% in. However, GlcN was present in mass spectra prior to GlcNAc, indicating its higher abundance and providing further evidence that glycosidic bond hydrolysis is favored between subunits involving at least one GlcN monomer. GlcNAc was visible after 24 h of exposure, indicating that H_2O_2 has a limited ability to cleave glycosidic bonds with

one GlcNAc residue. **Table 4.4** summarizes chitin polymer 1's degradation products following 24 h of exposure to 30% H_2O_2. No products were observed in mass spectra from chitin polymer 2 exposed to H_2O_2 for up to 24 h.

Table 4.4: Degradation products generated from chitin polymer 1 exposed to 30% H_2O_2 over 24 hours.

Analyte	*m/z* observed	1 h	2 h	24 h
GlcN, $[C_6H_{13}NO_5 + H]^+$	180 *m/z*		X	X
GlcNAc, $[C_8H_{15}NO_6 + H]^+$	222 *m/z*			X
GlcN/GlcNAc dimer $[C_{14}H_{26}N_2O_9 + H]^+$	383 *m/z*		X	X
GlcNAc dimer, $[C_{16}H_{28}N_2O_{11} + Na]^+$	447 *m/z*		X	X
1 GlcN, 2 GlcNAc trimer, $[C_{22}H_{39}N_3O_5 + H]^+$	586 *m/z*			X

Mass spectra acquired from exposing chitin polymer 1 and chitin polymer 2 to 30% H_2O_2 indicate that the chitin polymer 2 was fully acetylated. As shown in Appendix D, IR spectra failed to indicate notable differences between the two starting materials. However, prior observations show that GlcNAc is produced more slowly from both highly deacetylated and slightly deacetylated copolymers. If it is assumed that chitin polymer 2 are roughly fully acetylated, the data acquired from these experiments indicate that H_2O_2 is ineffective at cleaving GlcNAc-GlcNAc bonds. GlcNAc's production from chitin polymer 1 and chitosan polymer in previous degradations can be rationalized if it is only liberated as a terminal group attached to a GlcN residue. This provides an explanation as to why GlcNAc is only observed after GlcN monomers following exposure to H_2O_2. Although literature reports the use of H_2O_2 to degrade chitin in tandem with other degrading agents[42,43], the inability of H_2O_2 to cleave glycosidic linkages

between *N*-acetylated residues suggests that alternatives should be used to degrade all but highly deacetylated polymers, as H_2O_2 is ineffective against these.

4.4.3 HCl degradation

Acidic hydrolysis of chitosan and chitin has been investigated extensively, with HCl being well-documented in literature[44–46]. Concentrated HCl and other strong acids are used to depolymerize chitin and chitosan alongside simultaneous deacetylation[47,48]. While various acid strengths can be used, it is generally accepted that higher concentration acids and elevated temperatures increase the rate of degradation[49]. In these experiments, chitosan polymer, chitin polymer 1, and chitin polymer 2 were exposed directly to 5 M HCl at 90 °C, removed aliquots at 1 h, 2 h, and 24 h, and analyzed the resulting products using direct injection ESI-TOF-MS. COS and monomers produced from the HCl degradation of all polymers can be found in **Table 4.5.**

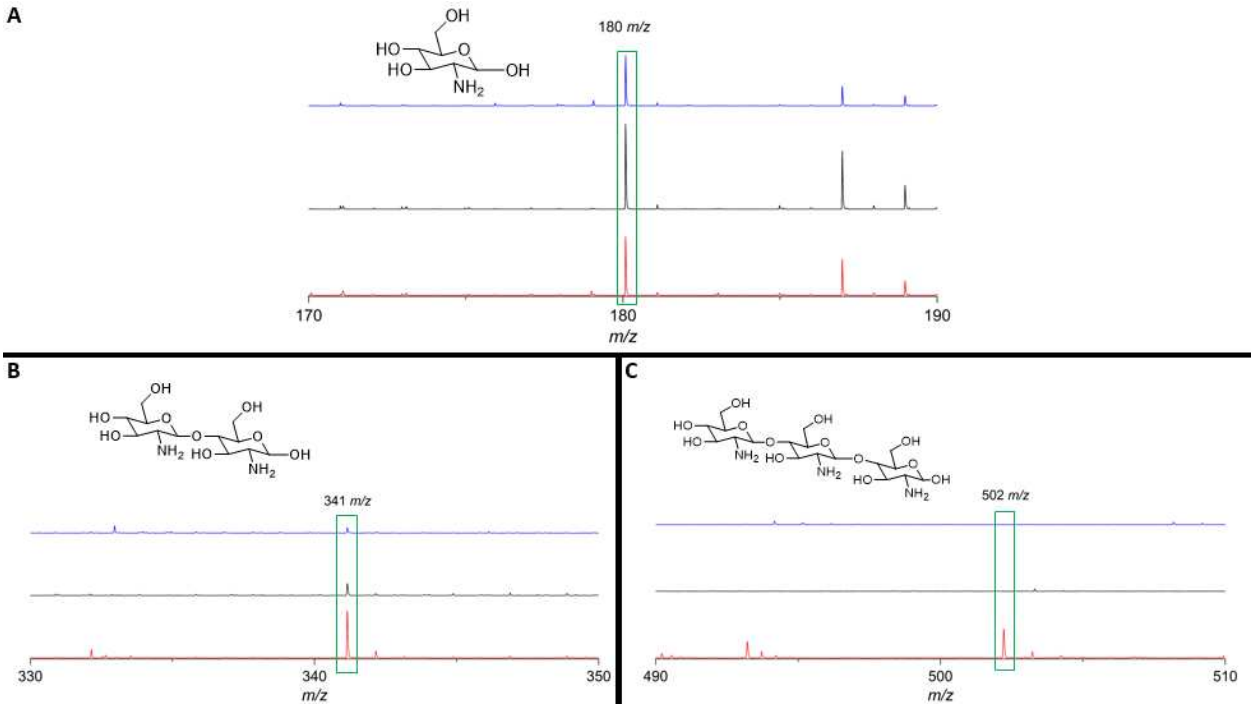

Figure 4.3: Mass spectra of chitin and chitosan polymers exposed to 5 M HCl for 1 h. Chitosan polymer (96% GlcN) is shown in red. Chitin polymer 1 (20-30% GlcN) is shown in black. Chitin polymer 2 (~0% GlcN) is shown in blue. Degradation products were observed in all three polymers

exposed to 5M HCl. Inset **A** shows a peak overlay for GlcN monomers produced from all polymers. Inset **B** shows an overlay for GlcN dimers produced from all polymers. Inset **C** shows an overlay for GlcN trimers only observed from chitosan polymer.

Table 4.5: Summary of low molecular weight degradation products following exposure to 5M HCl and characterized by ESI-TOF-MS.

Analyte	Observed species	1 h	2 h	24 h
GlcN	$[C_6H_{13}NO_5 + H]^+$	X	X	X
GlcNAc	$[C_8H_{15}NO_6 + H]^+$		X	X
GlcN dimer	$[C_{12}H_{24}N_2O_9 + H]^+$	X	X	X
GlcN/GlcNAc dimer	$[C_{14}H_{26}N_2O_9 + H]^+$		X	
GlcN trimer	$[C_{18}H_{35}N_3O_{13} + H]^+$	X		
GlcN tetramer	$[C_{24}H_{46}N_4O_{17} + H]^+$	X		
GlcN pentamer	$[C_{30}H_{57}N_5O_{21} + H]^+$	X		

Mass spectra from chitosan polymer exposed to 5 M HCl for 1 h contained signals at 180, 341, and 502 *m/z*. The signal at 180 *m/z* corresponds to an ion with a formula matching that of a protonated GlcN ion, $[C_6H_{13}NO_5 + H]^+$. The signal at 341 *m/z* corresponds to an ion with a formula matching that of a protonated GlcN dimer, $[C_8H_{15}NO_6 + H]^+$. The signal at 502 *m/z* corresponds to an ion with a formula matching that of a protonated GlcN trimer, $[C_{18}H_{35}N_3O_{13} + H]^+$. The same signals remained visible after 2 h; however, aliquots removed after 24 h displayed additional signal formation at 663 and 824 *m/z*. The signal at 663 *m/z* corresponds to an ion with a formula matching that of a protonated GlcN tetramer, $[C_{24}H_{46}N_4O_{17} + H]^+$. The signal at 824 *m/z* corresponds to an ion with a formula matching that of a protonated GlcN pentamer, $[C_{30}H_{57}N_5O_{21} + H]^+$. Replicates of all corresponding mass spectra can be found in Appendix D. **Table 4.6** summarizes chitosan polymer's degradation products following 24 h of exposure to 5M HCl.

Table 4.6: Degradation products generated from chitosan polymer exposed to 5 M HCl over 24 hours.

Analyte	*m/z* observed	1 h	2 h	24 h
GlcN, $[C_6H_{13}NO_5 + H]^+$	180 *m/z*	X	X	X
GlcN dimer, $[C_{12}H_{24}N_2O_9 + H]^+$	341 *m/z*	X	X	X
GlcN trimer, $[C_{18}H_{35}N_3O_{13} + H]^+$	502 *m/z*	X	X	X
GlcN tetramer, $[C_{24}H_{46}N_4O_{17} + H]^+$	663 *m/z*			X
GlcN pentamer, $[C_{30}H_{57}N_5O_{21} + H]^+$	824 *m/z*			X

The absence of larger oligomers (>663 *m/z*) in early aliquots does not necessarily preclude their presence. Rather, this may be explained by relative product scarcity of these species due to a lower time of exposure to the lysing agent. A higher proportion of GlcN and its oligomers were observed over GlcNAc after chitosan polymer was exposed to 5 M HCl, which was expected given acid's propensity to deaminate *N*-acetyl groups. Although some acetylated compounds were observed in low quantities, the abundance of these ions decreased relative to deacetylated COS and GlcN over 24 h. While these experiments did not investigate chemical modifications beyond 24 h, data suggests that sufficient exposure to HCl would yield exclusively deacetylated products.

Mass spectra of chitin polymer 1 exposed to 5 M HCl for 1 h contained signals at 180, 222, 341, and 383 *m/z*. The signals at 180 and 341 *m/z* correspond to ions with formulas matching those of protonated GlcN monomers and dimers, respectively. The signal at 222 *m/z* corresponds to an ion with a molecular formula matching that of protonated GlcNAc. The signal at 383 *m/z* corresponds to an ion with a molecular formula matching that of a protonated dimer composed of GlcN and GlcNAc. Signals observed in mass spectra taken after 2 h of exposure remained constant with the exception of the 383 *m/z* signal, which disappeared. Spectra taken after 24 h of exposure

were identical taken to those after 2 h. **Table 4.7** summarizes chitin polymer 1's degradation products following 24 h of exposure to 5M HCl.Replicates of all corresponding mass spectra can be found in Appendix D.

Table 4.7: Degradation products generated from chitin polymer 1 exposed to 5 M HCl.

Analyte	*m/z* observed	1 h	2 h	24 h
GlcN, $[C_6H_{13}NO_5 + H]^+$	180 *m/z*	X	X	X
GlcNAc, $[C_8H_{15}NO_6 + H]^+$	222 *m/z*	X	X	X
GlcN dimer, $[C_{12}H_{24}N_2O_9 + H]^+$	341 *m/z*	X	X	X
GlcN/GlcNAc dimer $[C_{14}H_{26}N_2O_9 + H]^+$	383 *m/z*	X		

Despite there being a lower proportion of GlcN to GlcNAc residues, the most prominent signal at all measured times was GlcN, providing evidence that HCl deacetylates GlcNAc polymers as it depolymerizes them. Notably, signals at 222 *m/z*, corresponding to $[C_8H_{15}NO_6 + H]^+$ ions, were present in all aliquots, indicating that HCl can degrade GlcNAc polymers prior to deacetylation. Literature reports that chitosan's degree of acetylation decreases following exposure to HCl[50], and results indicate that these tendencies apply to more acetylated chitin polymers as well.

Mass spectra of chitin polymer 2 exposed to 5 M HCl for 1 h contained signals at 180 and 222 *m/z*. These correspond to ions with molecular formulas matching those of protonated GlcN and GlcNAc ions, respectively. These signals were observed in mass spectra of aliquots taken after 2 h and 24 h as well, with the addition of an ion at 341 *m/z*. This signal corresponds to an ion with a formula matching that of a protonated dimer composed of GlcN and GlcNAc. Replicates of all mass spectra can be found in Appendix D. Given earlier results indicating the high degree of

acetylation of the chitin polymer 2 used in these studies, these results serve to indicate that HCl rapidly and effectively degrades chitin and chitosan polymers with any degree of deacetylation, producing primarily deacetylated products. Although dilute HCl has been reported to hydrolyze glycosidic linkages as roughly the same rate as it deacetylates *N*-acetyl groups, concentrated acid hydrolyzes polymers more than 10 times faster than it deacetylates these[49]. Although relatively concentrated HCl (5 M) was used in tandem with highly acetylated chitin polymers (70-80% acetylated), the prevalent low molecular weight degradation product observed was still GlcN. This suggests a higher susceptibility of reducing end glycosidic linkages involving GlcN; equal susceptibilities would result in higher initial proportions of GlcNAc to GlcN. **Table 4.8** summarizes chitin polymer 2's degradation products following 24 h of exposure to 5M HCl.

Table 4.8: Degradation products generated from chitin polymer 2 exposed to 5 M HCl over 24 hours.

Analyte	*m/z* observed	1 h	2 h	24 h
GlcN, $[C_6H_{13}NO_5 + H]^+$	180 *m/z*	X	X	X
GlcNAc, $[C_8H_{15}NO_6 + H]^+$	222 *m/z*	X	X	X
GlcN dimer, $[C_{12}H_{24}N_2O_9 + H]^+$	341 *m/z*		X	X

4.4.4 HNO_2 degradation

As free HNO_2 decomposes rapidly, it is generally generated *in situ*. Nitrous acid's propensity to degrade chitosan at low temperatures has been shown at 0 °C[51]; however, to the best of our knowledge, its effect on chitin has not been investigated. To assess the ability of HNO_2 to degrade chitin and chitosan at elevated temperatures, chitosan polymer, chitin polymer 1 and chitin polymer 2 were exposed to HNO_2. Nitrous acid was generated *in situ* at 90 °C by the addition of

stoichiometric quantities of HCl and $NaNO_2$. Aliquots were drawn at 1 h, 2 h and 24 h and analyzed using direct injection ESI-TOF-MS in negative ion mode.

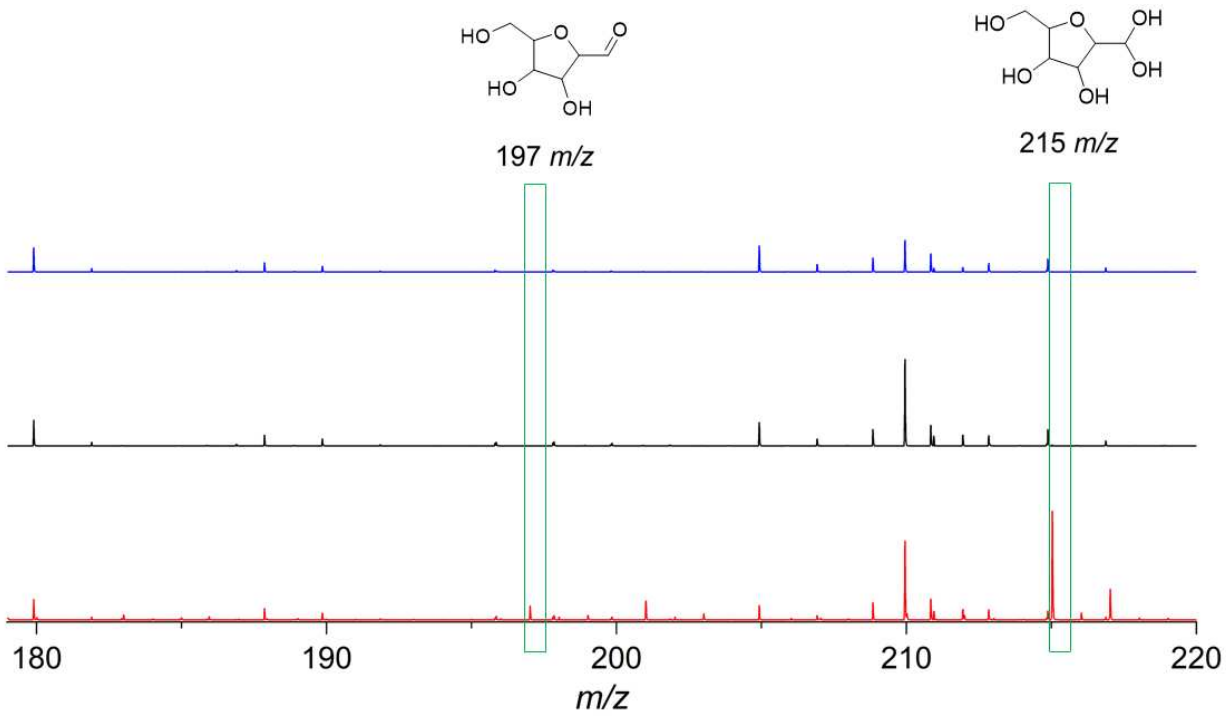

Figure 4.4: Mass spectra of chitin and chitosan polymers exposed to 0.5 M HNO_2 for 1 h. Chitosan polymer (96% GlcN) is shown in red. Chitin polymer 1 (20-30% GlcN) is shown in black. Chitin polymer 2 (~0% GlcN) is shown in blue. Only chitosan polymer was degraded by the HNO_2 degradation protocol used. Peaks at 197 and 215 *m/z* correspond to 2,5-AM and its hydrated form as chlorinated adducts in negative ion mode ESI-MS.

Mass spectra of chitosan polymer exposed to 0.5 M HNO_2 for 1 h contained signals at 197 and 214 *m/z*. The signal at 197 *m/z* corresponds to an ion with a molecular formula matching that of a chlorinated 2,5 anhydro-d-mannose (2,5-AM) ion $[C_6H_{10}O_5 + Cl]^-$. The signal at 215 *m/z* corresponds to an ion with a molecular formula matching that of a chlorinated hydrated 2,5-AM ion, $[C_6H_{12}O_6 + Cl]^-$. The same signals were visible in mass spectra taken after 2 h, as well as after 24 h of exposure. Only 2,5-AM and its hydrated form were observed in all mass spectra obtained. Replicates of all corresponding mass spectra can be found in Appendix D.

2,5-AM forms upon exposure to HNO_2 when GlcN's primary amine is nitrosated, producing NO, N_2, and a carbocation. Lone pairs on the heterocyclic oxygen interact with the carbocation as NO and N_2 depart, resulting in a ring contraction and a 5 membered ring in the form of 2,5-AM[24]. Signals corresponding to 2,5-AM and its hydrated form were only observed using negative ion mode mass spectrometry. Given 2,5-AM's lack of electronegative functional groups, the absence of 2,5-AM ions in mass spectra is likely explained by low ionization efficiency conferred by its inability to form positively charged ions. Additionally, these results indicate that 2,5-AM has an increased propensity to form $[M + Cl]^-$ adducts, likely involving residual Cl^- in solution from the reaction of HCl and $NaNO_2$, as deprotonated adducts were not observed in negative ion mode mass spectra.

It may be noted that the polymer mass used in this protocol was 10x higher than the concentration in experiments using HCl or H_2O_2. The concentrations used originally matched those in HCl and H_2O_2 chemical degradation protocols; however, no GlcN or GlcNAc monomers were observed in mass spectra using overall concentrations of 1 mg/mL. Upon increasing the analyte concentrations to 10 mg/mL, however, new signal formation was observed in mass spectra chitosan polymer exposed to HNO_2. The lack of observed products at polymer concentrations of 1 mg/mL points to a decreased ability of HNO_2 to degrade chitosan, lower ionization efficiency of 2,5-AM, or a combination of both factors. No oligomers were observed in mass spectra, indicating that depolymerization occurred in reducing end monomers and that ring rearrangement happened prior to GlcN's release.

No degradation products were observed in spectra taken of chitin polymer 1 or polymer 2 exposed to 0.5 M HNO_2 at any measured time up through 24 h. This indicates that HCl and $NaNO_2$ react immediately upon exposure in solution to form HNO_2 and degrade chitosan via a mechanism

distinct from that of HCl, as studies exposing chitin polymers and chitin polymer 2 to HCl resulted in swift degradation. A stepwise mechanism in which chitin and chitosan were depolymerized by HCl rather than HNO_2 followed by ring contraction would have been indicated by chitin's degradation, which was not observed.

4.4.5 Enzymatic degradations

LC-MS analysis of degradation products taken over 7 days of exposure indicated that lysozyme degraded chitosan polymer. A broad peak appeared from 5.0 – 7.5 minutes exposure that increased in size relative to other chromatographic peaks with time. Although this peak was absent in the aliquot taken at 1 hour, it appeared at aliquots taken at 4 hours and beyond. Mass spectra extracted from this peak contained signals at 144, 162 and 180 *m/z,* indicative of $[C_6H_{13}NO_5 + H]^+$, $[C_6H_{13}NO_5 - H_2O + H]^+$, and $[C_6H_{13}NO_5 - 2H_2O + H]^+$, all identified as adducts of GlcN. In addition, a signal at 204 *m/z* was observed, corresponding to a compound with a molecular formula matching that of protonated GlcNAc, $[C_8H_{15}NO_6 + H]^+$. Low abundances of GlcN and GlcNAc oligomers were also observed. The presence of these compounds was suggested by signals at 323 and 341 *m/z,* indicative of ions with molecular formulas matching protonated and sodiated GlcN dimers, $[C_{12}H_{24}N_2O_9 + H]^+$ and $[C_{12}H_{24}N_2O_9 + Na]^+$. Signals were observed at 365 and 383 *m/z,* indicative of compounds with formulas matching those of GlcN-GlcNAc dimers, $[C_{14}H_{26}N_2O_9 + H]^+$ and $[C_{14}H_{26}N_2O_9 + Na]^+$. A signal was observed at 526 *m/z,* indicative of protonated trimers composed of 2 GlcN and 1 GlcNAc, $[C_{20}H_{37}N_3O_{14} + H]^+$. Signals were also observed at 568 and 586 *m/z,* indicating the presence of trimers composed of 1 GlcN and 2 GlcNAc, $[C_{22}H_{39}N_3O_5 + H]^+$ and $[C_{22}H_{39}N_3O_5 + Na]^+$, respectively. Signals observed in this first peak are summarized in **Table 4.9**. Chromatograms and mass spectra from these experiments can be found in Appendix B.

Table 4.9: Summary of low molecular weight degradation products following exposure to lysozyme and characterized by LC-MS.

1st peak: 5-7 minutes

Degradation product	Observed species	Chitosan	Chitin 1	Chitin 2
GlcN	$[C_6H_{13}NO_5 + H]^+$	X		
GlcNAc	$[C_8H_{15}NO_6 + H]^+$	X		
GlcN dimer	$[C_{12}H_{24}N_2O_9 + H]^+$	X		
GlcN-GlcNAc dimer	$[C_{14}H_{26}N_2O_9 + H]^+$	X		
2 GlcN, 1 GlcNAc trimer	$[C_{20}H_{37}N_3O_{14} + H]^+$	X		
1 GlcN, 2 GlcNAc trimer	$[C_{22}H_{39}N_3O_5 + H]^+$	X		

In aliquots taken at three and seven days, a broad peak eluting from ~13-16 minutes protruding slightly above baseline was observed. This contained several signals indicative of GlcNAc monomers and oligomers with degrees of polymerization of up to 4. Signals observed in this second peak are summarized in **Table 4.10.** Chromatograms and mass spectra from these experiments can be seen in Appendix D.

Table 4.10: Summary of low molecular weight degradation products following exposure to lysozyme and characterized by LC-MS.

2nd peak: 13-16 minutes

Degradation product	Observed species	Chitosan	Chitin 1	Chitin 2
GlcNAc	$[C_8H_{15}NO_6 + H]^+$	X	X	
GlcNAc dimer	$[C_{16}H_{28}N_2O_{11} + H]^+$	X	X	
GlcNAc trimer	$[C_{24}H_{41}N_3O_{16} + H]^+$	X	X	
GlcNAc tetramer	$[C_{32}H_{54}N_4O_{21} + H]^+$	X	X	

LC-MS data indicated that lysozyme degraded slightly deacetylated (20-30% GlcN) chitin polymers as well. Chitin polymer 1 produced oligomers and monomers in a chromatographic peak following three days of exposure to lysozyme. This peak eluted from ~13-16 minutes and contained exclusively GlcNac monomers, dimers, trimers, and tetramers. Figures showing LC chromatograms with mass spectrometric insets can be found in Appendix D. Degradation was not observed in chitin polymer 2 at any measured time.

GlcNAc was observed to elute at multiple times; first at 5-7 minutes, and again at 13-16 minutes. This is likely the result of oligomers fragmenting in the ESI source. While ESI is considered to be a soft ionization source, its ability to fragment weak bonds in molecules has been well documented[52]. Multiple elution times for both copolymer constituents indicate that the the β-1,4-glycosidic bond connecting GlcN and GlcNAc residues were fragmented within the source. The presence of multiple COS species confirms that lysozyme degrades chitosan given sufficient time; however, it occurs at a considerably slower rate than chemical degradation processes.

Lipase and Hemicellulase

LC-MS analysis indicated that lipase and hemicellulase degradation protocols did not produce low molecular weight products from chitin and chitosan polymers. Chromatograms obtained from these experiments failed to reveal the peaks previously observed at 5-7 minutes or 13-16 minutes that were observed using lysozyme degradation protocols. Additionally, extracted ion chromatogram (EIC) surveys did not indicate the presence of compounds with formulas matching those observed during degradation by lysozyme, or during chemical degradation protocols.

4.5 Conclusions

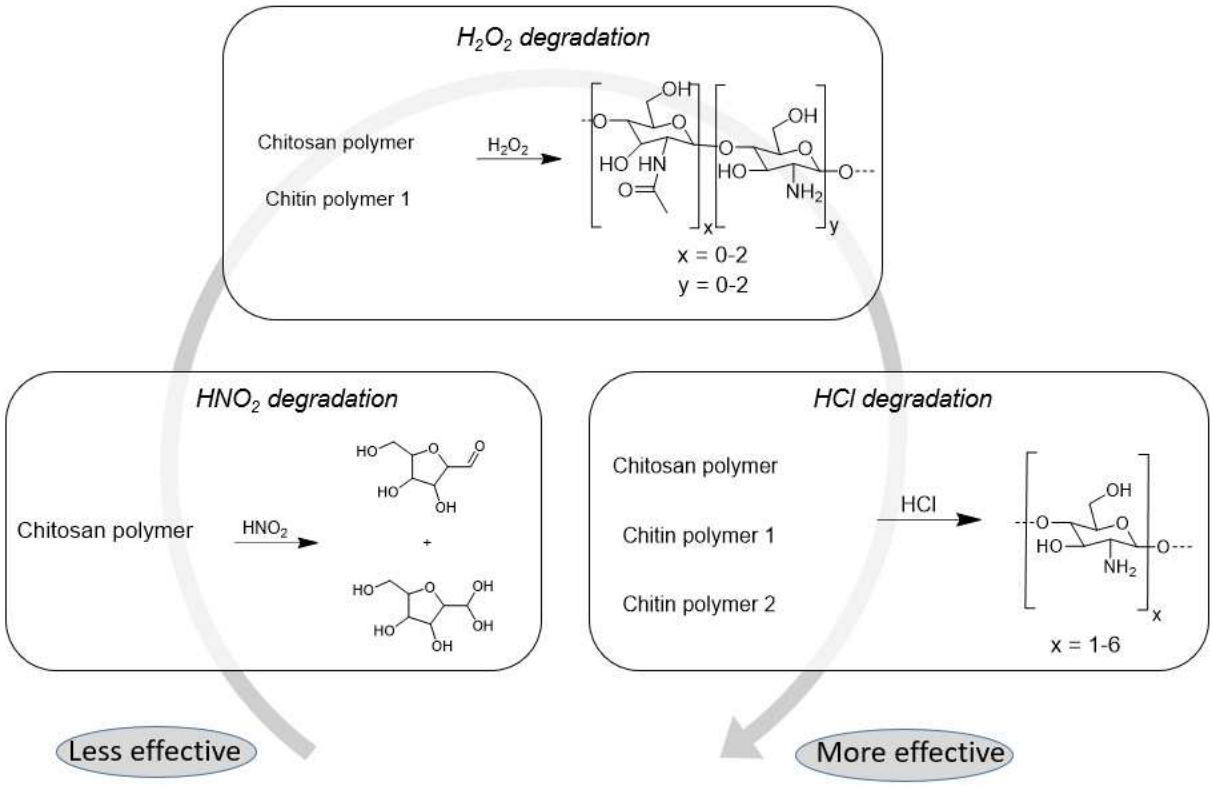

Figure 4.5: Summary of the primary products formed by the degradation protocols tested. Assessments of "more" and "less" effective protocols are based on the protocol's ability to degrade chitin and chitosan polymers with varying degrees of deacetylation. Nitrous acid was effective at degrading only chitosan polymers. Hydrogen peroxide was able to degrade polymers more effectively as their degree of deacetylation increased. Hydrochloric acid was shown to degrade all polymers tested.

Our identification of specific products stands in contrast to methods like HPLC or viscometry which fail to identify specific products form from degradation protocols. These ESI-MS methods can be used in a standalone fashion or to compliment traditional methods of characterizing COS. We proposed that degradation protocols used to produce COS yield distinct products, and that the compositions of these products are dependent on both the degrading agent and the composition of the polymers used. The data acquired confirm this, indicating that HCl, H_2O_2, and HNO_2 degrade chitin and chitosan based on the copolymers' proportion of GlcN to

GlcNAc. The mechanisms responsible for degradation account for the distinct products generated by the protocols studied. For HNO_2, nitrosation and ring rearrangements of terminal GlcN residues produces 2,5-AM monomers[24,25]. Exposure to H_2O_2 results in glycosidic bond scission instigated by radical reactions; these result in proton abstraction from GlcN residues[53]. Hydrochloric acid hydrolyzes glycosidic bonds and also deacetylates GlcNAc residues[47]. Each of these degrading agents generates distinct COS and monomer units, which allows the selection of appropriate degradation protocols to produce COS of desired compositions. Our results indicate that H_2O_2 degrades deacetylated chitosan effectively. Chitin and chitosan's susceptibility to H_2O_2 degradation increases along with its degree of deacetylation. A range of acetylated and deacetylated COS and monomers are generated that result from GlcN-GlcN and GlcN-GlcNAc cleavage within starting polymers. Hydrochloric acid effectively degrades all polymers that were tested, generating GlcN monomers and oligomers by both depolymerizing and deacetylating chitin and chitosan. Nitrous acid degraded only deacetylated chitosan, producing 2,5-AM residues that resulted from reducing end GlcN undergoing a ring rearrangement and being released. Of the three enzymes tested, only lysozyme degraded chitin and chitosan. While lysozyme, hemicellulase, and lipase have all been reported to degrade chitosan or chitin, our results indicated that degradation occurs more quickly using chemical means. Given our quick positive results with chemical degradation methods, we decided the best course of action was to pursue these rather than to optimize the enzymatic degradation methods used. In summary, our use of ESI-TOF-MS to compare these degradation protocols by COS and monomer units produced provides a precise overview of the products one can expect to generate, thereby enabling production of COS that may facilitate more predictable results. Production of COS with composed of both GlcN and GlcNAc can be achieved by using H_2O_2 to degrade starting polymers. Researchers derivatizing the amine

in COS will benefit from using HCl degradations. Simultaneous deacetylation of chitin or chitosan polymers will provide highly deacetylated COS, which may translate into higher yields during modifications. Additionally, as the antibacterial properties of COS are conferred by its primary amine, we strongly recommend the use of HCl to produce a higher proportion of deacetylated oligomers in studies when this is relevant.

CHAPTER 4 – REFERENCES

(1) Rebelo, R.; Fernandes, M.; Fangueiro, R. ScienceDirect ScienceDirect Biopolymers in Medical Implants : A Brief Review. *Procedia Eng.* **2017**, *200*, 236–243. https://doi.org/10.1016/j.proeng.2017.07.034.

(2) Rinaudo, M. Chitin and Chitosan: Properties and Applications. *Progress in Polymer Science (Oxford)*. Pergamon July 1, 2006, pp 603–632. https://doi.org/10.1016/j.progpolymsci.2006.06.001.

(3) Zou, P.; Yang, X.; Wang, J.; Li, Y.; Yu, H.; Zhang, Y.; Liu, G. Advances in Characterisation and Biological Activities of Chitosan and Chitosan Oligosaccharides. *Food Chem.* **2016**, *190* (12), 1174–1181. https://doi.org/10.1016/j.foodchem.2015.06.076.

(4) Gbenebor, O. P.; Adeosun, S. O.; Lawal, G. I.; Jun, S.; Olaleye, S. A. Engineering Science and Technology , an International Journal Acetylation , Crystalline and Morphological Properties of Structural Polysaccharide from Shrimp Exoskeleton. *Eng. Sci. Technol. an Int. J.* **2017**, *20* (3), 1155–1165. https://doi.org/10.1016/j.jestch.2017.05.002.

(5) Peniche, C.; Goycoolea, M. Chitin and Chitosan : Major Sources , Properties and Applications. *1*.

(6) Antonino, R. S. C. M. D. Q.; Fook, B. R. P. L.; Lima, V. A. D. O.; Rached, R. Í. D. F.; Lima, E. P. N.; Lima, R. J. D. S.; Covas, C. A. P.; Fook, M. V. L. Preparation and Characterization of Chitosan Obtained from Shells of Shrimp (Litopenaeus Vannamei Boone). *Mar. Drugs* **2017**, *15* (5). https://doi.org/10.3390/md15050141.

(7) Pillai, C. K. S.; Paul, W.; Sharma, C. P. Progress in Polymer Science Chitin and Chitosan

Polymers : Chemistry , Solubility and Fiber Formation. **2009**, *34*, 641–678. https://doi.org/10.1016/j.progpolymsci.2009.04.001.

(8) Fathi, M.; Donsi, F.; McClements, D. J. Protein-Based Delivery Systems for the Nanoencapsulation of Food Ingredients. *Comprehensive Reviews in Food Science and Food Safety*. Blackwell Publishing Inc. July 1, 2018, pp 920–936. https://doi.org/10.1111/1541-4337.12360.

(9) Sinha, V. R.; Singla, A. K.; Wadhawan, S.; Kaushik, R.; Kumria, R.; Bansal, K.; Dhawan, S. Chitosan Microspheres as a Potential Carrier for Drugs. *International Journal of Pharmaceutics*. Elsevier April 15, 2004, pp 1–33. https://doi.org/10.1016/j.ijpharm.2003.12.026.

(10) Bansal, V.; Sharma, P. K.; Sharma, N.; Pal, O. P.; Malviya, R. Applications of Chitosan and Chitosan Derivatives in Drug Delivery. **2011**, *5* (1), 28–37.

(11) Lutzke, A.; Pegalajar-Jurado, A.; Neufeld, B. H.; Reynolds, M. M. Nitric Oxide-Releasing S-Nitrosated Derivatives of Chitin and Chitosan for Biomedical Applications. *J. Mater. Chem. B* **2014**, *2* (42), 7449–7458. https://doi.org/10.1039/c4tb01340a.

(12) Yin, H.; Du, Y.; Dong, Z. Chitin Oligosaccharide and Chitosan Oligosaccharide : Two Similar but Different Plant Elicitors. **2016**, *7* (April), 2014–2017. https://doi.org/10.3389/fpls.2016.00522.

(13) Kasaai, M. R.; Arul, J.; Charlet, G. Fragmentation of Chitosan by Acids. **2013**, *2013*.

(14) Muanprasat, C.; Chatsudthipong, V. Chitosan Oligosaccharide: Biological Activities and Potential Therapeutic Applications. *Pharmacology and Therapeutics*. Elsevier Inc.

February 1, 2017, pp 80–97. https://doi.org/10.1016/j.pharmthera.2016.10.013.

(15) Wang, Y.; Khan, A.; Liu, Y.; Feng, J.; Dai, L.; Wang, G.; Alam, N.; Tong, L.; Ni, Y. Chitosan Oligosaccharide-Based Dual PH Responsive Nano-Micelles for Targeted Delivery of Hydrophobic Drugs. *Carbohydr. Polym.* **2019**, *223*, 115061. https://doi.org/10.1016/j.carbpol.2019.115061.

(16) Kim, S. Competitive Biological Activities of Chitosan and Its Derivatives: Antimicrobial, Antioxidant, Anticancer, and Anti-Inflammatory Activities. **2018**. https://doi.org/10.1155/2018/1708172.

(17) Jiang, L.; Lu, Y.; Liu, X.; Tu, H.; Zhang, J.; Shi, X.; Deng, H.; Du, Y. Layer-by-Layer Immobilization of Quaternized Carboxymethyl Chitosan/Organic Rectorite and Alginate onto Nanofibrous Mats and Their Antibacterial Application. *Carbohydr. Polym.* **2015**, *121*, 428–435. https://doi.org/10.1016/j.carbpol.2014.12.069.

(18) Guerry, A.; Cottaz, S.; Fleury, E.; Bernard, J.; Halila, S. Redox-Stimuli Responsive Micelles from DOX-Encapsulating Polycaprolactone-g-Chitosan Oligosaccharide. *Carbohydr. Polym.* **2014**, *112*, 746–752. https://doi.org/10.1016/j.carbpol.2014.06.052.

(19) Holme, K. R.; Perlin, A. S. Chitosan N-Sulfate. A Water-Soluble Polyelectrolyte. *Carbohydr. Res.* **1997**, *302* (1–2), 7–12. https://doi.org/10.1016/s0008-6215(97)00117-1.

(20) Lu, Y.; Shah, A.; Hunter, R. A.; Soto, R. J.; Schoenfisch, M. H. Acta Biomaterialia S - Nitrosothiol-Modified Nitric Oxide-Releasing Chitosan Oligosaccharides as Antibacterial Agents. *Acta Biomater.* **2015**, *12*, 62–69. https://doi.org/10.1016/j.actbio.2014.10.028.

(21) Ramos, V. M.; Rodríguez, N. M.; Rodríguez, M. S.; Heras, A.; Agulló, E. Modified

Chitosan Carrying Phosphonic and Alkyl Groups. *Carbohydr. Polym.* **2003**, *51* (4), 425–429. https://doi.org/10.1016/S0144-8617(02)00211-4.

(22) Kittur, F. S.; Vishu Kumar, A. B.; Varadaraj, M. C.; Tharanathan, R. N. Chitooligosaccharides—Preparation with the Aid of Pectinase Isozyme from Aspergillus Niger and Their Antibacterial Activity. *Carbohydr. Res.* **2005**, *340* (6), 1239–1245. https://doi.org/10.1016/j.carres.2005.02.005.

(23) Ngo, D.; Lee, S.; Kim, M.; Kim, S. Production of Chitin Oligosaccharides with Different Molecular Weights and Their Antioxidant Effect in RAW 264 . 7 Cells. *J. Funct. Foods* **2009**, *1* (2), 188–198. https://doi.org/10.1016/j.jff.2009.01.008.

(24) Claustre, S.; Bringaud, F.; Azéma, L.; Baron, R.; Périé, J.; Willson, M. An Easy Stereospecific Synthesis of 1-Amino-2,5-Anhydro-1-Deoxy-D-Mannitol and Arylamino Derivatives. *Carbohydr. Res.* **1999**, *315* (3–4), 339–344. https://doi.org/10.1016/s0008-6215(99)00040-3.

(25) Horton, D.; Philips, K. D. The Nitrous Acid Deamination of Glycosides and Acetates of 2-Amino-2-Deoxy-D-Glucose. *Carbohydr. Res.* **1973**, *30* (2), 367–374. https://doi.org/10.1016/S0008-6215(00)81823-6.

(26) Chang, K. L. B.; Tai, M.; Cheng, F. Kinetics and Products of the Degradation of Chitosan by Hydrogen Peroxide. **2001**. https://doi.org/10.1021/jf001469g.

(27) Li, M.; Han, J.; Xue, Y.; Dai, Y.; Liu, J.; Gan, L.; Xie, R.; Long, M. Hydrogen Peroxide Pretreatment Efficiently Assisting Enzymatic Hydrolysis of Chitosan at High Concentration for Chitooligosaccharides. *Polym. Degrad. Stab.* **2019**, *164*, 177–186. https://doi.org/10.1016/j.polymdegradstab.2019.04.011.

(28) Hai, N. T. T.; Thu, L. H.; Nga, N. T. T.; Hoa, T. T.; Tuan, L. N. A.; Van Phu, D.; Hien, N. Q. Preparation of Chitooligosaccharide by Hydrogen Peroxide Degradation of Chitosan and Its Effect on Soybean Seed Germination. *J. Polym. Environ.* **2019**, *27* (9), 2098–2104. https://doi.org/10.1007/s10924-019-01479-y.

(29) Somashekar, D.; Joseph, R. Chitosanases - Properties and Applications: A Review. *Bioresource Technology*. Elsevier Science Ltd January 1, 1996, pp 35–45. https://doi.org/10.1016/0960-8524(95)00144-1.

(30) Singh Rathore, A.; Gupta, R. D. Chitinases from Bacteria to Human: Properties, Applications, and Future Perspectives. **2015**. https://doi.org/10.1155/2015/791907.

(31) Zelechowska, P.; Agier, J.; Brzezińska-Błaszczyk, E. Endogenous Antimicrobial Factors in the Treatment of Infectious Diseases. *Central European Journal of Immunology*. Termedia Publishing House Ltd. 2016, pp 419–425. https://doi.org/10.5114/ceji.2016.65141.

(32) Zimoch-Korzycka, A.; Gardrat, C.; Castellan, A.; Coma, V.; Jarmoluk, A. The Use of Lysozyme to Prepare Biologically Active Chitooligomers. *Polimeros* **2015**, *25* (1), 35–41. https://doi.org/10.1590/0104-1428.1630.

(33) Lončarević, A.; Ivanković, M.; Rogina, A. Lysozyme-Induced Degradation of Chitosan: The Characterisation of Degraded Chitosan Scaffolds. *J. Tissue Repair Regen.* **2017**, *1* (1), 12–22. https://doi.org/10.14302/issn.2640-6403.jtrr-17-1840.

(34) Shin, S. S.; Lee, Y. C.; Chan, L. The Degradation of Chitosan with the Aid of Lipase from Rhizopus Japonicus for the Production of Soluble Chitosan. *J. Food Biochem.* **2001**, *25* (4), 307–321. https://doi.org/10.1111/j.1745-4514.2001.tb00742.x.

(35) Qin, C.; Du, Y.; Zong, L.; Zeng, F.; Liu, Y.; Zhou, B. Effect of Hemicellulase on the Molecular Weight and Structure of Chitosan. *Polym. Degrad. Stab.* **2003**, *80* (3), 435–441. https://doi.org/10.1016/S0141-3910(03)00027-2.

(36) Knill, C. J.; Kennedy, J. F.; Mistry, J.; Miraftab, M.; Smart, G.; Groocock, M. R.; Williams, H. J. Acid Hydrolysis of Commercial Chitosans. *J. Chem. Technol. Biotechnol.* **2005**, *80* (11), 1291–1296. https://doi.org/10.1002/jctb.1327.

(37) Li, B.; Zhang, J.; Bu, F.; Xia, W. Determination of Chitosan with a Modified Acid Hydrolysis and HPLC Method. *Carbohydr. Res.* **2013**, *366*, 50–54. https://doi.org/10.1016/j.carres.2012.11.005.

(38) Tian, F.; Liu, Y.; Hu, K.; Zhao, B. Study of the Depolymerization Behavior of Chitosan by Hydrogen Peroxide. *Carbohydr. Polym.* **2004**, *57* (1), 31–37. https://doi.org/10.1016/j.carbpol.2004.03.016.

(39) Lu, Y.; Slomberg, D. L.; Schoen, M. H. Biomaterials Nitric Oxide-Releasing Chitosan Oligosaccharides as Antibacterial Agents. **2014**, *35*, 1716–1724. https://doi.org/10.1016/j.biomaterials.2013.11.015.

(40) Tian, F.; Liu, Y.; Hu, K.; Zhao, B. The Depolymerization Mechanism of Chitosan by Hydrogen Peroxide. *J. Mater. Sci.* **2003**, *38* (23), 4709–4712. https://doi.org/10.1023/A:1027466716950.

(41) Chang, K. L. B.; Tai, M. C.; Cheng, F. H. Kinetics and Products of the Degradation of Chitosan by Hydrogen Peroxide. *J. Agric. Food Chem.* **2001**, *49* (10), 4845–4851. https://doi.org/10.1021/jf001469g.

(42) Kuusk, S.; Bissaro, B.; Kuusk, P.; Forsberg, Z.; Eijsink, V. G. H.; Sørlie, M.; Valjamae, P. Kinetics of H2O2-Driven Degradation of Chitin by a Bacterial Lytic Polysaccharide Monooxygenase. *J. Biol. Chem.* **2018**, *293* (2), 523–531. https://doi.org/10.1074/jbc.M117.817593.

(43) Wojtasz-pająk, A.; Szumilewicz, J. DEGRADATION OF CHITIN WITH HYDROGEN PEROXIDE N A MICROWAVE FIELD. **2007**, 13–24.

(44) Jang, J. H.; Hui, C. H.; Ike, M.; Inoue, C.; Fujita, M.; Yoshida, T. Acid Hydrolysis and Quantitative Determination of Total Hexosamines of an Exopolysaccharide Produced by Citrobacter Sp. *Biotechnol. Lett.* **2005**, *27* (1), 13–18. https://doi.org/10.1007/s10529-004-6305-y.

(45) Novikov, V. Y. Acid Hydrolysis of Chitin and Chitosan. *Russ. J. Appl. Chem.* **2004**, *77* (3), 484–487. https://doi.org/10.1023/B:RJAC.0000031297.24742.b9.

(46) Li, J.; Revol, J.; Marchessault, R. H. Effect of Degree of Deacetylation of Chitin on the Properties of Chitin Crystallites. **1996**, 373–380.

(47) Einbu, A.; Vårum, K. M. Depolymerization and De-N-Acetylation of Chitin Oligomers in Hydrochloric Acid. **2007**, 309–314. https://doi.org/10.1021/bm0608535.

(48) Rupley, J. A. The Hydrolysis of Chitin by Concentrated Hydrochloric Acid, and the Preparation of Low-Molecular-Weight Substrate for Lysozyme. *BBA - Spec. Sect. Mucoproteins Mucopolysaccharides* **1964**, *83* (3), 245–255. https://doi.org/10.1016/0926-6526(64)90001-1.

(49) Varum, K. M.; Ottoy, M. H.; Smidsrod, O. Acid Hydrolysis of Chitosans. *Carbohydr.*

Polym. **2001**, *46* (1), 89–98. https://doi.org/10.1016/S0144-8617(00)00288-5.

(50) Li, J.; Revol, J. -F.; Marchessault, R. H. Effect of Degree of Deacetylation of Chitin on the Properties of Chitin Crystallites. *J. Appl. Polym. Sci.* **1997**, *65* (2), 373–380. https://doi.org/10.1002/(SICI)1097-4628(19970711)65:2<373::AID-APP18>3.0.CO;2-0.

(51) Allison, C. L.; Lutzke, A.; Reynolds, M. M. Examining the Effect of Common Nitrosating Agents on Chitosan Using a Glucosamine Oligosaccharide Model System. *Carbohydr. Polym.* **2019**, *203*. https://doi.org/10.1016/j.carbpol.2018.09.052.

(52) Demarque, D. P.; Crotti, A. E. M.; Vessecchi, R.; Lopes, J. L. C.; Lopes, N. P. Fragmentation Reactions Using Electrospray Ionization Mass Spectrometry: An Important Tool for the Structural Elucidation and Characterization of Synthetic and Natural Products. *Natural Product Reports*. Royal Society of Chemistry March 1, 2016, pp 432–455. https://doi.org/10.1039/c5np00073d.

(53) Qin, C.; Li, H.; Xiao, Q.; Liu, Y.; Zhu, J.; Du, Y. Water-Solubility of Chitosan and Its Antimicrobial Activity. *Carbohydr. Polym.* **2006**, *63* (3), 367–374. https://doi.org/10.1016/j.carbpol.2005.09.023.

CHAPTER 5

DETECTION OF FUNGAL-DERIVED GLUCOSAMINE USING LC-MS

5.1 Overview

Up to this point, the work contained in this dissertation has applied degradation and analysis methods to chitin model systems designed to mimic the structural polysaccharides found in fungi. Chapter 5 takes this research a step further, highlighting the application of these methods to *Aspergillus niger*, a species of fungi relevant to pulmonary infections. In Chapters 3 and 4 of this dissertation, studies revolved around the analysis of chitin and its derivatives via the characterization of their low molecular weight degradation products. These compounds, including glucosamine (GlcN), *N*-acetylglucosamine (GlcNAc), 2,5-anhydro-D-mannose (2,5-AM), and chitosan oligosaccharides (COS), can be produced through a wide assortment of degradation protocols. Previous work in this dissertation explored the efficacy of nitrous acid (HNO_2), hydrogen peroxide (H_2O_2), hydrochloric acid (HCl), lysozyme, lipase, and hemicellulase to degrade both chitin and chitosan polymers with differing degrees of acetylation. HCl degradation protocols were shown to quickly and effectively degrade all polymers tested, producing a chemical fingerprint made up of GlcN, and to a lesser extent, GlcN oligomers. Given its effectiveness, HCl degradation protocols were used exclusively for experiments in this chapter.

Chitin, and chitosan to a lesser extent, are constituents of the cell walls of fungi, composing 10-30% of their mass. While most fungal species are harmless, a minority can cause deadly

infections in immunocompromised patients. One such example is *Aspergillus niger,* a species of fungus commonly found in soil and vegetative material. In studies contained in this chapter, *A. niger* fungi were obtained and cultured, then subjected to cell lysis and cleanup steps. Lysed cells were subjected to HCl degradation protocols. Products were extracted into aqueous solutions then analyzed using LC-MS methods making use of hydrophilic interaction liquid chromatography (HILIC) separations. Exposing *A. niger* to these extraction and degradation protocols resulted in the formation of GlcN residues, as previously established in experiments exposing chitin and chitosan polymers to HCl. We verified our results by comparing the chromatograms from the degradation of *A. niger* to chromatograms obtained from the degradation of two chitin polymers also exposed to HCl. The observed retention times and accurate mass measurements provided a two-step validation that GlcN was produced from the degradation of fungal-derived chitin. By applying the methods and knowledge developed in earlier chapters to a relevant fungal species, the results contained in this chapter indicate that the initial premise of this dissertation holds true: LC-MS has the potential to serve as a screening method for pulmonary fungal infections via the detection of chitin. While a significant body of work is still necessary to move these methods from the research laboratory to clinical facilities, these experiments provide proof-of-concept evidence that justifies this dissertation's original postulation, as well as warranting continued study.

5.2 Introduction

Chitin is a β-1-4-linked homopolymer of GlcNAc residues[1]. It is the second most abundant natural polysaccharide in the world, behind cellulose[2,3]. Chitin is a component of crustacean and arthropod exoskeletons and is found in fungal cell walls, where it confers rigidity to its parent organism[4]. Chitin exists in nature as nearly-straight microfibrils with average diameters of ~2.8 nm and of indeterminate lengths[5]. Its size has been reported from ~100 GlcNAc residues in yeast

to 5-8000 GlcNAc residues in crab exoskeletons[6]. While most species of yeasts contain only 1-2% chitin, its abundance is much higher in filamentous fungi, ranging from 10-30%[1]. Chitin is found in the cell walls and septa of all species of pathogenic fungi[7]. Some fungi produce chitin deacetylase enzymes that modify chitin to chitosan during biosynthesis; however, chitosan's abundance in most fungi has not been well-defined[1,8,9].

Fungi are largely innocuous with regard to humans, with fewer than 1% of species having pathogenic capabilities[10]. However, a minority of fungal species are extremely effective opportunistic pathogens[11]. Worldwide, over 300 million cases of serious fungal infections occur annually[12]. Fungal infections can occur superficially (e.g. athlete's foot) or as systemic infections such as candidemia or aspergillosis[13–16]. Fungal spores are found ubiquitously in the environment, and most individuals are exposed to a huge number of airborne fungi with no notable health repercussions. However, those with compromised immune systems have an increased susceptibility to fungal pathogenesis[17]. Deep-seated fungal infections are a serious health risk to immunocompromised patients, and their diagnosis and treatment is often not straightforward[13]. Broadly, mycoses can be separated into two categories: community-acquired and nosocomial (hospital-acquired) infections[10]. In the case of community-acquired cases, fungal spores are often inhaled or ingested, while in nosocomial infections, implantation occurs during medical treatments or procedures[18,19].

Many serious fungal infections arise as secondary infections. Secondary infections are those that occur during or after an initial infection[20]. Initial infections originate from a variety of sources, ranging from cold and flu viruses to more severe conditions like HIV/AIDS and cancer[21]. Procedures like organ transplants and medical device implantation increase the risk of secondary infections, as well as some injuries like severe burns[22]. Fungal infections primarily affect

immunocompromised patients, including HIV/AIDS patients, cancer patients, and various others that require hospitalization. Pulmonary fungal infections compose a significant number of the fungal diseases, with global incidence of >10,000,000 patients. 1,400,000 of these result in fatalities annually[12]. A variety of genera such as *Aspergillus, Cryptococcus,* and *Pneumocystis* are responsible for these infections[23]. It is unlikely that healthy patients will develop fungal pulmonary infections; however, patients with HIV, transplant patients, cancer patients, and patients with emphysema, pneumonia, asthma, and cystic fibrosis are at an elevated risk for pulmonary fungal infections[24]. The Global Action Fund for Fungal Infections (GAFFI) lists four fungal diseases on its "Priority Fungal Infections" list, two of which are classified as being pulmonary infections[12]. The first of these is *Pneumocystis* pneumonia, which is caused by *Pneumocystis jirovecii.* It is most often seen in HIV patients, transplant patients, and those taking corticosteroids or immunomodulatory drugs. The second disease is chronic pulmonary aspergillosis. It is most often caused by *Aspergillus fumigatus* but can also be caused by *A. niger* or *A. flavus*[23]. Chronic pulmonary aspergillosis is most frequently seen in patients that have at one time had lung disease, such as tuberculosis, chronic obstructive pulmonary disease, or lung cancer[25]. With an increasing incidence of HIV in developing countries, especially sub-Saharan Africa, secondary pulmonary infections have increased per capita in recent years. Tuberculosis has experienced a significant resurgence in recent years, as well[26,27]. Although the overall number of patients infected with tuberculosis in modernized countries is quite low (~9000 in the U.S. in 2018), worldwide incidence exceeds 10 million[28].

Pulmonary disease in immunocompromised patients progresses rapidly, resulting in high mortality rates and necessitating prompt treatment[29,30]. As numerous fungal species may be responsible for pulmonary fungal infections, developing nonspecific screening methods is

significant. However, current screening methods have significant drawbacks. Microscopy can be used to detect fungi in stained pulmonary samples. However, these tests are prone to false negatives. The ability of microscopy to accurately detect fungi is dependent on the presence of hyphae in fungal species, which may not appear until later stages in their life cycles[31]. Cultures provide highly accurate diagnostics for fungal infections. Their primary drawback is the extended length of time they require to provide results, which be up to several weeks. We propose that liquid chromatography-mass spectrometry (LC-MS) can be used as a broad screening method for pulmonary fungal infections by detecting chitin contained within fungal cell walls. Chitin may be detected via the separation and detection of GlcN monomers and oligomers that are produced during the controlled degradation of chitin. The detection of polymeric chitin holds the potential to serve as a broad screening method for pulmonary fungal infections in hospital settings.

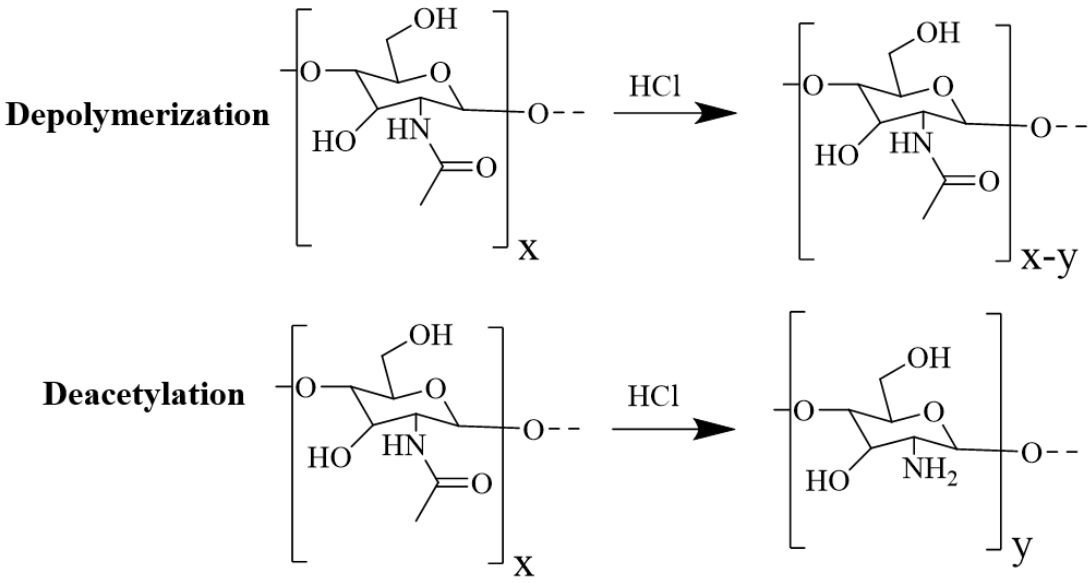

Figure 5.1: Simultaneous chemical modifications that occur upon the exposure of chitin to HCl. Polymers are simultaneously depolymerized and deacetylated, producing a low molecular weight chemical fingerprint that consists primarily of GlcN.

While chitin is not found endogenously in humans, it is ubiquitous in the cell walls of fungi, where it confers rigidity. In the following experiments, fungal-derived chitin was degraded from

Aspergillus niger, a filamentous fungal species, and the degradation products were characterized using LC-MS. Upon exposure to HCl, chitin is simultaneously depolymerized and deacetylated as shown in **Figure 5.1**, resulting in GlcN monomers and oligomers that can be related back to the presence of the parent polymer. These residues are soluble in aqueous liquids and can be separated and detected using LC-MS. Our research provides indication that chitin-derived GlcN can be detected from *Aspergillus niger* cells, a species that has been implicated in fungal pulmonary infections. To provide this proof-of-concept, we obtained *A. niger* cells and developed sample preparation steps to separate extracellular and intracellular components not of interest. We subjected fungi to cell lysis and degradation protocols, then used LC-MS to characterize the degradation products.

5.3 Materials and Methods

5.3.1 Materials

Aspergillus niger fungi were obtained from domestic cat hair samples and cultured on an agar medium. D-glucosamine hydrochloride was obtained from MP Biomedicals (Santa Ana, CA). Chitin polymer (100% acetylated) and *N*-acetyl-D-glucosamine (>98.0%) were obtained from TCI (Portland, OR). Chitin polymer (20-30% deacetylated) was obtained from Alfa Aesar. ACS-grade acetone and Optima LC-MS grade formic acid were obtained from Fisher Chemical (Waltham, MA). Hydrochloric acid was obtained from Ward's Science (Rochester, NY). LC-MS grade water, LC-MS grade acetonitrile, low molecular weight chitosan (96% deacetylated) and ammonium acetate (>98.0%) were obtained were obtained from EMD Millipore (Burlington, MA). 0.2-μm Captiva econo filters were obtained from Agilent (Palo Alto, CA). C18 Macro spin columns were obtained from Harvard Apparatus (Holliston, MA).

5.3.2 Sample preparation

Aspergillus niger was cultured on a dermatophyte test media (DTM) agar plate via standard toothbrush method. Fungi were obtained from domestic cat hair samples. The identification of the fungi was performed using colony morphology and ITS-2 sequencing. To obtain ITS-2 sequencing results, fungus was harvested for DNA extraction and used for conventional PCR analysis. PCR products were sent for sequencing at Macrogen and sequences were compared to entries in GenBank. *Aspergillus niger* cells were transferred into 15 mL centrifuge tubes in a biosafety hood. 5 mL chilled acetone (-20 °C) was added prior to removal from the hood. Samples were incubated for 60 minutes at -20 °C. Following incubation, samples were vortexed for 30 seconds then centrifuged for 10 minutes at 15k x *g*. The supernatant was removed, and samples were allowed to stand for 30 minutes to encourage the evaporation of residual acetone. Liquid nitrogen was added directly to the dried pellets to promote cell lysis. After 5 minutes, 5 mL of -20 °C acetone was added and the pellet vortexed again for 30 seconds. The supernatant was decanted, and the pellet was allowed to evaporate for 30 minutes. 4 mL 10 M HCl was added to the dried pellet. The pellet was vortexed, and the resulting suspension was transferred to a round-bottomed flask. The flask was heated in a water bath held at 90 °C and the acid evaporated over ~6 hours. Following evaporation, the dried material in the flask was reconstituted using Milli-Q grade water (18.2 MΩ•cm). Aliquots were drawn from the flask and passed through 0.2-µm filters. The eluent was added to C18 spin columns and centrifuged for 4 minutes at 2k x *g*. The filtrate was collected and analyzed via LC-MS.

5.3.3 LC-MS Methods

LC-MS analyses were carried out on an Agilent 6224 time-of-flight mass spectrometer coupled to an Agilent 1260 binary liquid chromatograph (Agilent, Palo Alto, CA). Separations

were performed using a Thermo Fisher Acclaim HILIC-10 column with dimensions of 4.6x150 mm and 5-µm particle sizes. The mobile phase was composed of LC-MS grade water and acetonitrile (ACN). Each mobile phase components contained 10 mM ammonium acetate and 0.05% formic acid with a final pH 4.0. The total length of chromatography runs was 50 minutes. Solvent flow rate was set to 0.350 mL/min for the duration of the separation. A gradient elution was used with initial solvent proportions of 90:10 ACN:H_2O. The solvent ratio was adjusted to 80:20 ACN:H_2O from 0-30 minutes. From 30-31 minutes, the solvents ratio was returned to the initial proportion of 90:10 ACN:H_2O. From 31-50 minutes, the column was allowed to reequilibrate and the baseline stabilize. The ion source used was a dual electrospray ionization source operating in positive ion mode. Ion source conditions were as follows: 3500 V capillary voltage, 120 V fragmentor voltage, 60 V skimmer voltage, 250 V octupole voltage, 10 L min^{-1} gas flow (N_2) at 300 °C, and 45 psig nebulizer pressure. The detection range was set to 95-3200 *m/z*.

5.3.4 LC-MS of Controls and Samples

Chitin polymer 1 and chitin polymer 2 were subjugated to HCl degradation (see **Table 5.2** for specific properties of these polymers). For LC-MS analysis of polymer degradation products, ~4 mg chitin polymer 1 and chitin polymer were 2 were added to a 50 mL round-bottomed flask. An appropriate quantity of 10 M HCl was added to the powdered samples. The flask was heated in a water bath held at 90 °C and the acid evaporated over ~6 hours. Following evaporation, the dried material in the flask was reconstituted using Milli-Q grade water (18.2 MΩ•cm). Aliquots were drawn from the flask and passed through 0.2-µm filters. The filtrate was collected and analyzed via LC-MS. Experiments were performed in triplicate.

5.3.5 Data Analysis

All data were analyzed using Agilent MassHunter Qualitative Analysis B.07.00 software. ESI optimization was performed prior to these experiments and a library of potential degradation products was generated to enable extracted ion chromatogram (EIC) scans for data deconvolution. Degradation experiments performed on *Aspergillus* samples were compared to the LC-MS results for chitin polymer degradations. Retention times and accurate mass measurements were both accounted for to provide a two-step validation confirming the identity of degradation products.

5.4 Results and Discussion

5.4.1 LC-MS analysis of GlcN

Using the LC-MS methods described above, GlcN eluted at 24 minutes. Several signals in mass spectral extractions from this chromatographic peak were corroborated with adducts of GlcN. A signal was observed at 162 *m/z,* indicating the presence of a protonated dehydrated GlcN ion, $[C_6H_{13}NO_5 - H_2O + H]^+$. A signal at 180 *m/z* was observed, indicating the presence of a protonated GlcN ion, $[C_6H_{13}NO_5 + H]^+$. A signal was observed at 202 *m/z,* indicating the presence of a sodiated GlcN ion, $[C_6H_{13}NO_5 + Na]^+$. A signal was observed at 381 *m/z* indicating the presence of two GlcN residues dimerized with a single sodium ion to form a $[(2)C_6H_{13}NO_5 + Na]^+$ adduct. All identified GlcN adducts observed are summarized in **Table 5.1**.

Table 5.1: All GlcN adducts observed in mass spectral extractions from LC-MS.

Signal observed (*m/z*)	**Adduct**
162	$[C_6H_{13}NO_5 - H_2O + H]^+$
180	$[C_6H_{13}NO_5 + H]^+$
202	$[C_6H_{13}NO_5 + Na]^+$

381	$[(2)C_6H_{13}NO_5 + Na]^+$

While it was expected that the most prevalent signal would be a protonated adduct at 180 *m/z*, the most abundant signal in mass spectra was shown at 381 *m/z.* To the best of our knowledge, dimerization has not been previously reported in ESI analysis of GlcN; however, $[2M + H]^+$, $[2M + Na]^+$, and variations of these dimerized adducts have been observed in other compounds[32,33]. Dimerized ESI adducts are proposed to result from noncovalent interactions between residues in solution, as Coulombic barriers preclude dimerization following electrospray ionization[34]. The signals at 162, 180, and 222 *m/z* are representative of commonly seen adducts. The 162 *m/z* signal results following the loss of water from GlcN and subsequent protonation, and has previously been observed in the ESI analysis of GlcN[35]. The 180 *m/z* ion is a protonated GlcN adduct, encouraged by the acidic pH in the mobile phase used, while the 222 *m/z* sodiated adduct likely originates from residual salts used in the glass manufacturing process[36].

5.4.2 LC-MS analysis of polymer degradation

The efficacy of degradation methods was established via identification of the degradation products from chitin polymers following exposure to HCl degradation protocols. In these experiments, two chitin polymers were exposed to HCl degradation protocols and the products were characterized using LC-MS. Information regarding the polymers used for degradation studies can be found in **Table 5.2**, along with a generic structure of chitin/chitosan shown in **Figure 5.3**.

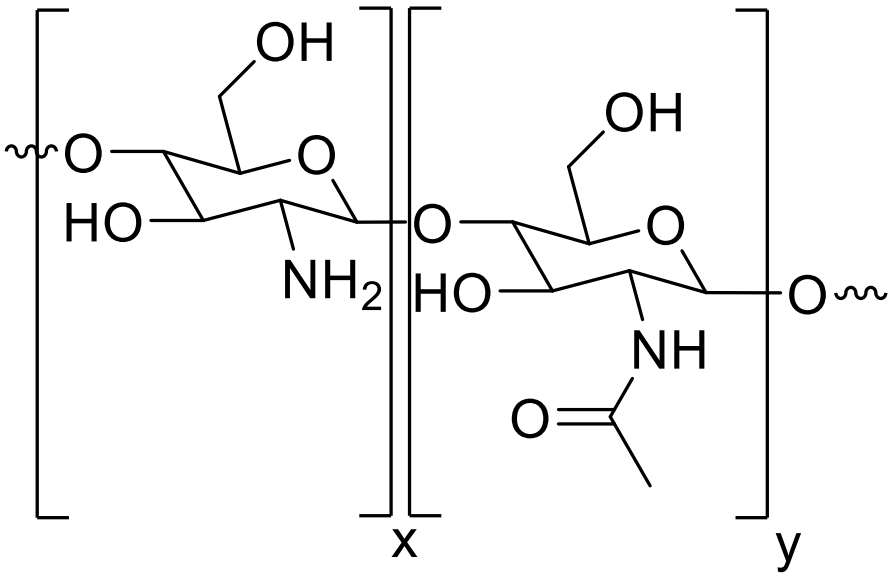

Figure 5.3. Generic structure of chitin (>50% GlcNAc) showing GlcN (x) and GlcNAc (y) subunits.

Table 5.2: Polymers used for degradation studies.

Polymer	**Supplier**	**% GlcN**	**% GlcNAc**
Chitin 1	Alfa Aesar	20-30[a]	70-80
Chitin 2	TCI	-	100[b]

[a]Alfa Aesar certificate of analysis; [b]TCI certificate of analysis

Analysis of degradation products from chitin polymer 1

The first polymer used in these studies had a composition of ~75:25 GlcNAc to GlcN residues. This polymer was exposed to 5 M HCl at a concentration of 1 mg/mL in a round bottomed flask. The acid was removed under heat and evaporation over approximately 6 hours. Milli-Q grade water (18.2 MΩ•cm) was added to the dry flask to resuspend soluble species. The resulting suspension was removed, filtered, and analyzed via LC-MS. The chromatogram obtained from these experiments is shown in **Figure 5.4**.

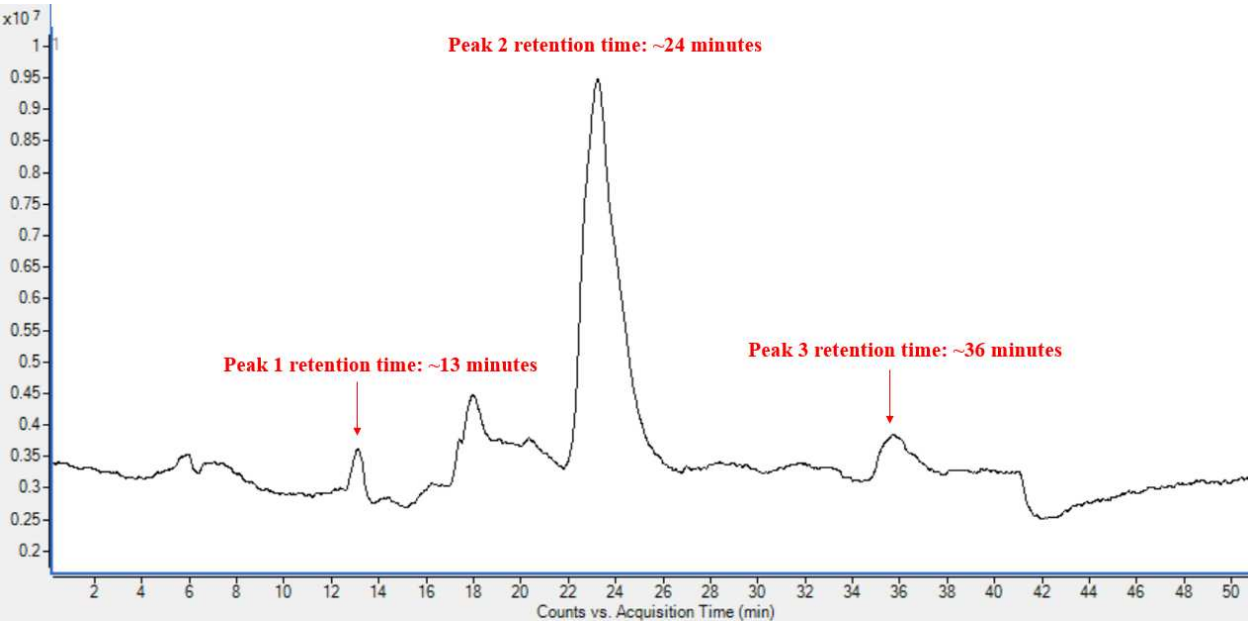

Figure 5.4: Chromatogram of chitin polymer 1 degradation products. Three peaks contained *m/z* signals that indicated the presence of the degradation products of chitin. Unlabeled peaks did not contain signals that correlated to chitin degradation products.

Three peaks in the chromatograms obtained from these experiments contained signals indicating the presence of the degradation products of chitin. The first of these peaks eluted at ~13 minutes and contained adducts of GlcNAc. The most prominent peak in this chromatogram eluted at ~24 minutes and contained adducts of GlcN. A third peak eluting at ~36 minutes contained GlcN dimer adducts. The peak containing GlcNAc adducts was small in proportion to the GlcN peak, which was expected given the ability of HCl to deacetylate GlcNAc residues. As noted in Chapter 4, concentrated HCl depolymerizes chitin polymers considerably faster than it deacetylates residues. Hence, observation of acetylated species was not surprising. GlcN was predicted to be the prevalent product from this degradation protocol, given it is the final product of the depolymerization and deacetylation of chitin polymer. This prediction was confirmed by the relative size of the peak eluting at 24 minutes. Given the propensity of concentrated acid to deacetylate chitin more rapidly than it deacetylates GlcNAc residues, the size of this peak also indicated that depolymerization was largely complete by the time the HCl had evaporated. The

peak at 36 minutes containing adducts of GlcN dimers was relatively small in size and was representative of fully deacetylated, partially depolymerized residues. A summary of the peaks and the compounds eluting in these can be seen in **Table 5.3.**

Table 5.3: Summary of peaks and the ions contained within these.

Retention time	**Compounds**	***m/z* signals identified**
13 minutes	GlcNAc	204, 222, 244, 465
24 minutes	GlcN	162, 180, 202, 381
36 minutes	GlcN dimers	341, 363, 703

The mass spectrum from the chromatographic peak eluting at 13 minutes contained four signals that were corroborated with GlcNAc adducts, as shown in the mass spectrum in **Figure 5.5**. The prominent signal at 465 *m/z* is indicative of a compound with a formula matching that of dimerized GlcNAc residues with an associated sodium ion to form a $[(2)C_8H_{15}NO_6 + Na]^+$ adduct. The signal at 244 *m/z* is indicative of an ion with a formula matching that of a sodiated GlcNAc adduct, $[C_8H_{15}NO_6 + Na]^+$. The signal at 222 *m/z* is indicative of a compound with a formula matching that of a protonated GlcNAc adduct, $[C_8H_{15}NO_6 + Na]^+$. The signal at 204 *m/z* is indicative of a compound with a formula matching that of a dehydrated protonated GlcNAc adduct, $[C_8H_{15}NO_6 - H_2O + H]^+$. Some signals, such as 424 *m/z,* were observed but did not match any predicted or previously observed adducts. These signals may be indictive of unrelated coeluting compounds or of ions that were formed as a result of source fragmentation. Regardless, the presence of multiple adducts provides clear indication of the presence of GlcNAc. Additionally, since this peak is a minor degradation product and would in theory disappear given sufficient polymer exposure to HCl, this was not investigated further.

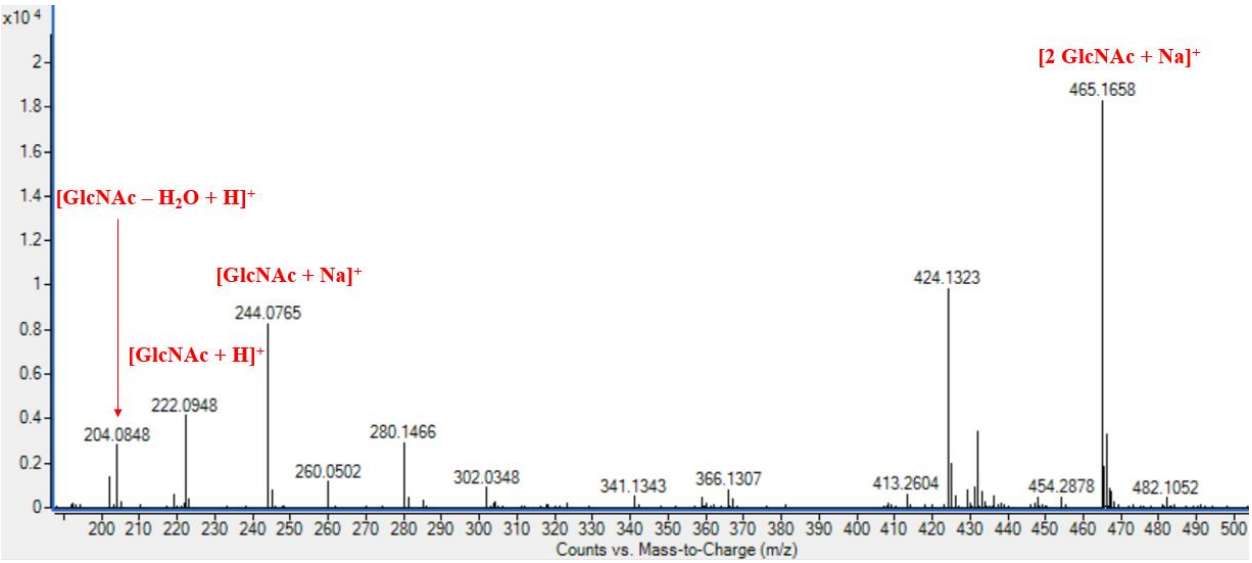

Figure 5.5: Mass spectrum of the 1st chromatographic peak eluting at 13 minutes. Four signals were identified as *m/z* ratios indicating the presence of compounds with molecular formulas matching those of GlcNAc adducts.

The mass spectrum from the chromatographic peak eluting at 24 minutes contained four signals consistent with GlcN adducts. The prominent signal at 381 *m/z* is indicative of a compound with a formula matching that of GlcN residues that dimerized with a sodium ion to form a $[(2)C_6H_{13}NO_5 + H]^+$ adduct. The signal at 202 *m/z* is indicative of a compound with a formula matching that of a sodiated GlcN adduct, $[C_6H_{13}NO_5 + Na]^+$. The signal at 180 *m/z* is indicative of a compound with a formula matching that of a protonated GlcN adduct, $[C_6H_{13}NO_5 + H]^+$. The signal at 162 *m/z* is indicative of a compound with a formula matching that of a dehydrated and protonated GlcNAc adduct, $[C_6H_{13}NO_5 - H_2O + H]^+$. Some signals, such as the cluster from 359 - 362 *m/z,* were observed but did not match any predicted or previously observed adducts. A $[(2)GlcN + H]^+$ dimerized adduct would result in a signal at 359 *m/z*; however, the isotope pattern of the cluster from 359 – 362 *m/z* indicates that the most abundant species is an isotope at 360 *m/z*. This makes $[(2)C_6H_{13}NO_5 + H]^+$ an unlikely assignment. Interestingly, this cluster was also noted in low abundances in the LC-MS of GlcN standards. The presence of this peak in both the GlcN

standard and chitin polymer degradation products provides indication that this signal may represent an unforeseen adduct related to GlcN. There are surprisingly few studies regarding the nature of the ESI ionization of amino sugar residues such as GlcN and GlcNAc. Further investigations into this would provide useful information to define how these molecules behave when ionized.

The mass spectrum from the chromatographic peak eluting at 36 minutes contained three signals consistent with GlcN dimer adducts, as shown in the mass spectrum in **Figure 5.6**. The prominent signal at 703 *m/z* is indicative of a compound with a formula matching that of two GlcN dimers with an associated sodium ion to form a $[(2)C_{12}H_{24}N_2O_9 + Na]^+$ adduct. The signal at 363 *m/z* is indicative of a compound with a formula matching that of a sodiated GlcN dimer, $[C_{12}H_{24}N_2O_9 + H]^+$. The signal at 341 *m/z* is indicative of a compound with a formula matching that of a protonated GlcN dimer, $[C_{12}H_{24}N_2O_9 + H]^+$.

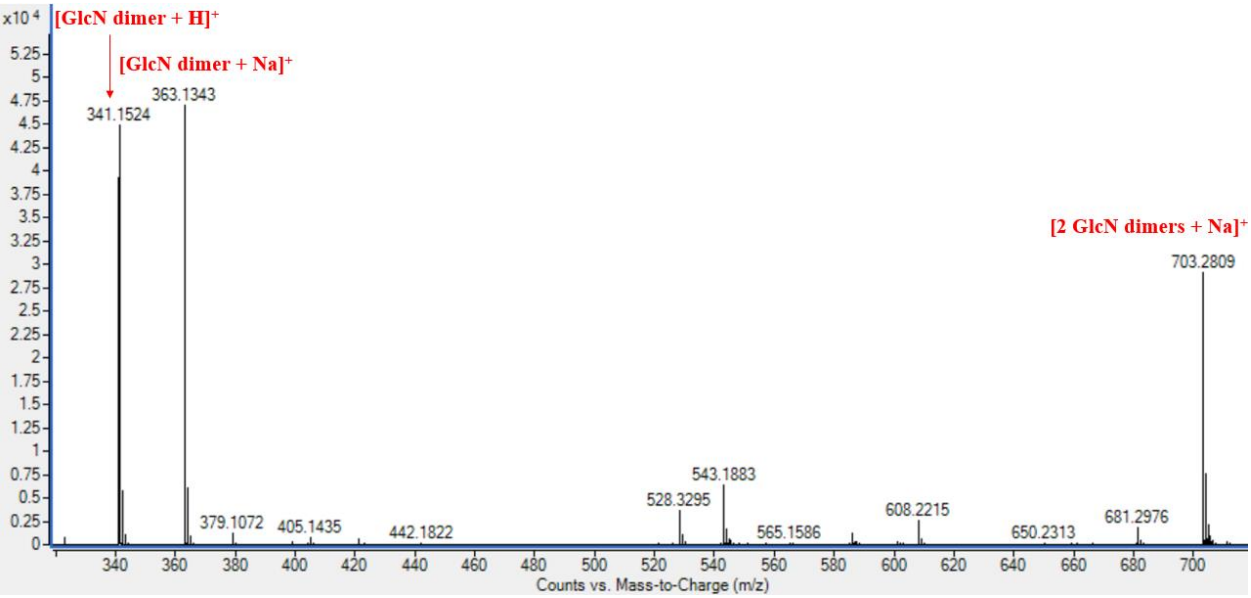

Figure 5.6: Mass spectrum of the 3rd chromatographic peak eluting at 36 minutes. Three signals were identified with *m/z* ratios indicating the presence of compounds with molecular formulas matching GlcNAc adducts.

Analysis of degradation products from chitin polymer 2

The second polymer used exposed to the HCl degradation protocol was chitin polymer 2, which had a composition of 100% GlcNAc. These studies mirrored those with chitin polymer 1, with this analyte being exposed to 10 M HCl at a concentration of 1 mg/mL in a round bottomed flask. The acid was removed under heat by evaporation over approximately 6 hours. Milli-Q grade water (18.2 MΩ•cm) was added to the dry flask to resuspend soluble species. The resulting suspension was removed, filtered, and analyzed via LC-MS. The chromatogram obtained from these experiments is shown in **Figure 5.7**.

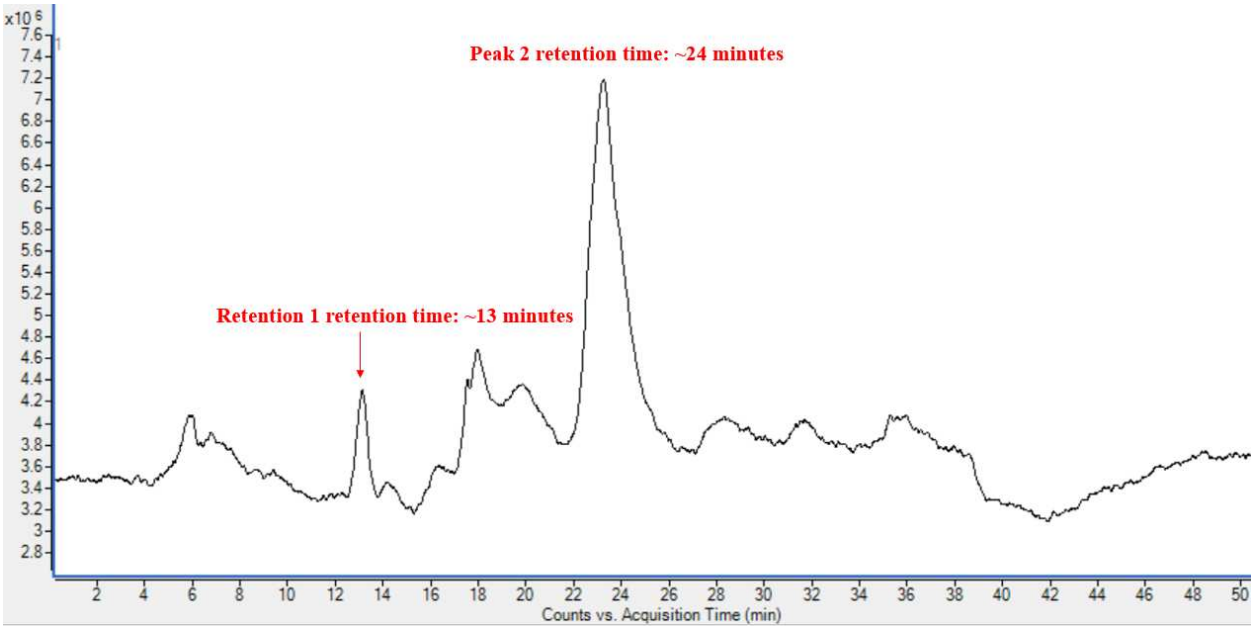

Figure 5.7: Chromatogram of chitin polymer 2 degradation products. Two peaks contained signals that indicated the presence of chitin degradation products. Remaining peaks did not contain signals representative of chitin degradation products.

Two peaks in the chromatograms obtained from these experiments contained signals representative of chitin's degradation products. The first of these peaks eluted at ~13 minutes and contained GlcNAc adducts. As was previously observed in degradation experiments using chitin polymer 1, the peak containing GlcNAc was small in comparison to the peak containing GlcN.

This was expected, given the ability of HCl to deacetylate GlcNAc residues. The mass spectrum extracted from this peak is shown in **Figure 5.8.** The second and most prominent peak in the chromatogram eluted at ~24 minutes and contained GlcN adducts. This was consistent with the analysis of the degradation products of chitin polymer 1. There was a small, poorly resolved peak eluting at 36 minutes that contained GlcN dimers. As this peak barely protruded over the baseline, mass spectral extractions from this peak have not been included.

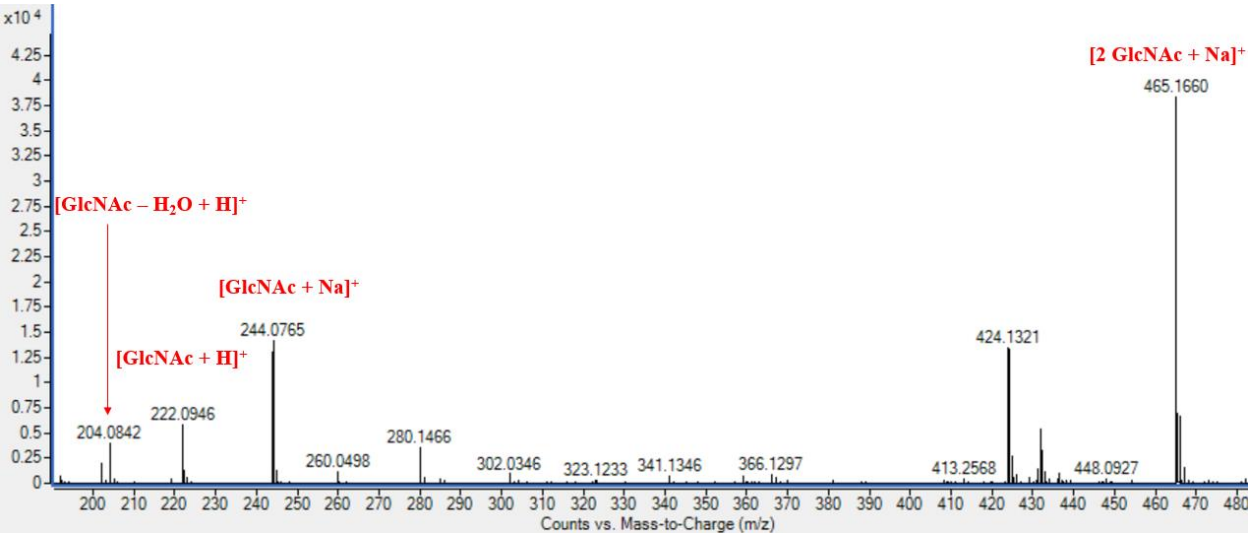

Figure 5.8: Mass spectrum of the 1st chromatographic peak which eluted at 13 minutes. Four signals indicated the presence of compounds with molecular formulas matching those of GlcNAc adducts.

The mass spectrum from the chromatographic peak eluting at 13 minutes contained four signals consistent with GlcNAc adducts. The prominent signal at 465 *m/z* is indicative of a compound with a formula matching that of dimerized GlcNAc with a sodium ion to form a $[(2)C_8H_{15}NO_6 + Na]^+$ adduct. The signal at 244 *m/z* is indicative of a compound with a formula matching that of a sodiated GlcNAc adduct, $[C_8H_{15}NO_6 + Na]^+$. The signal at 222 *m/z* is indicative of a compound with a formula matching that of a protonated GlcNAc adduct, $[C_8H_{15}NO_6 + Na]^+$. The signal at 204 *m/z* is indicative of a compound with a formula matching that of a dehydrated

and protonated GlcNAc adduct, $[C_8H_{15}NO_6 - H_2O + H]^+$. Once again, the signal at 424 *m/z* discussed earlier was observed.

As observed with the results from chitin polymer 1, the mass spectrum from the chromatographic peak eluting at 24 minutes contained four signals consistent with GlcN adducts. A representative mass spectrum from this peak is shown in **Figure 5.9**. However, the prominent signal in these spectrum was the species at 180 *m/z,* indicative of a compound with a formula matching that of a protonated GlcN adduct, $[C_6H_{13}NO_5 + H]^+$. The signal at 202 *m/z* is indicative of a compound with a formula matching that of a sodiated GlcN adduct, $[C_6H_{13}NO_5 + Na]^+$. The signal at 162 *m/z* is indicative of a compound with a formula matching that of a dehydrated and protonated GlcNAc adduct, $[C_6H_{13}NO_5 - H_2O + H]^+$. The signal at 381 *m/z* was observed once again, indicative of a compound with a formula matching that of dimerized GlcN residues with an associated sodium ion to form a $[(2)\ C_6H_{13}NO_5 + H]^+$ adduct. Additionally, the cluster from 359 - 362 *m/z,* was observed again in mass spectra extracted from this peak.

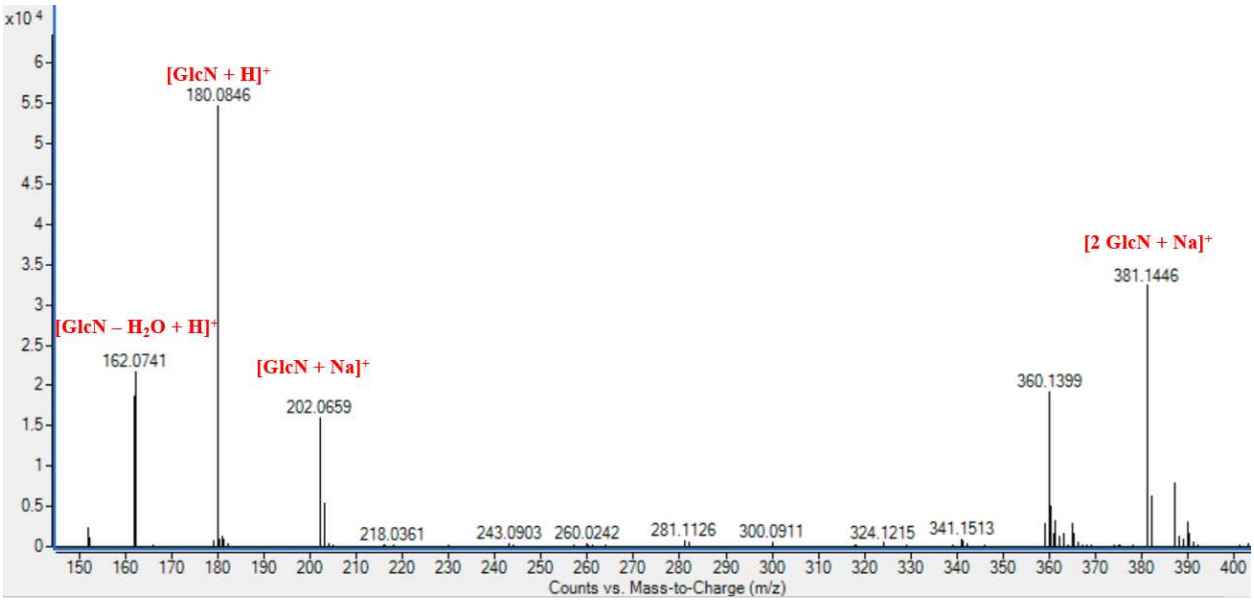

Figure 5.9: Mass spectrum of the 2nd chromatographic peak eluting at 24 minutes. Four signals were identified with *m/z* ratios indicating the presence of ions with molecular formulas matching GlcN adducts.

5.4.3 LC-MS of Aspergillus degradation products

Following the testing of LC-MS methods using chitin polymers, the ability of degradation methods in tandem with LC-MS to detect fungal-derived GlcN was explored. *Aspergillus niger* cells were used for these studies. Cell lysis and precipitation steps were performed first, followed by solid-phase extraction steps for sample cleanup. Following this, we analyzed the degradation products using LC-MS. A representative chromatogram from these experiments can be seen in **Figure 5.10**.

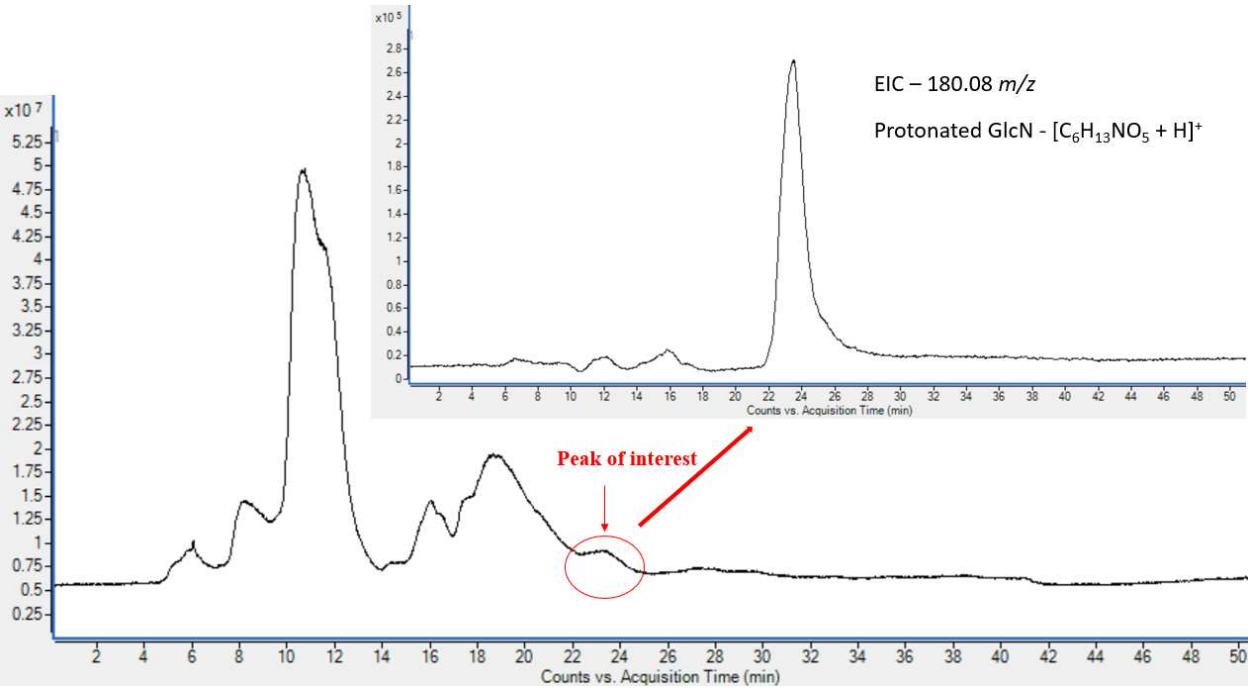

Figure 5.10: Chromatogram of *Aspergillus* degradation products. Analytes of interest eluted in a broad peak at ~24 minutes. The inset shows an extracted ion chromatogram for the monoisotopic mass of GlcN, 180.08.

The chromatogram obtained from the extraction and degradation of chitin from *Aspergillus* contained multiple peaks that overlapped in areas from 5-25 minutes. As a HILIC HPLC column

was used, it was inferred that compounds eluted from least hydrophilic to most hydrophilic. The final peak eluted at ~24 minutes and contained GlcN, along with signals representing coeluting compounds. An Extracted Ion Chromatogram (EIC) for the accurate mass *m/z* measurement of a protonated GlcN adduct was performed, and the peak was overlaid with those from chitin polymer degradation experiments. This overlay can be seen in **Figure 5.11.**

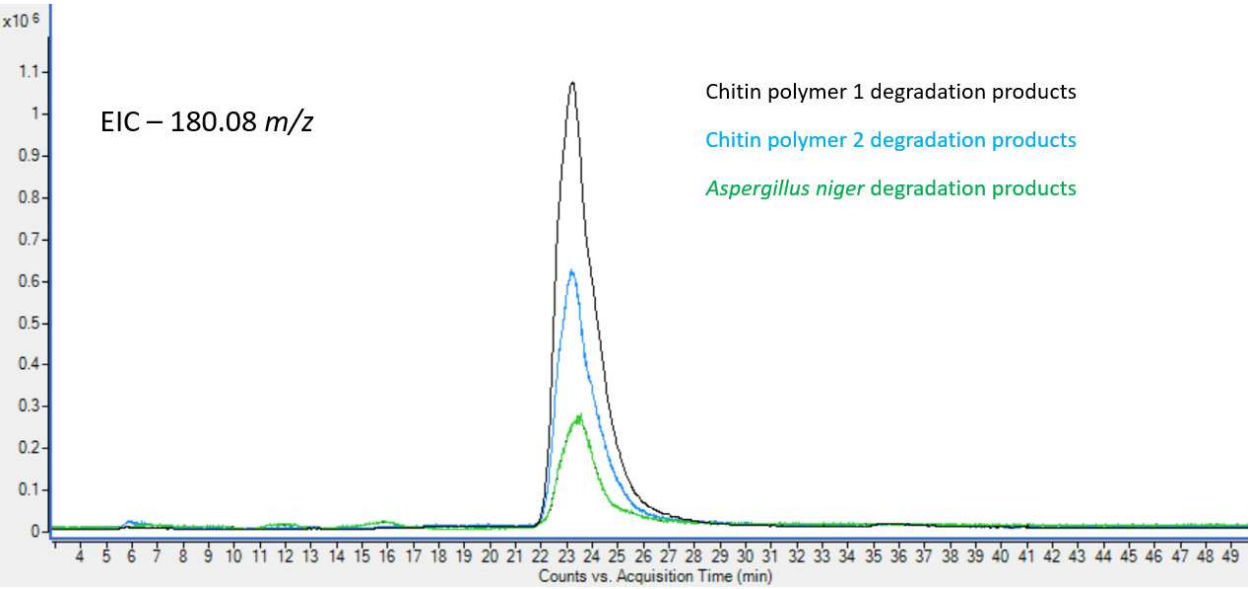

Figure 5.11: Overlay of EICs from degradation experiments. The value for EIC scans was set to 180.08 to highlight the elution of protonated GlcN. The black trace represents GlcN produced from chitin polymer 1. The blue trace represents GlcN produced from chitin polymer 2. The green trace represents GlcN produced from *Aspergillus* fungi.

An EIC is a reconstructed chromatogram in which ions of interest are highlighted via software extraction. They are performed for a variety purposes, such as increasing the resolution of coeluting compounds, for isomer differentiation, or for detecting of ions of interest. The use of EICs is common in proteomics, metabolomics, lipidomics, and other subfields in which sample complexity is high[37–39]. In this instance, we performed EIC extractions to specifically highlight the most abundant degradation product from the degradation of chitin, and to validate that polymer models and fungi both produce GlcN during degradation. The EIC overlays confirm the production

of GlcN from both chitin polymers studied, as well as the chitin contained in *Aspergillus niger* fungi. The chromatographic peaks for both chitin polymers as well as fungal extractions line up at ~24 minutes. We extracted mass spectra from these peaks, which can be found in **Figure 5.12.** Chromatographic elution times and analysis of *m/z* values suggest the presence of ions with identical polarity and molecular weights, providing a two-step validation of the presence of GlcN in all samples tested.

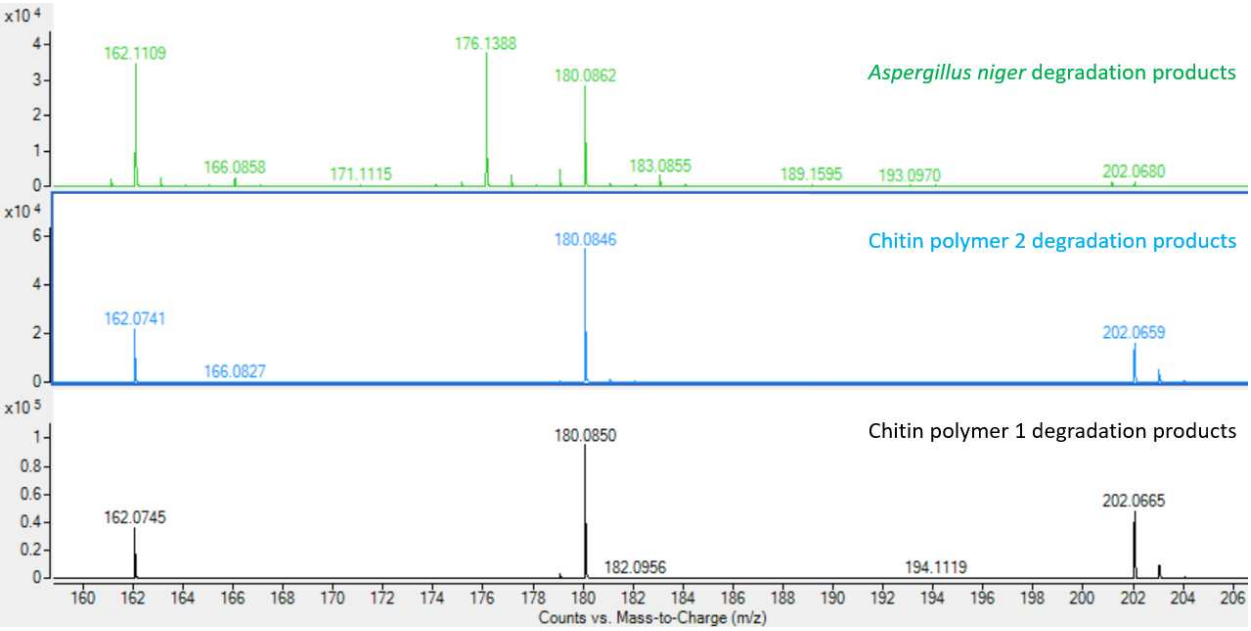

Figure 5.12: MS overlays from LC-MS analysis of polymer and fungal degradations.

Extractions of mass spectra from chromatographic peaks at ~24 minutes all displayed signals at 180 *m/z,* indicative of ions with formulas matching those of protonated GlcN adducts, $[C_6H_{13}NO_5 + H]^+$. The degradation of both chitin polymers displayed a signal at 202 *m/z,* indicative of ions with formulas matching those of sodiated GlcN adducts, $[C_6H_{13}NO_5 + Na]^+$. The mass spectrum of *Aspergillus* contained a signal at 202 *m/z*; however, its abundance was very low. The degradation products from chitin polymers also displayed signals at 162 *m/z*, indicative of ions with formulas matching those of protonated dehydrated GlcN adducts, $[C_6H_{13}NO_5 - H_2O + H]^+$.

While the mass spectrum of *Aspergillus* contained a signal at 162 *m/z,* its monoisotopic mass varied from that expected from a protonated dehydrated GlcN ion. Closer examination revealed that the peak at 162.1109 *m/z* was split, suggesting that two molecules with similar but not identical *m/z* ratios were present in mass spectra. Greater resolving power would be required necessary to distinguish between these peaks.

5.5 Conclusions

In this chapter, we used LC-MS to detect GlcN from fungal-derived chitin. To accomplish this, we obtained *Aspergillus niger* fungi and exposed these to cell lysis and sample cleanup steps. Lysed cells were exposed to previously developed degradation protocols using HCl. The acidic solution was evaporated and water-soluble analytes were resuspended into an aqueous suspension, which was filtered and analyzed using HILIC-ESI-MS. LC-MS analysis indicated the presence of a chromatographic peak with a retention time matching that of GlcN produced from the degradation of chitin. Mass spectral extractions of this peak provided secondary confirmation of its identity, showing the presence of a signal at 180.08 *m/z,* matching that of a protonated GlcN ion.

The studies performed in this chapter mark the first application of methods developed earlier in the dissertation. Mass spectrometric methods first studied in Chapter 2 led to the development of LC-MS methods used for these analyses. Degradation methods developed through Chapters 3 and 4 led to the selection of the protocol to break down fungal-derived chitin. The analyte produced from fungal degradation in Chapter 5 was consistent with those generated during the analysis and comparison of degradation protocols using several variations of chitin and chitosan. Retention times and accurate mass measurements were compared to validate that chitosan polymers, chitin polymers, as well as *A. niger* produce GlcN following exposure to HCl.

Additional studies are necessary to transfer these methods from research labs to clinical facilities. However, from start to finish, the research contained in this dissertation provides the groundwork and proof of concept studies necessary to confirm the potential of LC-MS to serve as a diagnostic method for pulmonary infections.

CHAPTER 5 – REFERENCES

(1) Ohno, N. *2.17 Yeast and Fungal Polysaccharides*.

(2) Verma, D.; Fortunati, E. Biopolymer Processing and Its Composites: An Introduction. In *Biomass, Biopolymer-Based Materials, and Bioenergy: Construction, Biomedical, and other Industrial Applications*; Elsevier, 2019; pp 3–23. https://doi.org/10.1016/B978-0-08-102426-3.00001-1.

(3) Bhat, G. S.; Rong, H. Biodegradable Nonwovens. In *Biodegradable and Sustainable Fibres: A Volume in Woodhead Publishing Series in Textiles*; Elsevier Ltd, 2005; pp 310–342. https://doi.org/10.1533/9781845690991.310.

(4) Lopez-Romero, E.; Ruiz-Herrera, J. The Role of Chitin in Fungal Growth and Morphogenesis. In *Chitin in Nature and Technology*; Springer US, 1986; pp 55–62. https://doi.org/10.1007/978-1-4613-2167-5_8.

(5) Resh, V. H. *Encyclopedia of Insects*; Elsevier Inc., 2009. https://doi.org/10.1016/B978-0-12-374144-8.X0001-X.

(6) Das, S.; Roy, D.; Sen, R. Utilization of Chitinaceous Wastes for the Production of Chitinase. In *Advances in Food and Nutrition Research*; Academic Press Inc., 2016; Vol. 78, pp 27–46. https://doi.org/10.1016/bs.afnr.2016.04.001.

(7) Lenardon, M. D.; Munro, C. A.; Gow, N. A. R. Chitin Synthesis and Fungal Pathogenesis. *Current Opinion in Microbiology*. Elsevier August 2010, pp 416–423. https://doi.org/10.1016/j.mib.2010.05.002.

(8) Winkler, S.; Kaplan, D. L. Biosynthesized Materials: Properties and Processing. *Encycl.*

Mater. Sci. Technol. **2001**, 609–615. https://doi.org/10.1016/b0-08-043152-6/00117-0.

(9) Pochanavanich, P.; Suntornsuk, W. Fungal Chitosan Production and Its Characterization. *Lett. Appl. Microbiol.* **2002**, *35* (1), 17–21. https://doi.org/10.1046/j.1472-765X.2002.01118.x.

(10) Veríssimo, C. Fungal Infections. In *Environmental Mycology in Public Health: Fungi and Mycotoxins Risk Assessment and Management*; Elsevier Inc., 2015; pp 27–34. https://doi.org/10.1016/B978-0-12-411471-5.00003-X.

(11) Pfaller, M. A.; Diekema, D. J. Rare and Emerging Opportunistic Fungal Pathogens: Concern for Resistance beyond Candida Albicans and Aspergillus Fumigatus. *Journal of Clinical Microbiology*. American Society for Microbiology Journals October 1, 2004, pp 4419–4431. https://doi.org/10.1128/JCM.42.10.4419-4431.2004.

(12) GAFFI. Fungal Disease Frequency | Gaffi - Global Action Fund for Fungal Infections https://www.gaffi.org/why/fungal-disease-frequency/ (accessed Apr 12, 2020).

(13) Badiee, P.; Hashemizadeh, Z. Opportunistic Invasive Fungal Infections: Diagnosis & Clinical Management. *Indian Journal of Medical Research*. Indian Council of Medical Research 2014, pp 195–204.

(14) Rautemaa-Richardson, R.; Richardson, M. D. Systemic Fungal Infections. *Medicine (United Kingdom)*. Elsevier Ltd December 1, 2017, pp 757–762. https://doi.org/10.1016/j.mpmed.2017.09.007.

(15) Wenzel, R. P. Nosocomial Candidemia: Risk Factors and Attributable Mortality. *Clin. Infect. Dis.* **1995**, *20* (6), 1531–1534. https://doi.org/10.1093/clinids/20.6.1531.

(16) Denning, D. W. *Invasive Aspergillosis*.

(17) CDC. Global Fungal Diseases | Fungal Diseases https://www.cdc.gov/fungal/global/index.html (accessed Apr 12, 2020).

(18) Jarvis, W. R. Epidemiology of Nosocomial Fungal Infections, with Emphasis on Candida Species. *Clin. Infect. Dis.* **1995**, *20* (6), 1526–1530. https://doi.org/10.1093/clinids/20.6.1526.

(19) Taplitz, R. A.; Ritter, M. L.; Torriani, F. J. Infection Prevention and Control, and Antimicrobial Stewardship. In *Infectious Diseases*; Elsevier, 2017; pp 54-61.e1. https://doi.org/10.1016/b978-0-7020-6285-8.00006-x.

(20) Bonagura, V. R. *Infections That Cause Secondary Immunodeficiency*; Elsevier Inc., 2014. https://doi.org/10.1016/B978-0-12-405546-9.00046-7.

(21) Hendaus, M. A.; Jomha, F. A.; Alhammadi, A. H. Therapeutics and Clinical Risk Management Dovepress Virus-Induced Secondary Bacterial Infection: A Concise Review. *Ther. Clin. Risk Manag.* **2015**, 11–1265. https://doi.org/10.2147/TCRM.S87789.

(22) Trottein, F.; Alcorn, J. F. *Editorial: Secondary Respiratory Infections in the Context of Acute and Chronic Pulmonary Diseases*; 2019; Vol. 10. https://doi.org/10.3389/fimmu.2019.02764.

(23) Fungi and Fungal Infections | Gaffi - Global Action Fund for Fungal Infections https://www.gaffi.org/why/fungi-fungal-infections/ (accessed Mar 9, 2020).

(24) Life http://www.life-worldwide.org/fungal-diseases/chronic-or-deep-tissue/ (accessed Mar 9, 2020).

(25) Bongomin, F.; Gago, S.; Oladele, R. O.; Denning, D. W. Global and Multi-National Prevalence of Fungal Diseases—Estimate Precision. *Journal of Fungi*. 2017. https://doi.org/10.3390/jof3040057.

(26) Ya Diul Mukadi; Maher, D.; Harries, A. Tuberculosis Case Fatality Rates in High HIV Prevalence Populations in Sub-Saharan Africa. *Aids* **2001**, *15* (2), 143–152. https://doi.org/10.1097/00002030-200101260-00002.

(27) Pneumonia https://www.who.int/news-room/fact-sheets/detail/pneumonia (accessed Mar 9, 2020).

(28) Fungal Diseases Homepage | CDC https://www.cdc.gov/fungal/index.html (accessed Mar 9, 2020).

(29) Bajaj, S. K.; Tombach, B. Respiratory Infections in Immunocompromised Patients: Lung Findings Using Chest Computed Tomography. *Radiol. Infect. Dis.* **2017**, *4* (1), 29–37. https://doi.org/10.1016/j.jrid.2016.11.001.

(30) Pragman, A. A.; Berger, J. P.; Williams, B. J. Understanding Persistent Bacterial Lung Infections: Clinical Implications Informed by the Biology of the Microbiota and Biofilms. *Clin. Pulm. Med.* **2016**, *23* (2), 57–66. https://doi.org/10.1097/CPM.0000000000000108.

(31) Life http://www.life-worldwide.org/fungal-diseases (accessed Apr 18, 2020).

(32) Pan, H. A Non-Covalent Dimer Formed in Electrospray Ionisation Mass Spectrometry Behaving as a Precursor for Fragmentations. *Rapid Commun. Mass Spectrom.* **2008**, *22* (22), 3555–3560. https://doi.org/10.1002/rcm.3767.

(33) Schug, K.; McNair, H. M. Adduct Formation in Electrospray Ionization Mass

Spectrometry: II. Benzoic Acid Derivatives. *J. Chromatogr. A* **2003**, *985* (1–2), 531–539. https://doi.org/10.1016/S0021-9673(02)01732-6.

(34) Smith, R. D.; Light-Wahl, K. J.; Winger, B. E.; Loo, J. A. Preservation of Non-covalent Associations in Electrospray Ionization Mass Spectrometry: Multiply Charged Polypeptide and Protein Dimers. *Org. Mass Spectrom.* **1992**, *27* (7), 811–821. https://doi.org/10.1002/oms.1210270709.

(35) Taguchi, R.; Hamakawa, N.; Maekawa, N.; Ikezawa, H. Application of Electrospray Ionization MS/MS and Matrix-Assisted Laser Desorption/Ionization-Time of Flight Mass Spectrometry to Structural Analysis of the Glycosyl-Phosphatidylinositol-Anchored Protein. *J. Biochem.* **1999**, *126* (2), 421–429. https://doi.org/10.1093/oxfordjournals.jbchem.a022467.

(36) Watson, D. D. Controlling Na and K Adducts in LC-MS https://www.chromacademy.com/chromatography-Na-and-K-Adducts-in-LC-MS.html (accessed Apr 14, 2020).

(37) Koulman, A.; Woffendin, G.; Narayana, V. K.; Welchman, H.; Crone, C.; Volmer, D. A. High-Resolution Extracted Ion Chromatography, a New Tool for Metabolomics and Lipidomics Using a Secondgeneration Orbitrap Mass Spectrometer. *Rapid Commun. Mass Spectrom.* **2009**, *23* (10), 1411–1418. https://doi.org/10.1002/rcm.4015.

(38) Zhang, W.; Zhao, P. X. Quality Evaluation of Extracted Ion Chromatograms and Chromatographic Peaks in Liquid Chromatography/Mass Spectrometry-Based Metabolomics Data. *BMC Bioinformatics* **2014**, *15* (11), S5. https://doi.org/10.1186/1471-2105-15-S11-S5.

(39) Lu, P.; Fan, M. J.; Zhang, Q.; Zheng, Q. X.; Liu, P. P.; Wang, B.; Guo, J. W.; Wang, S.; Fu, H. Y.; Yu, Y. J.; et al. A Novel Strategy for Extracted Ion Chromatogram Extraction to Improve Peak Detection in UPLC-HRMS. *Anal. Methods* **2018**, *10* (42), 5118–5126. https://doi.org/10.1039/c8ay01850b.

CHAPTER 6

CONCLUSIONS AND FUTURE DIRECTIONS

6.1 Conclusions

From its inception, this dissertation sought to answer whether LC-MS may serve as a diagnostic method for fungal infections. Over the course of the five preceding chapters, the research to address this has been summarized. Establishing the ability of LC-MS to screen for fungal infections necessitated a significant quantity of research on the central components studied, such as the degradation of chitin and chitosan, as well as the use of mass spectrometry to study these copolymers. Projects covered in this dissertation led to the completion of several milestones. Repeatable ESI methods were developed and optimized to detect the degradation products of chitin and chitosan. Following this, the susceptibility of chitosan to depolymerization by nitrosating agents was established and tracked using ESI mass spectrometry. Our results showed that nitrosating agents can depolymerize chitosan polymers, resulting in the production of low molecular weight compounds that should be accounted for in medically relevant applications. The scope of degradation studies was expanded to include chitin and chitosan polymers with wide degrees of acetylation. This model system was exposed to chemical and enzymatic degradation agents to comparatively assess their ability to degrade these polymers. The chemical fingerprint produced from each of these protocols was characterized using mass spectrometry or LC-MS. Separations methods were developed to separate and detect the compounds produced from chitin and chitosan, and degradation protocols were developed to produce GlcN from both chitin and

chitosan polymers with varying degrees of deacetylation. Ultimately, polymer degradation methods were used in tandem with LC-MS to detect fungal-derived GlcN, providing the proof of concept that LC-MS can detect compounds produced from pathogenic fungi.

6.2 Future directions

The experiments contained in this dissertation provide the proof-of-concept evidence that LC-MS is a feasible method to detect fungal-derived GlcN. However, to remove compounds that could result in ion suppression during LC-MS, it would be beneficial to implement additional sample cleanup steps. These cleanup steps fall into one of two categories: 1) precipitation steps using solvents with higher polarity than those currently used, or 2) the addition of solid-phase extraction (SPE) steps to remove compounds that coelute with GlcN. While significant milestones were achieved during this research, significant studies are still necessary for these methods to be implemented in clinical laboratories. Following the addition of sample cleanup steps, fungal degradation and GlcN separation methods should be tested using a biologically relevant medium. For applications involving pulmonary fungal infections, it is crucial that this model system utilize a mucin component. Mucins are a family of heavily glycosylated proteins that are a primary component of mucous. Once LC-MS methods have been testing using this model system, degradation and separation methods should be expanded to include additional species of fungi beyond *Aspergillus niger*. A more diverse survey of pathogenic fungi would verify that LC-MS could be effective as a broad screening technique for pulmonary fungal infections. Species should include *Cryptococcus* and *Pneumocystis* species, both of which are frequently implicated in fungal pulmonary disease. With clinical applicability in mind, LC-MS methods should be transferred to a ultra-high-performance liquid chromatography (UHPLC) in tandem with a triple quadrupole mass spectrometer. While transferring HPLC to UHPLC methods will be straightforward, new

method development will be necessary for detecting GlcN with a triple quadrupole. Transferring analysis methods to this system will decrease chromatography time and increase sensitivity. Since triple quadrupoles are prevalent in clinical labs, method transferal will make the proposed methods more widely applicable.

The final step in moving towards clinical applicability is to validate that the proposed methods can detect fungal-derived GlcN from patients with pulmonary fungal infections. Acquiring relevant samples (e.g. sputum, lavage) would necessitate partnership with at least one hospital. National surveillance does not exist for many fungal diseases; therefore, rates of infection are difficult to determine[1,2]. Estimates can still be made that account for patient susceptibility and infection rates, however. For example, organ transplant patients are at high risk for pulmonary fungal infections. The UCHealth Transplant Center at the Anschutz Medical Campus performs ~30 lung transplants annually[3]. Lung transplants are particularly susceptible to infection by *Aspergillus,* with around 33% of patients contracting Aspergillosis[4,5]. By those estimates, over the course of 18 months, a collaborative effort with this hospital would provide ~15 *Aspergillus*-positive samples. *Pneumocystis* pneumonia also occurs frequently in transplant patients. **Table 6.1** shows the number of transplants performed statewide at four hospitals in Colorado in 2018, along with transplant patient susceptibility to *Pneumocystis* pneumonia. From these numbers, we can estimate a range of positive samples that could be obtained from collaborating with the four hospitals in Colorado at which transplants occur. Making the assumption that the number of infections falls at the middle value in each range, we could obtain 65 samples that test positive for *Pneumocystis* pneumonia over an 18-month time period from exclusively transplant patients. Our estimates suggest that over 18 months, a total of ~500 samples of interest could be obtained. According to risk factors, ~80 of these would test positive for *Aspergillus* or *Pneumocystis* fungi.

At least 30 samples are require to establish a Gaussian reference range in clinical samples[6]. FDA clearance would require additional sample acquisition, however[7]. 500 total samples (with 80 positive) falls well within the range of previous studies proposing novel fungal detection assays[8,9].

Table 6.1: Transplants performed in Colorado in 2018 at UCHealth, Presbyterian/St. Luke's, Porter Adventist, and Children's Hospital Colorado[10].

Transplant type	**Transplants performed (2018)**[10]	**Risk of *Pneumocystis* pneumonia**[11]	**Number of samples that could be obtained in 12 months**	**Number of samples that could be obtained in 18 months**
Heart-lung/lung	52	6.5-43%	3-22	5-34
Heart	59	2-41%	1-24	2-36
Liver	98	3-11%	3-11	4-16
Kidney	268	0.6-14%	2-38	2-56

At the beginning of this dissertation, a novel concept was proposed that led to the completion of multiple projects. These were disseminated through various outlets, including publications[12–14], poster presentations, and oral presentations. The milestones accomplished during the completion of this research stand on their own as contributions to the fields of LC-MS methods development and polymer characterization; however, their potential is best assessed in the context of the overall goal presented in this dissertation. Ultimately, the results presented in this dissertation indicate that further studies on this project are highly warranted.

CHAPTER 6 – REFERENCES

(1) Aspergillosis Statistics | Aspergillosis | Types of Fungal Diseases | Fungal Diseases | CDC https://www.cdc.gov/fungal/diseases/aspergillosis/statistics.html (accessed May 17, 2020).

(2) Pneumocystis pneumonia | Fungal Diseases | CDC https://www.cdc.gov/fungal/diseases/pneumocystis-pneumonia/index.html (accessed May 17, 2020).

(3) UCHealth celebrates 25 years of lung transplant success | University of Colorado https://www.cu.edu/cu-careers/news/uchealth-celebrates-25-years-lung-transplant-success (accessed May 17, 2020).

(4) Solé, A.; Morant, P.; Salavert, M.; Pemán, J.; Morales, P.; Pastor, A.; Lozano, C.; Vicente, R.; Ramos, F.; Blasco, E.; et al. Aspergillus Infections in Lung Transplant Recipients: Risk Factors and Outcome. *Clin. Microbiol. Infect.* **2005**, *11* (5), 359–365. https://doi.org/10.1111/j.1469-0691.2005.01128.x.

(5) Patterson, J. E.; Peters, J.; Calhoon, J. H.; Levine, S.; Anzueto, A.; Al-Abdely, H.; Sanchez, R.; Patterson, T. F.; Rech, M.; Jorgensen, J. H.; et al. Investigation and Control of Aspergillosis and Other Filamentous Fungal Infections in Solid Organ Transplant Recipients. *Transpl. Infect. Dis.* **2000**, *2* (1), 22–28. https://doi.org/10.1034/j.1399-3062.2000.020105.x.

(6) Clinical Laboratory Statistics - UCSD Lab Medicine http://ucsdlabmed.wikidot.com/chapter-1 (accessed May 17, 2020).

(7) Lathrop, J. T.; Branch, H. *Analytical Validation and Points for Discussion*.

(8) Reinwald, M.; Spiess, B.; Heinz, W. J.; Heussel, C. P.; Bertz, H.; Cornely, O. A.; Hahn, J.; Lehrnbecher, T.; Kiehl, M.; Laws, H. J.; et al. Aspergillus PCR-Based Investigation of Fresh Tissue and Effusion Samples in Patients with Suspected Invasive Aspergillosis Enhances Diagnostic Capabilities. *J. Clin. Microbiol.* **2013**, *51* (12), 4178–4185. https://doi.org/10.1128/JCM.02387-13.

(9) Shin, J. H.; Ranken, R.; Sefers, S. E.; Lovari, R.; Quinn, C. D.; Meng, S.; Carolan, H. E.; Toleno, D.; Li, H.; Lee, J. N.; et al. Detection, Identification, and Distribution of Fungi in Bronchoalveolar Lavage Specimens by Use of Multilocus PCR Coupled with Electrospray Ionization/Mass Spectrometry. *J. Clin. Microbiol.* **2013**, *51* (1), 136–141. https://doi.org/10.1128/JCM.01907-12.

(10) Record-Breaking Year for Organ Donation in Colorado and Wyoming - Donor Alliance https://www.donoralliance.org/newsroom/media-info/press/release/record-breaking-year-for-organ-donation-in-colorado-and-wyoming/?cli_action=1589746357.066 (accessed May 17, 2020).

(11) Iriart, X.; Le Bouar, M.; Kamar, N.; Berry, A. Pneumocystis Pneumonia in Solid-Organ Transplant Recipients. *Journal of Fungi*. MDPI AG December 1, 2015, pp 293–331. https://doi.org/10.3390/jof1030293.

(12) Lutzke, A.; Melvin, A. C.; Neufeld, M. J.; Allison, C. L.; Reynolds, M. M. Nitric Oxide Generation from S-Nitrosoglutathione: New Activity of Indium and a Survey of Metal Ion Effects. *Nitric Oxide - Biol. Chem.* **2019**, *84*. https://doi.org/10.1016/j.niox.2019.01.005.

(13) Allison, C. L.; Lutzke, A.; Reynolds, M. M. Examining the Effect of Common Nitrosating Agents on Chitosan Using a Glucosamine Oligosaccharide Model System. *Carbohydr.*

Polym. **2019**, *203*. https://doi.org/10.1016/j.carbpol.2018.09.052.

(14) Melvin, A. C.; Jones, W. M.; Lutzke, A.; Allison, C. L.; Reynolds, M. M. S-Nitrosoglutathione Exhibits Greater Stability than S-Nitroso-N-Acetylpenicillamine under Common Laboratory Conditions: A Comparative Stability Study. *Nitric Oxide - Biol. Chem.* **2019**, *92*, 18–25. https://doi.org/10.1016/j.niox.2019.08.002.

APPENDIX A

SEPARATION AND DETETION OF GLUTATHIONE, S-NITROSOGLUTATHIONE, AND GLUTATHIOSE DISULFIDE USING LC-MS

A.1 Introduction

Glutathione (GSH) is a tripeptide that is found intracellularly in mammalian cells[1,2]. GSH is generated in cytoplasm and serves as the primary reducing agent in cells[3–5]. S-nitrosoglutathione (GSNO) is an endogenous mediator of the signaling effects of nitric oxide (NO)[6]. GSNO decomposes to spontaneously releases NO under the influence of stimuli such as heat, light, or trace metal ions[7]. Following the decomposition of GSNO, the residues dimerizes to form glutathione disulfide (GSSG)[8]. GSSG can also form via the oxidation of GSH[9]. Therefore, the development of methods to simultaneously determine GSH, GSNO, and GSSG offers a host potential applications. These include monitoring the effectiveness of derivatization reactions from GSH to GSNO, assessing the purity of one or all of these compounds, or tracking the decomposition of GSNO or GSH. Structures of these three compounds are shown in **Figure A.1**. In these studies, we developed an LC-MS method capable of simultaneously measuring GSH, GSNO, and GSSG.

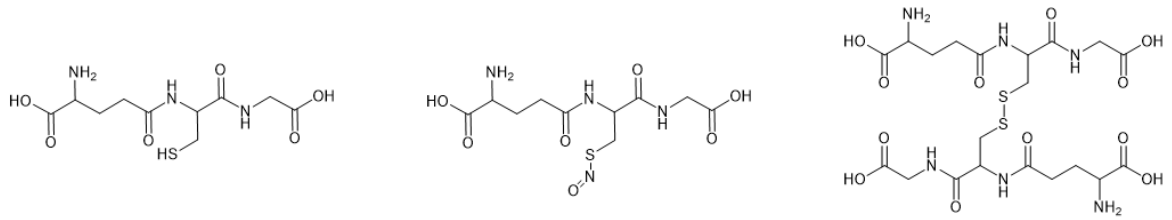

Figure A.1: Chemical structures of GSH, GSNO, and GSSG

A.2 Materials and Methods

A.2.1 Materials

Oxidized L-glutathione (GSSG, ≥98.0%) was obtained from Sigma-Aldrich (St. Louis, MO). Reduced glutathione (GSH, high purity grade) was obtained from VWR (Radnor, PA). Ammonium acetate (>98.0%), LC-MS grade water, and LC-MS grade methanol were obtained from EMD Millipore (Burlington, MA).

A.2.2 Methods

LC-MS analyses were carried out using an Agilent 6224 time-of-flight mass spectrometer couple to an Agilent 1260 binary liquid chromatograph (Agilent, Palo Alto, CA). Separations were performed using a Phenomenex Nucleosil C18 column with a 5 μm particle size (Phenomenex, Torrance, CA). An isocratic mobile phase was used with a composition of 90% water and 10% methanol, each with a 10 mM ammonium acetate additive. The total length of chromatography runs was 15 minutes.

A.2.3 Sample prep

Standard solutions of GSH, GSSG, and GSNO were made to concentrations of 5 mg/mL in LC-MS grade water. Each of these samples was tested individually. Following individual testing, 0.3 mL of each standard was transferred into an LC-MS vial to make a solution with final concentrations of 1.67 mg/mL of each analyte. Final analyses were performed in duplicate.

A.3 Results and Discussion

Three peaks were observed in chromatographs obtained from these experiments. The first peak eluted at 7.5 minutes and contained GSSG. The prominent signal in mass spectra extracted from this peak was observed at 307.08 *m/z,* indicative of a doubly protonated $[GSSG + 2H]^+$ adduct. The doubly charged adduct was supported by molecular weight calculations, as well as the isotopic pattern, which contained isotope signals separated by ~0.5 *m/z.* A second, slightly less prominent peak was observed at 613.16 *m/z,* indicative of a singly protonated $[GSSG + H]^+$ molecule. The second peak eluted at 8.9 minutes and contained GSH. The prominent signal in mass spectra extracted from this peak was observed at 308.09 *m/z,* indicative of a protonated $[GSH + H]^+$ adduct. The third peak eluted at 11.1 minutes and contained GSNO. The prominent signal in mass spectra extracted from this peak was observed at 337.08 *m/z,* indicative of a protonated $[GSNO + H]^+$ adduct.

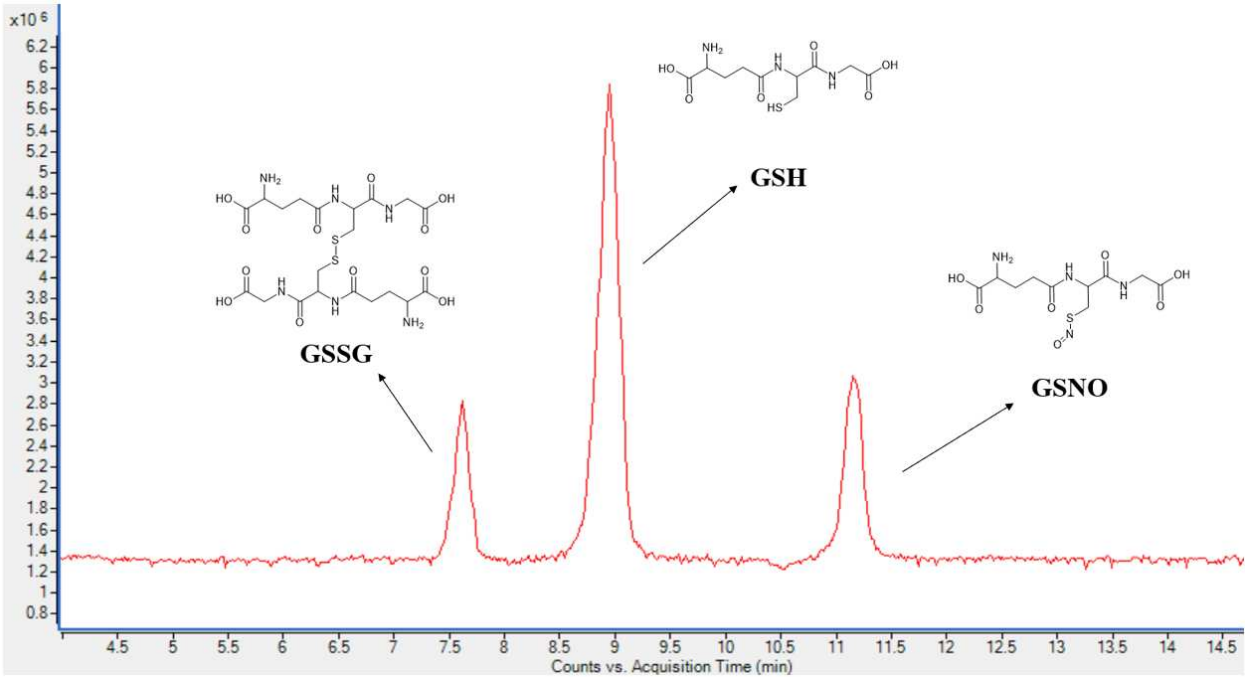

Figure A.2: Representative chromatogram showing the three peaks eluting during chromatography.

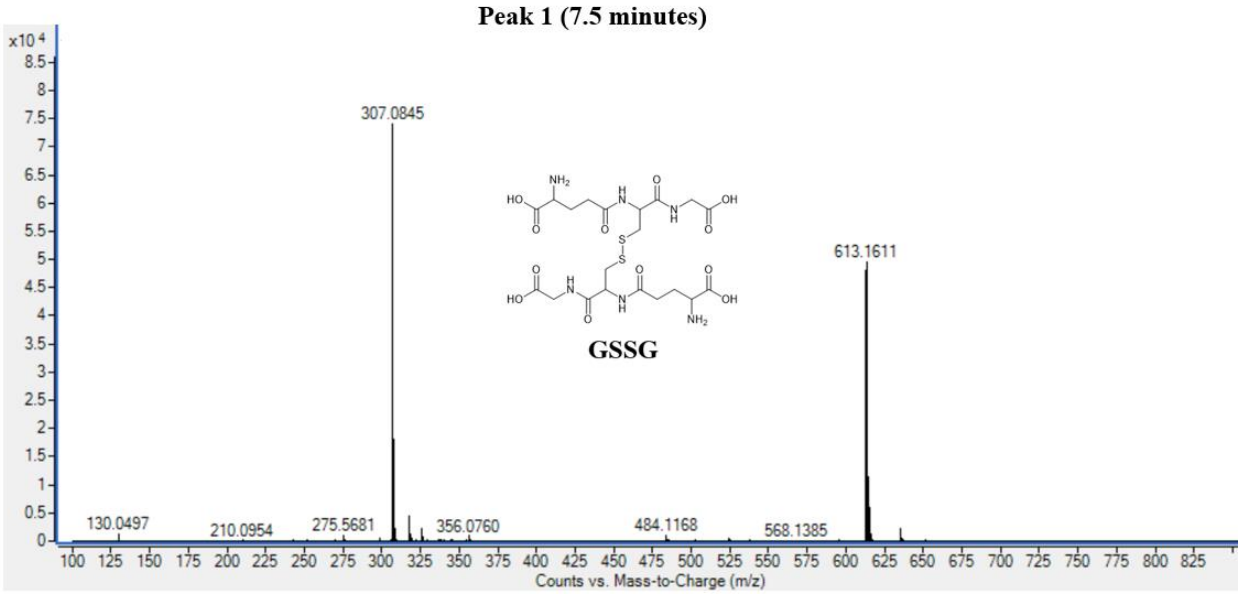

Figure A.3: Representative mass spectrum extracted from peak 1.

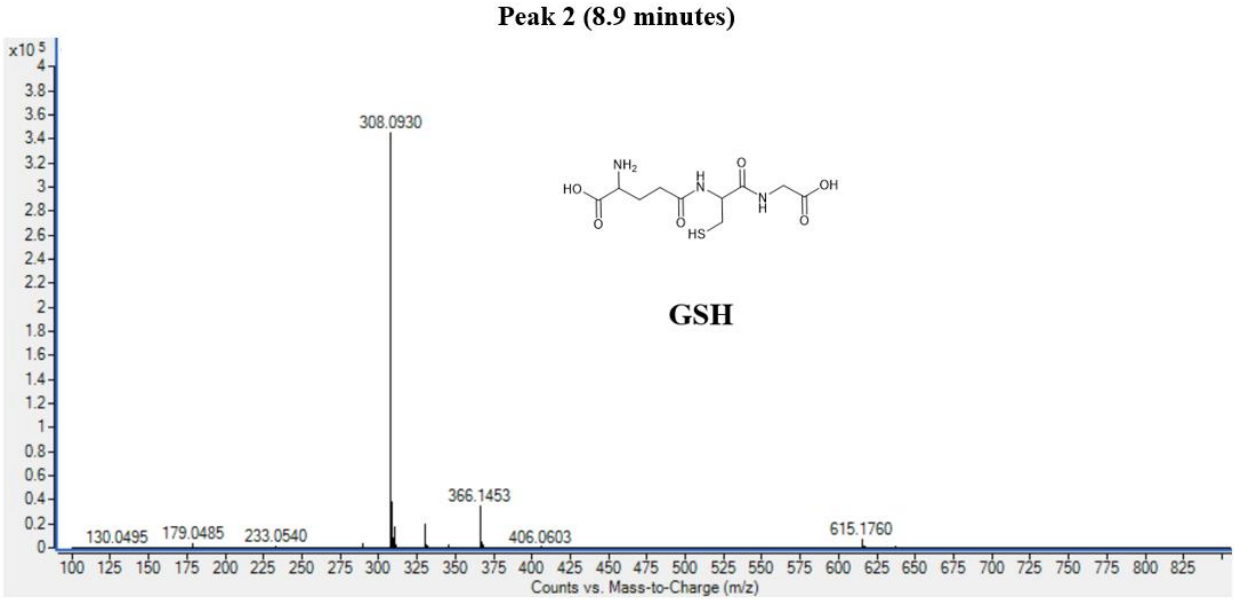

Figure A.4: Representative mass spectrum extracted from peak 2.

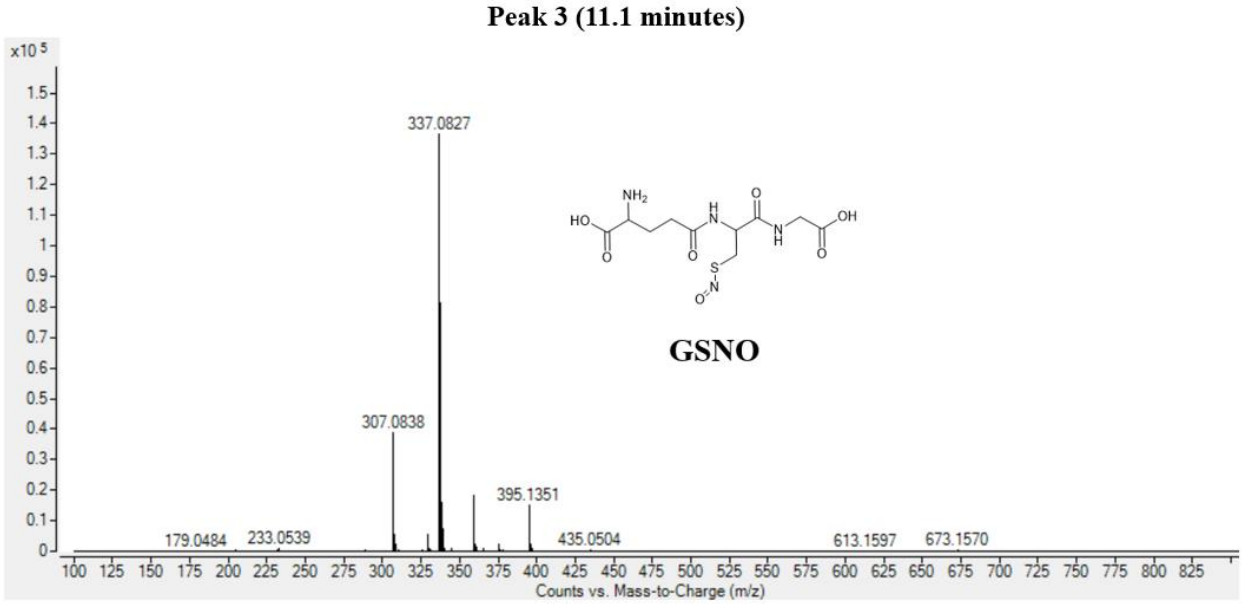

Figure A.5: Representative mass spectrum extracted from peak 3.

APPENDIX A – REFERENCES

(1) Abel, R. Age-Related Macular Degeneration. In *Integrative Medicine: Fourth Edition*; Elsevier, 2018; pp 838-846.e1. https://doi.org/10.1016/B978-0-323-35868-2.00085-2.

(2) Awadallah, S. Protein Antioxidants in Thalassemia. In *Advances in Clinical Chemistry*; Academic Press Inc., 2013; Vol. 60, pp 85–128. https://doi.org/10.1016/B978-0-12-407681-5.00003-9.

(3) Di, L.; Kerns, E. H. Toxicity Methods. In *Drug-Like Properties*; Elsevier, 2016; pp 433–445. https://doi.org/10.1016/b978-0-12-801076-1.00035-6.

(4) Fanucchi, M. V. Pulmonary Developmental Responses to Toxicants. In *Comprehensive Toxicology, Second Edition*; Elsevier Inc., 2010; Vol. 8, pp 199–221. https://doi.org/10.1016/B978-0-08-046884-6.00910-6.

(5) Gupta, P. K. Biotransformation. In *Fundamentals of Toxicology*; Elsevier, 2016; pp 73–85. https://doi.org/10.1016/b978-0-12-805426-0.00008-1.

(6) Broniowska, K. A.; Diers, A. R.; Hogg, N. S-Nitrosoglutathione. *Biochimica et Biophysica Acta - General Subjects*. Elsevier May 1, 2013, pp 3173–3181. https://doi.org/10.1016/j.bbagen.2013.02.004.

(7) Melvin, A. C.; Jones, W. M.; Lutzke, A.; Allison, C. L.; Reynolds, M. M. S-Nitrosoglutathione Exhibits Greater Stability than S-Nitroso-N-Acetylpenicillamine under Common Laboratory Conditions: A Comparative Stability Study. *Nitric Oxide - Biol. Chem.* **2019**, *92*, 18–25. https://doi.org/10.1016/j.niox.2019.08.002.

(8) Jit Singh, R.; Hogg, N.; Joseph, J.; Kalyanaraman, B. *Mechanism of Nitric Oxide Release*

from S-Nitrosothiols Downloaded From*; 1996; Vol. 271.

(9) Owen, J. B.; Allan Butterfiel, D. Measurement of Oxidized/Reduced Glutathione Ratio. In *Methods in Molecular Biology*; Humana Press Inc., 2010; Vol. 648, pp 269–277. https://doi.org/10.1007/978-1-60761-756-3_18.

APPENDIX B

SUPPLEMENTAL INFORMATION FOR CHAPTER 4: COMPARISON OF DEGRADATION METHODS FOR CHITIN AND CHIOSAN USING ESI-MS

Table B.1: Potential low molecular weight degradation products from chitin and chitosan with corresponding molecular formulas and *m/z* ratios for common ESI adducts. "D" corresponds to a deacetylated monomer GlcN unit and "A" corresponds to an acetylated monomer unit.

Species	**Formula**	**$[M-H_2O+H]^+$**	**$[M+H]^+$**	**$[M+Na]^+$**	**$[M-H]^-$**	**$[M+Cl]^-$**
2,5-AM	$C_6H_{10}O_5$	N/A	N/A	N/A	161.0455	197.0222
2,5-AM	$C_6H_{12}O_6$	N/A	N/A	N/A	179.0561	215.0328
D1A0	$C_6H_{13}NO_5$	162.0761	180.0866	202.0686	178.0721	214.0488
D0A1	$C_8H_{15}NO_6$	204.0866	222.0973	244.0792	220.0827	256.0593
D2A0	$C_{12}H_{24}N_2O_9$	323.1449	341.1555	363.1374	339.1409	375.1176
D1A1	$C_{14}H_{26}N_2O_{10}$	365.1555	383.1660	405.1480	381.1515	417.1281
D0A2	$C_{16}H_{28}N_2O_{11}$	407.1660	425.1766	447.1585	423.1620	459.1387
D3A0	$C_{18}H_{35}N_3O_{13}$	484.2137	502.2243	524.2062	N/A	N/A
D2A1	$C_{20}H_{37}N_3O_{14}$	526.2243	544.2348	566.2168	N/A	N/A
D1A2	$C_{22}H_{39}N_3O_{15}$	568.2348	586.2454	608.2273	N/A	N/A
D0A3	$C_{24}H_{41}N_3O_{16}$	610.2454	628.2560	650.2379	N/A	N/A
D4A0	$C_{24}H_{46}N_4O_{17}$	645.2825	663.2931	685.2750	N/A	N/A
D3A1	$C_{26}H_{48}N_4O_{18}$	687.2931	705.3036	727.2856	N/A	N/A
D2A2	$C_{28}H_{50}N_4O_{19}$	729.3036	747.3142	769.2961	N/A	N/A
D1A3	$C_{30}H_{52}N_4O_{20}$	771.3142	789.3248	811.3087	N/A	N/A
D5A0	$C_{30}H_{57}N_5O_{21}$	806.3513	824.3619	846.3438	N/A	N/A
D0A4	$C_{32}H_{54}N_4O_{21}$	813.3248	831.3353	853.3173	N/A	N/A
D3A2	$C_{34}H_{61}N_5O_{23}$	890.3724	908.3830	930.3650	N/A	N/A
D6A0	$C_{36}H_{68}N_6O_{25}$	967.4201	985.4307	1007.4126	N/A	N/A

Table B.2: IR assignments with corresponding functional groups noted in starting materials.

Functional group	**Frequencies (approximate values, cm^{-1})**
O – H (stretching)	3550-3200

N – H (stretching)	3330-3250
N – H (bending)	1650-1580
C – H (stretching)	3000-2840
C = O (stretching)	1650
C – N (stretching)	1342-1266
C – H (stretching)	1375
C – H (bending)	1465
C – O – C (stretching)	1150-1085
C – O (stretching)	1075-1020

Spectral analysis of glucosamine

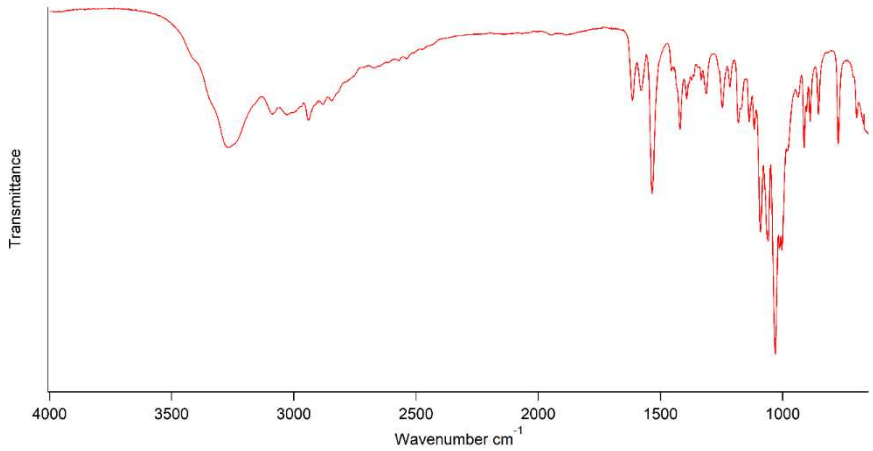

Figure B.1: ATR-FTIR spectrum of glucosamine. ATR-FTIR: 3267, 3088, 3027, 2941, 2880, 2845, 1615, 1579, 1534, 1420, 1393, 1314, 1248, 1217, 1182, 1138, 1116, 1091, 1060, 1031, 1013, 1004 cm^{-1}.

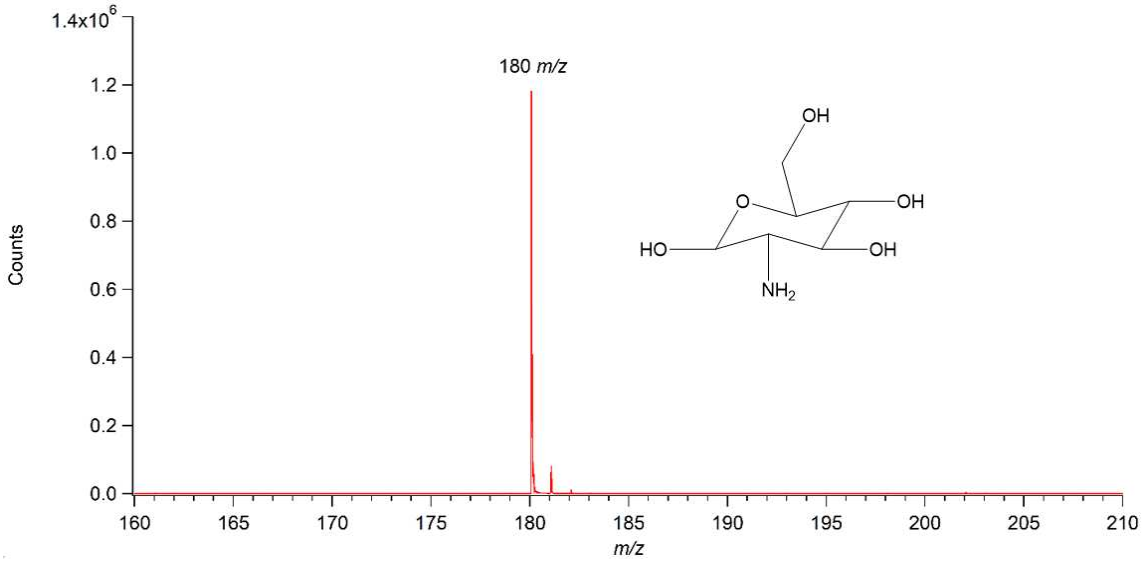

Figure B.2: Mass spectrum of glucosamine obtained via direct injection. The peak at 180 *m/z* is indicative of a compound with a molecular formula consistent with a protonated glucosamine ion, $[C_6H_{13}NO_5 + H]^+$.

Spectral analysis of *N*-acetylglucosamine

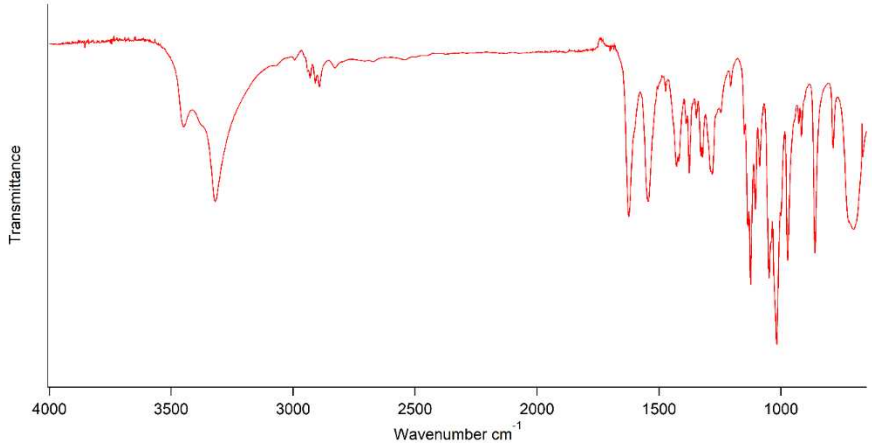

Figure B.3: ATR-FTIR spectrum of *N*-acetylglucosamine. ATR-FTIR: 3449, 3319, 2930, 2909, 2892, 2828, 1624, 1545, 1428, 1419, 1389, 1376, 1347, 1329, 1322, 1282, 1247, 1206, 1150, 1136, 1125, 1105, 1088, 1049, 1018 $cm^{-1.}$

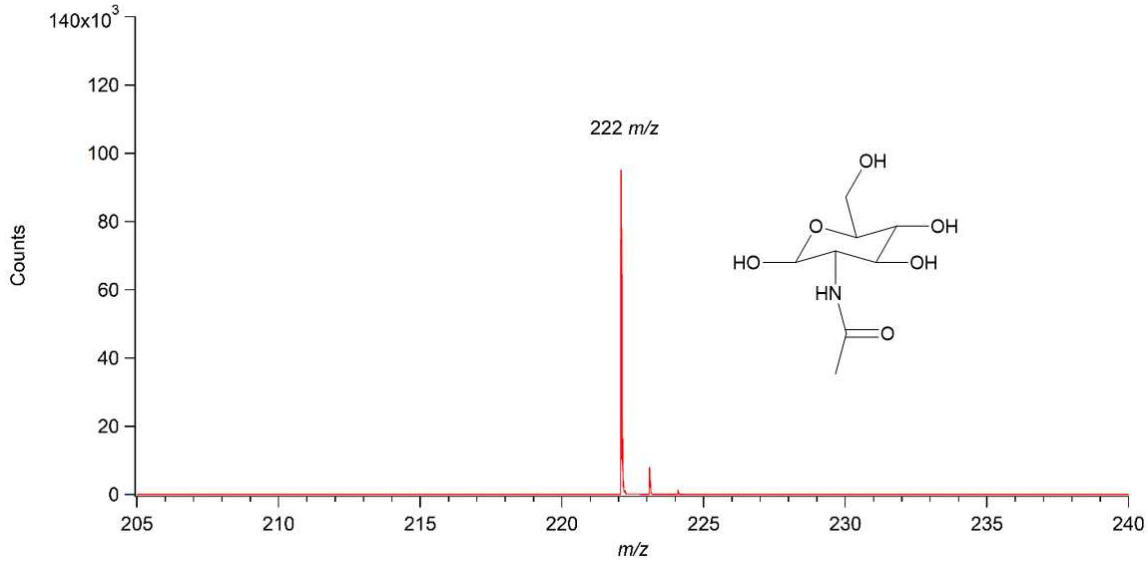

Figure B.4: Mass spectrum of *N*-acetylglucosamine obtained via direct injection. The peak at 222 *m/z* is indicative of a compound with a molecular formula consistent with a protonated *N*-acetylglucosamine ion, $[C_8H_{15}NO_6 + H]^+$.

Spectral analysis of chitosan oligosaccharides

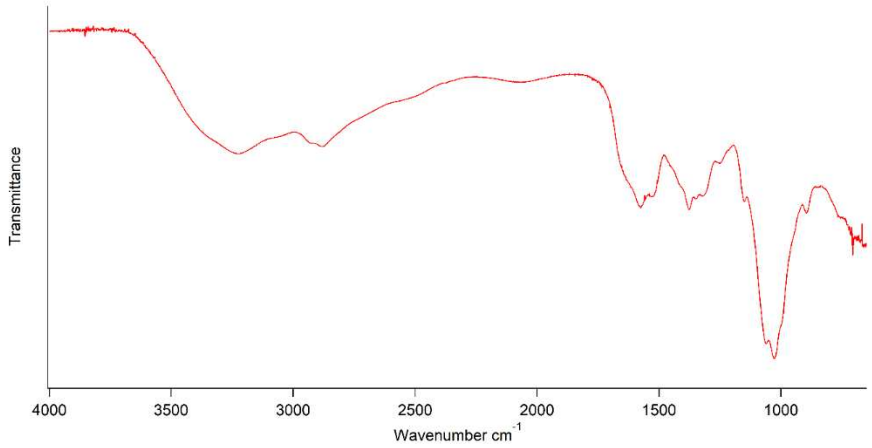

Figure B.5: ATR-FTIR spectrum of chitosan oligosaccharides. ATR-FTIR: 3700-3000, 2922, 2881, 1576, 1530, 1377, 1349, 1321, 1251, 1150, 1062, 1028 cm^{-1}.

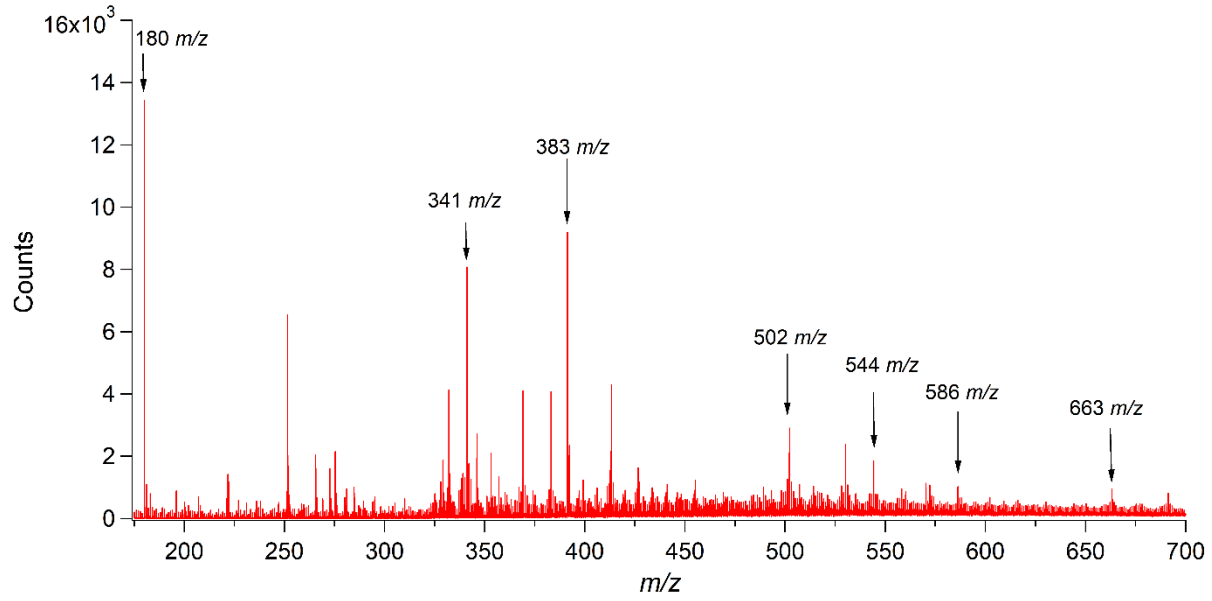

Figure B.6: Mass spectrum of chitosan oligosaccharides obtained via direct injection. The signals shown are indicative of compounds show in **Table B.1.**

Spectral analysis of chitosan polymer

Figure B.7: ATR-FTIR spectrum of chitosan polymer. ATR-FTIR: 3700-3000, 3352, 3283, 2912, 2866, 1652, 1588, 1419, 1373, 1316, 1150, 1063, 1025 cm^{-1}.

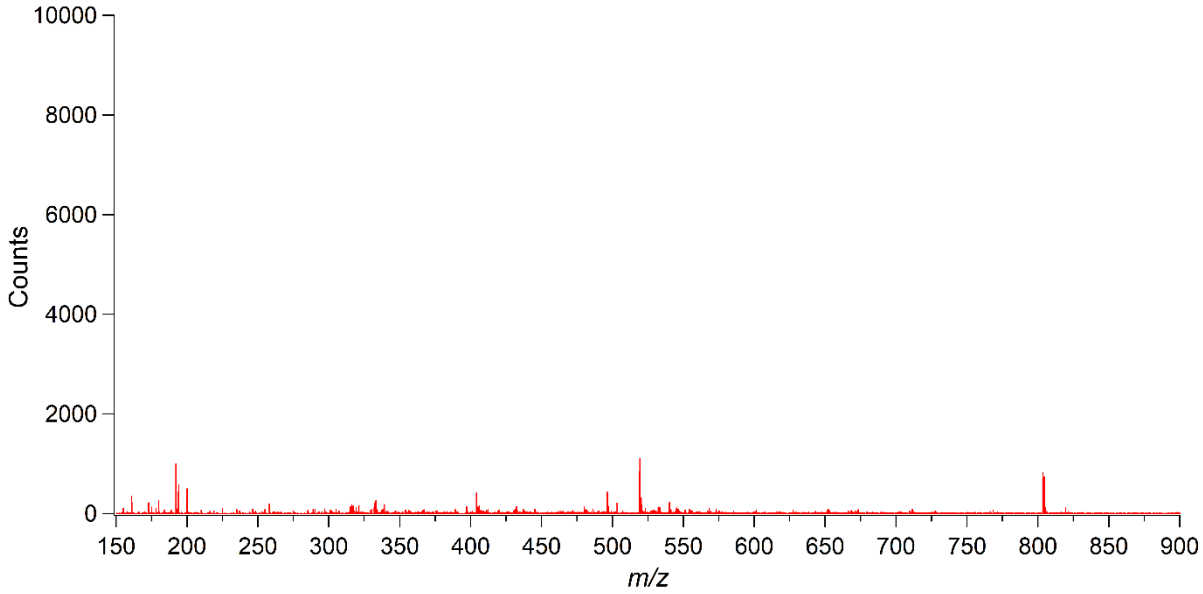

Figure B.8: Mass spectrum of chitosan polymer obtained via direct injection. Peaks shown are not of interest and are likely artefacts of material processing or the solvent systems used.

Spectral analysis of chitin polymer 1

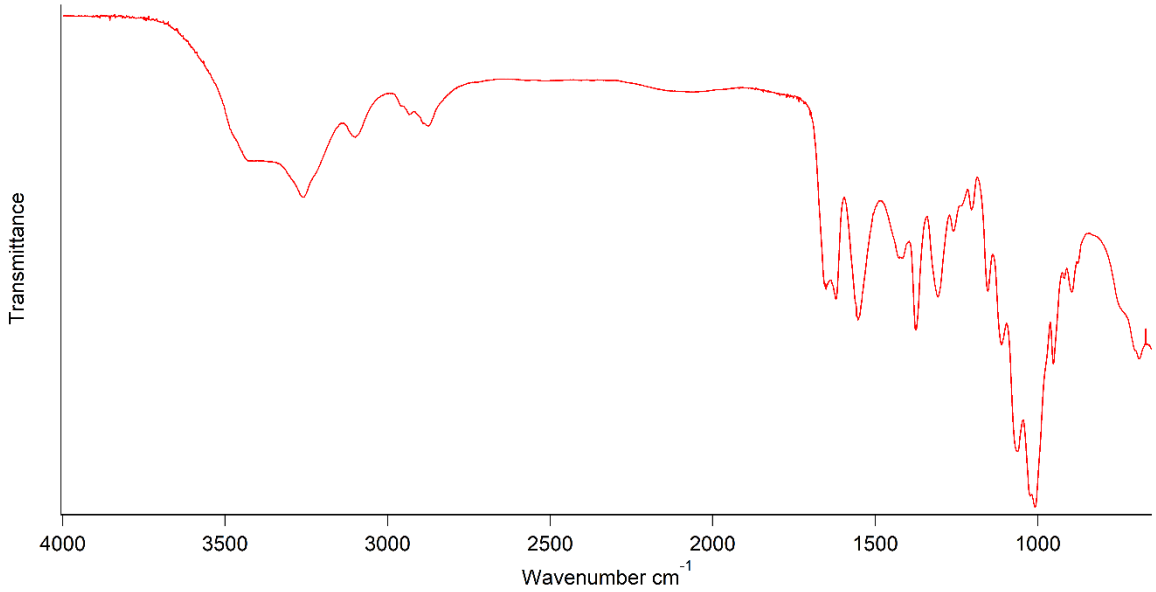

Figure B.9: ATR-FTIR spectrum of chitin polymer 1. ATR-FTIR: 3256, 3100, 2873, 1652, 1620, 1553, 1415, 1376, 1307, 1260, 1204, 1154, 1113, 1068, 1007 cm^{-1}.

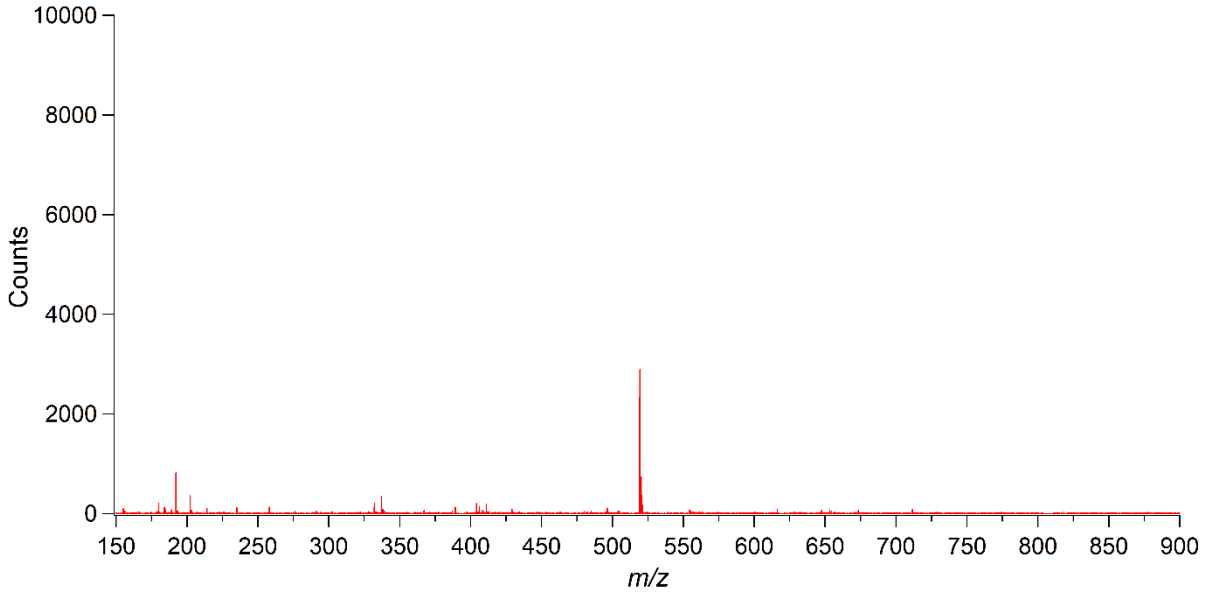

Figure B.10: Mass spectrum of chitin polymer 1 obtained via direct injection. Peaks shown are not of interest and are likely artefacts of material processing or the solvent systems used.

Spectral analysis of chitin polymer 2

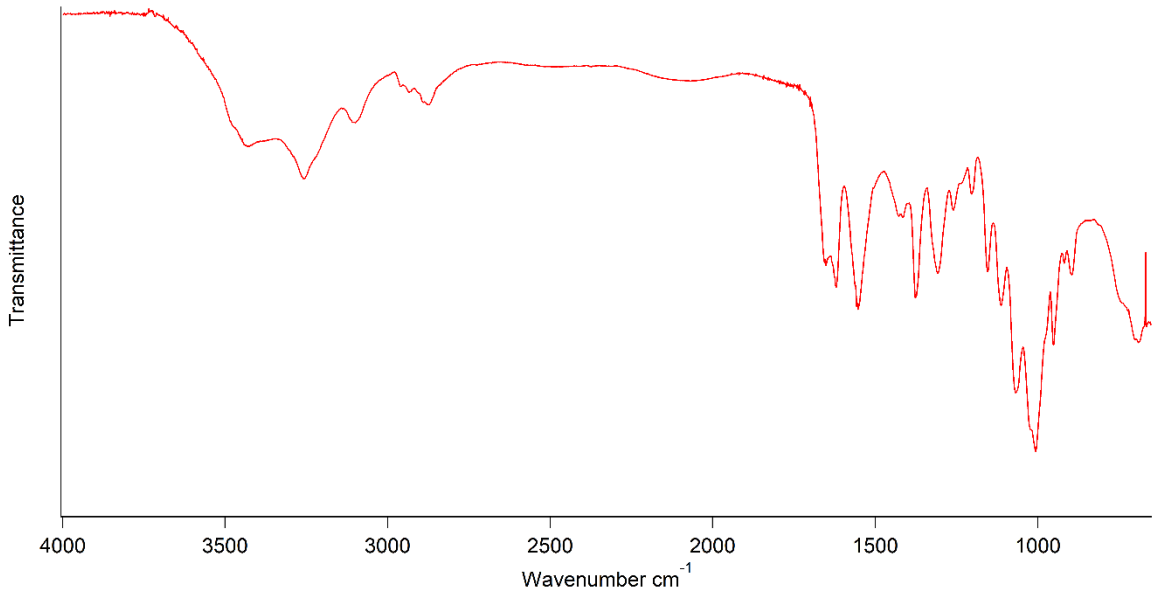

Figure B.11: ATR-FTIR spectrum of chitin polymer 2. ATR-FTIR: 3256, 3100, 2873, 1652, 1620, 1553, 1415, 1376, 1307, 1260, 1204, 1154, 1113, 1068, 1007 cm^{-1}.

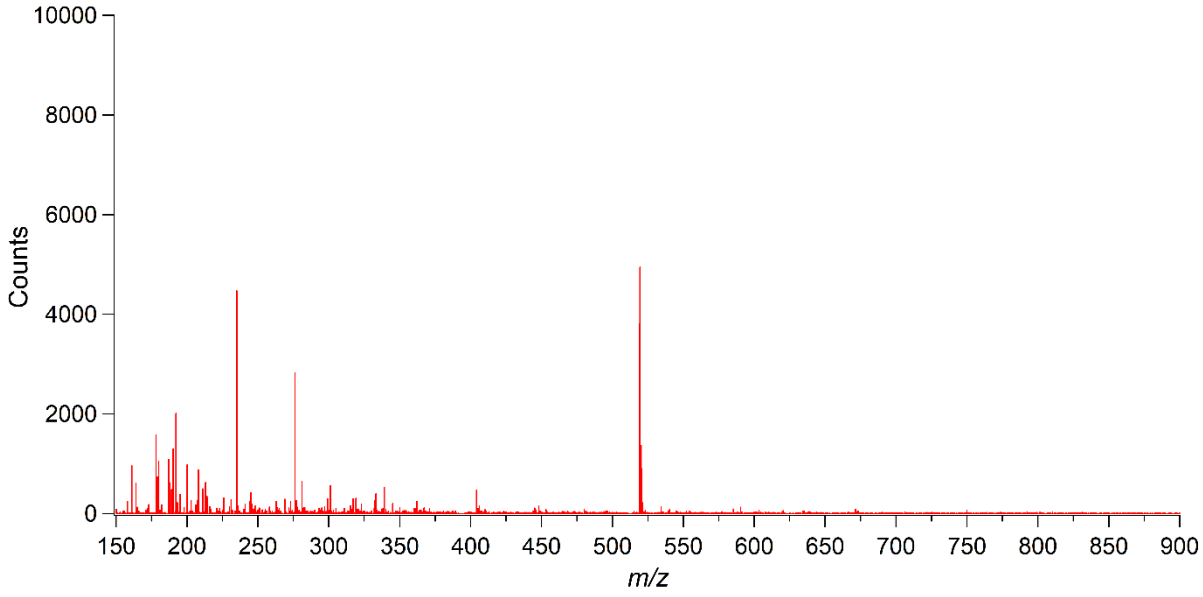

Figure B.12: Mass spectrum of chitin polymer 2 obtained via direct injection. Peaks shown are not of interest and are likely artefacts of material processing or the solvent systems used.

Spectral analysis of H_2O_2 degradation products

Chitosan polymer

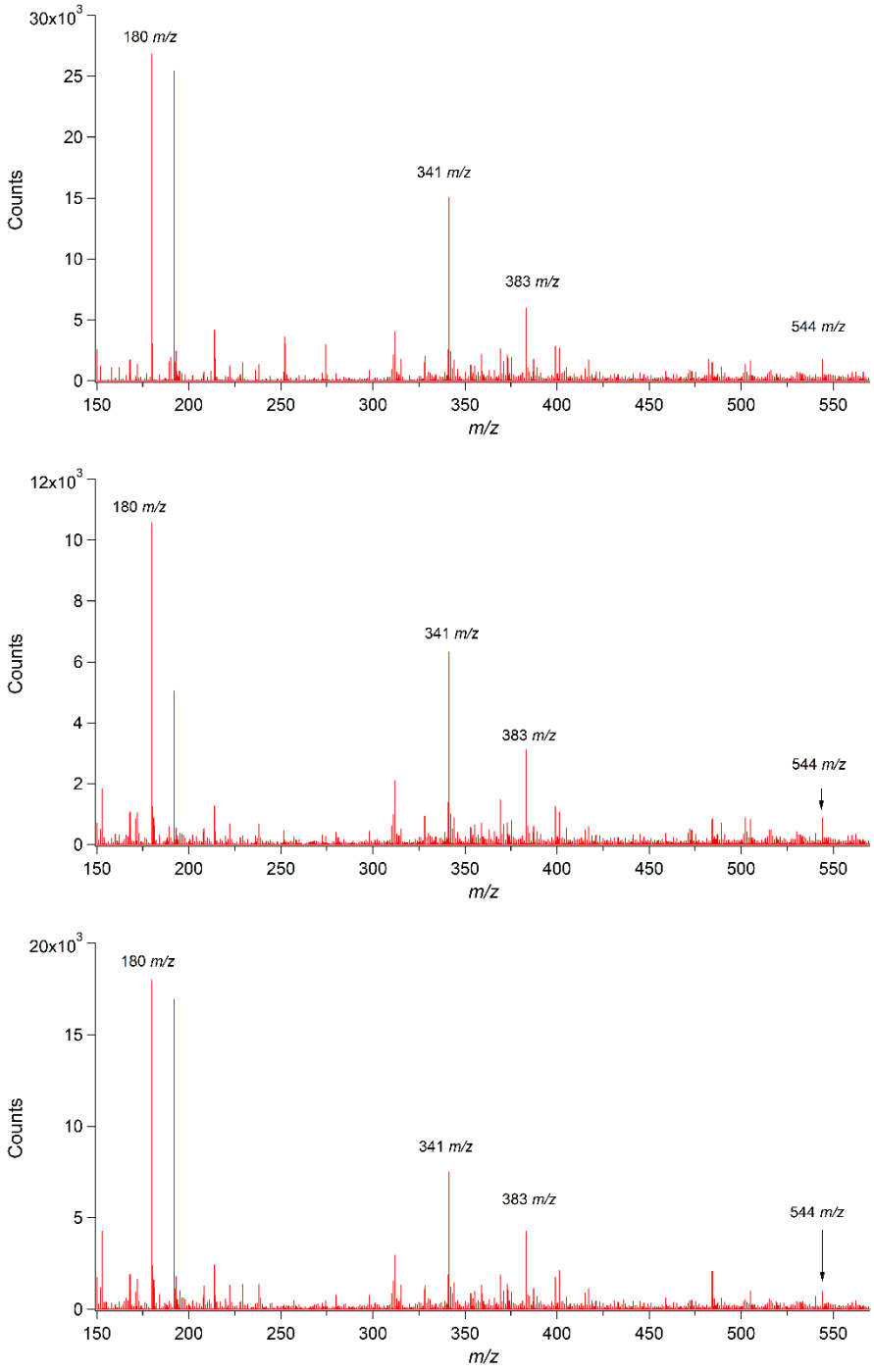

Figure B.13: MS of chitosan polymer after exposure to 30% H_2O_2 for 1 hour. Labeled peaks are indicative of compounds with molecular formulas consistent with predicted degradation products found in **Table B.1.** Remaining unlabeled peaks represent ions that occur as a result of unexpected adducts or are artefacts of chemical reagents used to degrade the analyte. These are still visible due to there being no separation step prior to ionization.

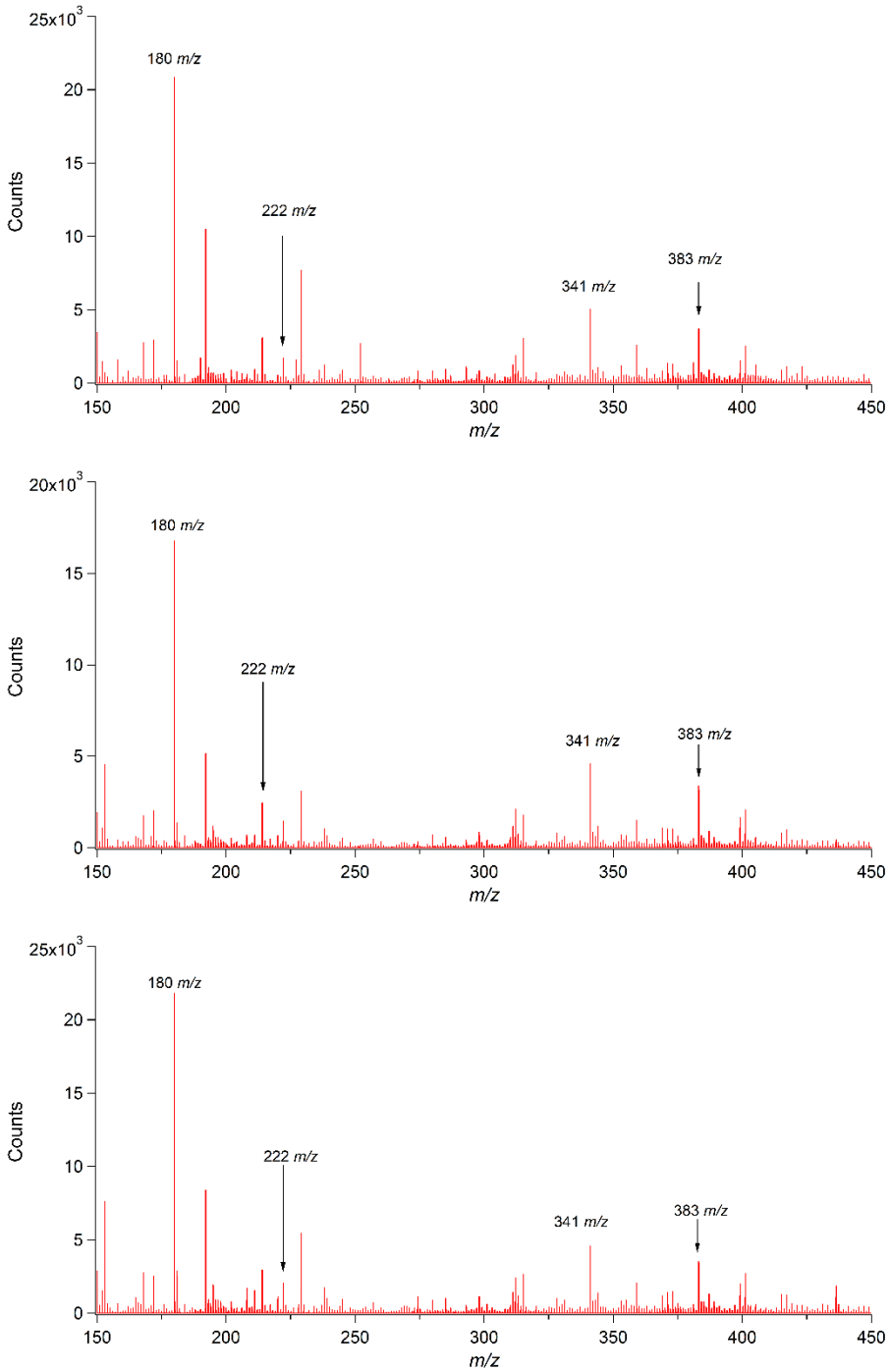

Figure B.14: MS of chitosan polymer after exposure to 30% H_2O_2 for 2 hours. Labeled peaks are indicative of compounds with molecular formulas consistent with predicted degradation products found in **Table B.1.** Remaining unlabeled peaks represent ions that occur as a result of unexpected adducts or are artefacts of chemical reagents used to degrade the analyte. These are still visible due to there being no separation step prior to ionization.

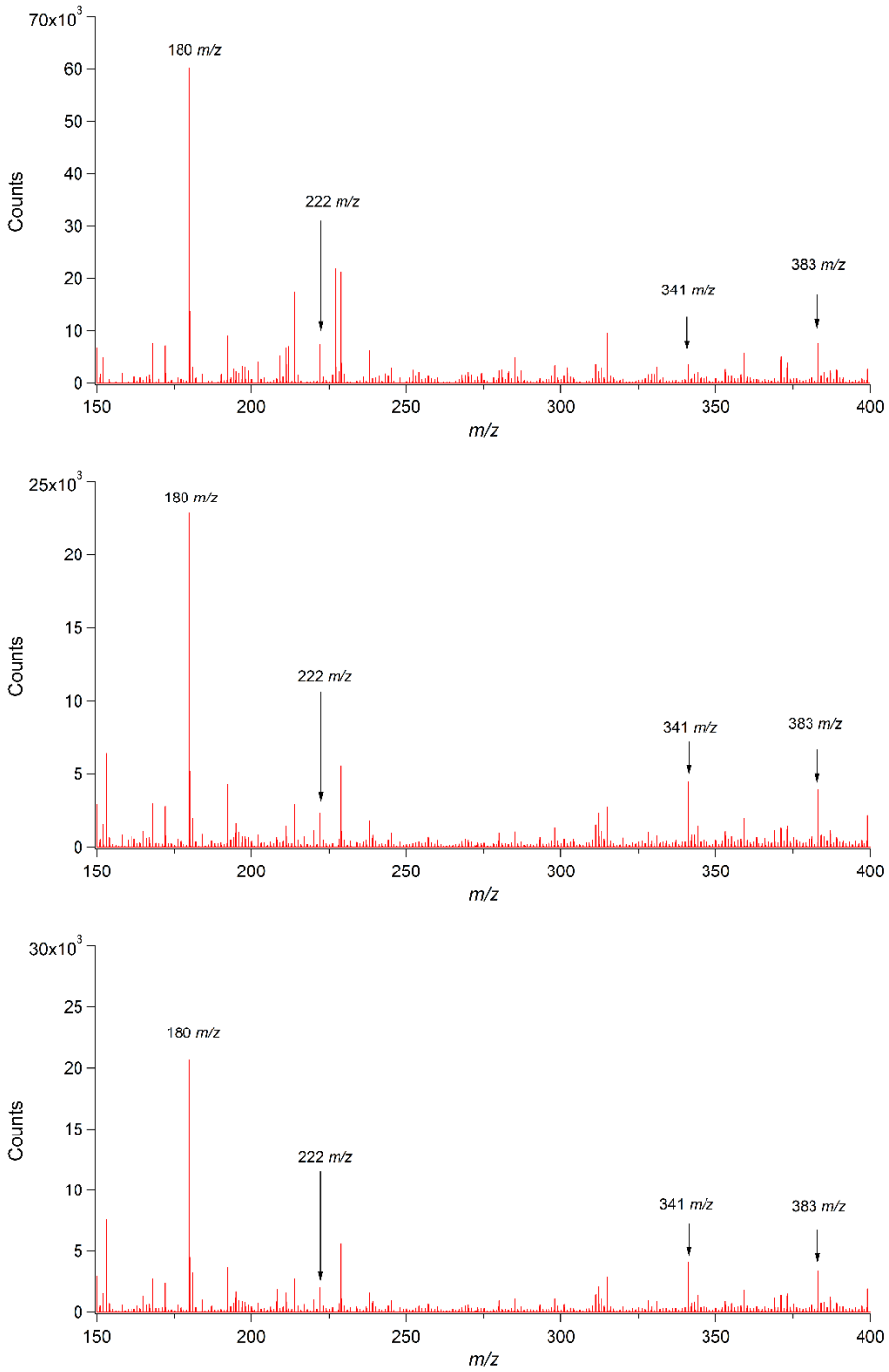

Figure B.15: MS of chitosan polymer after exposure to 30% H_2O_2 for 24 hours. Labeled peaks are indicative of compounds with molecular formulas consistent with predicted degradation products found in **Table B.1.** Remaining unlabeled peaks represent ions that occur as a result of unexpected adducts or are artefacts of chemical reagents used to degrade the analyte. These are still visible due to there being no separation step prior to ionization.

Chitin polymer 1

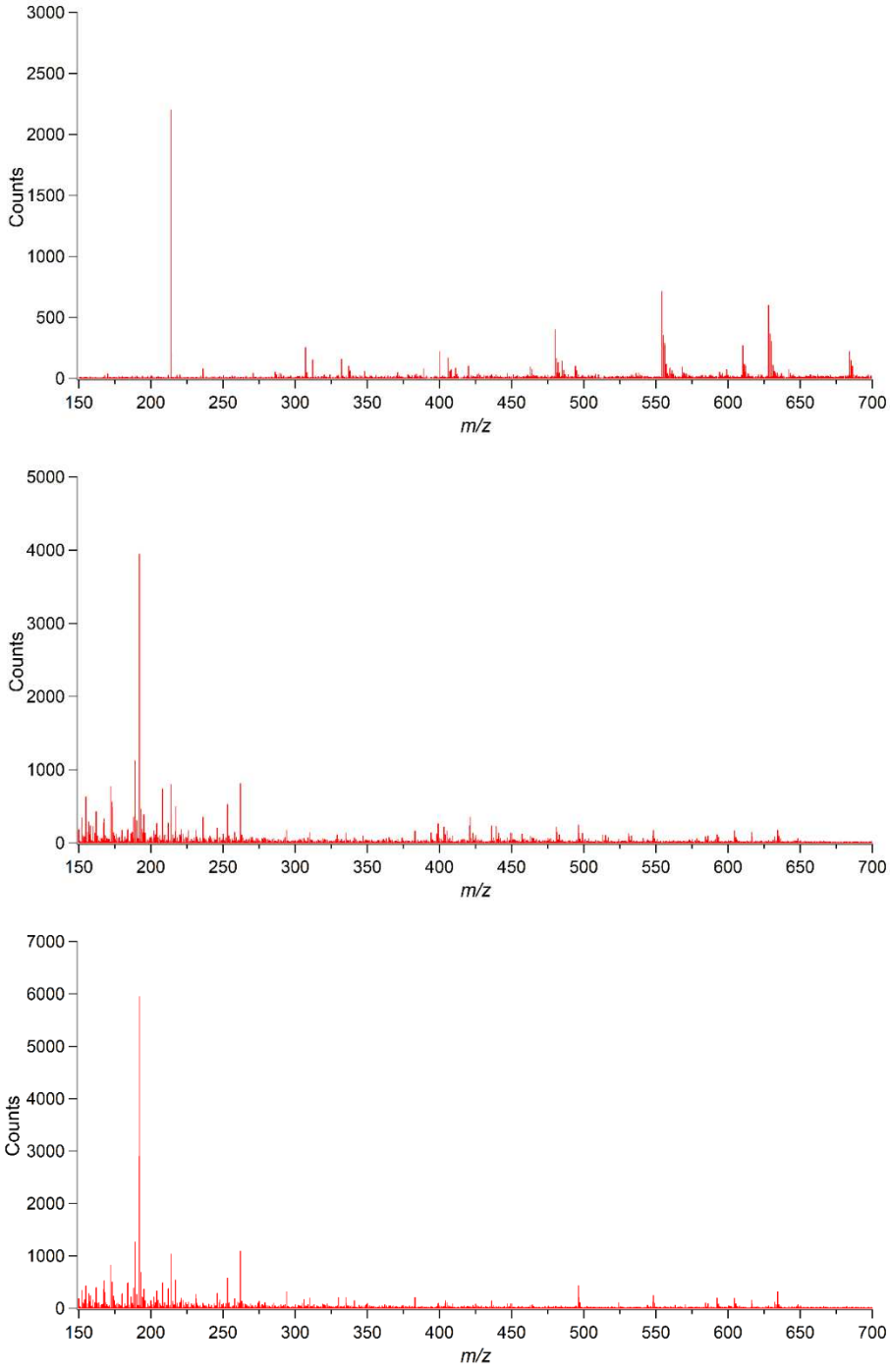

Figure B.16: MS of chitin polymer 1 after exposure to 30% H_2O_2 for 1 hour. Unlabeled peaks represent ions that occur as a result of unexpected adducts or are artefacts of chemical reagents used to degrade the analyte. These are still visible due to there being no separation step prior to ionization.

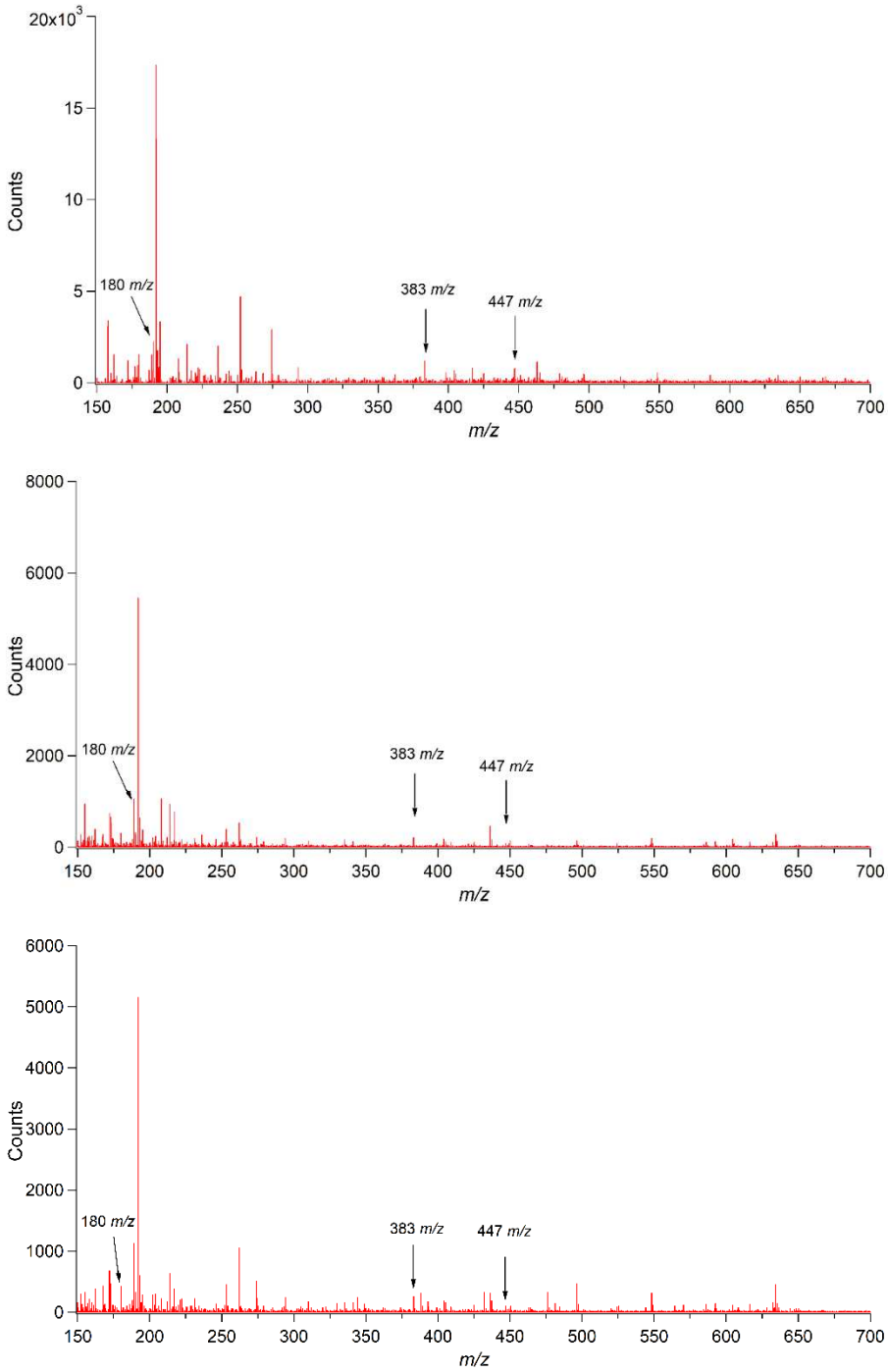

Figure B.17: MS of chitin polymer 1 after exposure to 30% H_2O_2 for 2 hours. Labeled peaks are indicative of compounds with molecular formulas consistent with predicted degradation products found in **Table B.1.** Remaining unlabeled peaks represent ions that occur as a result of unexpected adducts or are artefacts of chemical reagents used to degrade the analyte. These are still visible due to there being no separation step prior to ionization.

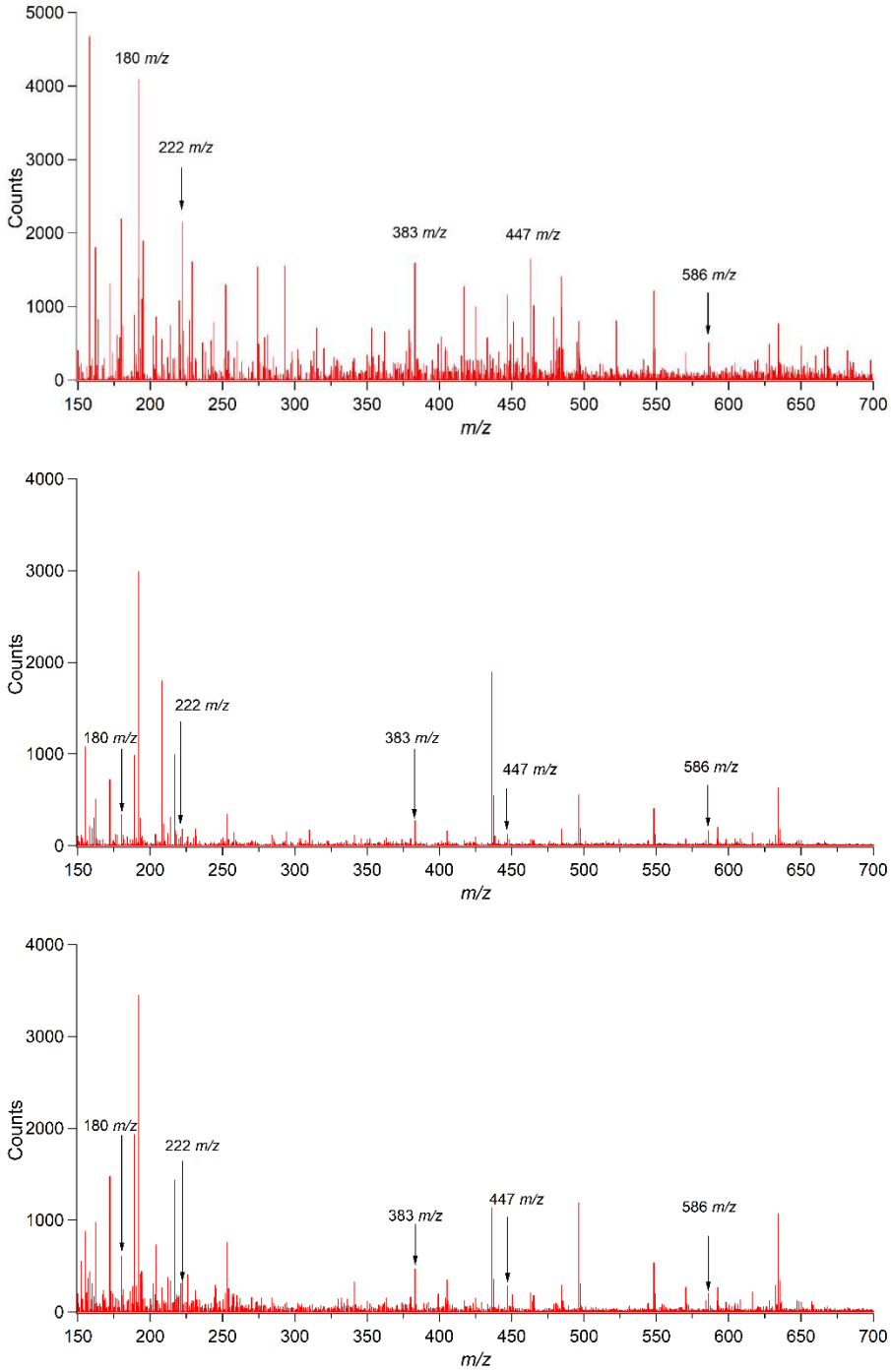

Figure B.18: MS of chitin polymer 1 after exposure to 30% H_2O_2 for 24 hours. Labeled peaks are indicative of compounds with molecular formulas consistent with predicted degradation products found in **Table B.1.** Remaining unlabeled peaks represent ions that occur as a result of unexpected adducts or are artefacts of chemical reagents used to degrade the analyte. These are still visible due to there being no separation step prior to ionization.

Chitin polymer 2

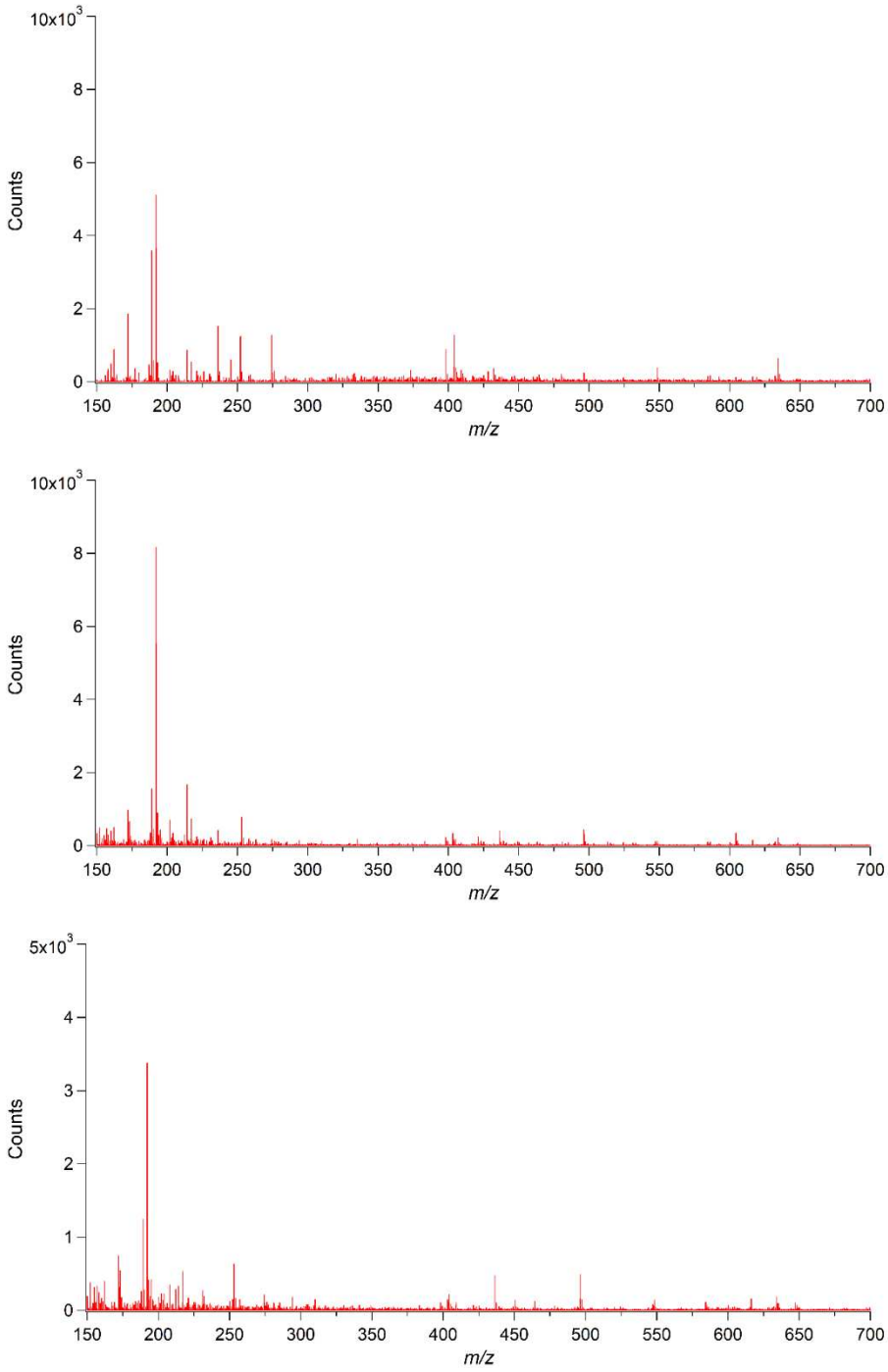

Figure B.19: MS of chitin polymer 2 after exposure to 30% H_2O_2 for 1 hour. Unlabeled peaks represent ions that occur as a result of unexpected adducts or are artefacts of chemical reagents used to degrade the analyte. These are still visible due to there being no separation step prior to ionization.

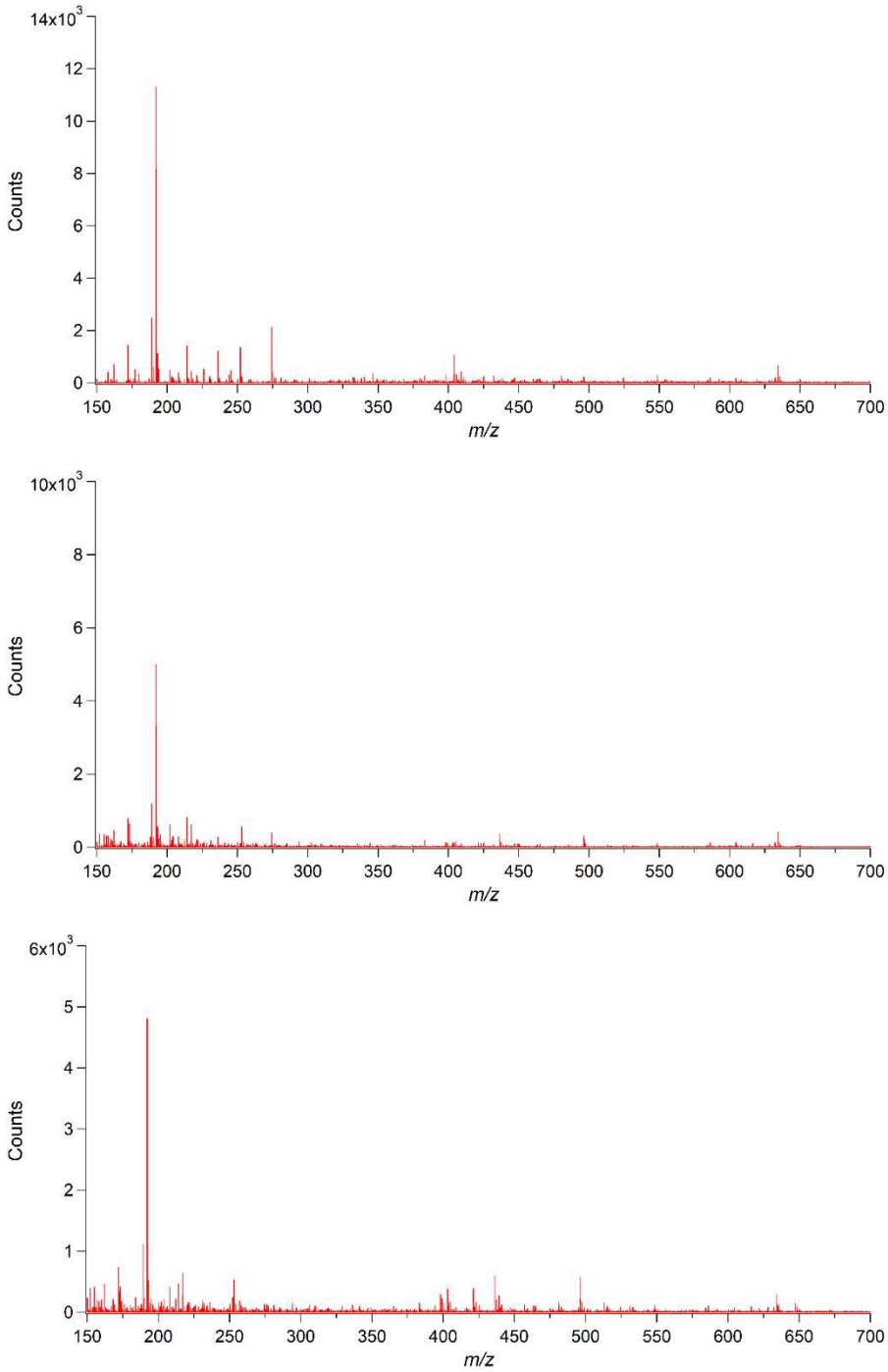

Figure B.20: MS of chitin polymer 2 after exposure to 30% H_2O_2 for 2 hours. Unlabeled peaks represent ions that occur as a result of unexpected adducts or are artefacts of chemical reagents used to degrade the analyte. These are still visible due to there being no separation step prior to ionization.

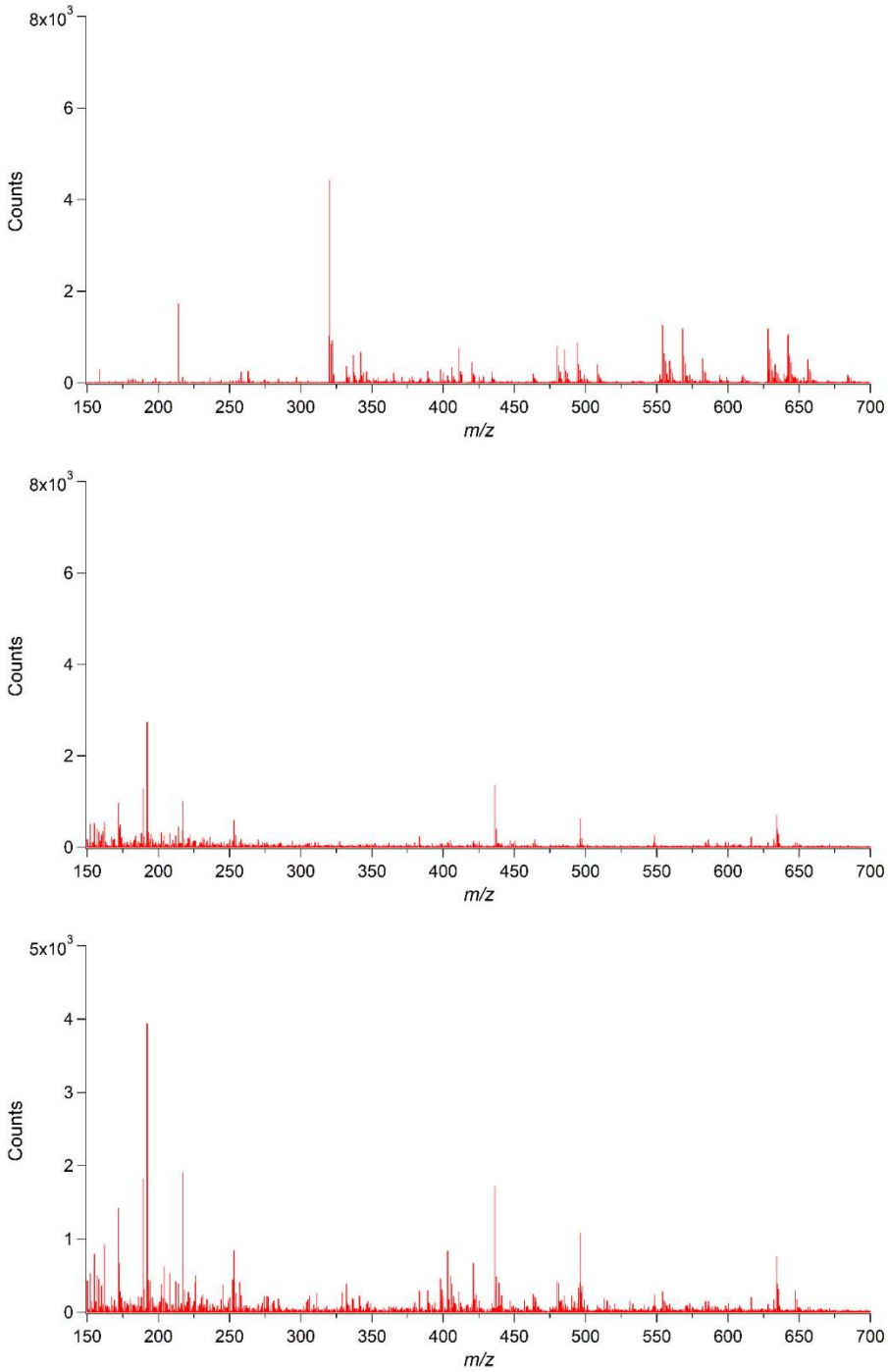

Figure B.21: MS of chitin polymer 1 after exposure to 30% H_2O_2 for 24 hours. Unlabeled peaks represent ions that occur as a result of unexpected adducts or are artefacts of chemical reagents used to degrade the analyte. These are still visible due to there being no separation step prior to ionization.

Spectral analysis of HNO_2 degradation products

Chitosan polymer

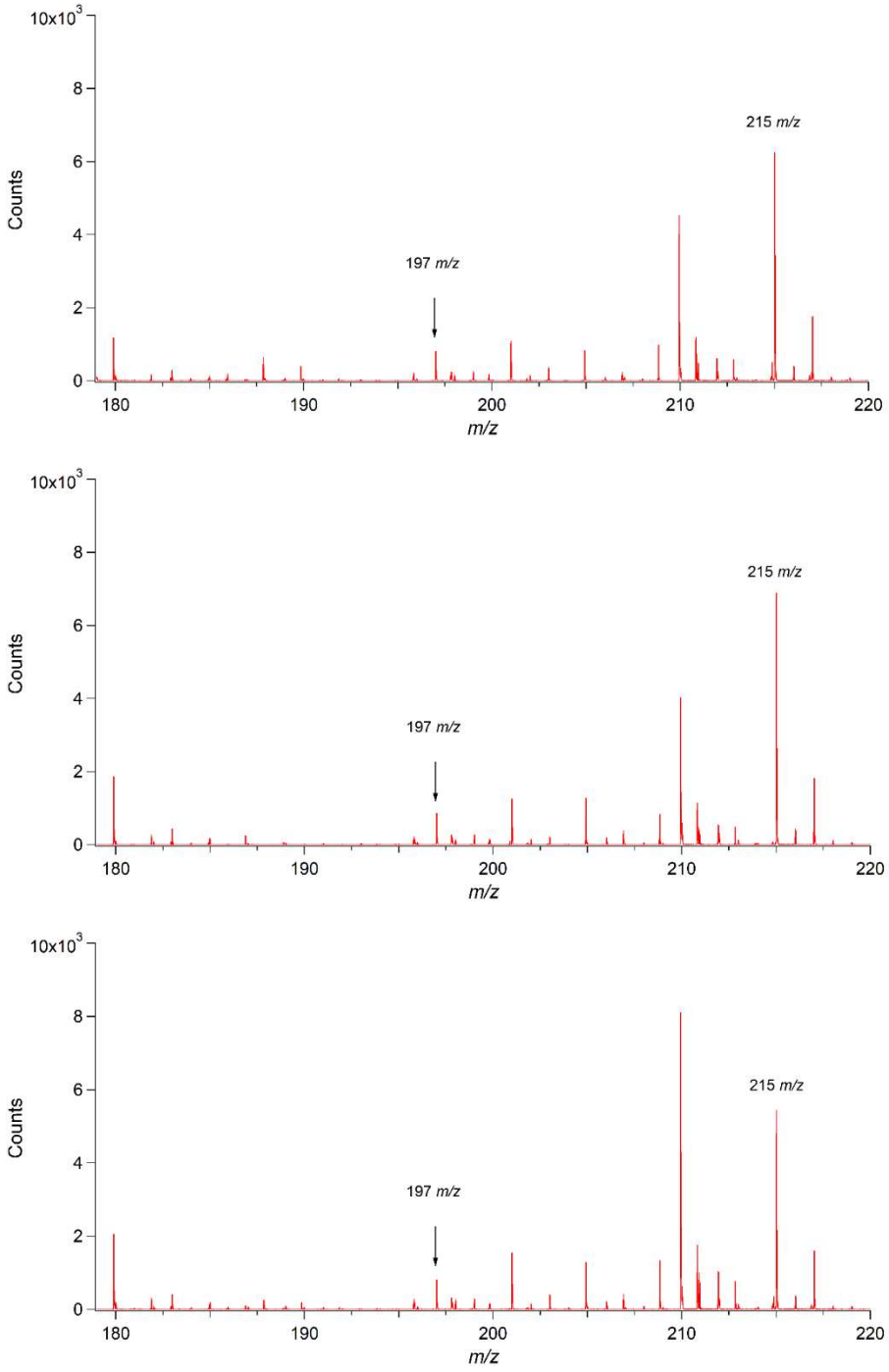

Figure B.22: MS of chitosan polymer after exposure to 0.5M HNO_2 for 1 hour. Labeled peaks are indicative of compounds with molecular formulas consistent with predicted degradation products found in **Table B.1.** Remaining unlabeled peaks represent ions that occur as a result of unexpected adducts or are artefacts of chemical reagents used to degrade the analyte. These are still visible due to there being no separation step prior to ionization.

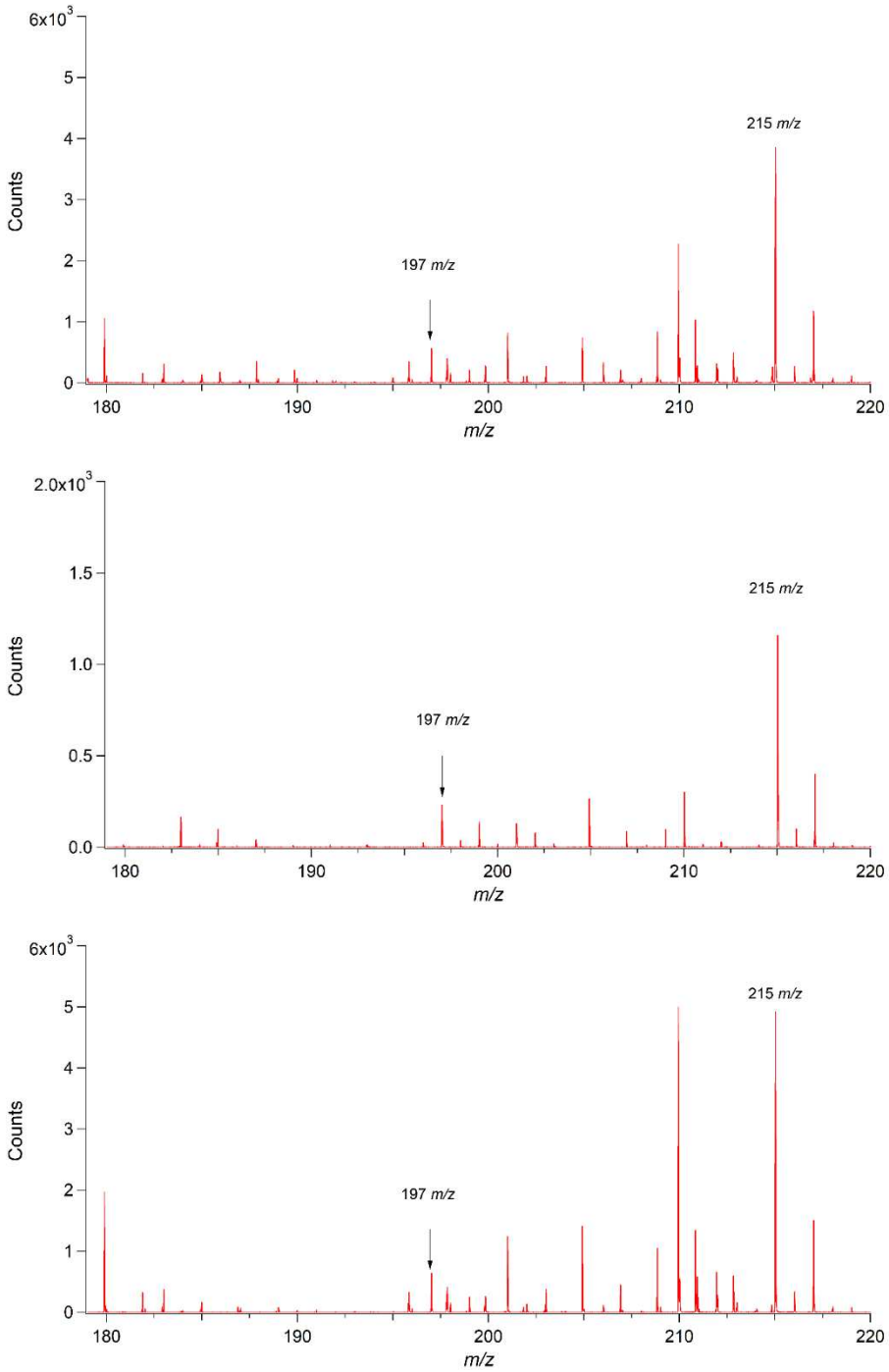

Figure B.23: MS of chitosan polymer after exposure to 0.5M HNO_2 for 2 hours. Labeled peaks are indicative of compounds with molecular formulas consistent with predicted degradation products found in **Table B.1.** Remaining unlabeled peaks represent ions that occur as a result of unexpected adducts or are artefacts of chemical reagents used to degrade the analyte. These are still visible due to there being no separation step prior to ionization.

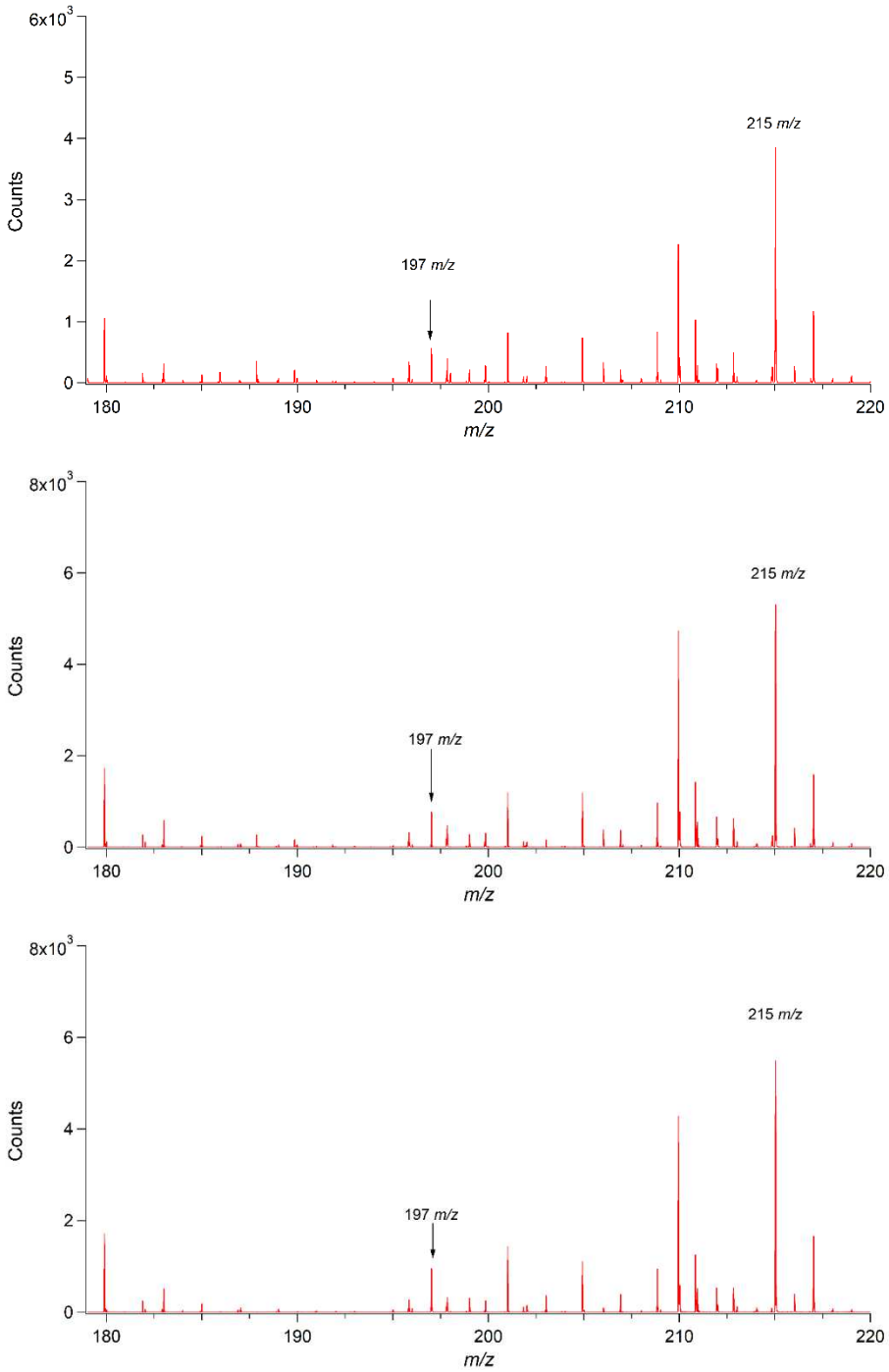

Figure B.24: MS of chitosan polymer after exposure to 0.5M HNO_2 for 2 hours. Labeled peaks are indicative of compounds with molecular formulas consistent with predicted degradation products found in **Table B.1.** Remaining unlabeled peaks represent ions that occur as a result of unexpected adducts or are artefacts of chemical reagents used to degrade the analyte. These are still visible due to there being no separation step prior to ionization.

Chitin polymer 1

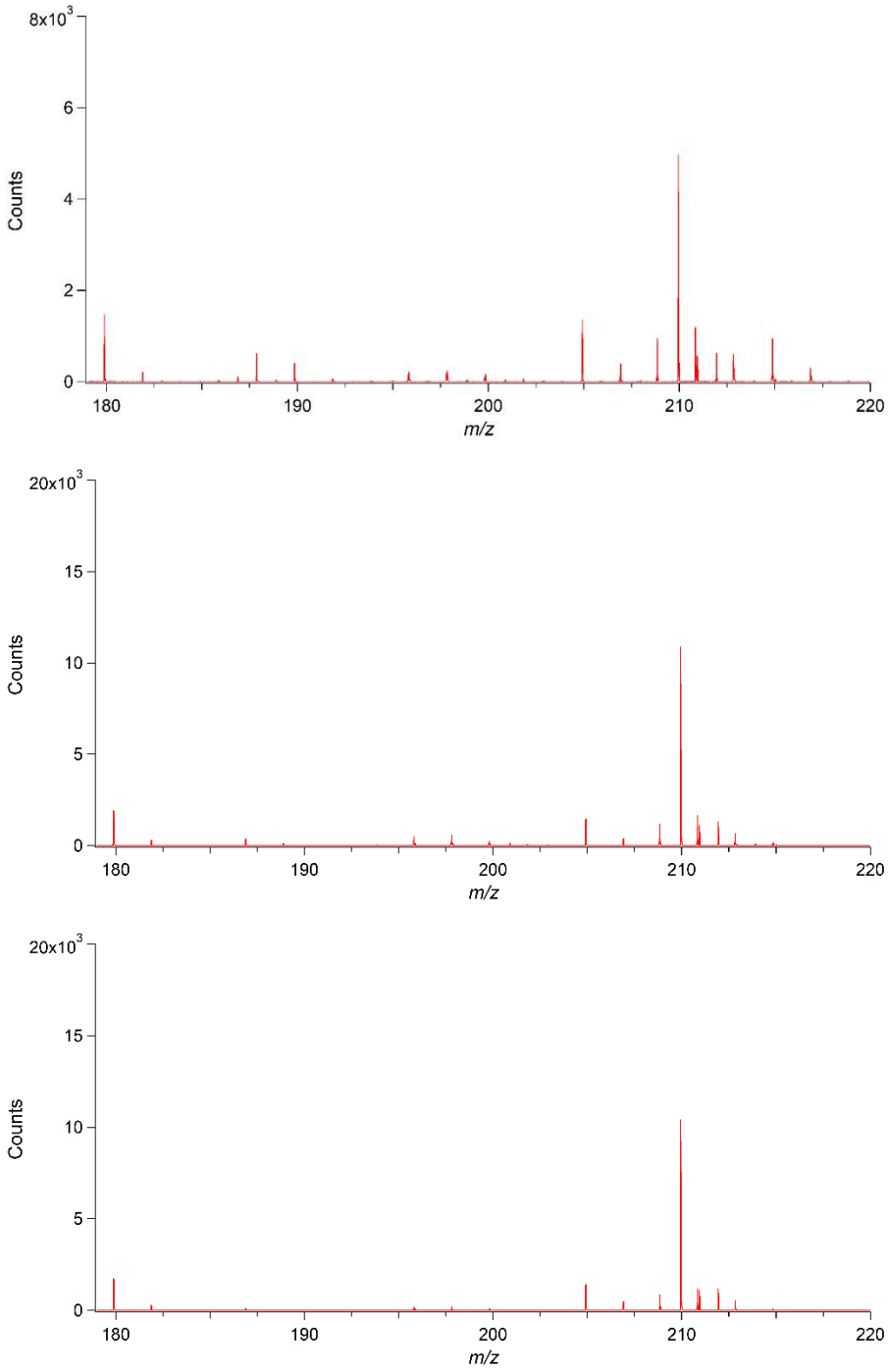

Figure B.25: MS of chitin polymer 1 after exposure to 0.5M HNO_2 for 1 hour. Unlabeled peaks represent ions that occur as a result of unexpected adducts or are artefacts of chemical reagents used to degrade the analyte. These are still visible due to there being no separation step prior to ionization.

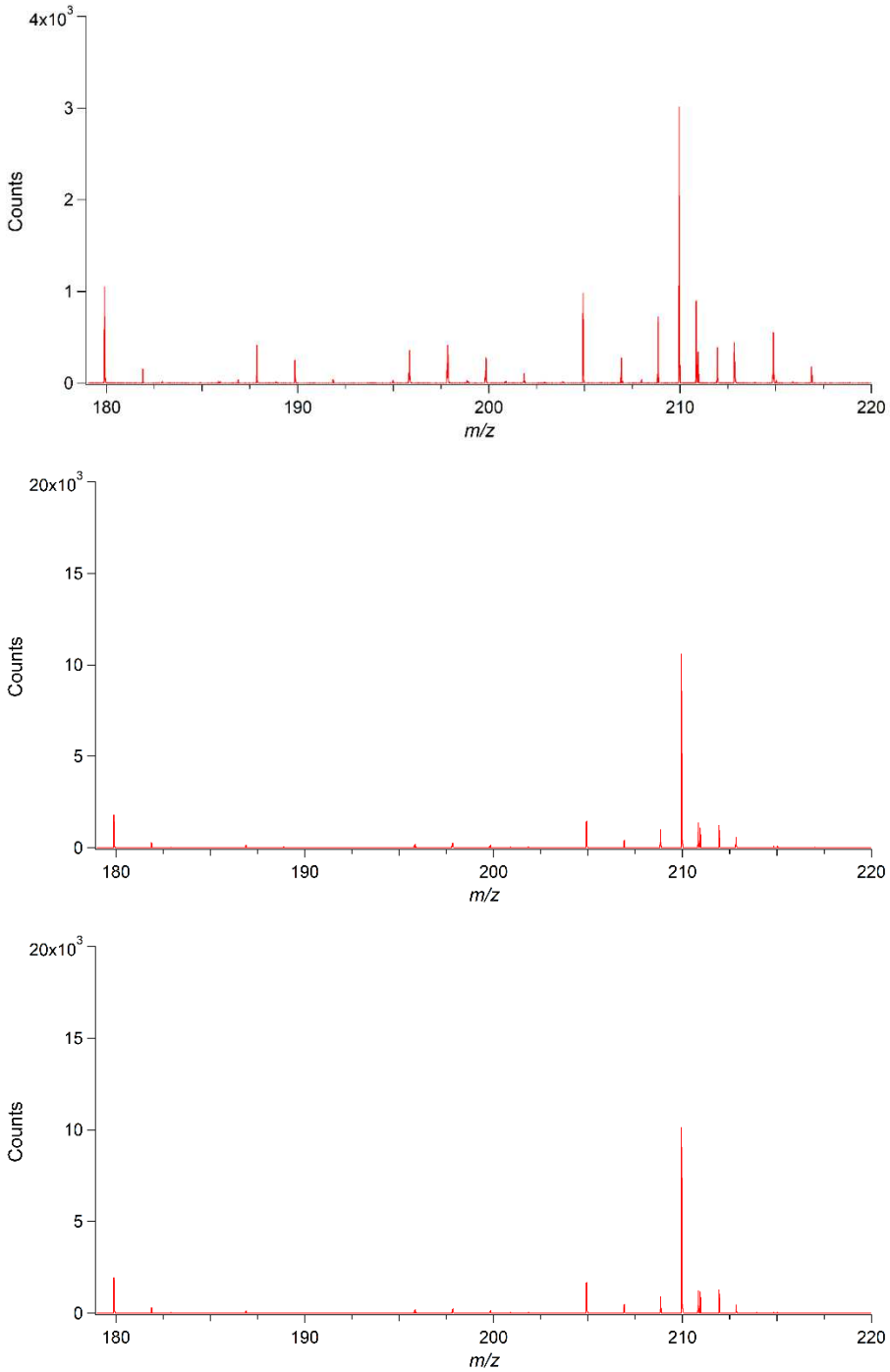

Figure B.26: MS of chitin polymer 1 after exposure to 0.5M HNO_2 for 2 hours. Unlabeled peaks represent ions that occur as a result of unexpected adducts or are artefacts of chemical reagents used to degrade the analyte. These are still visible due to there being no separation step prior to ionization.

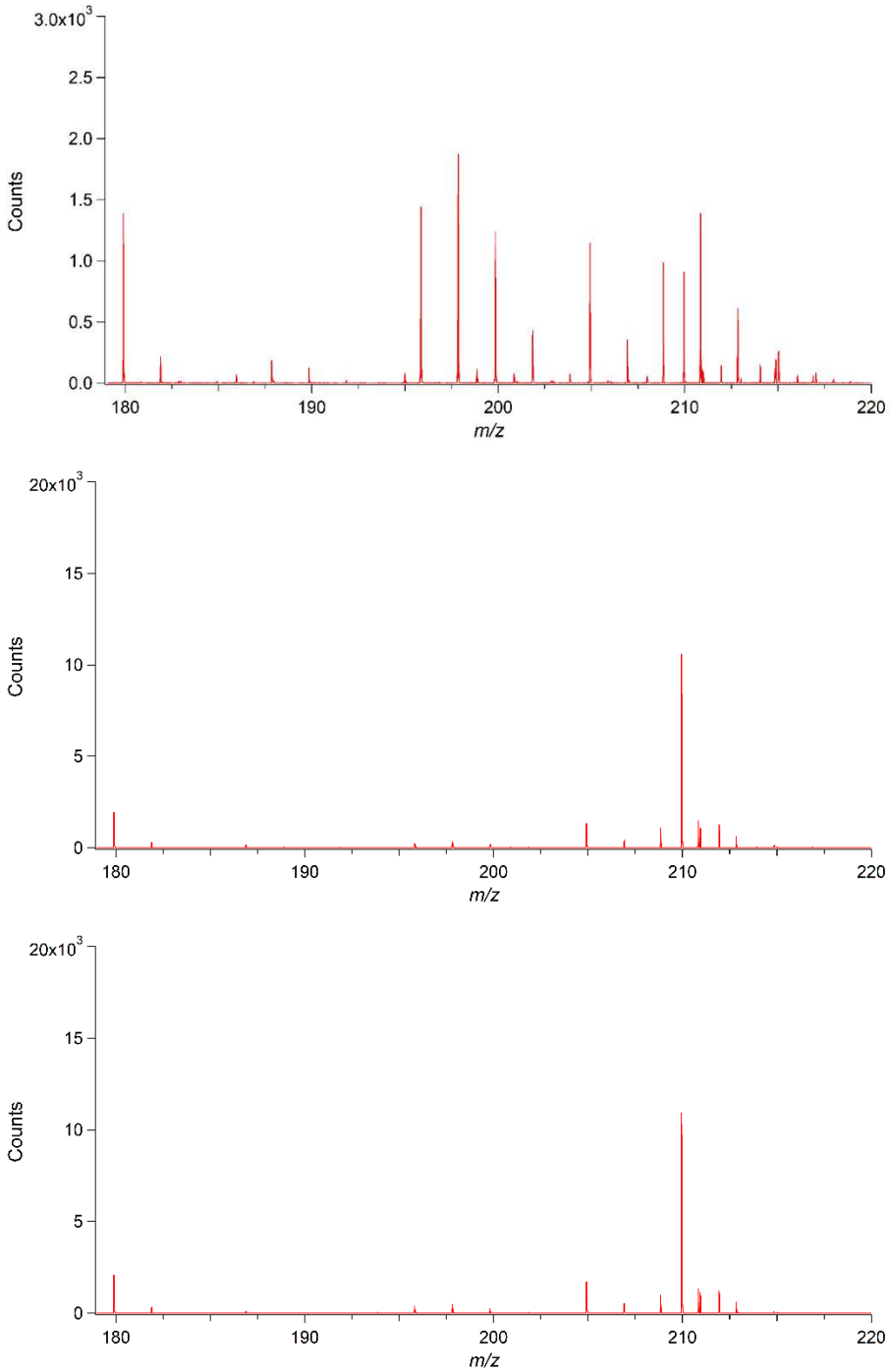

Figure B.27: MS of chitin polymer 1 after exposure to 0.5M HNO_2 for 24 hours. Unlabeled peaks represent ions that occur as a result of unexpected adducts or are artefacts of chemical reagents used to degrade the analyte. These are still visible due to there being no separation step prior to ionization.

Chitin polymer 2

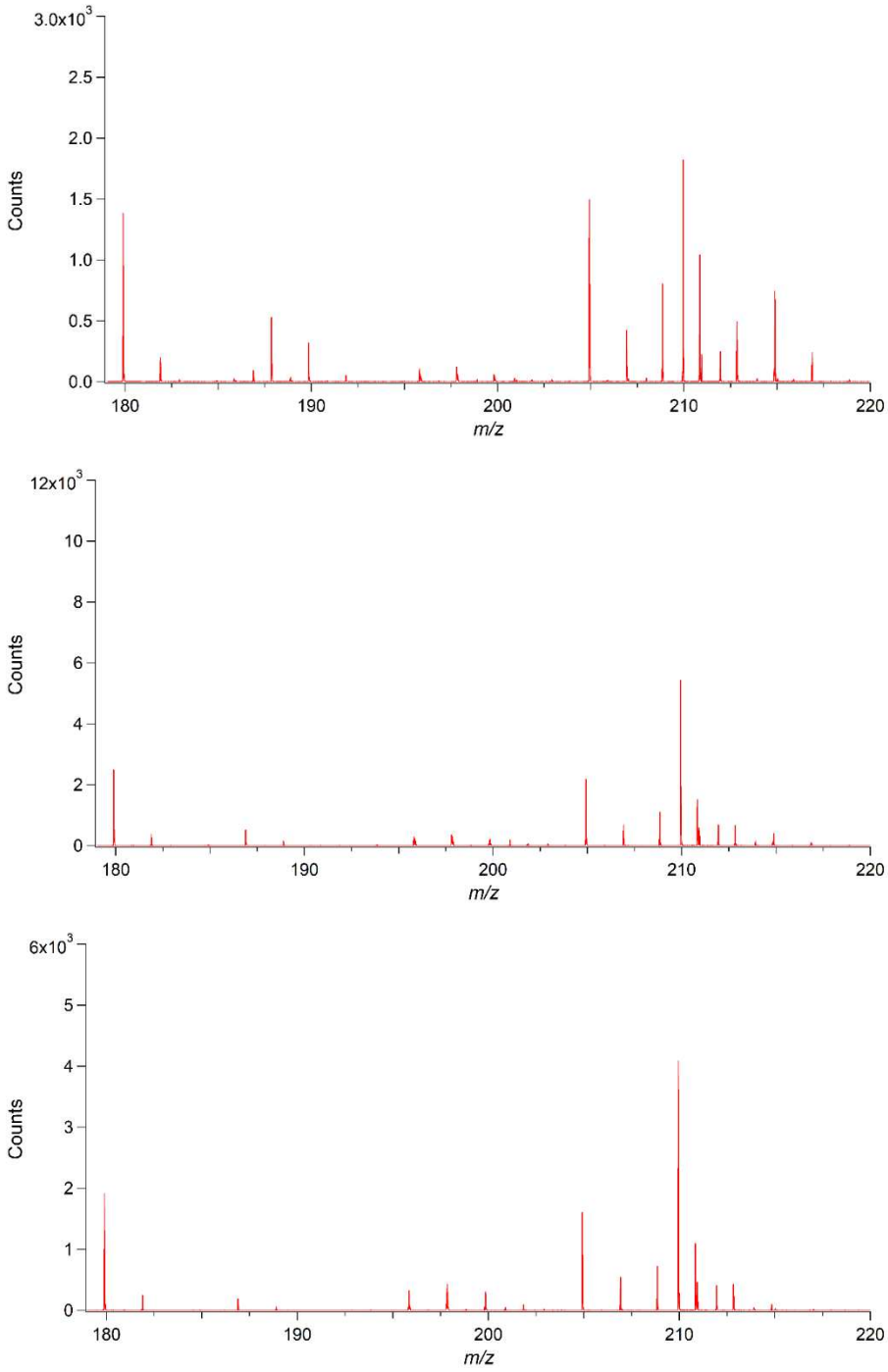

Figure B.28: MS of chitin polymer 2 after exposure to 0.5M HNO_2 for 1 hour. Unlabeled peaks represent ions that occur as a result of unexpected adducts or are artefacts of chemical reagents used to degrade the analyte. These are still visible due to there being no separation step prior to ionization.

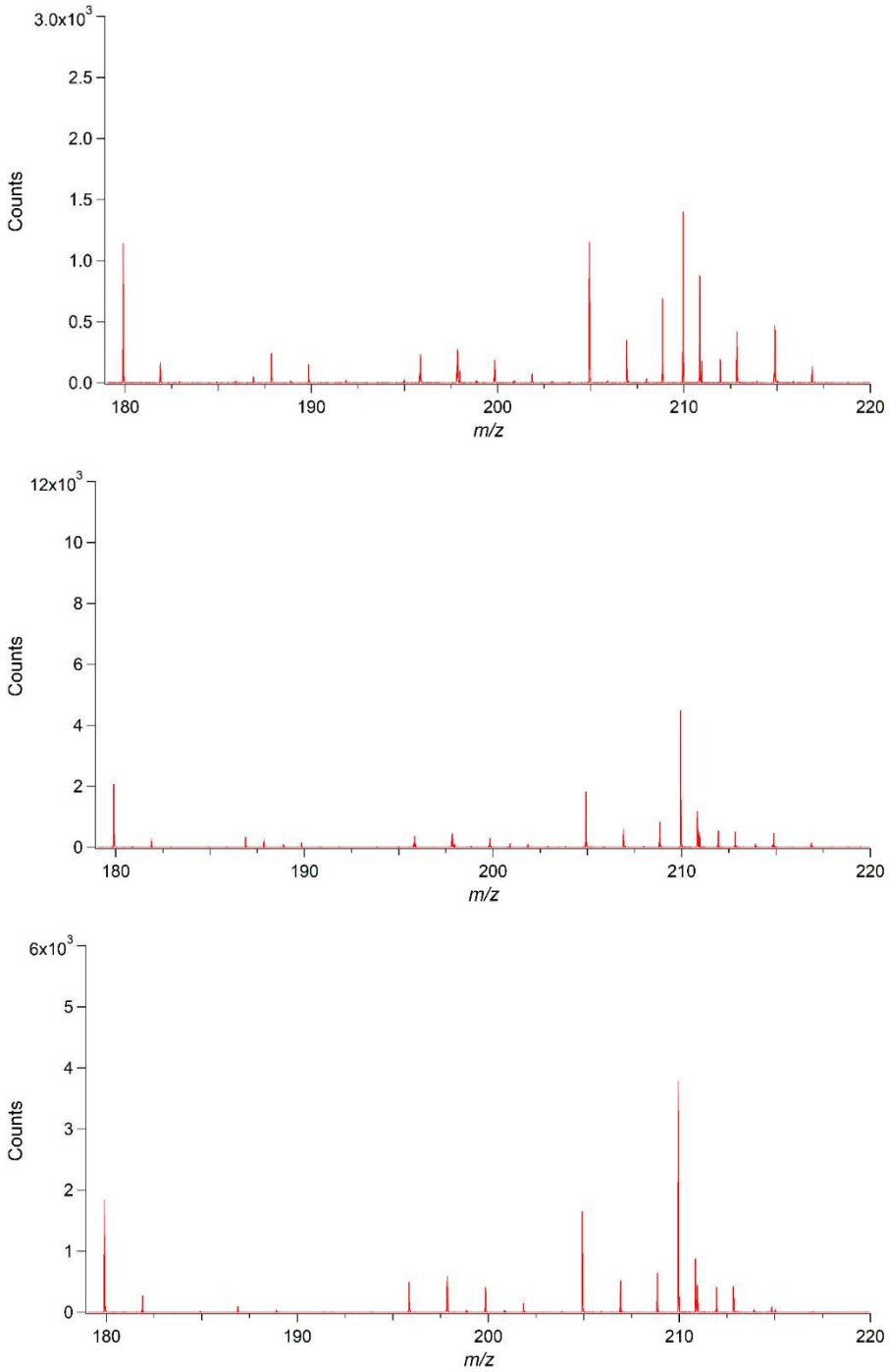

Figure B.29: MS of chitin polymer 2 after exposure to 0.5M HNO_2 for 2 hours. Unlabeled peaks represent ions that occur as a result of unexpected adducts or are artefacts of chemical reagents used to degrade the analyte. These are still visible due to there being no separation step prior to ionization.

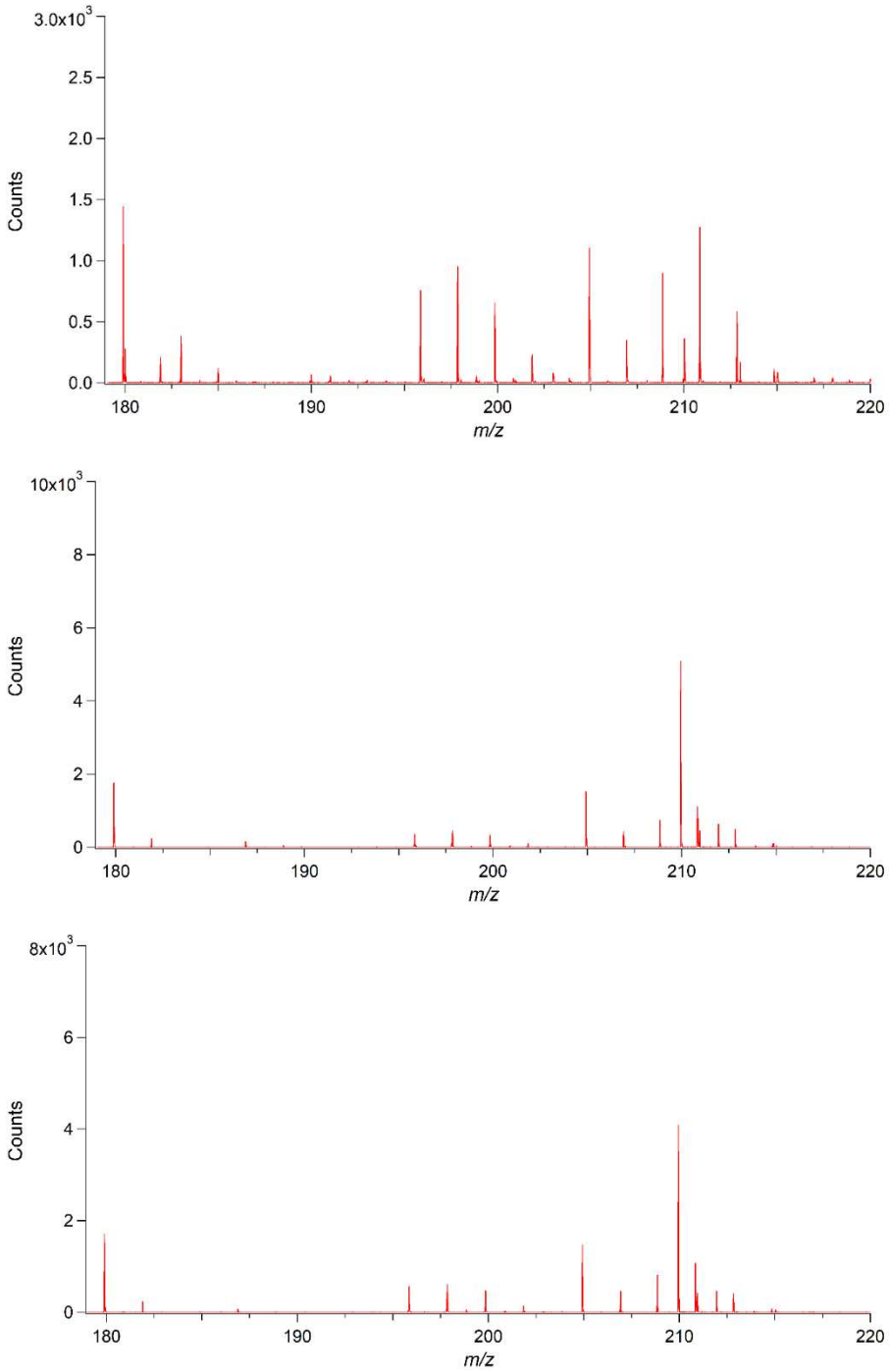

Figure B.30: MS of chitin polymer 2 after exposure to 0.5M HNO_2 for 24 hours. Unlabeled peaks represent ions that occur as a result of unexpected adducts or are artefacts of chemical reagents used to degrade the analyte. These are still visible due to there being no separation step prior to ionization.

Spectral analysis of HCl degradation products

Chitosan polymer

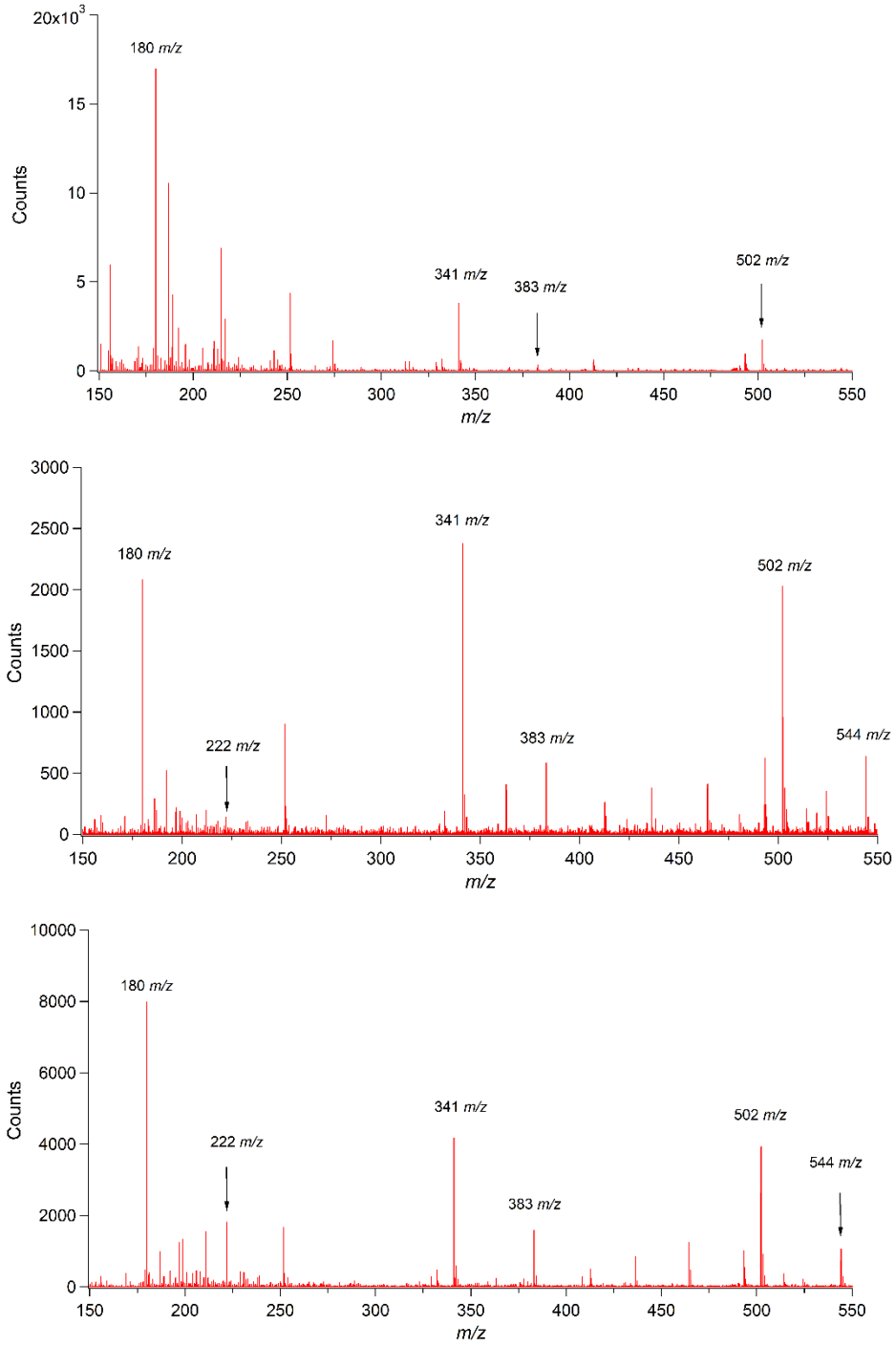

Figure B.31: MS of chitosan polymer after exposure to 5M HCl for 1 hour. Labeled peaks are indicative of compounds with molecular formulas consistent with predicted degradation products found in **Table B.1.** Remaining unlabeled peaks represent ions that occur as a result of unexpected

adducts or are artefacts of chemical reagents used to degrade the analyte. These are still visible due to there being no separation step prior to ionization.

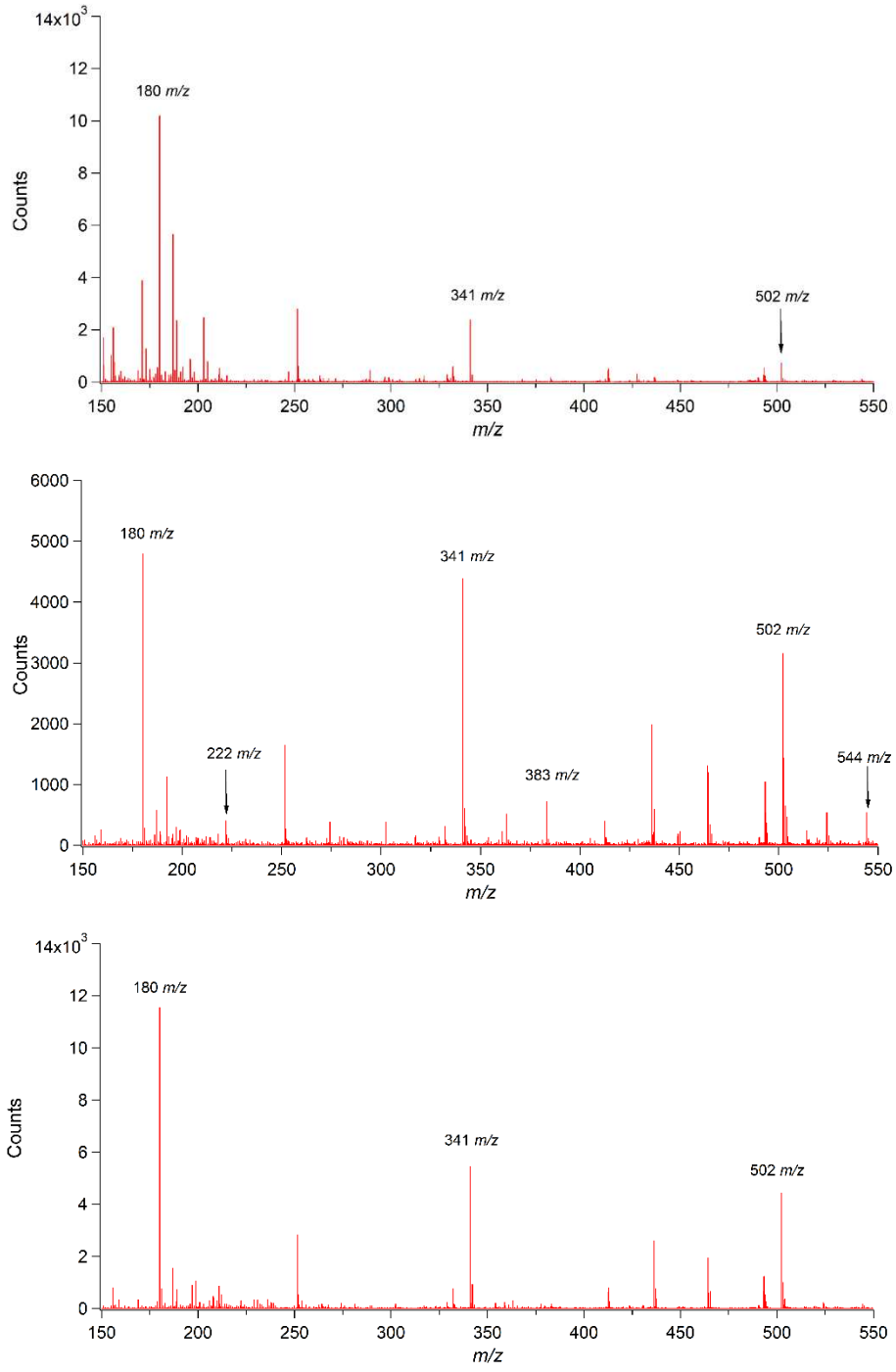

Figure B.32: MS of chitosan polymer after exposure to 5M HCl for 2 hours. Labeled peaks are indicative of compounds with molecular formulas consistent with predicted degradation products found in **Table B.1.** Remaining unlabeled peaks represent ions that occur as a result of unexpected adducts or are artefacts of chemical reagents used to degrade the analyte. These are still visible due to there being no separation step prior to ionization.

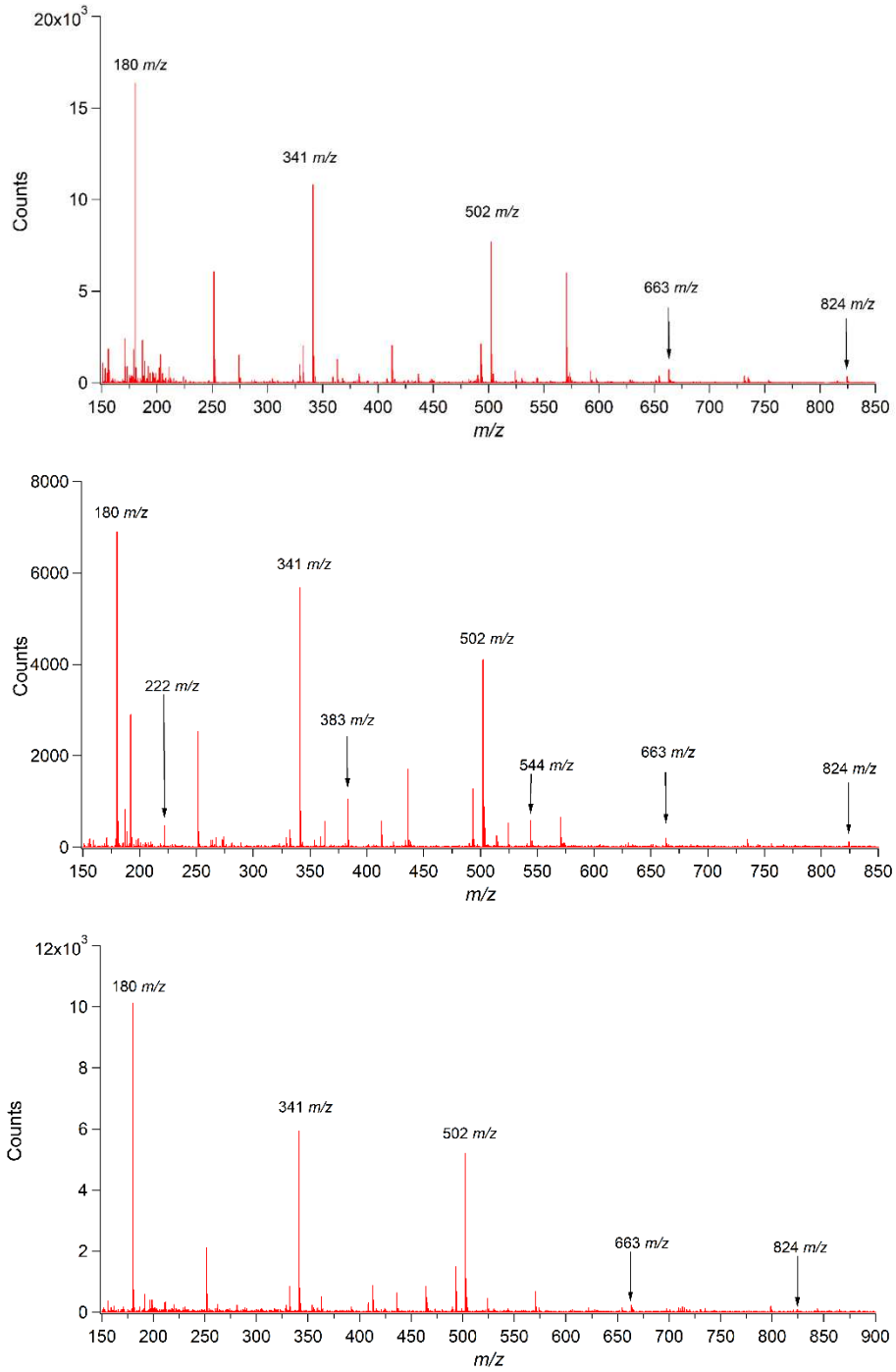

Figure B.33: MS of chitosan polymer after exposure to 5M HCl for 24 hours. Labeled peaks are indicative of compounds with molecular formulas consistent with predicted degradation products found in **Table B.1.** Remaining unlabeled peaks represent ions that occur as a result of unexpected adducts or are artefacts of chemical reagents used to degrade the analyte. These are still visible due to there being no separation step prior to ionization.

Chitin polymer 1

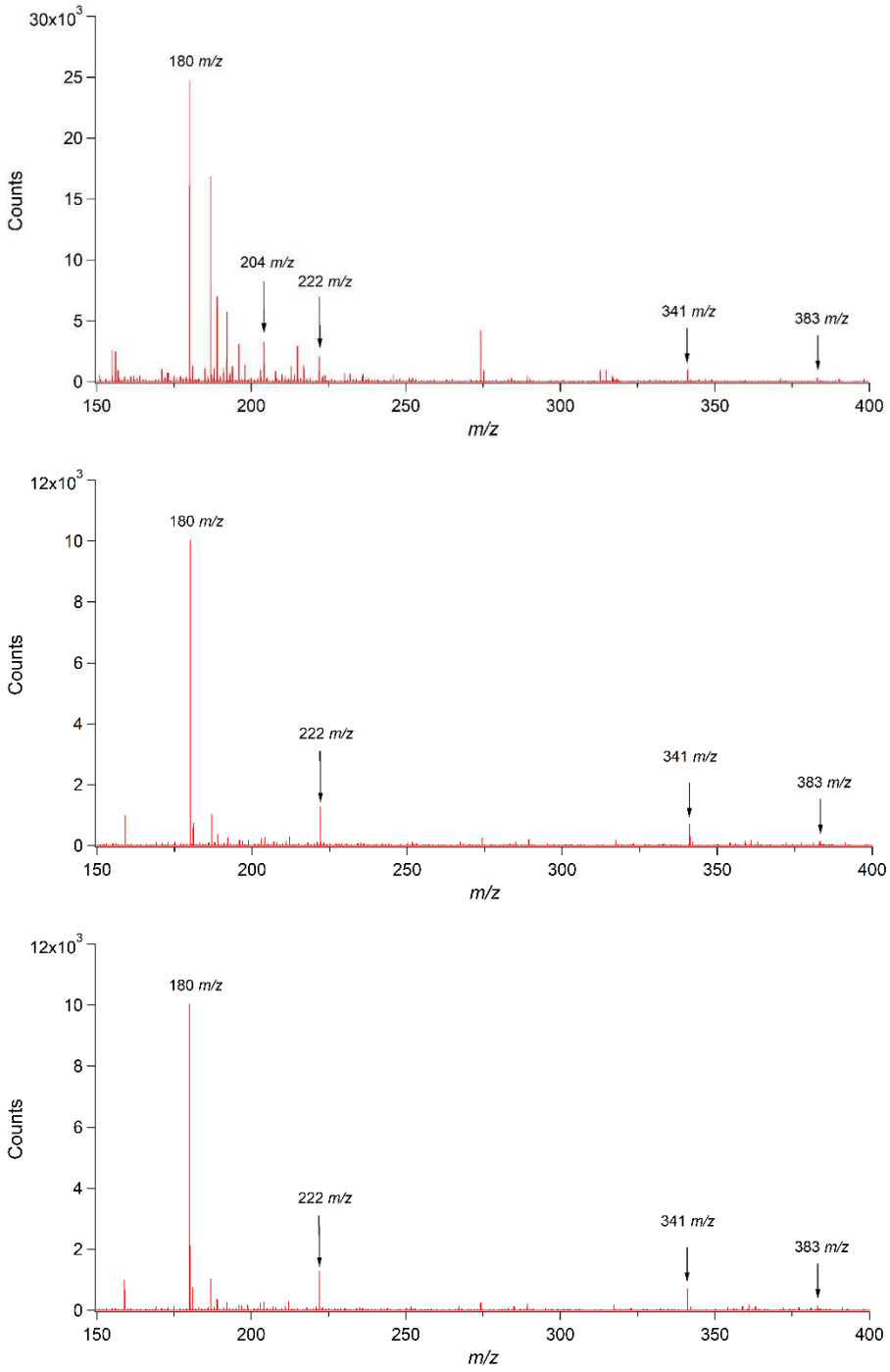

Figure B.34: MS of chitin polymer 1 after exposure to 5M HCl for 1 hour. Labeled peaks are indicative of compounds with molecular formulas consistent with predicted degradation products found in **Table B.1.** Remaining unlabeled peaks represent ions that occur as a result of unexpected adducts or are artefacts of chemical reagents used to degrade the analyte. These are still visible due to there being no separation step prior to ionization.

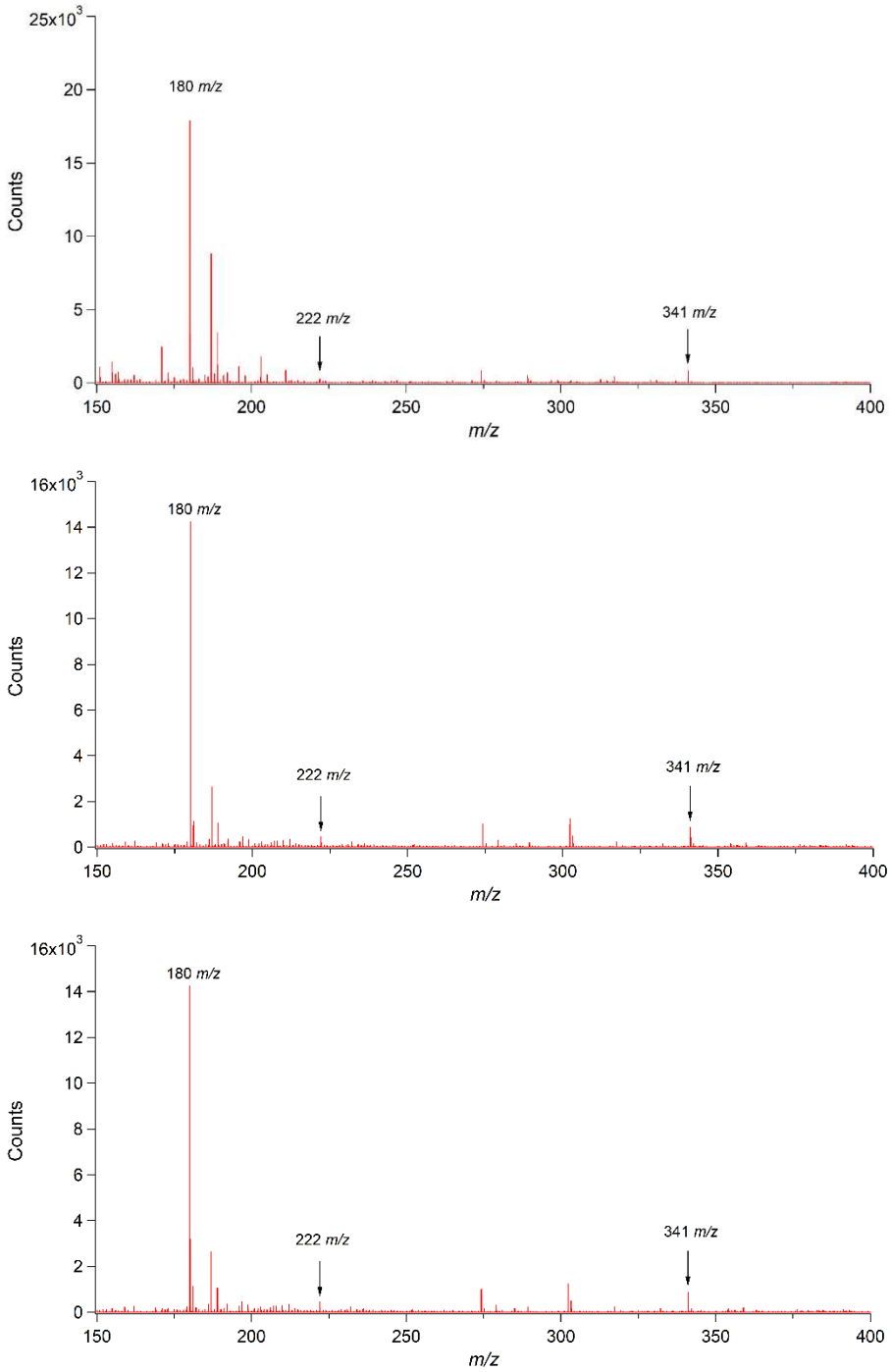

Figure B.35: MS of chitin polymer 1 after exposure to 5M HCl for 2 hours. Labeled peaks are indicative of compounds with molecular formulas consistent with predicted degradation products found in **Table B.1.** Remaining unlabeled peaks represent ions that occur as a result of unexpected adducts or are artefacts of chemical reagents used to degrade the analyte. These are still visible due to there being no separation step prior to ionization.

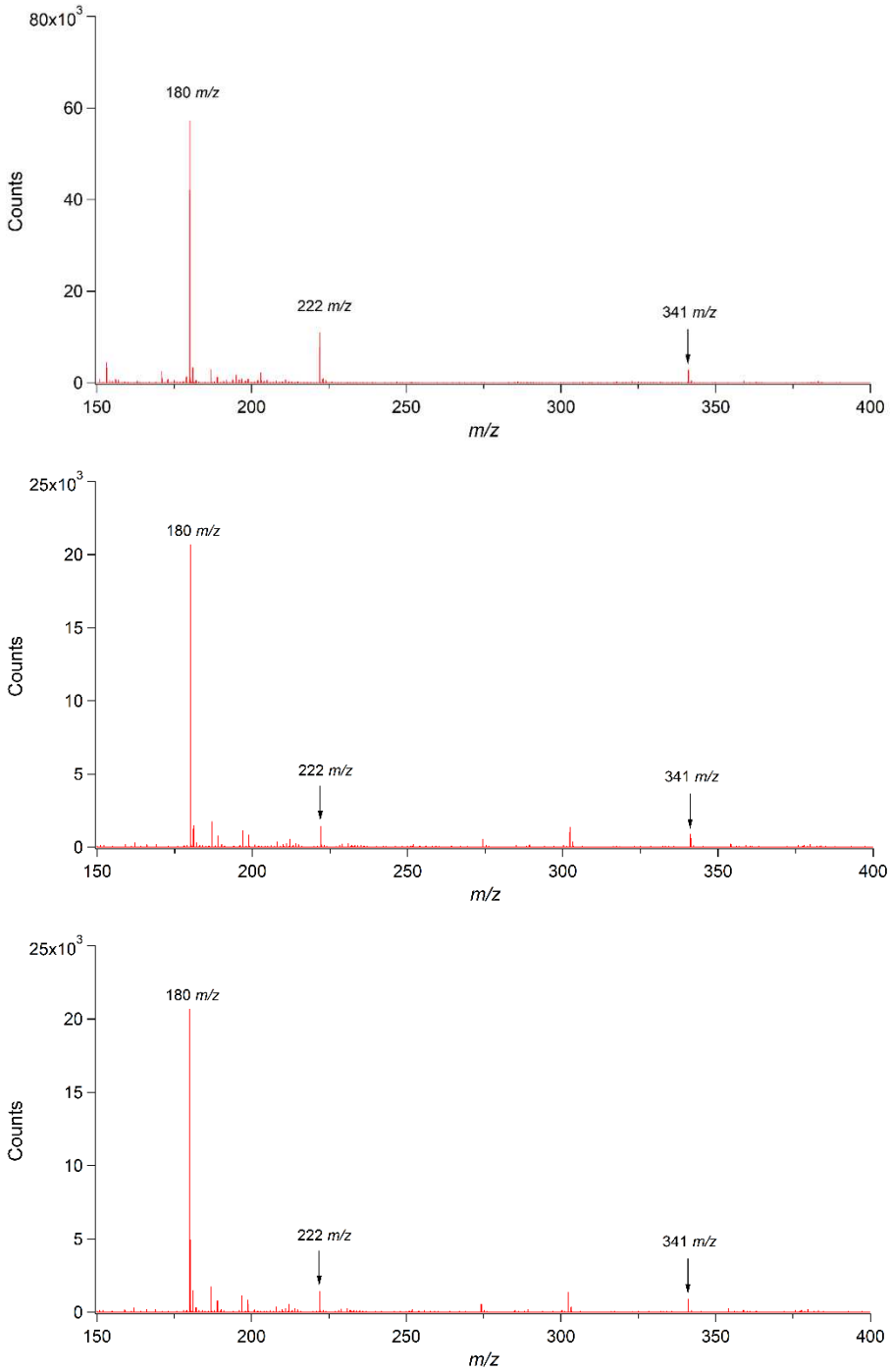

Figure B.36: MS of chitin polymer 1 after exposure to 5M HCl for 24 hours. Labeled peaks are indicative of compounds with molecular formulas consistent with predicted degradation products found in **Table B.1.** Remaining unlabeled peaks represent ions that occur as a result of unexpected adducts or are artefacts of chemical reagents used to degrade the analyte. These are still visible due to there being no separation step prior to ionization.

Chitin polymer 2

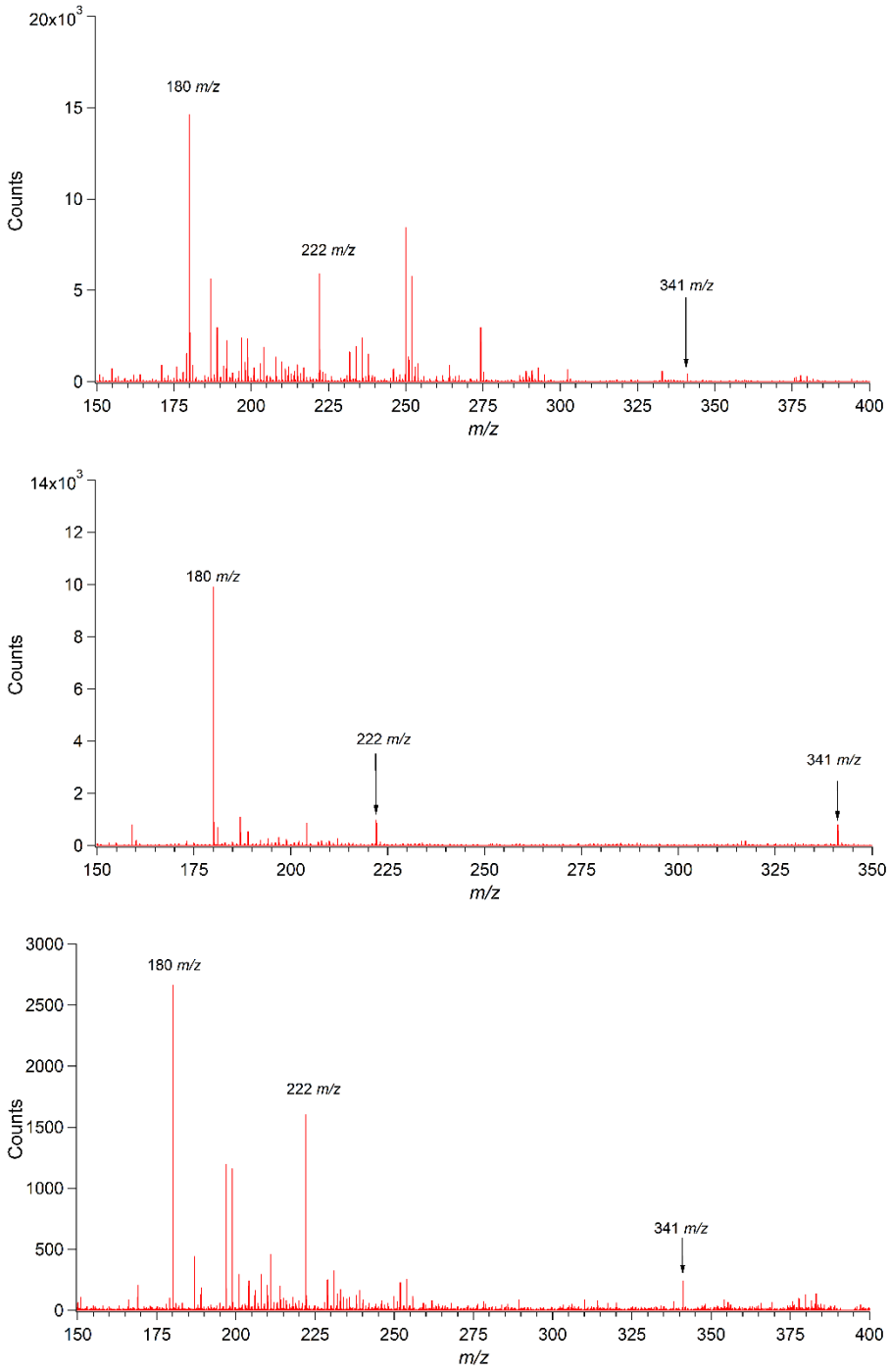

Figure B.37: MS of chitin polymer 2 after exposure to 5M HCl for 1 hour. Labeled peaks are indicative of compounds with molecular formulas consistent with predicted degradation products found in **Table B.1.** Remaining unlabeled peaks represent ions that occur as a result of unexpected adducts or are artefacts of chemical reagents used to degrade the analyte. These are still visible due to there being no separation step prior to ionization.

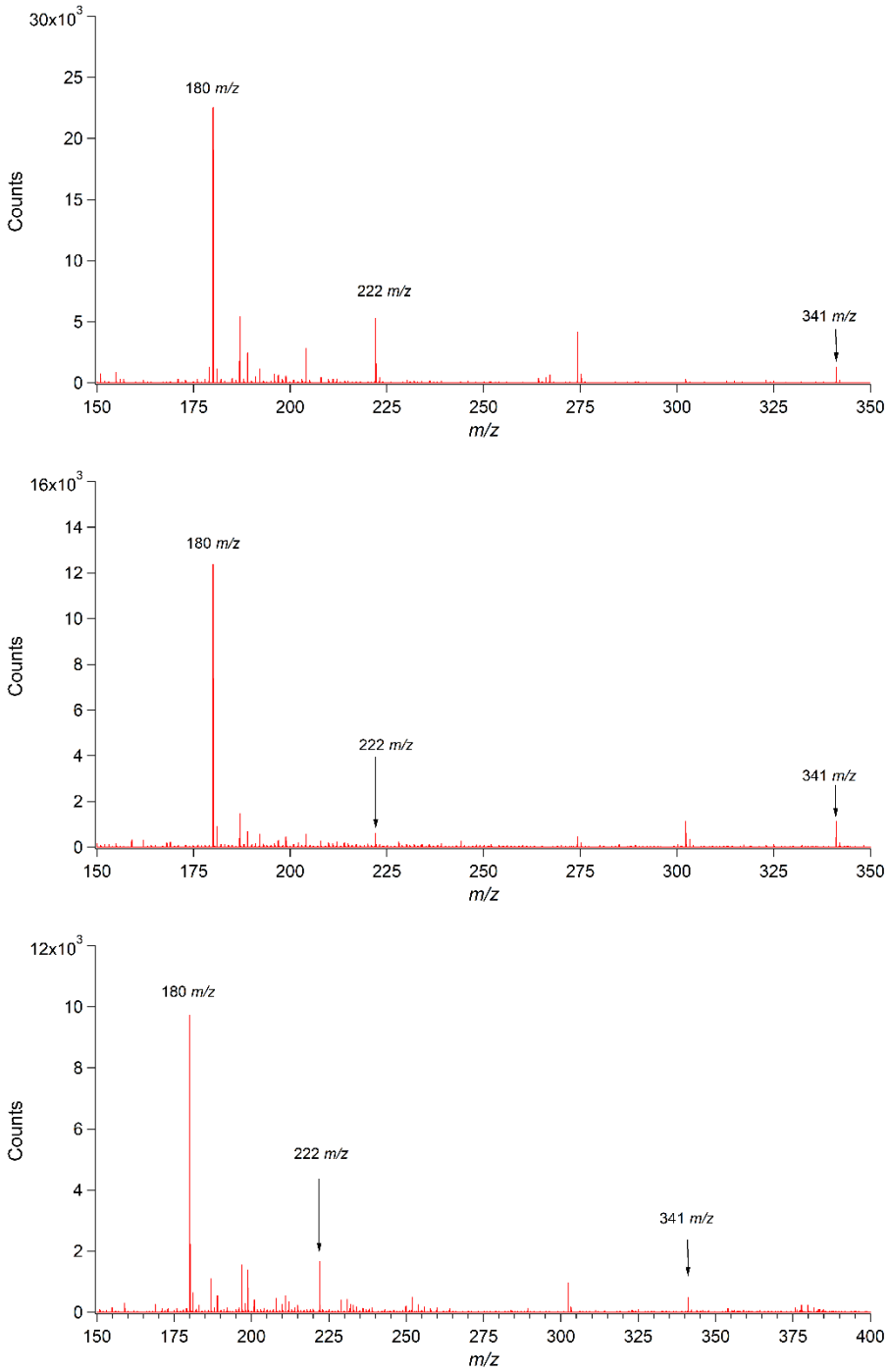

Figure B.38: MS of chitin polymer 2 after exposure to 5M HCl for 2 hours. Labeled peaks are indicative of compounds with molecular formulas consistent with predicted degradation products found in **Table B.1.** Remaining unlabeled peaks represent ions that occur as a result of unexpected adducts or are artefacts of chemical reagents used to degrade the analyte. These are still visible due to there being no separation step prior to ionization.

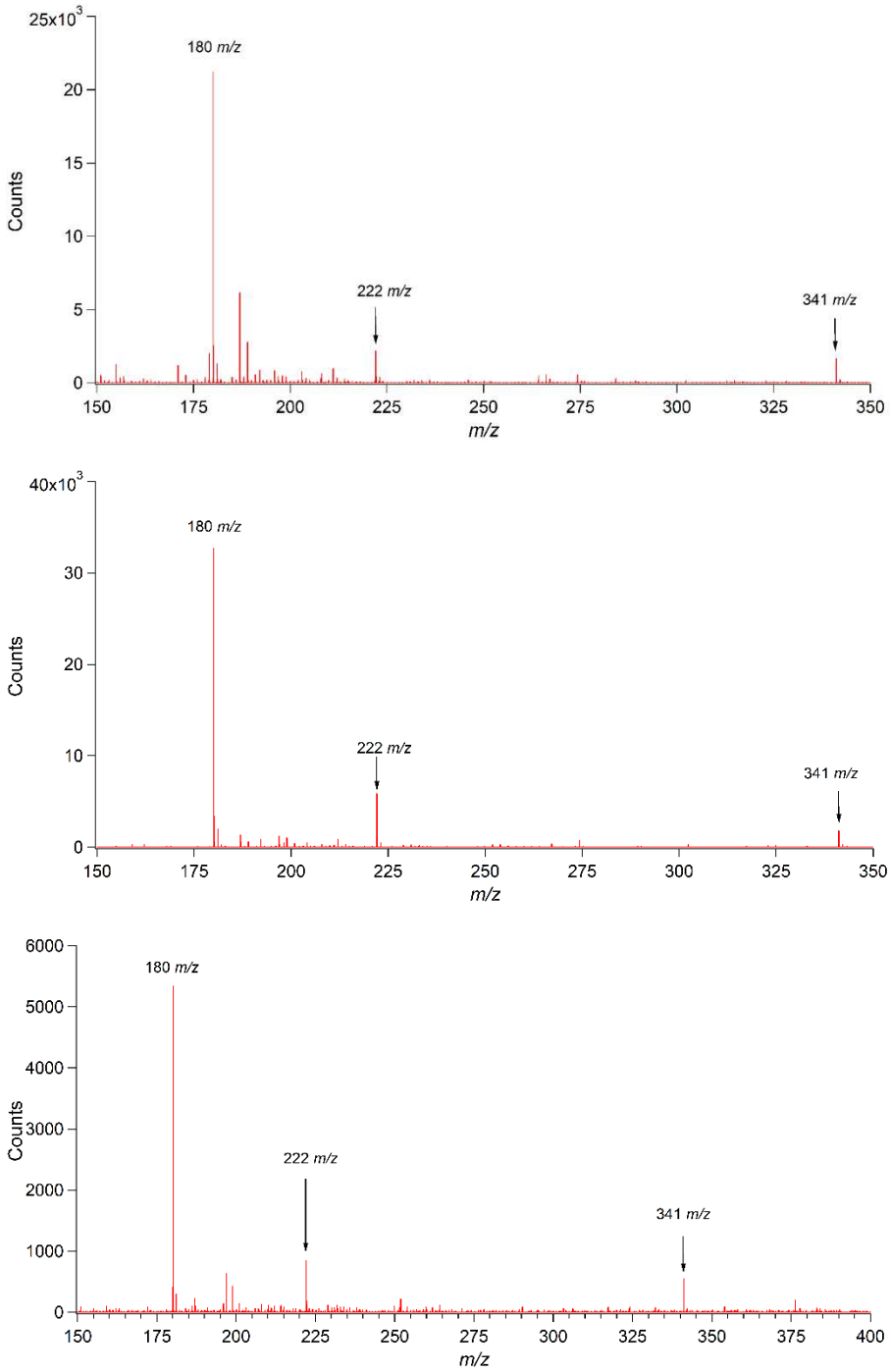

Figure B.39: MS of chitin polymer 2 after exposure to 5M HCl for 24 hours. Labeled peaks are indicative of compounds with molecular formulas consistent with predicted degradation products found in **Table B.1.** Remaining unlabeled peaks represent ions that occur as a result of unexpected adducts or are artefacts of chemical reagents used to degrade the analyte. These are still visible due to there being no separation step prior to ionization.

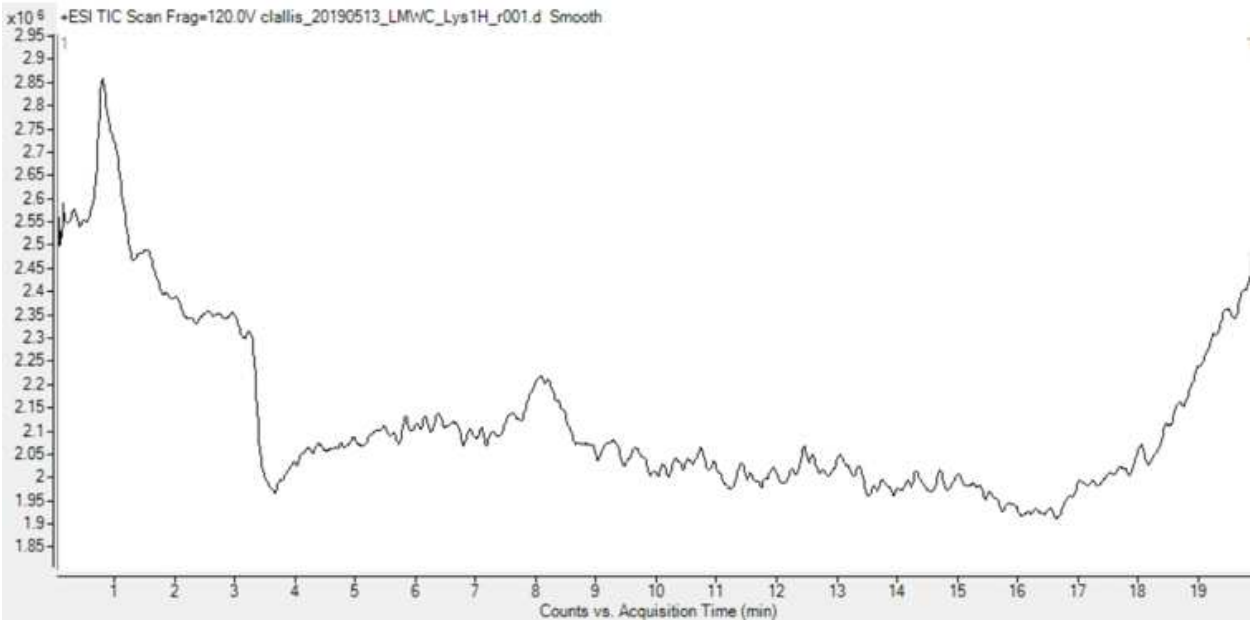

Figure B.40: LC chromatogram with MS insert of chitosan polymer following exposure to lysozyme for 1 hour. Peaks shown in MS are indicative of compounds with molecular formulas consistent with predicted degradation products found in **Table B.1**. Remaining unlabeled peaks represent ions that occur as a result of unexpected adducts or are artefacts of chemical reagents used to degrade the analyte.

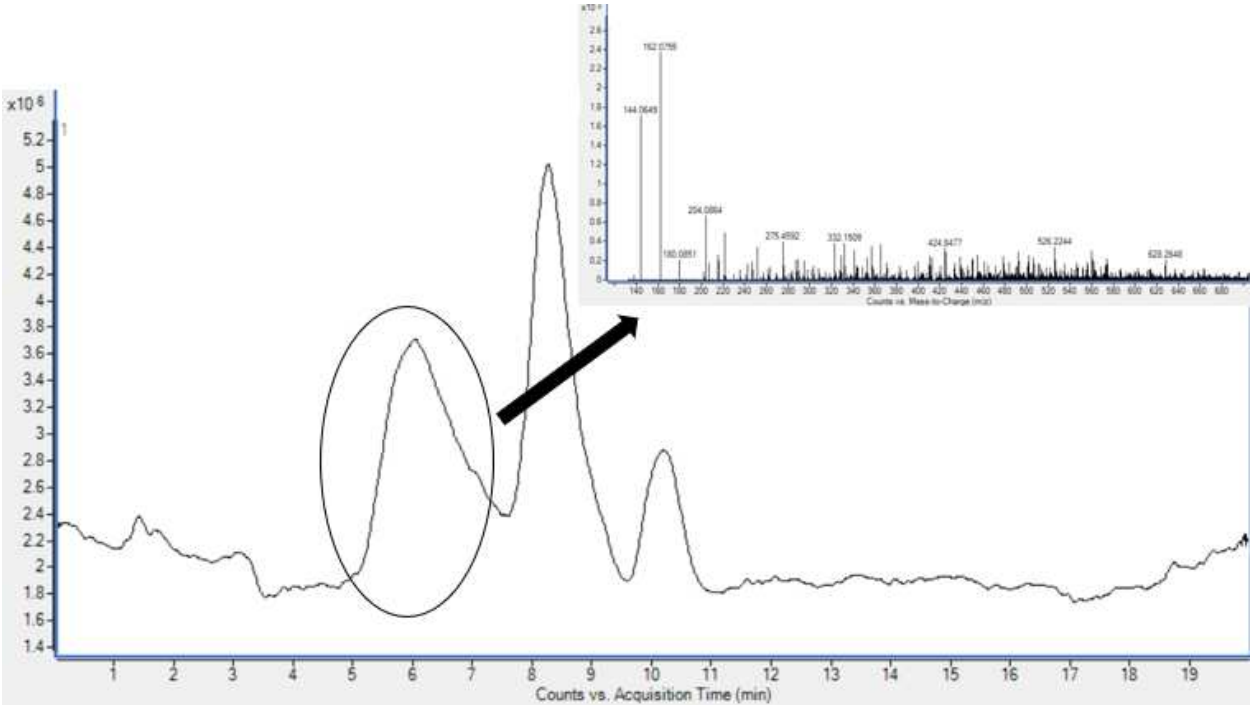

Figure B.41: LC chromatogram with MS insert of chitosan polymer following exposure to lysozyme for 4 hours. Peaks shown in MS are indicative of compounds with molecular formulas consistent with predicted degradation products found in **Table B.1**. Remaining unlabeled peaks

represent ions that occur as a result of unexpected adducts or are artefacts of chemical reagents used to degrade the analyte.

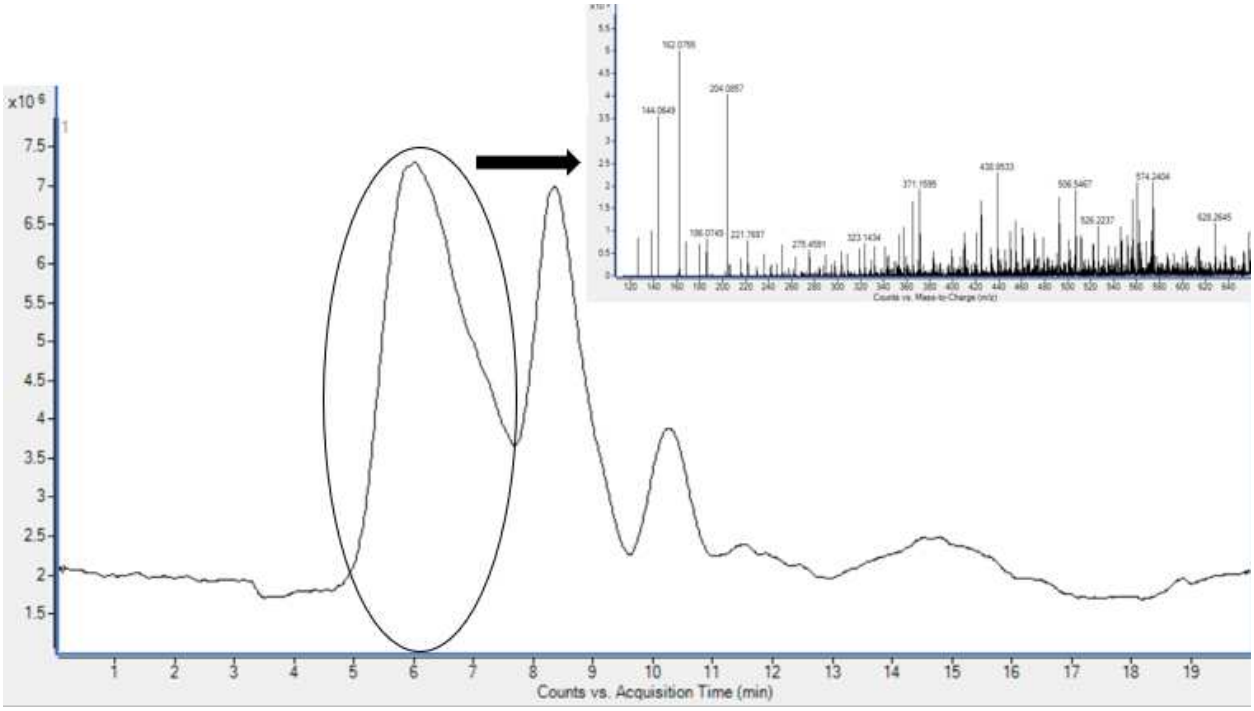

Figure B.42: LC chromatogram with MS insert of chitosan polymer following exposure to lysozyme for 24 hours. Peaks shown in MS are indicative of compounds with molecular formulas consistent with predicted degradation products found in **Table B.1**. Remaining unlabeled peaks represent ions that occur as a result of unexpected adducts or are artefacts of chemical reagents used to degrade the analyte.

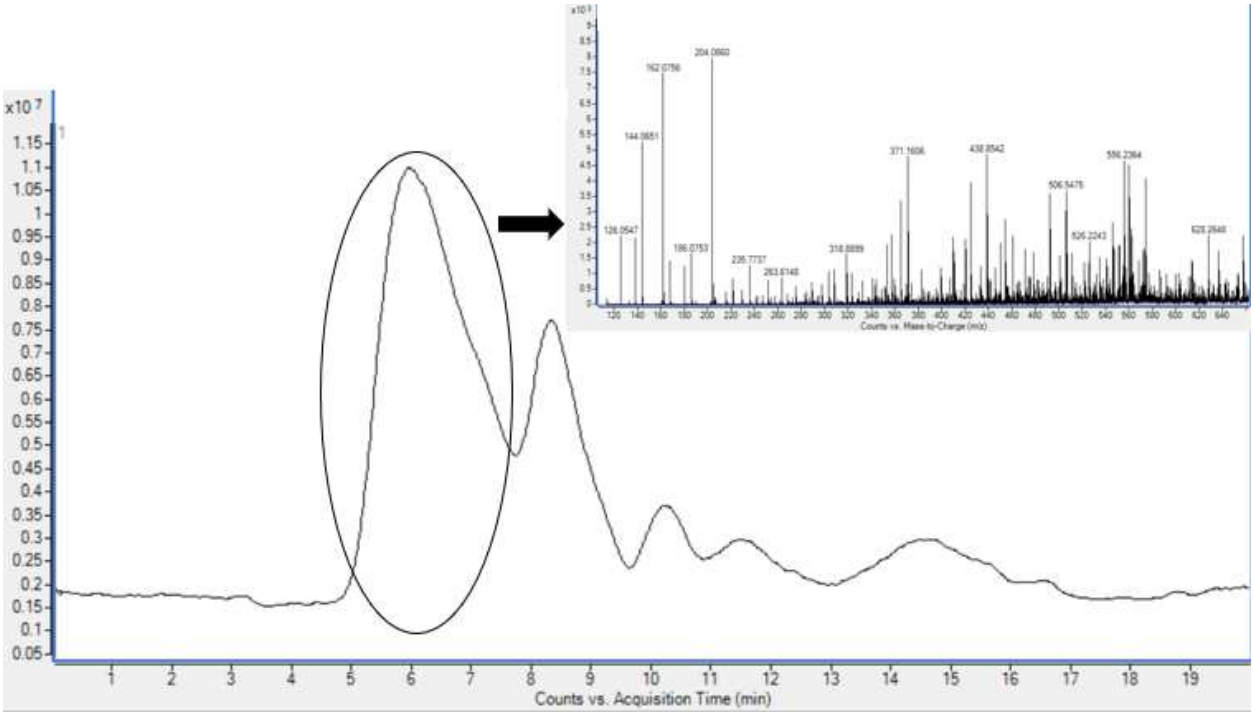

Figure B.43: LC chromatogram with MS insert of chitosan polymer following exposure to lysozyme for 3 days. Peaks shown in MS are indicative of compounds with molecular formulas consistent with predicted degradation products found in **Table B.1**. Remaining unlabeled peaks represent ions that occur as a result of unexpected adducts or are artefacts of chemical reagents used to degrade the analyte.

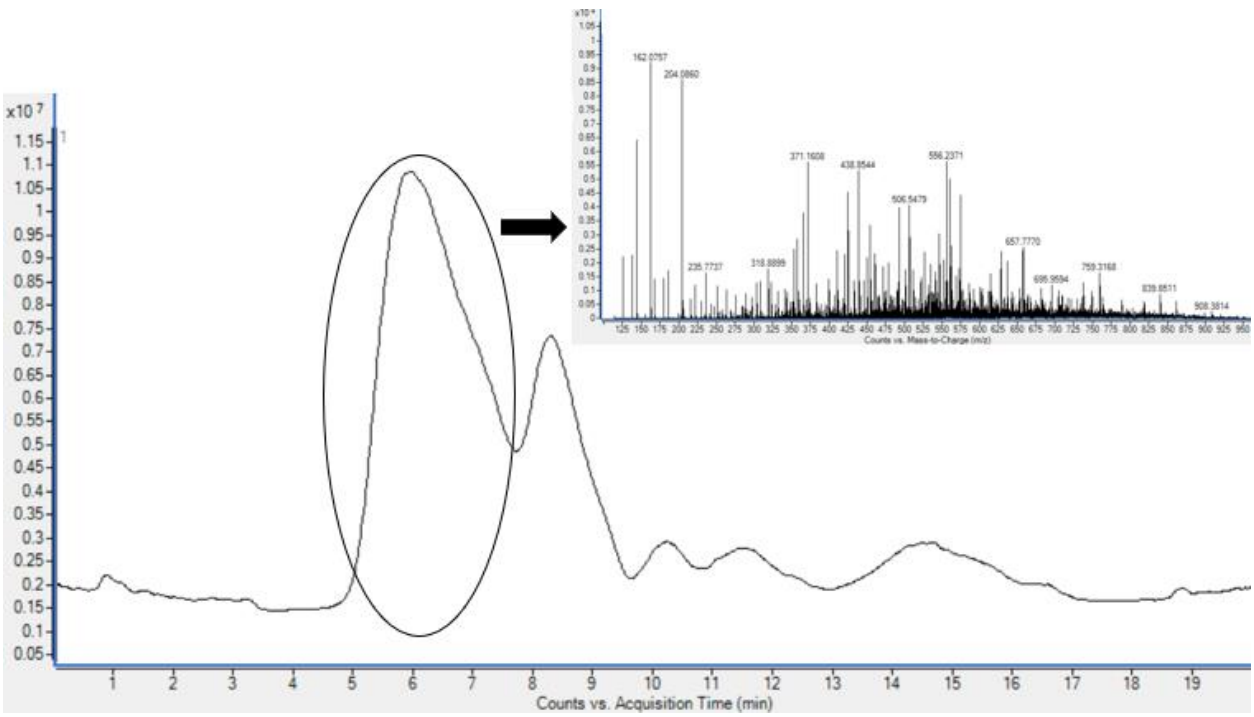

Figure B.44: LC chromatogram with MS insert of chitosan polymer following exposure to lysozyme for 7 days. Peaks shown in MS are indicative of compounds with molecular formulas consistent with predicted degradation products found in **Table B.1**. Remaining unlabeled peaks represent ions that occur as a result of unexpected adducts or are artefacts of chemical reagents used to degrade the analyte.

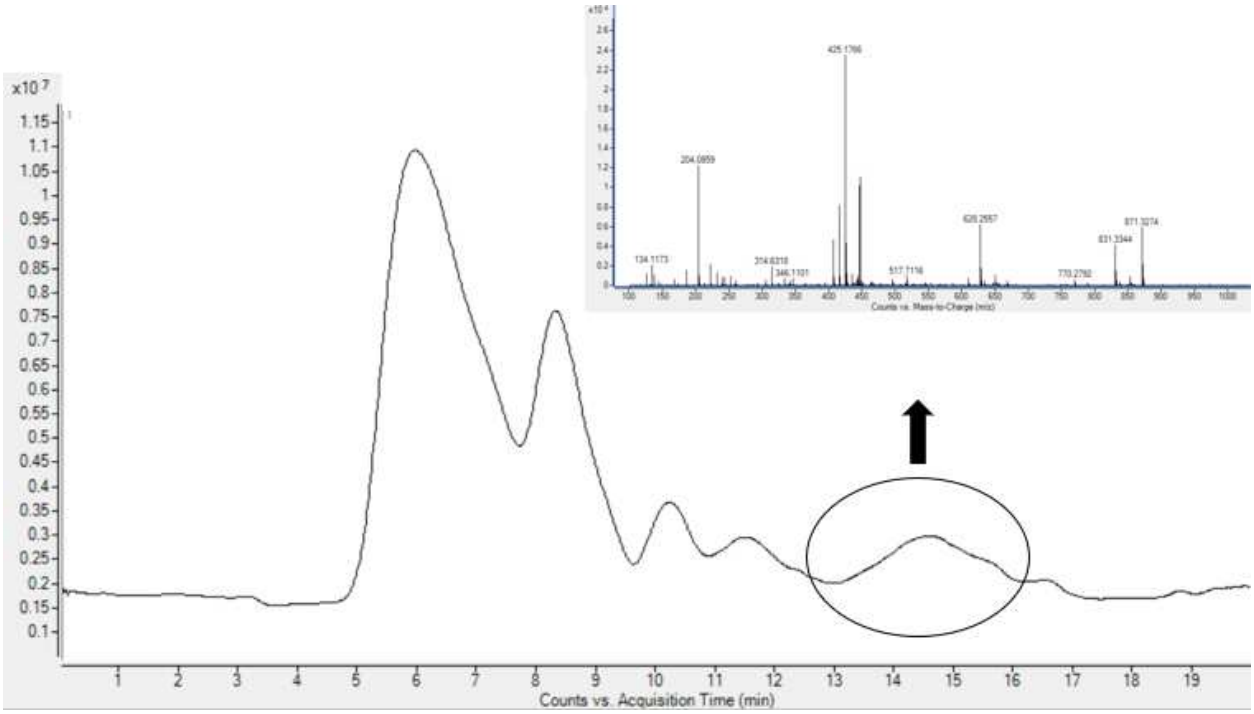

Figure B.45: LC chromatogram with MS insert of chitosan polymer following exposure to lysozyme for 3 days. Peaks shown in MS are indicative of compounds with molecular formulas consistent with predicted degradation products found in **Table B.1**. Remaining unlabeled peaks represent ions that occur as a result of unexpected adducts or are artefacts of chemical reagents used to degrade the analyte.

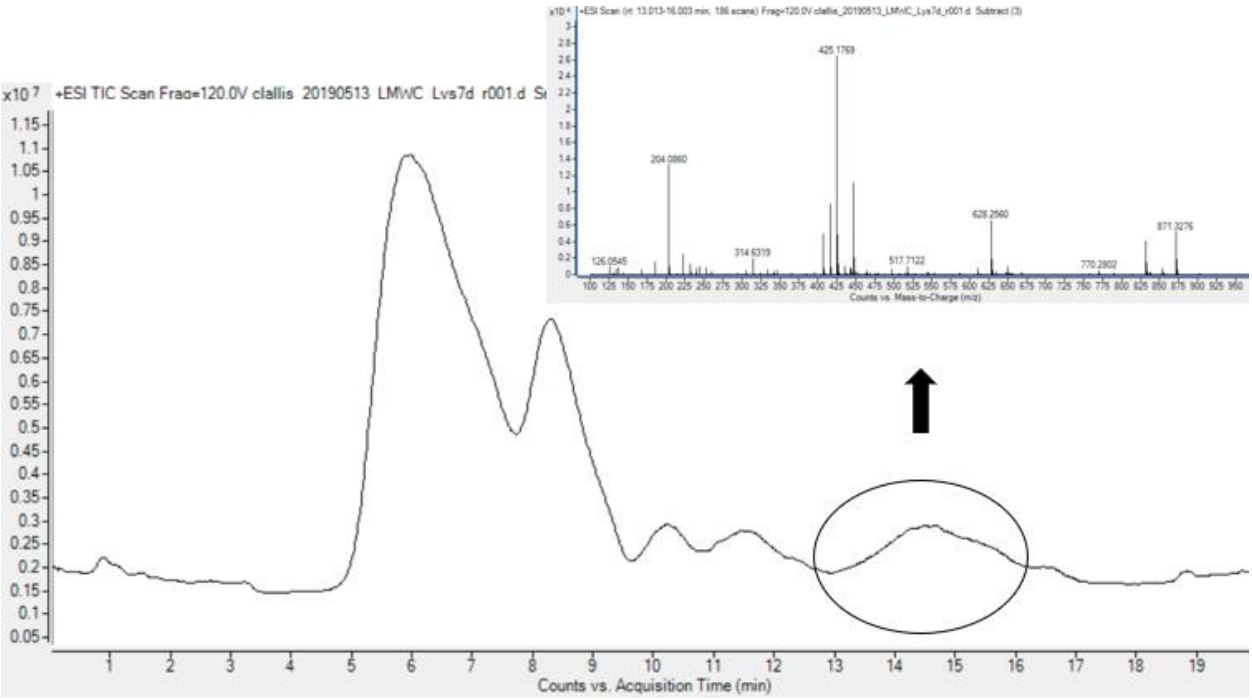

Figure B.46: LC chromatogram with MS insert of chitosan polymer following exposure to lysozyme for 7 days. Peaks shown in MS are indicative of compounds with molecular formulas consistent with predicted degradation products found in **Table B.1**. Remaining unlabeled peaks represent ions that occur as a result of unexpected adducts or are artefacts of chemical reagents used to degrade the analyte.

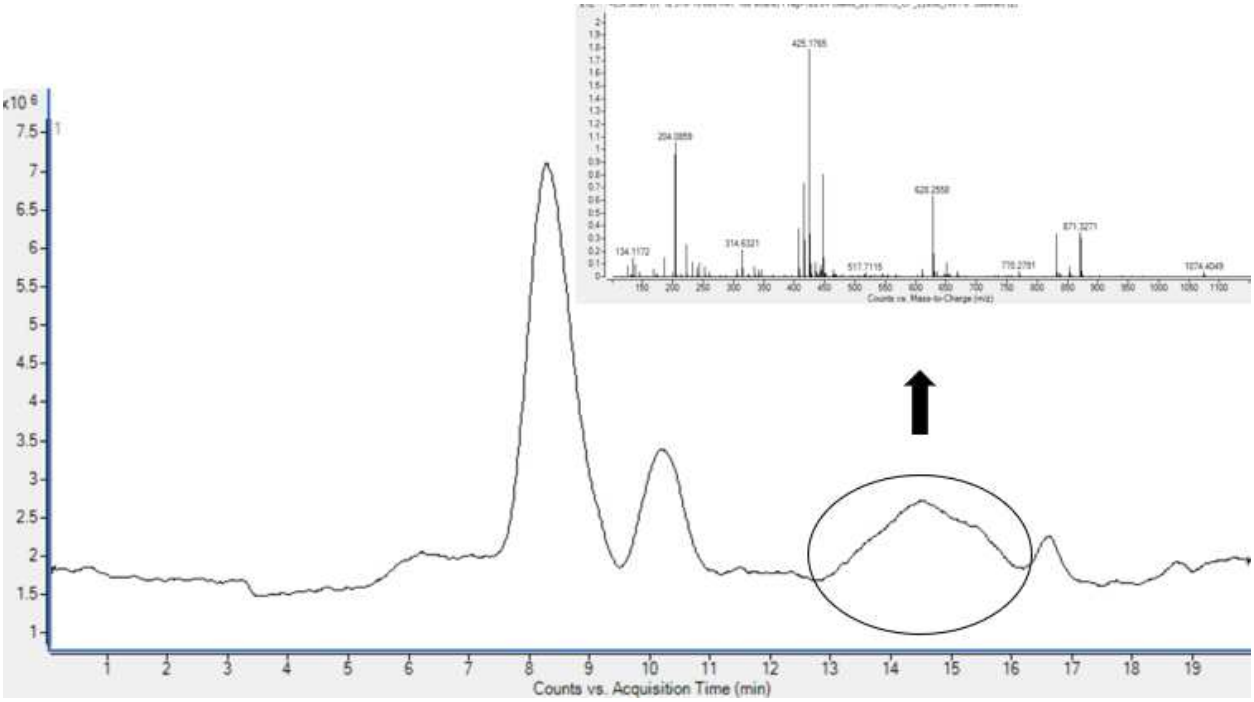

Figure B.47: LC chromatogram with MS insert of chitin polymer 1 following exposure to lysozyme for 3 days. Peaks shown in MS are indicative of compounds with molecular formulas

consistent with predicted degradation products found in **Table B.1**. Remaining unlabeled peaks represent ions that occur as a result of unexpected adducts or are artefacts of chemical reagents used to degrade the analyte.

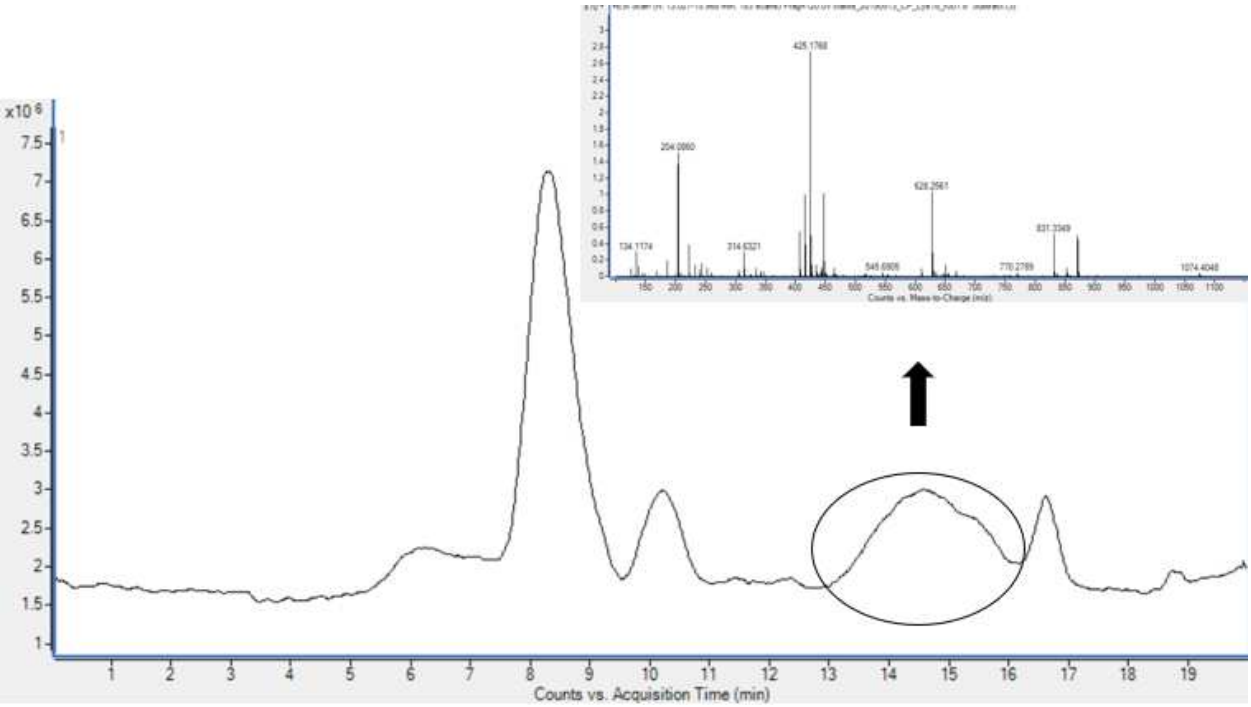

Figure B.48: LC chromatogram with MS insert of chitin polymer 1 following exposure to lysozyme for 7 days. Peaks shown in MS are indicative of compounds with molecular formulas consistent with predicted degradation products found in **Table B.1**. Remaining unlabeled peaks represent ions that occur as a result of unexpected adducts or are artefacts of chemical reagents used to degrade the analyte.